

**Development of novel genetically encoded
fluorescent sensors for real-time monitoring of
subcellular NADPH/NADP⁺ dynamics in living cells**

Dissertation

zur Erlangung des Grades
der Doktorin der Naturwissenschaften
der Naturwissenschaftlich-Technischen Fakultät
der Universität des Saarlandes

von

Marie Scherschel

Saarbrücken

2022

Tag des Kolloquiums: 15. Dezember 2022

Dekan: Prof. Dr. Ludger Santen

Berichterstatter: Prof. Dr. Bruce Morgan
Prof. Dr. Robert Ernst

Vorsitz: Prof. Dr. Alexandra K. Kiemer

Akad. Mitarbeiter: Dr. Eva Steinmetz

Table of Contents

Table of Contents	I
Summary	VI
Zusammenfassung	VII
List of Figures	VIII
List of Tables	X
Abbreviations	XI
1 Introduction	1
1.1 The model organism <i>Saccharomyces cerevisiae</i>	1
1.2 NAD and NADP coenzymes	1
1.2.1 NAD ⁺ biosynthesis	2
1.2.2 NAD-dependent redox reactions in central carbon metabolism	4
1.2.3 NADP biosynthesis	5
1.2.4 NADP-dependent redox reactions	5
1.2.5 NAD(P)H shuttles	7
1.3 Antioxidant defense systems	8
1.3.1 The GSH-based system	9
1.3.2 The Trx-based system	10
1.4 The yeast metabolic cycle	11
1.5 Genetically encoded fluorescent indicators	13
1.5.1 Redox-sensitive GFIs	16
roGFP2-Grx1 (GSSG/2GSH)	16
roGFP2-Tsa2ΔC _R (H ₂ O ₂)	17
HyPer7 (H ₂ O ₂)	17
1.5.2 pH-sensitive GFIs	18
SypHer	18
pHluorin	18
1.6 Methods to quantify NAD and NADP metabolites	19
1.6.1 Conventional NAD(P) quantification methods	19
1.6.2 NAD- and NADP-sensitive GFIs	21
The transcriptional repressor Rex	22
The Peredox sensor family (NADH/NAD ⁺)	24
The SoNar sensor (NADH/NAD ⁺)	26
The iNap sensor family (NADPH)	27

1.7	Research objectives	29
2	Results	31
2.1	Characterization of SoNar and iNap in <i>S. cerevisiae</i>	31
2.1.1	SoNar and iNap are functional in <i>S. cerevisiae</i>	32
2.1.2	Fluorescence of SoNar and iNap strongly depends on pH.....	34
	Construction of mSI-SoNar and mSI-iNap sensors.....	37
2.1.3	SoNar and mSI-SoNar respond to NAD(P)H in semipermeabilized cells ..	37
2.1.4	iNap and mSI-iNap respond to NADPH in semipermeabilized cells	38
2.2	Characterization of Pdx-mC and Pdx-mC DS in <i>S. cerevisiae</i>	41
2.2.1	Pdx-mC (DS) are functional in <i>S. cerevisiae</i>	41
2.2.2	Pdx-mC (DS) show minor pH dependency	43
2.2.3	Maturation time discrepancies between cpTS and mC are minor	44
2.2.4	Pdx-mC (DS) respond to NAD(P)H in semipermeabilized cells.....	46
2.3	Design of novel NADPH/NADP ⁺ -responsive NAPstar sensors.....	47
2.3.1	In vitro characterization of NAPstar probes.....	49
2.3.2	NAPstar sensors are functional in <i>S. cerevisiae</i>	50
2.3.3	NAPstar sensors show minor pH dependency	50
2.3.4	NAPstar sensors have improved fluorescence intensities.....	53
2.3.5	NAPstar sensors respond to NADPH in semipermeabilized cells	54
2.4	Multiparameter imaging during acute oxidative stress	56
2.4.1	Effect of exogenous H ₂ O ₂ on cytosolic NAD(P) redox states	56
	NADPH is robustly maintained during H ₂ O ₂ challenge.....	58
	NADH/NAD ⁺ ratio is transiently reduced by exogenous H ₂ O ₂	60
2.4.2	Effect of exogenous diamide on cytosolic NAD(P) redox states.....	61
	Diamide-induced NADP oxidation resembles cytosolic acidification	63
	NADH/NAD ⁺ ratio is transiently reduced by exogenous diamide.....	65
2.4.3	Effect of exogenous TBHP on cytosolic NAD(P) redox states.....	66
	NADPH is robustly maintained during TBHP challenge	67
	NADH/NAD ⁺ is not affected by exogenous TBHP	69
2.5	Role of the PPP in NADPH production during acute oxidative stress.....	70
2.6	Influence of GSH- and Trx-based antioxidant systems on cytosolic NAD(P) redox homeostasis during oxidative stress	73
2.6.1	<i>GLR1</i> deletion abolishes any detectable H ₂ O ₂ - and diamide-induced NADPH oxidation.....	73
2.6.2	<i>TRX1 TRX2</i> double deletion renders NADP and NAD pools more robust towards H ₂ O ₂ and diamide.....	76

2.6.3	<i>TSA1 TSA2</i> double deletion increases the robustness of cytosolic NAD(P) redox states towards diamide, but not H ₂ O ₂	77
2.7	Expanded NAPstar toolbox covers a range of different NAD(P) binding properties	78
2.7.1	Responses of novel NAPstar sensors to NADPH resemble that of NAPstar3 in semipermeabilized WT cells	79
	The ‘mixed’ NAPstar approach	79
	Rational mutagenesis of the iNap1 T-Rex domain	82
	Alternative NADPH-binding T-Rex variants	83
2.7.2	Novel NAPstar sensors show minor pH dependency	84
2.7.3	Novel NAPstar sensors possess the desired NADPH/NADP ⁺ binding properties	85
2.8	NAD and NADP redox states during the YMC	88
2.8.1	Plasmid-expressed HyPer7 confirms H ₂ O ₂ oscillations	88
2.8.2	NADH/NAD ⁺ cycles periodically during the YMC	90
2.8.3	NADPH/NADP ⁺ oscillations during the YMC could not be clearly detected	91
3	Discussion	95
3.1	T-Rex-based sensor design	95
3.1.1	Comparison of Pdx-mC (DS) and SoNar probes (NADH/NAD ⁺)	96
3.1.2	Comparison of NAPstar (NADPH/NADP ⁺) and iNap probes (NADPH)	97
	Optimization of iNap3	100
3.1.3	Interim conclusion and outlook for future sensor development	100
3.2	NAD(P) transhydrogenase-like activity of semipermeabilized cells	101
3.3	Redox mechanisms during acute oxidative stress	104
3.3.1	Relevance of GSH and Trx systems in NAD(P) oxidation	105
3.3.2	Regulation of NAD metabolism during acute oxidative stress	107
3.4	NAD(P) during the yeast metabolic cycle	109
3.5	Concluding remarks and outlook	114
4	Material and Methods	115
4.1	Key resources	115
4.2	Molecular biological methods	118
4.2.1	Oligonucleotides	118
4.2.2	Plasmids	120
4.2.3	DNA quantification	122
4.2.4	DNA sequencing	122
4.2.5	Agarose gel electrophoresis	122

4.2.6	Restriction and ligation	122
4.2.7	Polymerase chain reaction.....	122
	DNA modification for subcloning	123
	Site-directed mutagenesis.....	123
	Resistance cassette amplification.....	123
	Confirmation PCR	124
4.3	Bacteriological methods	125
4.3.1	Bacteria handling.....	125
4.3.2	Preparation of chemically competent <i>E. coli</i> cells	125
4.3.3	Heat-shock transformation.....	125
4.3.4	Plasmid DNA isolation	125
4.4	Yeast methods	126
4.4.1	Yeast strains.....	126
4.4.2	Yeast culture handling	126
	Yeast peptone dextrose medium and antibiotics	126
	Hartwell's complete medium.....	127
4.4.3	Gene deletion via homologous recombination	128
4.4.4	One-step transformation of plasmids	128
4.5	Multiwell plate reader-based fluorescence spectroscopy	128
4.5.1	NAD(P)H titration and pH dependency experiments	130
4.5.2	roGFP2 measurements	130
4.5.3	Induction of Peredox-mCherry DS expression	130
4.5.4	Calculations.....	131
	Calculation of OxD value (roGFP2 sensors).....	131
	Calculation of 420/480 nm (SypHer, SoNar, iNap) and 399/470 nm ratios (pHluorin)	131
	Calculation of (norm.) cpTS/mC (Pdx, NAPstar) and 420 nm/mSI ratios (mSI-iNap, -SoNar)	131
	Calculation of sensor occupancy.....	132
4.6	YMC in continuous culture.....	132
4.6.1	YMC establishment in the bioreactor	132
4.6.2	Online fluorimetry during chemostat cultivation.....	133
5	References	135
Appendix	153
	List of supplementary figures	153
	List of supplementary tables	153
	Supplementary figures.....	154

Supplementary tables	165
Gene sequences.....	167
SoNar and iNap sequences	167
Pdx-mC and NAPstar sequences	169
Acknowledgement	181

Summary

The essential and ubiquitous NADH/NAD⁺ and NADPH/NADP⁺ redox couples are central for cellular metabolism. NADPH is also the ultimate source of reductive power for the thiol-based antioxidant systems. Our current picture of NAD(P) redox metabolism is incomplete, in part due to the limitations of former measurement methods. The development of genetically encoded fluorescent sensors now permits the specific monitoring of changes in the NADH/NAD⁺ ratio and in NADPH concentration in living cells in defined subcellular compartments.

Here, the pH-resistant NADH/NAD⁺ probe, Peredox, was used as a scaffold to develop novel NADPH/NADP⁺ ratio sensors. By rational mutagenesis of the NAD binding site, a series of NADPH/NADP⁺ sensors with a broad spectrum of NADPH binding affinities was generated, termed NAPstar probes. The characterization of these sensors in *Saccharomyces cerevisiae* cells demonstrated their specificity for NADPH/NADP⁺ changes, pH resistance, and high brightness relative to other genetically encoded NADH/NAD⁺ and NADPH probes.

The application of the NAPstar sensors in yeast demonstrated an extreme robustness of the cytosolic NADPH pool against oxidative perturbation. Furthermore, NADPH/NADP⁺ monitoring to assess the relative electron fluxes through the thioredoxin and glutathione/glutaredoxin pathways revealed a surprising importance for glutathione reductase compared to the thioredoxin system under pro-oxidative conditions.

Zusammenfassung

Die essentiellen, ubiquitären Redoxpaare NADH/NAD⁺ und NADPH/NADP⁺ sind von zentraler Bedeutung für den Zellmetabolismus. NADPH stellt ferner die Reduktionskraft für die Thiol-basierten antioxidativen Systeme bereit. Unser aktuelles Wissen über den NAD(P)-Redoxmetabolismus ist unvollständig, was zum Teil auf Limitierungen früherer Messmethoden zurückzuführen ist. Die Entwicklung von genetisch kodierten Fluoreszenzsensoren ermöglicht nun die gezielte Messung von Veränderungen des NADH/NAD⁺-Verhältnisses und der NADPH-Konzentration in lebenden Zellen in definierten Zellkompartimenten.

Auf Grundlage des pH-resistenten NADH/NAD⁺-Sensors Peredox wurden neue Sensoren für das NADPH/NADP⁺-Verhältnis entwickelt. Durch gezielte Mutagenese der NAD-Bindungsstelle wurde eine Reihe von NADPH/NADP⁺-Sensoren mit unterschiedlichen NADPH-Affinitäten erzeugt, die NAPstar Sensoren. Die Charakterisierung dieser Sensoren in *Saccharomyces cerevisiae* zeigte ihre Spezifität für NADPH/NADP⁺, ihre pH-Beständigkeit und ihr starkes Fluoreszenzsignal im Vergleich zu anderen NADH/NAD⁺- und NADPH-Sonden.

Die Anwendung der NAPstar-Sensoren in Hefe offenbarte eine starke Robustheit des zytosolischen NADPH-Pools gegenüber oxidativen Störungen. Zudem enthüllte das NADPH/NADP⁺-Verhältnis zur Beurteilung der relativen Elektronenflüsse durch das Thioredoxin- und das Glutathion/Glutaredoxinsystem eine überraschende Relevanz der Glutathionreduktase im Vergleich zum Thioredoxinsystem unter prooxidativen Bedingungen.

List of Figures

Figure 1.1: Chemical structures of NAD and NADP metabolites.....	2
Figure 1.2: Simplified model of NAD(P) metabolism and NADPH-dependent antioxidative mechanisms in <i>S. cerevisiae</i>	3
Figure 1.3: Oscillations in dO_2 and oxygen consumption rate during YMC.	12
Figure 1.4: Redox-sensitive roGFP2- and cpYFP-based GFIs.....	15
Figure 1.5: Design and mechanism of T-Rex-based Pdx-mC (DS), SoNar and iNap sensors.	23
Figure 2.1: Characterization of SoNar and iNap in WT cells.	33
Figure 2.2: pH dependencies of SoNar and iNap in semipermeabilized WT cells.	36
Figure 2.3: NADH and NADPH titration to semipermeabilized WT cells expressing (mSI-) SoNar.....	38
Figure 2.4: NADPH titration to semipermeabilized WT cells expressing (mSI-) iNap.	40
Figure 2.5: Characterization of Pdx-mC (DS) in WT cells.	42
Figure 2.6: pH dependencies of Pdx-mC (DS) sensors in semipermeabilized WT cells...	44
Figure 2.7: Maturation of cpTS and mC after induction of Pdx-mC DS expression.	45
Figure 2.8: NADH and NADPH titration to semipermeabilized WT cells expressing Pdx-mC (DS).....	46
Figure 2.9: Design of novel Pdx-mC-based NADPH/NADP ⁺ -specific NAPstar sensors. ..	49
Figure 2.10: Characterization of NAPstar3 and NAPstarC in WT cells.....	51
Figure 2.11: pH dependencies of NAPstar3 and NAPstarC in semipermeabilized WT cells.	52
Figure 2.12: Fluorescence intensities of cpYFP- and cpTS-based NAD(P)-specific GFIs..	54
Figure 2.13: NADPH and NADH titration to semipermeabilized WT cells expressing NAPstar1-4 or NAPstarC.	55
Figure 2.14: Cytosolic mechanisms of NADPH oxidation after exogenous oxidant application to <i>S. cerevisiae</i> cells.	57
Figure 2.15: Influence of exogenous H_2O_2 on cytosolic roGFP2-Tsa2 Δ C _R , roGFP2-Grx1, and pH in WT strain.	58

Figure 2.16: Influence of exogenous H ₂ O ₂ on cytosolic NADP in WT strain.	59
Figure 2.17: Influence of exogenous H ₂ O ₂ on cytosolic NAD in WT strain.....	62
Figure 2.18: Influence of exogenous diamide on cytosolic roGFP2-Tsa2ΔC _R , roGFP2-Grx1, and pH in WT strain.	63
Figure 2.19: Influence of exogenous diamide on cytosolic NADP in WT strain.....	64
Figure 2.20: Influence of exogenous diamide on cytosolic NAD in WT strain.	66
Figure 2.21: Influence of exogenous TBHP on cytosolic roGFP2-Tsa2ΔC _R , roGFP2-Grx1, and pH in WT strain.....	67
Figure 2.22: Influence of exogenous TBHP on cytosolic NADP in WT strain.....	68
Figure 2.23: Influence of exogenous diamide on cytosolic NAD in WT strain.	69
Figure 2.24: Influence of exogenous H ₂ O ₂ , diamide, and TBHP on cytosolic roGFP2-Tsa2ΔC _R , roGFP2-Grx1, NAPstar3, and Pdx-mC DS in Δ <i>zwf1</i> strain.	72
Figure 2.25: Influence of exogenous H ₂ O ₂ on cytosolic roGFP2-Tsa2ΔC _R , roGFP2-Grx1, NAPstar3, and Pdx-mC DS in Δ <i>glr1</i> , Δ <i>trx1Δtrx2</i> , and Δ <i>tsa1Δtsa2</i> strains.....	74
Figure 2.26: Influence of exogenous diamide on cytosolic roGFP2-Tsa2ΔC _R , roGFP2-Grx1, NAPstar3, and Pdx-mC DS in Δ <i>glr1</i> , Δ <i>trx1Δtrx2</i> , and Δ <i>tsa1Δtsa2</i> strains. ..	75
Figure 2.27: Design principle of ‘mixed’ NAPstar sensors.	80
Figure 2.28: NADPH titration to semipermeabilized WT cells expressing novel NAPstar variants.....	81
Figure 2.29: pH dependencies of novel NAPstar variants in semipermeabilized WT cells.	84
Figure 2.30: H ₂ O ₂ treatment of WT cells expressing novel NAPstar variants.....	86
Figure 2.31: Diamide treatment of WT cells expressing novel NAPstar variants.	87
Figure 2.32: Fluorescence ratios of cytosolic HyPer7 and HyPer7 C121S during YMC....	89
Figure 2.33: Fluorescence ratios of cytosolic Pdx-mC (DS) and pHluorin during YMC.....	91
Figure 2.34: Fluorescence ratios of cytosolic NAPstar probes during YMC.....	92
Figure 3.1: Reactions implicated in the reported transhydrogenase-like shunt.	103
Figure 3.2: Overview over the cytosolic GFI-determined parameters during the YMC....	110

List of Tables

Table 1.1: Average whole cell concentrations of NAD(P) metabolites and free cytosolic NAD(P)H/NAD(P) ⁺ ratios reported for prototrophic yeast strains.	20
Table 1.2: Reported in vitro NAD(P) binding affinities of NADH/NAD ⁺ -sensing Pdx-mC (DS) and SoNar sensors.	25
Table 2.1: Mutations and in vitro NADPH binding affinities of NAPstar and iNap variants.	48
Table 2.2: pH-dependent fold change in fluorescence ratio of different NAD(P)-specific GFIs.	53
Table 2.3: Steady state readouts of roGFP2-Tsa2ΔC _R , roGFP2-Grx1, NAPstar3 and Pdx-mC DS expressed in the cytosol of the investigated yeast strains.	71
Table 4.1: Key resources used in this study.	115
Table 4.2: Oligonucleotides used in this study.	118
Table 4.3: Plasmids used in this study.	120
Table 4.4: Ligation reaction program.	123
Table 4.5: PCR program for site-directed mutagenesis.	124
Table 4.6: PCR program for resistance cassette confirmation.	124
Table 4.7: <i>S. cerevisiae</i> strains used in this study.	126
Table 4.8: Composition of HC medium.	127
Table 4.9: Composition of 10X dropout mix.	127
Table 4.10: Plate reader settings for fluorescence measurements.	129
Table 4.11: Fermenter medium for yeast continuous culture.	133
Table 4.12: Spectrophotometer settings for fluorescence measurements during continuous culture.	133

Abbreviations

ATP, ADP, AMP	Adenosine tri-, di-, monophosphate
B-Rex	<i>Bacillus subtilis</i> Rex protein
cp	Circularly permuted
DHA	Dihydroxyacetone
DNA	Deoxyribonucleic acid
δ	Dynamic range
δ'	Maximum sensor response
dO ₂	Dissolved oxygen
DS (index)	Peredox-mCherry DS
E_{GSH}	Glutathione redox potential
ETC	Electron transport chain
FP	Fluorescent protein
G6PDH (yeast Zwf1)	Glucose-6-phosphate dehydrogenase
GAPDH (yeast Tdh3)	Glyceraldehyde-3-phosphate dehydrogenase
GFI	Genetically encoded fluorescent indicator
GFP	Green fluorescent protein
Glr	Glutathione reductase
Grx	Glutaredoxin
GSH	Glutathione, reduced form
GSSG	Glutathione disulfide
HOC	High oxygen consumption
iN (index)	iNap
$K_d(')$	(Apparent) Dissociation constant
LOC	Low oxygen consumption
mC	mCherry
mSI	mScarlet-I
NAD	Nicotinamide adenine dinucleotide, reduced and oxidized forms
NAD ⁺	Nicotinamide adenine dinucleotide, oxidized form

Abbreviations

NADH	Nicotinamide adenine dinucleotide, reduced form
NADP	Nicotinamide adenine dinucleotide phosphate, reduced and oxidized forms
NADP ⁺	Nicotinamide adenine dinucleotide phosphate, oxidized form
NADPH	Nicotinamide adenine dinucleotide phosphate, reduced form
NBD	Nucleotide binding domain
norm.	Normalized
Ns (index)	NAPstar
OxD	Degree of oxidation
PCR	Polymerase chain reaction
Pdx	Peredox
Pdx (index)	Peredox-mCherry
PPP	Pentose phosphate pathway
Prx	Peroxiredoxin
RFP	Red fluorescent protein
ro	Redox-sensitive
SoN (index)	SoNar
TBHP	<i>tert</i> -Butyl hydroperoxide
TCA	Tricarboxylic acid cycle
TORC1	Target of rapamycin complex I
T-Rex	<i>Thermus aquaticus</i> Rex protein
Trr	Thioredoxin reductase
Trx	Thioredoxin
TS	T-Sapphire
WT	Wild type
YFP	Yellow fluorescent protein

1 Introduction

1.1 The model organism *Saccharomyces cerevisiae*

For thousands of years, *Saccharomyces cerevisiae* (Brewer's or Baker's yeast) has been employed to manufacture food such as wine or bread (Nielsen, 2019). The unicellular fungus has a diameter of 5 to 10 μm and divides by budding. It was the first eukaryotic organism whose complete genome (5800 protein-encoding genes) was successfully sequenced in 1996 (Goffeau et al., 1996). *S. cerevisiae* achieved growing importance as a model organism, mainly because its genome is easily accessible to genomic manipulations (Westermann and Klecker, 2022). Novel insights obtained by the investigation of various genetically-modified strains are regularly updated in the public *Saccharomyces Genome Database* (SGD, <https://www.yeastgenome.org/>). Meanwhile, *S. cerevisiae* belongs to the best studied and described eukaryotic model organisms and is broadly used in science and biotechnology (Nielsen, 2019; Parapouli et al., 2020; Westermann and Klecker, 2022). Furthermore, yeast and humans show a high degree of conservation regarding important genes (enabling complementation studies), compartmentalization, and central cellular processes such as protein folding, translocation, secretion, or signal transduction pathways (Nielsen, 2019). Compared to the handling of mammalian cell material or animals, the cultivation of budding yeast is faster, less complex, and cheaper. Those and many more characteristics render *S. cerevisiae* suitable for medicinal research to study pathophysiological phenotypes and potential therapies (Botstein and Fink, 2011). Omic approaches allow a deep insight into the yeast physiology. But still, the acquirement of metabolic data remains difficult due to fast turnover rates, reaction compartmentation and chemical diversity of metabolites (Nielsen, 2019; Villas-Bôas et al., 2005). Critical metabolites include the coenzymes of central cellular energy and redox metabolism, such as adenosine triphosphate (ATP), nicotinamide adenine dinucleotide (NAD) and NAD phosphate (NADP).

1.2 NAD and NADP coenzymes

NAD and NADP are essential cellular redox coenzymes and either present in their oxidized (NAD^+ and NADP^+) or reduced states (NADH and NADPH) (**Figure 1.1**) (Bakker et al., 2001). As the NADP biosynthesis is based on the NAD^+ precursor, NAD and NADP partly share common synthetic pathways. The NAD and NADP coenzymes are involved in

a variety of redox reactions. Despite their structural similarity, NAD and NADP fulfill very different functions within the cell.

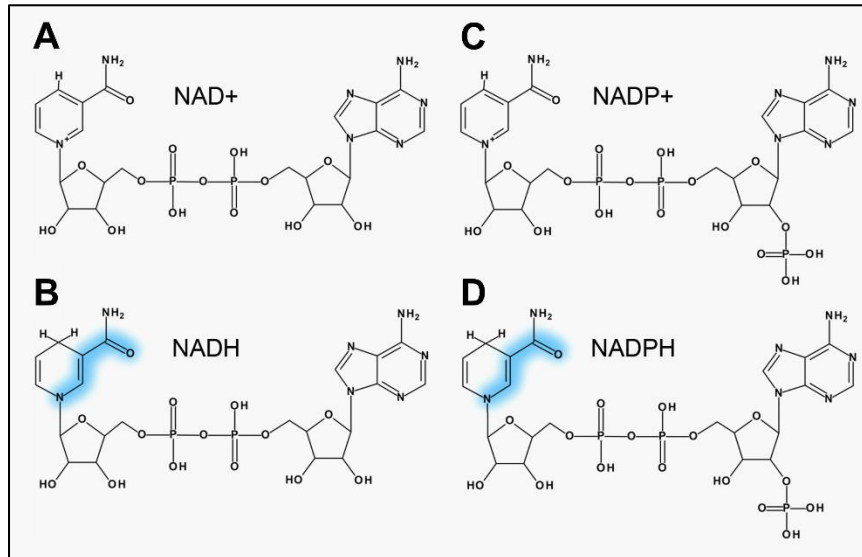


Figure 1.1: Chemical structures of NAD and NADP metabolites.

NAD⁺ (A) differs from NADP⁺ (C) in a phosphate group at the second carbon of the AMP moiety. Hydride ion transfer to the NAM ring generates the reduced forms NADH (B) and NADPH (D) (adapted from Blacker and Duchen, 2016). Light absorption shifts the electron density to the amide group (blue) causing the autofluorescence of the reduced metabolites.

1.2.1 NAD⁺ biosynthesis

The synthesis of NAD⁺ is highly regulated by various factors and feed-back loops on different levels such as on the transcriptional or the enzyme activity level (Croft et al., 2020). *S. cerevisiae* continuously secretes and takes up small NAD⁺ precursors to flexibly adapt the rate of NAD⁺ production to its cellular requirements (Croft et al., 2020). In humans and yeasts, the NAD⁺ synthesis proceeds in the cytosol via three different pathways: (i) the de novo synthesis from tryptophan, (ii) the nicotinic acid (NA, niacin)/ nicotinamide (NAM) salvage or (iii) the nicotinamide riboside (NR) salvage pathways (**Figure 1.2**) (Croft et al., 2020; Kato and Lin, 2014; Koju et al., 2022). The de novo synthesis involves six enzymatic steps (catalyzed by Bna1, Bna2, and Bna4-7) and one non-enzymatic step to produce nicotinic acid mononucleotide (NaMN) (Croft et al., 2020; Kato and Lin, 2014). As some of these reaction steps require oxygen, anoxic grown cultures depend on the salvage pathways to generate NAD⁺. At the level of the NaMN intermediate, the de novo and the salvage pathways converge.

activity and the 5'-capping of RNA (**Figure 1.2**) (Imai et al., 2000; Walters et al., 2017). The produced NAM is hydrolyzed by Pnc1 to NA (Ghislain et al., 2002). The phosphoribose group of phosphoribosyl pyrophosphate (PRPP) is subsequently transferred to NA by Npt1, producing NaMN (Croft et al., 2020). NaMN receives an adenosine monophosphate (AMP) group from ATP via the Nma1- and Nma2-catalyzed reaction forming deamido-NAD⁺ (NaAD) (Kato and Lin, 2014). Subsequent NaAD amidation by Qns1 finally results in the generation of NAD⁺ (Bieganowski et al., 2003).

During the NR salvage pathway, NR is phosphorylated by Nrk1 to nicotinamide mononucleotide (NMN) (Bieganowski and Brenner, 2004; Croft et al., 2020). Afterwards, the AMP moiety of ATP is transferred to NMN by Nma1, Nma2 and Pof1, generating NAD⁺ (Emanuelli et al., 1999, 2003; Kato and Lin, 2014). In contrast to the other NAD⁺ synthesis pathways, the NR salvage is more flexible due to the differential compartmentalization of precursors and enzymes (Croft et al., 2020). Especially the vacuole plays an important role in the storage of intermediates, in particular NR and NMN (Lu and Lin, 2011). Alternatively, NR can be metabolized to NAM feeding the NA/NAM salvage pathway (Croft et al., 2020; Kato and Lin, 2014).

The cytosolic and mitochondrial pyridine nucleotide pools are separated as the molecules cannot freely cross the mitochondrial inner membrane (von Jagow and Klingenberg, 1970). Since NAD⁺ is synthesized in the cytosol, it must be imported into the mitochondrial matrix. In *S. cerevisiae*, this transport is mediated by Yia6 (Ndt1) and Yea6 (Ndt2) (**Figure 1.2**) (Todisco et al., 2006).

1.2.2 NAD-dependent redox reactions in central carbon metabolism

As NAD predominantly serves as an electron acceptor in catabolic reactions, the cytosolic NADH/NAD⁺ redox ratio is kept low to allow a high dissimilatory rate (Bakker et al., 2001). During glycolysis, the glucose dissimilation to pyruvate is coupled to the reduction of NAD⁺ via the glyceraldehyde-3-phosphate dehydrogenase (GAPDH, *S. cerevisiae* Tdh1-3) (**Figure 1.2**). The peroxisomal fatty acid beta-oxidation is another source of cytosolic NADH (Croft et al., 2020). Cytosolic NADH then feeds electrons into the electron transport chain (ETC) that localizes to the mitochondrial inner membrane (respiration). *S. cerevisiae* harbor two external NADH dehydrogenases (Nde1, Nde2) that accept the electrons from cytosolic NADH feeding them directly into the ETC by reducing ubiquinone to ubiquinol (Luttik et al., 1998). Alternatively, NADH can be shuttled into the mitochondrial matrix (**Section 1.2.5**) where it is oxidized by the internal NADH dehydrogenase (Ndi1) (Li et al., 2006).

To ensure the sufficient regeneration of cytosolic NAD^+ at low oxygen availability or at high glucose concentrations, *S. cerevisiae* utilizes the decarboxylation of pyruvate to produce acetaldehyde, which is subsequently reduced to ethanol in an NADH-dependent manner (Ald1/4/5) (ethanol or alcoholic fermentation, **Figure 1.2**) (Bakker et al., 2001). Although the ATP yield of alcoholic fermentation is lower than that of respiration, it proceeds in the presence of oxygen and sugars, partly due to the repression of respiratory genes (Crabtree effect). Cytosolic pyruvate is alternatively transported via the mitochondrial pyruvate carrier into the mitochondrial matrix where it gets further oxidized to acetyl-CoA or oxaloacetate and fed into the tricarboxylic acid (TCA) cycle (**Figure 1.2**) (Murray et al., 2011). The produced reduction equivalents finally fuel the ETC for ATP production.

1.2.3 NADP biosynthesis

In the *S. cerevisiae* cytosol, NADP^+ is primarily synthesized from NAD^+ by the ATP-dependent Utr1 and Yef1 kinases with Utr1 representing the major isoform (**Figure 1.2**) (Kawai et al., 2001; Shi et al., 2005). In contrast, the mitochondrial Pos5 kinase phosphorylates both NADH and NAD^+ to produce NADPH and NADP^+ , respectively (Miyagi et al., 2009; Strand et al., 2003). Since the only source of NADP^+ in *S. cerevisiae* is the ATP-dependent phosphorylation of NAD by one of these kinases, the triple deletion mutant $\Delta utr1\Delta yef1\Delta pos5$ is inviable (Miyagi et al., 2009) but also the $\Delta utr1\Delta pos5$ double deletion was reported to be lethal (Bieganowski et al., 2006). Under physiological conditions, Yef1 is present at low abundance (Ghaemmaghami et al., 2003) and the $\Delta yef1$ deletion mutant does not show hampered growth, even in double knockout strains in combination with *UTR1* or *POS5* (Bieganowski et al., 2006). Thus, Yef1 is thought to contribute only moderately to the cytosolic NADP^+ production. It was suggested that relocalization of Pos5 to the cytosol compensates for NAD kinase activity in the $\Delta utr1$ and $\Delta utr1\Delta yef1$ strains (Bieganowski et al., 2006). How NADP is transported to or produced in the mitochondrial matrix of a $\Delta pos5$ deletion strain remains elusive.

1.2.4 NADP-dependent redox reactions

Anabolic reactions, such as the biosynthesis of amino acids, lipids and nucleotides, but also some antioxidant defense mechanisms (**Section 1.3**) rely on NADPH as an electron donor (Murray et al., 2011). The generated NADP^+ must be reduced quickly to keep the NADPH/ NADP^+ ratio high to provide the optimal conditions for biomass accumulation and to counter oxidative stress. Under fermentative conditions, in the presence of glucose, the pentose phosphate pathway (PPP) is almost solely responsible for the cytosolic NADPH

production (**Figure 1.2**) (Celton et al., 2012; Frick and Wittmann, 2005). During the oxidative PPP, two irreversible enzymatic reactions are responsible for the reduction of NADP⁺. The first and rate-limiting step is catalyzed by the glucose-6-phosphate dehydrogenase (G6PDH, *S. cerevisiae* Zwf1) (Nogae and Johnston, 1990) and the second, NADPH-producing step is catalyzed by Gnd1 (and Gnd2) (Sinha and Maitra, 1992). The carbon flux through the PPP seems to be dictated by the need for NADPH, but not for carbon precursor molecules. Hence, a mechanism has evolved inactivating the GAPDH (Tdh3) during oxidative challenge rerouting the flux from the glycolysis to the PPP to upregulate the NADPH production (Peralta et al., 2015; Ralser et al., 2007). The shift from oxidative to fermentative growth leads to the carbon flux redirection from the PPP to the glycolysis which decreases the NADPH supply from ~100% to 60% of total NADPH (Frick and Wittmann, 2005).

Besides the PPP, the acetaldehyde dehydrogenase Ald6 was demonstrated to be an important source of cytosolic NADPH during growth on glucose (Grabowska and Chelstowska, 2003), whereas the cytosolic NADP-specific isocitrate dehydrogenase Idp2 seems to be relevant during non-fermentable growth (Minard and McAlister-Henn, 2005) (**Figure 1.2**). Cytosolic Ald6, Ald2 and Ald3 as well as mitochondrial Ald4 and Ald5 are involved in the pyruvate dehydrogenase (PDH) bypass with the NADP⁺-dependent Ald6 and Ald5 representing the major isoforms (Saint-Prix et al., 2004). The PDH bypass via Ald6 is the sole source of cytosolic acetyl-CoA required for fatty acid synthesis (Pronk et al., 1996). The mitochondrial PDH bypass contributes to the mitochondrial reduction of NADP⁺ via the activity of Ald4 and Ald5. Thus, it represents next to the Pos5 kinase another source of mitochondrial NADPH (Miyagi et al., 2009). Further, the NADP⁺-dependent Idp1 and the malic enzyme Mae1 also potentially contribute to the mitochondrial NADPH production when the flux through the TCA cycle is high.

NADPH is important for the major antioxidant defense systems (**Section 1.3**). Hence, several enzymes involved in NADPH production are upregulated during oxidative stress and the phenotypes of the respective gene deletion strains are similar to those observed for redox mutants. For instance, *ZWF1* is constitutively expressed and upregulated in a H₂O₂- and Yap1-dependent manner (Lee et al., 1999; Minard and McAlister-Henn, 2005). The deletion of *ZWF1* decreases the whole cell NADPH concentration and leads to methionine auxotrophy (Hector et al., 2009; Masselot and De Robichon-Szulmajster, 1975; Yoshikawa et al., 2021). Moreover, the $\Delta zwf1$ mutant is more robust to low concentrations of H₂O₂ but more sensitive towards high doses of H₂O₂ and diamide (Larochelle et al., 2006; Ng et al., 2008; Nogae and Johnston, 1990; Yoshikawa et

al., 2021). A recent study demonstrated the constitutive activation of Yap1 in a $\Delta zwf1$ strain, compensating for the limited antioxidative capacity by increased cytosolic catalase T (Ctt1) activity, which would explain the enhanced fitness in the presence of low H_2O_2 concentrations (Yoshikawa et al., 2021). Additional deletion of the glutathione reductase *GLR1* in a $\Delta zwf1$ background did not further affect the strain sensitivity against oxidative stress, suggesting that the Glr1 activity relies on the NADPH produced by Zwf1 (Izawa et al., 1998; Yoshikawa et al., 2021). Likewise, the NAD⁺-dependent Ald enzymes have been reported to be inactivated during enhanced oxidative challenge to increase the NADPH production by the NADP⁺-dependent Ald isoforms (Y. Zhang et al., 2020).

1.2.5 NAD(P)H shuttles

Different shuttle systems exist that enable for the indirect exchange of NADH or NADPH between the cytosol and the mitochondrial matrix via distinct enzyme-coupled reactions. For instance, the ethanol-acetaldehyde shuttle transfers NADH reduction equivalents in *S. cerevisiae* (Bakker et al., 2001; von Jagow and Klingenberg, 1970). Both, ethanol and acetaldehyde are freely diffusible via the mitochondrial membranes and can be interconverted by alcohol dehydrogenases (Adhs) located in both compartments. In total, seven Adhs were reported for *S. cerevisiae*, but only NADH-dependent Adh1-3 are important for ethanol metabolism, with minor contribution of Adh4 and Adh5 (de Smidt et al., 2012). These Adh enzymes show different affinities i.e., Adh1, Adh3, and Adh4 prefer the reduction of acetaldehyde to ethanol during glucose fermentation whereas Adh2 rather oxidizes ethanol to acetaldehyde (Bakker et al., 2001; Murray et al., 2011). In this way, cytosolic Adh1, Adh2 and mitochondrial Adh3 enable for the balancing of the NAD homeostasis between the cytosol and the mitochondrial matrix (Bakker et al., 2000). An expansion of the ethanol-acetaldehyde shuttle has been proposed to balance the NADPH/NADP⁺ ratio between the cytosol and the mitochondrial matrix via Ald enzymes (Murray et al., 2011).

Mostly, the shuttle system reactants are not freely diffusible and require transport proteins to cross the inner mitochondrial membrane (Ferramosca and Zara, 2021). The malate-oxaloacetate shuttle is based on two malate dehydrogenases, the mitochondrial Mdh1 and the cytosolic Mdh2 (Bakker et al., 2001). In the first step, oxaloacetate is NADH-dependently reduced to malate by Mdh2 (Minard and McAlister-Henn, 1991). Malate is then imported into the mitochondrial matrix by the dicarboxylate carrier Dic1 (Kakhniashvili et al., 1997), where it is oxidized to oxaloacetate by Mdh1 producing NADH (Thompson et al., 1988). Oxaloacetate is finally shuttled to the cytosol by Oac1 closing the circuit (Palmieri et

al., 1999). The malate-aspartate shuttle can be regarded as an extension to the malate-oxaloacetate shuttle with an additional NADH-dependent deamination step from aspartate to oxaloacetate (aspartate aminotransferase Aat2) and the reverse reaction occurring in mitochondrial matrix (Aat1) (Murray et al., 2011). The resulting aspartate is shuttled via the aspartate-glutamate carrier (Agc1) (Cavero et al., 2003).

The shuttling of NADH into the mitochondrial matrix to fuel the ETC can be bypassed in *S. cerevisiae*. For instance, cytosolic NADH can be directly oxidized by the external NADH dehydrogenases Nde1 and Nde2 producing reduced ubiquinol (**Section 1.2.2**). But also, the glycerol-3-phosphate shuttle transfers electrons from the cytosolic NADH pool into the ETC (Bakker et al., 2001; Murray et al., 2011). This shuttle is composed of the cytosolic, NAD-dependent glycerol-3-phosphate dehydrogenases Gpd1 and Gpd2 that catalyze the reduction of dihydroxyacetone-phosphate to glycerol-3-phosphate. Gut2, localized at the inner mitochondrial membrane, is responsible for the oxidation of glycerol-3-phosphate to dihydroxyacetone-phosphate, thereby reducing ubiquinone.

The citrate-oxoglutarate shuttle was reported to shuttle NADPH reduction equivalents via antiport (Yhm2) of oxoglutarate into and citrate out of the mitochondrial matrix (Castegna et al., 2010; Ferramosca and Zara, 2021). In the cytosol, citrate is converted to isocitrate (Aco1) and oxidized by Idp2 in an NADP⁺-dependent manner to oxaloacetate, producing NADPH. On the mitochondrial site, oxoglutarate is converted to isocitrate by Idp1. The citrate-isocitrate interconversion is mediated by Aco1 (Castegna et al., 2010).

1.3 Antioxidant defense systems

Free radicals are highly reactive species with one or more unpaired valence electrons. The extra electron usually derives from the leakage of an electron carrier system, such as the respiratory chain (Murray et al., 2011). Free radicals react readily with other species, thereby transmitting an electron. For instance, the superoxide anion (O₂^{•-}) and H₂O₂ arise from the reduction of oxygen and belong to the so-called reactive oxygen species (ROS). In *S. cerevisiae*, the ETC is considered the main ROS production site under respiratory conditions (**Figure 1.2**) (Ayer et al., 2014). Other physiological processes like the peroxisomal fatty acid beta-oxidation or oxidative protein folding in the endoplasmic reticulum (ER) additionally contribute to the cellular H₂O₂ generation (Hashimoto and Hayashi, 1990; Zito, 2015). Different enzymatic antioxidant defense mechanisms protect the cell from ROS-induced damage (Toledano et al., 2003). Superoxide dismutase (Sod) enzymes catalyze the disproportionation of superoxide to H₂O₂ via a transition-metal center.

S. cerevisiae has two Sods, cytosolic Sod1 and mitochondrial Sod2 (Culotta et al., 2006). Besides Sods, yeast harbor two catalases catalyzing the dismutation of H₂O₂ to water and O₂, peroxisomal Cta1 and cytosolic Ctt1 (Herrero et al., 2008). Besides Sods and catalases, two thiol-based redox systems have important roles in ROS detoxification: (i) the glutathione- (GSH-, reduced form) and (ii) the thioredoxin- (Trx-) based systems. These systems rely on thiol-disulfide exchange reactions and on NADPH as the final electron donor.

1.3.1 The GSH-based system

GSH is a tripeptide (gamma-glutamyl-cysteinyl-glycine) which is synthesized in the cytosol in two ATP-consuming steps (Oestreicher and Morgan, 2019). GSH is the most abundant low-molecular weight thiol in eukaryotic cells. The cytosolic GSH pool is highly reduced and often regarded as the major redox buffer system in eukaryotic cells (Herrero et al., 2008; Morgan et al., 2013). Hence, the ratio of GSH to glutathione disulfide (GSSG, oxidized form) or the respective redox potential (E_{GSH}) are often considered to reflect the overall redox status of the cell. GSH is readily oxidized upon xenobiotic conjugation (X-SG), protein refolding, or oxidative challenge (**Figure 1.2**). The formation of GSH-mixed disulfides (protein-S-SG, S-glutathionylation) is reversible and their reduction leads to GSSG formation. Oxidized GSSG is reduced by the NADPH-dependent glutathione reductase (Glr1), producing NADP⁺ and two molecules of GSH (Collinson and Dawes, 1995; Deponte, 2013; Outten and Culotta, 2004). Due to alternative start-codons, Glr1 is localized in both, the cytosol, and the mitochondrial matrix (Outten and Culotta, 2004). Alternative pathways were reported to play important roles in maintaining a reduced GSSG/2GSH ratio in the yeast cytosol such as the export of accumulated GSSG into the vacuole via Ycf1 or the action of cytosolic Grx2- and Trx2-dependent pathways (Morgan et al., 2013). S-glutathionylation protects proteins from detrimental thiol group hyperoxidation and is known to regulate protein activity as a post-translational modification (Netto et al., 2007). For instance, the GAPDH (*S. cerevisiae* Tdh3) catalytic cysteine is specifically oxidized by H₂O₂ and subsequently glutathionylated leading to its inactivation (Grant et al., 1999; Peralta et al., 2015).

Thiol peroxidases specifically detoxify peroxides and are thereby reversibly oxidized (Herrero et al., 2008; Netto et al., 2007). Depending on the electron donor employed for the reduction, thiol peroxidases can be divided in two groups: GSH peroxidases (Gpxs) and thioredoxin peroxidases (or peroxiredoxins, Prxs). The thiol group (-SH, sulfhydryl group) of their active site cysteine is highly sensitive to oxidation by specific oxidants, generating

a sulphenic acid (-SOH). Thiol peroxidase hyperoxidation to a sulphinic acid (-SO₂H; slowly reversible) or to a sulphonic acid (-SO₃H, irreversible) leads to enzyme inactivation (Herrero et al., 2008; Winterbourn, 2013). Yeast harbor three different Gpxs, Gpx1, Gpx2 and Gpx3 (also known as Hyr1 or Orp1), which reduce phospholipid hydroperoxides and soluble peroxide species (**Figure 1.2**). Interestingly, despite their Gpx structure, they functionally behave more like Prxs. Additionally, Orp1 fulfills an important function as a hydroperoxide sensor activating the Yap1 transcription factor during oxidative challenge (Delaunay et al., 2002). Yap1, in turn, upregulates the transcription of genes involved in the antioxidant defense. These include *CTT1*, *CCP1* (mitochondrial cytochrome C peroxidase), *SOD1*, *SOD2* and members of the Trx- and GSH-based defense systems (*TRR1*, *GLR1*, *TRX2*, *TSA1*, *TSA2*, *AHP1*, *GSH1*) as well as *ZWF1* to enhance the production of NADPH (Lee et al., 1999).

Glutaredoxin (Grx) and thioredoxin (Trx) family members are oxidoreductases, accepting electrons from either GSH (Grxs) or the NADPH-dependent thioredoxin reductase (Trxs) (**Figure 1.2**) (Grant, 2001; Herrero et al., 2008; Muller, 1996; Toledano et al., 2003). Cytosolic Grxs and Trxs have overlapping functions as the quadruple deletion *TRX1 TRX2 GRX1 GRX2* is lethal and the expression of only one of these genes restores the cell viability (Draculic et al., 2000; Zimmermann et al., 2020). Grxs are involved in the reduction of GSH-mixed disulfides and protein disulfides producing GSSG (Collinson and Grant, 2003). The Grx family is versatile. *S. cerevisiae* has three dithiol Grxs located in the cytosol, Grx1, Grx2, and Grx8, with Grx2 being also present in the mitochondrial matrix (Herrero et al., 2008; Luikenhuis et al., 1998). In vitro studies revealed Grx1 and Grx2 possessing Gpx and glutathione-S-transferase activity whereas Grx8 was far less active (Eckers et al., 2009). Moreover, *S. cerevisiae* harbor five monothiol Grxs in various compartments (Herrero et al., 2008). Monothiol Grxs tend to be inactive in vitro and to fulfill other functions such as iron trafficking or iron-sulfur cluster biogenesis.

1.3.2 The Trx-based system

S. cerevisiae possesses five different Prxs: cytosolic Tsa1, Tsa2, and Ahp1, nuclear Dot5, and mitochondrial Prx1 (**Figure 1.2**) (Herrero et al., 2008). Particularly Tsa1 and Tsa2 seem to play important roles in the defense against oxidative and nitrosative stresses acting in concert with each other and with other antioxidative mechanisms, including the GSH-based system. Tsa1 demonstrates the highest abundance of all *S. cerevisiae* Prxs (Herrero et al., 2008; Netto et al., 2007; Park et al., 2000). In contrast, the basal expression levels of Tsa2 are low but highly upregulated upon hydroperoxide-induced oxidative challenge

(Herrero et al., 2008; Munhoz and Netto, 2004; Park et al., 2000). In addition to their peroxidase function, Tsa1 and Tsa2 can act as chaperones (Jang et al., 2004; Troussicot et al., 2021). Prxs have further important regulatory and signaling functions. For instance, the mitochondrial Prx1 has been shown to regulate H₂O₂-induced cell death (Calabrese et al., 2019) and Tsa1 seems to play a crucial role in light sensing, ageing, and the regulation of metabolic pathways (Bodvard et al., 2017; Irokawa et al., 2016; Kritsiligkou et al., 2021a; Roger et al., 2020). Hence, ROS species are not only regarded as harmful compounds, but also as important signaling molecules linked to the regulation of numerous physiological processes and to the development of several diseases (Finkel, 2011; Netto et al., 2007; Winterbourn, 2008).

S. cerevisiae has separate cytosolic- and matrix-localized Trx systems, composed of Trx and the NADPH-dependent Trx reductase (Trr) (Gan, 1991; Pedrajas et al., 1999). The cytosolic system consists of Trx1, Trx2, and Trr1, whereas Trx3 and Trr2 are enzymes of the mitochondrial system. During oxidative challenge, Trxs maintain reduced Prx pools (Le Moan et al., 2006). Especially Trx2 is important for the detoxification of exogenously added hydroperoxides, most probably due to its role in Tsa1 reduction (Ocón-Garrido and Grant, 2002). Moreover, Trx reduction is important for the enzymatic activities of 3'-phosphoadenosine-5'-phosphosulfate (PAPS) reductase for sulfur assimilation and of ribonucleotide reductase (RNR) during deoxynucleotide (dNTP) synthesis (Toledano et al., 2003). Altogether, the NADPH-dependent Trx- and GSH-based antioxidant systems form a complex redox interaction network having cooperative but also distinct functions.

1.4 The yeast metabolic cycle

Sustained biological oscillations, highly diverse in their period, have been described for all kingdoms of life (Lloyd, 2019; Tu and McKnight, 2006). For instance, circadian rhythms that underly transcription/ translation feedback loops (TTFLs) are well investigated but also other clock systems exist (Milev et al., 2018). Biological oscillations can be observed on different levels, such as cellular, organismal or the population level. On the single-cell level, the rhythmic metabolic behavior is thought to optimize metabolite fluxes by temporal compartmentalization (Tu and McKnight, 2006). In this way, different reactions and processes are separated from each other in time to minimize unwanted side reactions.

Various interlinked ultradian (period shorter than 24 h) metabolic oscillations have been described for *S. cerevisiae* such as the yeast metabolic cycle (YMC, or yeast respiratory oscillation, YRO). The YMC shows periods of about four hours and is connected to, but different from, the cell division cycle (Amponsah et al., 2021; O'Neill, 2021).

Spontaneous YMC synchronization takes place at a high population density under nutrient-limited, aerobic conditions, at constant pH, and low dilution rate (Lloyd, 2019; Satroutdinov et al., 1992). Practically, the YMC is induced in a bioreactor where a yeast cell culture has been aerobically grown to stationary phase and starved for several hours for cell synchronization (**Figure 1.3A**). The subsequent supplementation of fresh medium under continuous culturing conditions results in periodic changes in the oxygen consumption rate (**Figure 1.3B**). The oxygen consumption rate is commonly monitored via the dissolved oxygen concentration (dO_2) inside the culture medium. The YMC is marked by phases of low oxygen consumption (LOC) and high oxygen consumption (HOC). Similar to circadian clock systems, many transcripts and metabolites, including NADP, NADH, and H_2O_2 , were demonstrated to oscillate during YMC (Amponsah et al., 2021; Murray et al., 2007; Tu et al., 2007). Moreover, several signaling processes occur in synchrony with the YMC, such as the Prx oxidation level potentially coupling the YMC to the cell division cycle (Amponsah et al., 2021). In mammalian cells, the SIRT complex (Sir complex in *S. cerevisiae*) or the NAD^+ salvage pathway activities were reported to be connected to the circadian clock, generating oscillations in NAD^+ levels (Milev et al., 2018).

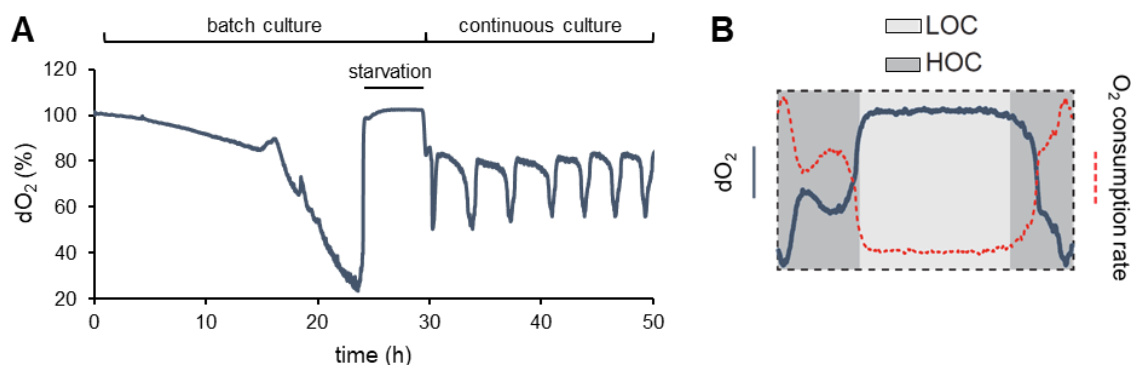


Figure 1.3: Oscillations in dO_2 and oxygen consumption rate during YMC.

The YMC is established by the inoculation of a yeast strain into the bioreactor ($t = 0$ h) (**A**, adapted from Amponsah et al., 2021; Tu et al., 2005). When the cells were grown to the stationary phase, they enter a starvation phase marked by a high $\sim 100\%$ dO_2 ($t = 23$ h). After 5 to 6 h of starvation, fresh medium is supplemented under continuous culture conditions that induce the YMC. The oxygen consumption rate (red) mirrors dO_2 (**B**, adapted from Amponsah et al., 2021). The YMC is characterized by phases of high (HOC) and low oxygen consumption rate (LOC).

Recently, a model has been proposed in which cellular processes during the YMC are linked to the 'energy status' of the cell via the pH-dependent activation of the target of rapamycin complex 1 (TORC1) and the sequestration of macromolecular proteins into biomolecular condensates (O'Neill et al., 2020). TORC1 is a master regulator that regulates

the switch between anabolic phases of enhanced protein synthesis and catabolic phases of high protein turnover and autophagy (Dilova et al., 2007; O'Neill et al., 2020). In this way, the TORC1 activity is thought to restrict the processes of protein synthesis to a distinct phase during the YMC due to their high energy demand. The mechanistic details of the model described in the following, including the respective references, is provided by O'Neill et al., 2020 (Fig. 5 and Table S1). The LOC is regarded as 'default sequester and store state'. Low cytosolic pH keeps TORC1 inactive and promotes the accumulation of macromolecules, including glycolytic enzymes, into biomolecular condensates. During this phase, the ATP is produced by the respiration of autophagic products and acetate, sufficiently driving the proton export activity via the plasma membrane H⁺-ATPase Pma1. The carbon fluxes are directed in favor of lipid, nucleotide, and polysaccharide biosynthesis. When carbohydrate storages are filled, the overwhelming ATP and glucose further stimulate Pma1 activity, increasing the cytosolic pH. The elevated pH mediates the entrance into HOC by liberating proteins from the biomolecular condensates. This accelerates the glycolytic rate and additionally increases the pH due to increased ATP availability. The elevated cytosolic pH activates TORC1, stimulating protein synthesis. Thereby, stored amino acids and carbohydrates fuel the enhanced biosynthetic activity. The end of HOC is initiated by TORC1 inactivation which is caused by the acidification of the cytosol (ATP depletion) and/or by the exhaustion of other storages.

1.5 Genetically encoded fluorescent indicators

The field of genetically encoded fluorescent indicators (GFIs) is rapidly evolving and indispensable for biological research. A vast variety of GFIs were developed to monitor numerous metabolites or physiological parameters like voltage, ions, second messengers, ATP, glucose, kinase activities, or ROS (Bilan and Belousov, 2017; Kostyuk et al., 2019; Liu et al., 2019; Zhang et al., 2018; Z. Zhang et al., 2020). GFIs can be heterologously expressed with minimal to none interference with the host metabolism enabling for real-time quantifications in living cells. They can be additionally equipped with a targeting sequence allowing for specific compartmental investigations of e.g., the mitochondrial matrix, the nucleus, or the endoplasmic reticulum lumen (Calabrese et al., 2019; Hoseki et al., 2016; Hung et al., 2011; Lim et al., 2020). When purified, GFIs can also be used for in vitro studies e.g., together with enzymes or even organelles (Steinbeck et al., 2020). The fluorescence readout is recorded by commonly available spectrofluorometric techniques, rendering GFIs suitable for broad applications and high-throughput methods (Zhao et al., 2015). In this way, metabolite changes can be specifically followed in vivo with high spatiotemporal resolution,

making even single-cell measurements possible (Dodd and Kralj, 2017; Hung et al., 2017; Karagiannis and Young, 2001). All these characteristics make GFIs very powerful tools. Although a variety of GFIs was hitherto successfully applied in various biological backgrounds, they keep a high development potential. For instance, the substrate affinity can be altered by targeted mutagenesis or the color can be tuned by the exchange of the fluorophore (Cameron et al., 2016; Steinbeck et al., 2020; Tao et al., 2017; Z. Zhang et al., 2020).

In general, most GFIs are composed of a sensory domain specifically interacting with the ligand (or substrate) of interest thereby inducing a change in the spectral properties of the fluorescent reporter domain (Kostyuk et al., 2019). This mechanism can be realized in many ways. For reporter domain construction, either a Förster resonance energy transfer (FRET) pair or a fluorescent protein (FP) with modulable fluorescence spectrum is most commonly employed (Kostyuk et al., 2019). The latter group includes redox-sensitive (ro) and circularly permuted (cp) FPs which are frequently utilized to report changes in either the sensor's oxidation state (roFPs) or conformation (cpFPs). On the one hand, roFPs are generated by the introduction of two cysteine residues located on the FP beta barrel structure surface close to the chromophore, neighboring each other (**Figure 1.4A**). Cysteine oxidation leads then to disulfide formation inducing structural alterations and a shift in fluorescence spectra (**Figure 1.4B**) (Müller-Schüssele et al., 2021). On the other hand, cpFPs are designed by the linkage of the original FP N- and C-termini via a short peptide sequence, forming the new termini near the chromophore (**Figure 1.4C**). The overall beta barrel structure is not disturbed by the circular permutation but the new N- and C-termini destabilize the hydrogen bond network around the chromophore enabling for inducible changes in fluorescence properties (**Figure 1.4D**) (Kostyuk et al., 2019; Meyer and Dick, 2010).

Depending on the sensor domain design, the GFI readout is either intensimetric or ratiometric (Bilan and Belousov, 2017). An intensimetric GFI possesses a FP with single excitation and emission maxima such as cpT-Sapphire (cpTS). The overall fluorescence intensity of an intensimetric reporter depends on the ligand binding state of the sensory domain. To discriminate further between the fluorescence changes mediated by the binding state from those deriving from altered sensor expression levels, a second, constantly fluorescent protein of another color e.g., mCherry (mC), can be fused to the sensor construct to allow for signal normalization. In contrast, ratiometric FPs, such as the circularly permuted yellow fluorescent protein (cpYFP) or the redox-sensitive green fluorescent

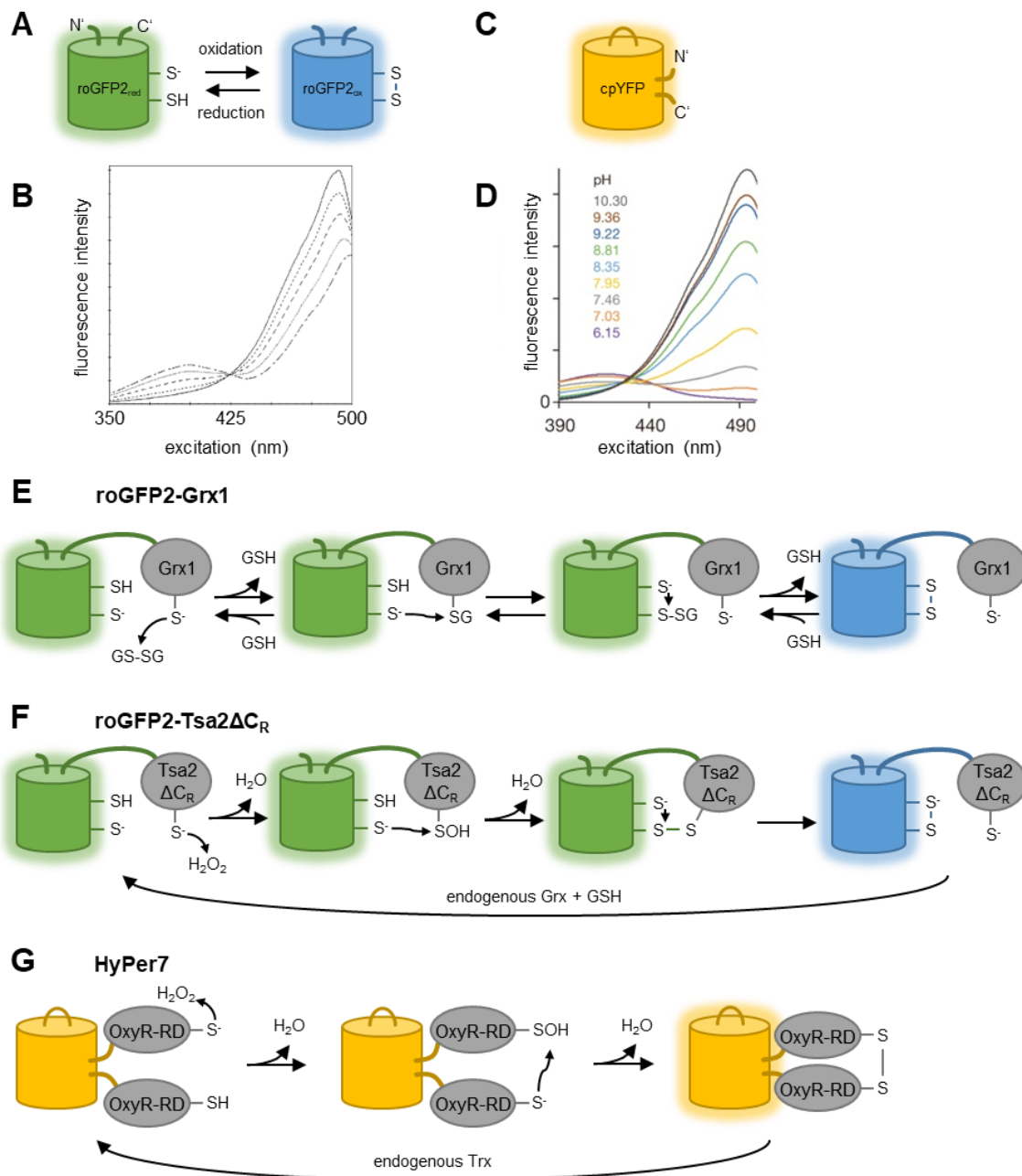


Figure 1.4: Redox-sensitive roGFP2- and cpYFP-based GFIs.

roGFP2 was designed by the introduction of, inter alia, S147C and Q204C mutations (marked as -SH and -S⁻) of EGFP (A). Excitation spectra of roGFP2 at 511 nm (B, adapted from Hanson et al., 2004). cpYFP was generated by the linkage of the original cpYFP N- and C-termini forming the novel termini close to the chromophore (C) (Nagai et al., 2001). Excitation spectra of cpYFP in dependency of pH (D, adapted from Schwarzländer et al., 2014). The fusion to Grx1 enables the fast equilibration of roGFP2 with E_{GSH} (E, adapted from Zimmermann and Morgan, 2022). The second active site cysteine of Grx1 is not displayed since it is not involved in the reaction mechanism. Reaction mechanisms of the ultrasensitive H₂O₂ sensor roGFP2-Tsa2 Δ C_R (F, adapted from Zimmermann and Morgan, 2022). The H₂O₂-sensitive HyPer7 probe was designed by cpYFP integration into the OxyR regulatory domain (OxyR-RD) (G, adapted from Pak et al., 2020).

protein 2 (roGFP2), often possess dual-wavelength excitation spectra and one emission maximum (**Figure 1.4B,D**) (Kostyuk et al., 2019; Müller-Schüssele et al., 2021). The ratiometric characteristics are inherited by the GFP ancestor which also harbors two excitation maxima at 400 and 480 nm, also referred to as A- and B-band, as well as one excitation maximum at 510 nm (Meyer and Dick, 2010). These two bands represent the two chromophore ionization states, the A-band corresponds to the protonated and the B-band to the de-protonated form. Since a GFP molecule can be only present in one of the two states, the fluorescence intensities measured at both excitation maxima behave inversely to each other i.e., the fluorescence intensity excited at the first maximum is rising, while the intensity excited at the second maximum is dropping, and vice versa. For ratiometric GFIs, the calculation of the intrinsic ratio of both fluorescence intensities enables the determination of the parameter of interest, irrespective of the sensor concentration, rendering a second fluorescent protein for a normalization dispensable.

Another critical GFI determinant is the dynamic range δ that describes the maximal possible change in fluorescence readout (Meyer and Dick, 2010). It is mainly determined by the complex interplay of sensory and reporter domains.

1.5.1 Redox-sensitive GFIs

A variety of redox-sensitive GFIs has been developed so far (Ezeriņa et al., 2014; Kostyuk et al., 2019; Meyer and Dick, 2010; Müller-Schüssele et al., 2021; Pang et al., 2021; Schwarzländer et al., 2016; Zimmermann and Morgan, 2022). They differ from other GFIs by the direct involvement in redox relay cascades, thereby being themselves oxidized or reduced. It must be noted that redox-sensitive GFIs rather report the redox equilibrium than the actual electron flux through the respective redox relay. Two different, frequently used redox-sensitive GFI families will be introduced in more detail: roGFP2-based and HyPer family probes.

roGFP2-Grx1 (GSSG/2GSH)

Inspired by the redox-sensitive YFP (rxYFP), roGFP2 was developed by the introduction of two cysteine mutations into the EGFP beta barrel structure (**Figure 1.4A**) (Dooley et al., 2004; Hanson et al., 2004). roGFP2 has a minor excitation peak at 400 nm and a major excitation maximum at 480 nm (**Figure 1.4B**). The oxidation of roGFP2 increases the fluorescence intensity excited at the A-band while reducing the B-band signal. The reduction of roGFP2 is catalyzed by the GSH-based system, whereas Trxs are not able to reduce oxidized roGFP2, most likely due to steric hindrance (Gutscher et al., 2008; Meyer

and Dick, 2010). The ratiometric readout of roGFP2 allows to calculate the degree of oxidation (OxD value, between 0 and 1) using a concomitant sensor calibration technique (Meyer and Dick, 2010). This procedure enables for the reliable comparability between different experiments. By tethering roGFP2 as a reporter domain via a flexible linker to Prx, Gpx or Grx as sensor moiety, it is possible to equilibrate the roGFP2 oxidation with the redox pair of interest or to monitor the redox activity of the sensory domain (Gutscher et al., 2008; Liedgens et al., 2020; Morgan et al., 2016; Zimmermann et al., 2020; Zimmermann and Morgan, 2022). In this way, the Grx1-roGFP2 sensor was developed as a fusion product of human Grx1 and roGFP2 enabling roGFP2 to equilibrate specifically with the GSSG/2GSH (or 2GSH/GSSG) ratio (**Figure 1.4E**) (Gutscher et al., 2008; Meyer and Dick, 2010). The resulting roGFP2 OxD value of the Grx1 sensor can then be utilized for E_{GSH} determination.

roGFP2-Tsa2 Δ C_R (H₂O₂)

For the development of a sensitive H₂O₂-specific GFI, *S. cerevisiae* thiol peroxidases were fused to a roGFP2 reporter and screened for H₂O₂-induced oxidation in vivo (Morgan et al., 2016). Orp1, Tsa1, and Tsa2 fusions sensitively oxidized roGFP2 in vitro. As roGFP2-Tsa2 was barely more sensitive as the established roGFP2-Orp1, the resolving Tsa2 cysteine was mutated to alanine, abolishing the reduction by endogenous Trxs. The resulting ultrasensitive roGFP2-Tsa2 Δ C_R sensor (**Figure 1.4F**) is oxidized by H₂O₂, *tert*-butyl hydroperoxide (TBHP) and hypochlorite in vitro. Its fluorescence readout is robust to pH changes in a broad range between pH 6.0 and pH 8.5 (Morgan et al., 2016). The reduction of the roGFP2-Tsa2 Δ C_R sensor has been shown to be mediated by the GSH- but not the Trx-based reductive system in vivo.

HyPer7 (H₂O₂)

HyPer was generated as a H₂O₂-specific sensor by the insertion of cpYFP into a surface loop of the *E. coli* OxyR regulatory domain (**Figure 1.4G**) (Belousov et al., 2006). The HyPer OxyR regulatory domain is specifically oxidized by H₂O₂ subsequently forming an intramolecular disulfide bond, thereby altering the fluorescence spectra of cpYFP. Hyper2 and HyPer3 were generated by optimization of HyPer to increase the dynamic range and to accelerate the reaction kinetics (Bilan et al., 2013; Markvicheva et al., 2011). Nonetheless, all three probes suffer from strong pH sensitivity deriving from the cpYFP moiety (**Figure 1.4D**) (Schwarzländer et al., 2014). To generate the pH-insensitive HyPer7 probe, the *E. coli* OxyR regulatory domain was exchanged by that of *Neisseria meningitidis*, and several rounds of mutagenesis were performed to optimize brightness, H₂O₂ sensitivity,

and pH robustness (Pak et al., 2020). HyPer7 has a major excitation peak at 490 nm and a second one at 400 nm. The fluorescence emission peaks at 520 nm. Upon oxidation, the fluorescence intensity excited at 490 nm rises whereas that at 400 nm decreases. Reduction leads to the reverse effect. Thus, the calculation of the 490/400 nm ratio enables for the calculation of the probe oxidation state. Interestingly, the calibration of HyPer7 to determine an OxD in *S. cerevisiae* was not possible using dithiothreitol (DTT) as reductant (Kritsiligkou et al., 2021b). The direct comparison of the roGFP2-Tsa2 Δ C_R and HyPer7 probes in yeast revealed HyPer7 being less sensitive to H₂O₂ while having a bigger dynamic range (Kritsiligkou et al., 2021b; Zimmermann et al., in preparation). Most interestingly, the different reduction kinetics clearly demonstrated HyPer7 being predominantly reduced by Trxs whereas roGFP2-Tsa2 Δ C_R is reduced by the GSH-based system (Kritsiligkou et al., 2021b). Hence, the probes were considered complementary providing information about the reductive capacities of the respective system.

1.5.2 pH-sensitive GFIs

The fact that the FP fluorescence properties depend on the chromophore protonation state provides excellent conditions for the design of pH indicators. To this end, FPs with acidic dissociation constants (pK_a values) in the physiological range are highly desired.

SypHer

The cpYFP moiety of the H₂O₂-sensitive HyPer probe was found to be highly pH dependent (see above). The HyPer mutagenesis of either C199S, C207S or both were reported to fully abolish its H₂O₂-induced oxidation (Belousov et al., 2006), generating sensor variants which were responsive to pH changes, but not to H₂O₂. HyPer C199S was renamed SypHer (synthetic pH sensor) and established as pH-sensitive GFI (Poburko et al., 2011). An increase in the pH value leads to a rise in the 490/420 nm ratio of SypHer. The in situ calibration of SypHer demonstrated a large 20-fold dynamic range from pH 7 to pH 10 with a pK_a of ~8.7. Besides SypHer, also the cpYFP itself is frequently used to monitor pH in vivo (Schwarzländer et al., 2014; Wagner et al., 2019; Zhao et al., 2015).

pHluorin

Two pH-sensitive pHluorin probes were generated by the targeted mutagenesis of GFP to visualize pH changes during synaptic transmission (Miesenböck et al., 1998). The ecliptic pHluorin possesses an excitation maximum at 400 nm that vanishes with decreasing

pH values down to pH 6. In contrast, ratiometric pHLuorin demonstrates two excitation maxima at 400 and 480 nm. The first excitation maximum rises and drops with pH. Oppositely, the fluorescence intensity excited at the second maximum rises with decreasing pH values and vice versa. The ratiometric pHLuorin sensor enables for dynamic pH measurements in the range of pH 6 to pH 8 (Miesenböck et al., 1998; Shen et al., 2013).

1.6 Methods to quantify NAD and NADP metabolites

The NADH/NAD⁺ redox ratio is widely accepted as an important parameter for the cellular metabolic state and it has been shown to influence the gene expression via the Sir2-mediated silencing and the 5'-capping of RNA (Bird et al., 2018; Croft et al., 2020). Further, the NADPH/NADP⁺ redox balance is considered as a readout of the cellular reduction capacity required for the accumulation of biomass and for antioxidative defense. Moreover, an altered metabolism of NAD or NADP has been connected to a range of pathophysiological conditions such as dementia, Parkinson, several types of cancer, or diabetes (Covarrubias et al., 2021; Okabe et al., 2019; Xiao et al., 2018). In many respects, the ratios of NADH/NAD⁺ and NADPH/NADP⁺ are important parameters that depend on reliable quantification methods.

1.6.1 Conventional NAD(P) quantification methods

Since the mid-twentieth century, reduced pyridine nucleotides have been quantified by autofluorescence measurements. Chance and co-workers established this parameter as a valuable readout of mitochondria-localized NADH (Chance et al., 1962; Chance and Thorell, 1959). The reduced nicotinamide rings of NAD(P)H absorb light at ~340 nm, leading to an electron density shift from the ring region towards the oxygen atom of the amide group (excited state) (**Figure 1.1**). The relaxation back to the ground state leads to a photon emission resulting in fluorescence emitted at ~460 nm (Blacker and Duchon, 2016). The fluorescence spectra of NADH and NADPH are indistinguishable and thus, often referred to as NAD(P)H autofluorescence. As the quantum yield of the autofluorescence is low, high intensities of ultraviolet light are needed resulting in the photodamage of the sample. An advanced method of autofluorescence spectrometry promises to overcome these disadvantages: Fluorescence lifetime imaging (FLIM) enables for the absolute quantification of and for the discrimination between protein-bound NADH and NADPH (Blacker et al., 2014). Nonetheless, FLIM requires expensive special optical equipment, suffers from a low throughput rate as well as from complex data evaluation. Moreover, only

the protein-bound pools are can be measured and important information about the free coenzyme pools, which are relevant to drive enzymatic reactions, are missing.

Besides fluorescence measurements, lysate-based methods are broadly applied for the specific quantification of NAD(P) metabolites. These include enzymatic recycling assays but also chromatography-, mass spectrometry- or HPLC-based analyses. Unfortunately, the cell lysis mixes the NAD(P) pools of different cell compartments. Additionally, dynamic measurements require a high effort of sample processing. These lysate-based techniques enabled to calculate the average whole cell NAD(P) concentrations for prototrophic yeast strains of ~ 2.8 mM NAD⁺, ~ 0.37 mM NADH, ~ 0.19 mM NADP⁺ and ~ 0.20 mM NADPH, resulting in NADH/NAD⁺ and NADPH/NADP⁺ ratios of 0.133 and 1.05, respectively (**Table 1.1**).

Table 1.1: Average whole cell concentrations of NAD(P) metabolites and free cytosolic NAD(P)H/NAD(P)⁺ ratios reported for prototrophic yeast strains.

Published values were determined for Cen.PK strains expressing bacterial NAD(P)-specific dehydrogenases. ^A cytosolic pH 7.0 to pH 6.5; ^B NAD(P)H and NAD(P)⁺ concentrations were originally reported in mmol/gDW and converted using the factor 2.38 mL_{cell}/gDW (Theobald et al., 1997). DW, dry weight.

Parameter	Cytosolic free	Whole cell total	Reference
NADH/NAD ⁺	0.001 to 0.003 ^A	0.133	Canelas et al., 2008
NADH	—	0.37 mM ^B	
NAD ⁺	—	2.8 mM ^B	
NADPH/NADP ⁺	15.6	1.05	Zhang et al., 2015
NADPH	—	0.20 mM ^B	
NADP ⁺	—	0.19 mM ^B	

NAD(P) coenzyme purification can be circumvent via coupled sensor reactions (Williamson et al., 1967). For instance, the cytosolic pyruvate/lactate ratio readily equilibrates with the NADH/NAD⁺ ratio via the reaction catalyzed by the lactate dehydrogenase in the cytosol of mammalian cells (Bücher et al., 1972; Hung et al., 2011). The quantification of pyruvate and lactate in the extracellular matrix enables then to draw conclusions about the cytosolic NADH/NAD⁺ ratio. Advantageously, this method reports in a compartment-specific manner the redox state of the free NAD(P) pool, what is important regarding the estimation of $\sim 80\%$ of total cellular NAD(P) being protein-bound (Blinova et al., 2005; Murray et al., 2011; Yu and Heikal, 2009). These methods led so far to the most accurate determinations of the NAD and NADP redox states. Notwithstanding, appropriate

enzyme reactions have to meet a number of requirements to allow for precise measurements (Canelas et al., 2008; Zhang et al., 2015). In addition, the kinetic assumptions for in vivo NAD(P)H/NAD(P)⁺ calculation can be inaccurate for certain conditions, like during dynamic changes, altered pH or limited substrate uptake. Moreover, the sampling, extraction, and analysis of the participating reactants and internal standards is laborious. Additionally, the activity of heterologously expressed dehydrogenases potentially influences the host metabolism leading to measurement artifacts. For the prototrophic yeast strains mentioned above, the enzymatic activities of recombinantly expressed NAD- and NADP-specific dehydrogenases enabled to determine the cytosolic free NADH/NAD⁺ and NADPH/NADP⁺ ratios to be ~0.002 and ~15.6, respectively (**Table 1.1**). The strong deviation from the data obtained by cell lysates under the same experimental conditions clearly demonstrate the high discrepancy between whole cell and cytosolic free ratios.

Other approaches like transcriptional fluorescent reporter systems (Huang et al., 2016; Knudsen et al., 2014; Liu et al., 2019; Siedler et al., 2014; Zhang et al., 2016) only report long-term qualitative effects and do not enable for dynamic, quantitative measurements. In contrast, data obtained with GFIs at single-cell resolution indicated highly dynamic and heterogenic behaviors of pH, NAD(P)H and ATP (see below) (Dodd and Kralj, 2017; Papagiannakis et al., 2017). Altogether, the NAD(P) quantification methods discussed in this section suffer from individual limitations. The ideal NAD(P) determination method should be highly specific for the metabolite and the compartment of interest, not interfere with the host metabolism, discriminate free from protein-bound coenzyme, and enable for dynamic, real-time measurements in the living organism. The GFIs introduced in the following section meet these requirements and thus represent a significant progress in the quantification of NAD(P) metabolites.

1.6.2 NAD- and NADP-sensitive GFIs

So far, various approaches were used to develop a variety of NAD(P)-specific GFIs (**Appendix, Table S1**). The majority of these probes has been designed by the combination of a nucleotide-binding sensor domain with a cpFP reporter domain (Bilan and Belousov, 2017; Zhao et al., 2018). Especially the bacterial transcription factor Rex has been proven worthy as sensor domain.

The transcriptional repressor Rex

The bacterial repressor Rex was first discovered in *Streptomyces coelicolor* and is present in most Gram-positive bacteria (**Figure 1.5A**) (Brekasis and Paget, 2003; Ravcheev et al., 2012). Rex acts as homodimer regulating the expression of its target genes in an oxygen-dependent manner via the NADH/NAD⁺ ratio. In the presence of sufficient oxygen amounts, NADH can be efficiently oxidized to NAD⁺ via respiration. The NADH/NAD⁺ ratio is low and Rex in the NAD⁺-bound state (**Figure 1.5B**). It possesses an open conformation and binds to the consensus Rex operator site, repressing target genes (McLaughlin et al., 2010; Sickmier et al., 2005). When the oxygen availability decreases, less NADH is oxidized and the NADH/NAD⁺ ratio rises. The Rex-bound NAD⁺ is replaced by two molecules of NADH, inducing a conformational change to the closed state. Rex dissociates from the operator site, enabling for target gene expression. Target operons are organism-specific and were reported to be implicated in energy and carbohydrate metabolism, fermentation, and NAD(P)H biogenesis pathways (Ravcheev et al., 2012).

Detailed structural and mechanistic information is available on the Rex protein from *Thermus aquaticus* (T-Rex, **Figure 1.5A**) (McLaughlin et al., 2010; Sickmier et al., 2005). Its compact, 'butterfly-like' structure likely arises from the adaptation to high temperatures. The symmetric bilobed homodimeric structure is similar to the Rex structures of other species (Nakamura et al., 2007; Sickmier et al., 2005; Wang et al., 2008). Each T-Rex monomer consists of an N-terminal DNA-binding domain (T-Rex residues 2-76), which is characterized by a winged helix motif, and a C-terminal nucleotide-binding domain (NBD, T-Rex residues 81-187). Although the NBD harbors a Rossmann fold, that is typically found in NAD⁺-depending dehydrogenases, T-Rex lacks dehydrogenase activity (Sickmier et al., 2005). The nucleotide-binding site is located at the dimer interface forming asymmetric interactions with the bound nucleotide(s). Either two molecules of NADH or one molecule of NAD⁺ are bound by T-Rex mediating a closed or open conformation, respectively (McLaughlin et al., 2010; Wang et al., 2011). The conformational change thereby describes a 'caliper-like' movement, where the N- and C-terminal domains act together as relatively stiff bodies performing in total a 40° rotation. This rearrangement is mediated by the C-terminal alpha helix (T-Rex residues 188-203) forming a 'domain-swapping' arm that is buried in the interdomain region of the reciprocal subunit (McLaughlin et al., 2010; Sickmier et al., 2005; Wang et al., 2008). Although the rotation induces a marginal conformation change in the NBD, the distance between the DNA-binding subunits is dramatically altered, thereby tuning DNA-binding.

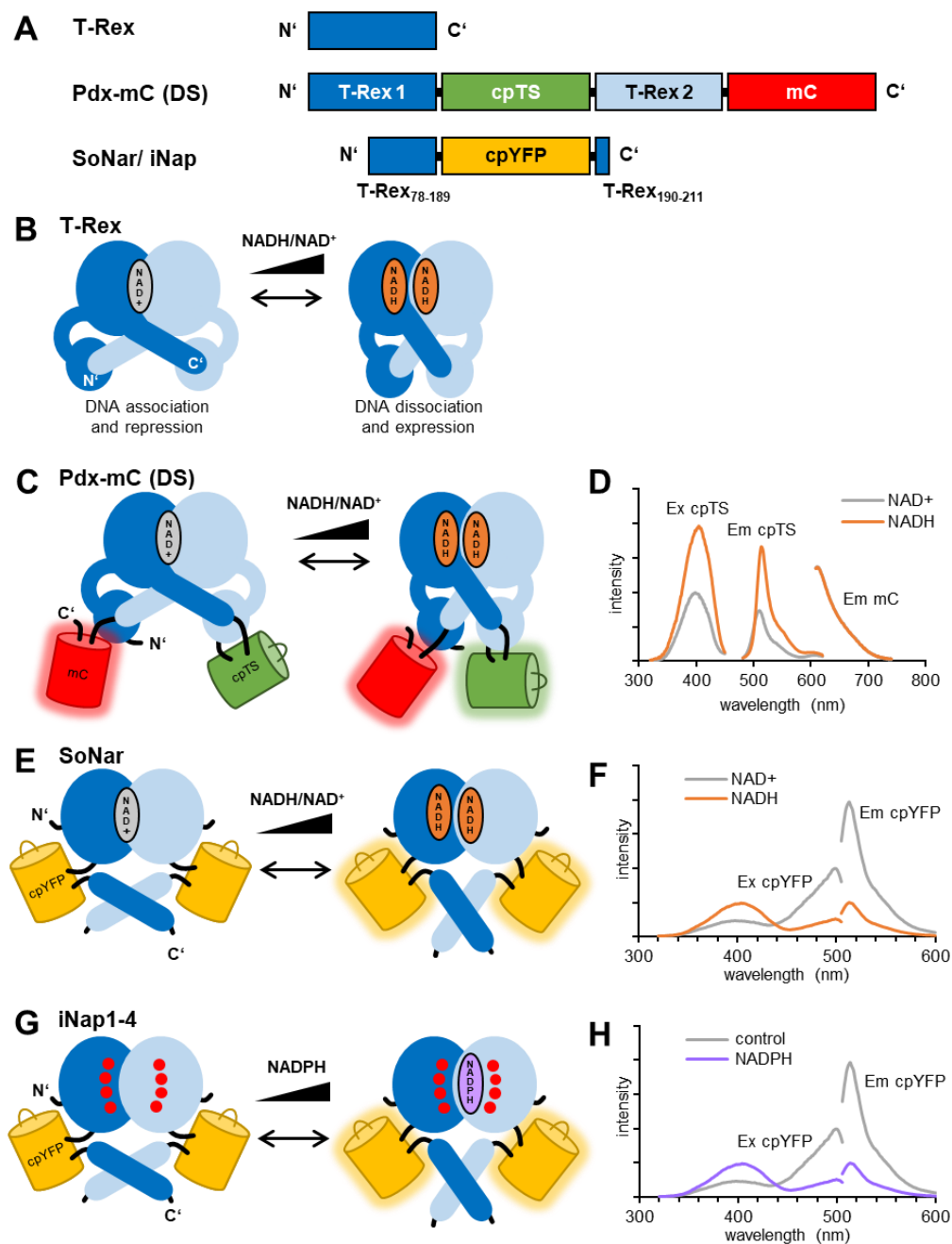


Figure 1.5: Design and mechanism of T-Rex-based Pdx-mC (DS), SoNar and iNap sensors.

The T-Rex protein sequence served as template for Pdx-mC (DS) and SoNar (iNap) design (A, adapted from Zhao et al., 2018). The dimeric T-Rex (blue) acts as a transcriptional repressor in dependency of the NADH/NAD⁺ ratio (B, adapted from McLaughlin et al., 2010). Pdx-mC was designed by cpTS insertion in between two T-Rex sequences and C-terminal attachment of mC (C, adapted from Hung et al., 2011). Fluorescence intensity of cpTS reports NADH/NAD⁺ whereas mCherry fluorescence remains constant (D). SoNar was created by truncation of the T-Rex DNA-binding domain and insertion of cpYFP into a T-Rex surface loop (E, adapted from Zhao et al., 2015). Ratio of fluorescence intensities determined at 420 nm and 480 nm excitation (at 520 nm emission) reflects NADH/NAD⁺ (F). iNap sensors were created by site-directed mutagenesis of the T-Rex NBD of SoNar (G, red dots). Ratio of fluorescence intensities determined at 420 nm and 480 nm excitation (at 520 nm emission) reflects NADPH concentration (H, adapted from Tao et al., 2017). C-F, adapted from Bilan and Belousov, 2017.

T-Rex represents an ideal candidate for NAD(P) GFI design since (i) its conformation depends specifically on NADH/NAD⁺ ratio, (ii) it lacks enzymatic activity, and (iii) detailed structural information is available, providing ideal prerequisites for rational sensor design. Many powerful GFIs were designed based on T-Rex (**Appendix, Table S1**), such as NADH/NAD⁺-specific Peredox-mCherry (Pdx-mC) and SoNar sensors.

The Peredox sensor family (NADH/NAD⁺)

The NADH/NAD⁺ ratio sensor Peredox (Pdx) was constructed by the insertion of a cpTS sequence in between two T-Rex domains (**Figure 1.5A,C**) (Hung et al., 2011). Additionally, mutagenesis was performed to avoid the dimerization of cpTS, the interaction with DNA, NADPH binding, and pH dependency, as well as to accelerate the binding and dissociation kinetics. The fluorescence intensity of cpTS peaks at 400 nm excitation and at 510 nm emission (**Figure 1.5D**). Pdx is an intensimetric sensor demonstrating increasing fluorescence intensity with increasing NADH/NAD⁺ ratios. A constantly fluorescent mC (590 nm excitation, 610 nm emission) was C-terminally linked to Pdx for the normalization of the cpTS signal, resulting in the final Pdx-mC construct. The cpTS/mC ratio of Pdx-mC is specifically reporting the NADH/NAD⁺ ratio, independent of related metabolites like NADPH, NADP⁺, ADP ribose, NAM, NMN, AMP or adenosine (Hung et al., 2011). Moreover, the Pdx-mC readout is independent of pH in the physiological range (Hartmann et al., 2018; Hung et al., 2011; Steinbeck et al., 2020). The dynamic range of Pdx-mC is about 2.2-fold to 3-fold (**Table 1.2**) (Chang et al., 2017; Hartmann et al., 2018; Hung et al., 2011; Steinbeck et al., 2020). As sensor control, a Pdx Y98D mutant, which is unresponsive to NADH, can be used (Hung et al., 2017).

Next to Pdx-mC, a Pdx-mCitrine variant was designed. The exchange of mC by mCitrine enables for the simultaneous measurement of a second, red fluorescent dye or GFI, such as pHRed (Hung and Yellen, 2014). Thus, Pdx-mCitrine expands the 'color palette' of NADH/NAD⁺ probes, facilitating multiple-parameter imaging. Due to partial spectral overlap of cpTS and mCitrine the dynamic range of Pdx-mCitrine is diminished (Hung et al., 2017). In 2020, the Pdx-mC DS variant was described (Steinbeck et al., 2020). Both Pdx-mC T-Rex domains were subjected to D112S mutation, lowering the NADH-binding affinity of the GFI without affecting its pH robustness. The dynamic range in vitro was thereby increased from 2.2 to 2.88 (**Table 1.2**). The NADH binding kinetics were accelerated whereas the replacement of NADH with NAD⁺ was slower compared to the original Pdx-mC construct. Since the cpTS/mC readout of Pdx-mC DS was less influenced by NAD⁺, it was proposed to predominantly report the NADH concentration instead of the NADH/NAD⁺ ratio.

Table 1.2: Reported in vitro NAD(P) binding affinities of NADH/NAD⁺-sensing Pdx-mC (DS) and SoNar sensors.

δ , dynamic range; N.D., not determined; $R' = [\text{NADH}] \times 1000 / [\text{NAD}^+]$; ^A values were calculated from K_R or K_d .

Sensor	δ	K_d NADH [μM]	K_R	K_d NADPH [μM]	Reference
Pdx-mC	2.5	0.0069 \pm 0.0036 (0 μM NAD ⁺)		N.D.	Tejwani et al., 2017
		0.464 \pm 0.064 (80 μM NAD ⁺) ^A	5.8 \pm 0.8	N.D.	
		11.7 \pm 3.6 (3 mM NAD ⁺) ^A	3.8 \pm 1.2	N.D.	
	2.2	1.2 \pm 0.15 (0.5 mM NAD ⁺)	2.4 \pm 0.3 ^A	531 \pm 12 (150 μM NADP ⁺)	Steinbeck et al., 2020
Pdx-mC DS	2.88	31.4 \pm 4.4 (0.5 mM NAD ⁺)	62.8 \pm 8.8 ^A	324 \pm 18 (150 μM NADP ⁺)	
SoNar	15	\sim 0.2 (K_d NAD ⁺ \sim 5 μM)	\sim 36 ^A	150 μM	Lim et al., 2020 Tao et al., 2017 Zhao et al., 2015

As T-Rex binds to NADH and NAD⁺ with different affinities, the description of Pdx sensor binding kinetics is complex, even a contribution of the total AXP concentration was described (Hung et al., 2011). The in vitro characterization of the Pdx ligand binding was performed by different labs in different setups, in dependency on the target organism (Hartmann et al., 2018; Hung et al., 2011; Steinbeck et al., 2020; Tejwani et al., 2017). Either the NAD⁺/NADH or NADH/NAD⁺ ratio at half maximal cpTS/mC readout were estimated as $K_{\text{NAD}^+/\text{NADH}}$ or $K_{\text{NADH}/\text{NAD}^+}$, respectively. Alternatively, a K_R value was determined with $R' = [\text{NADH}] \times 1000 / [\text{NAD}^+]$ ($R = 1/R'$). The standardization of the different kinetic parameters enables for a better comparison of the different results (**Table 1.2**). The K_R of Pdx-mC is \sim 5.8 in the presence of 80 μM NAD⁺ which differs only slightly from the K_R in the presence of 3 mM NAD⁺ (\sim 3.8). Although the total NAD pool is increased about a factor of 38, K_R is changed by a factor of only 1.5 (Tejwani et al., 2017). In the presence of 500 μM NAD⁺, the dissociation constants (K_d values) of Pdx-mC and Pdx-mC DS are 1.2 μM and 31.4 μM NADH, while the NADPH affinities in the presence of 150 μM NADP⁺ are much lower ($K_d = 531$ and 324 μM NADPH). Consequently, the Pdx readout should not be significantly influenced by changes in the total NAD pool size or by NADPH in vivo.

Up to date, the Pdx sensors were successfully applied in various primary cell cultures and cell lines (Hung et al., 2017, 2011; Masia et al., 2018; Sandbichler et al., 2018; Schöndorf et al., 2018), brain tissue (two-photon FLIM) (Díaz-García et al., 2017; Mongeon et al., 2016), plants (Steinbeck et al., 2020; Wagner et al., 2019), fungi (Hartmann et al.,

2018), and bacteria (Bhat et al., 2016a; Ishikawa et al., 2017; Tejwani et al., 2017). So far, the mitochondrial targeting of a Pdx construct has not been reported, whereas nuclear targeting was possible (Hung et al., 2011). Most likely, the big protein size impedes the import into the mitochondrial matrix (Steinbeck et al., 2020).

The SoNar sensor (NADH/NAD⁺)

A second NADH/NAD⁺-sensing GFI, SoNar, was constructed by the insertion of a cpYFP sequence into a surface loop of the T-Rex protein, in between F189 and L190 (**Figure 1.5A,E**) (Zhao et al., 2015). In addition, the N-terminal DNA-binding domain of T-Rex (T-Rex residues 1-77) has been truncated to minimize the sensor size and the interaction with DNA. The readout of SoNar is ratiometric, showing characteristic cpYFP fluorescence spectra with two excitation maxima at 420 nm and 490 nm wavelength as well as a single emission maximum at 515 nm (**Figure 1.5F**). In vitro analyses confirmed that the binding of NAD⁺ increases the fluorescence intensity of SoNar excited at 490 nm without affecting the 420 nm fluorescence. In contrast, NADH-binding to the sensor rises its fluorescence at 420 nm excitation whereas the intensity at 490 nm decreases. As a result, the ratio of SoNar fluorescence intensities when excited at 420 and 490 nm (420/490 nm) describes the NADH/NAD⁺ ratio. As the two excitation maxima behave opposingly, the SoNar ratiometric readout has a big 15-fold dynamic range in vitro and 9-fold in vivo (**Table 1.2**). SoNar is specific for NADH and NAD⁺, without significant influence of NAD analogs such as NADPH, NADP⁺, ATP or ADP. The K_d values for NAD⁺ and NADH are very low (~5.0 μ M NAD⁺ and ~0.2 μ M NADH), making sure that the sensor is occupied in vivo by either of the two pyridine nucleotides. The $K_{NAD^+/NADH}$ of SoNar is ~40 which is corresponding to a K_R value of ~25. Another study confirmed a similar K_R of ~36 (Lim et al., 2020). Although the K_d (NADH) of SoNar is lower, the K_R of SoNar is in between those of Pdx-mC and Pdx-mC DS due to its high NAD⁺ affinity. This feature also partly responsible for the fast binding and dissociation kinetics of SoNar, especially the replacement of NADH by NAD⁺ happens much faster compared to Pdx-mC (Zhao et al., 2015). When expressed in a H1299 cell line, the fluorescence intensity of SoNar, particularly at 490 nm excitation, was much brighter than that of other GFIs (Frex, cpYFP, HyPer, roGFP1, Peredox) (Zhao et al., 2015). Unfortunately, the 490 nm fluorescence is strongly pH-dependent, whereas the fluorescence at 420 nm is less affected (**Section 1.5** and **Figure 1.4D**). Consequently, the resulting 420/490 nm readout is also pH-sensitive (Zhao et al., 2015). To control for significant pH alterations in different experimental setups, a cpYFP-based pH control, such as cpYFP, SypHer or iNapc, should be carried in parallel. This control allows for

normalization of the pH-sensitive SoNar readout to exclude pH artifacts from the final output (see below) (F.-L. Zhao et al., 2016; Zou et al., 2018).

So far, SoNar was applied in a vast variety of primary cell cultures and cell lines, where it could be targeted to the nucleus or transplanted as xenografts into mice (Chugunova et al., 2019; Hao et al., 2019; Hu et al., 2020; Ji et al., 2017; Kim et al., 2019; Oldham et al., 2015; Shokhina et al., 2019; Tao et al., 2017; Titov et al., 2016; Y. Zhao et al., 2016; Zhao et al., 2015). SoNar was also expressed in transgenic mice (Chen et al., 2021; Gu et al., 2020) and plants (Lim et al., 2020). It was successfully localized to plastids, but peroxisomal and mitochondrial targeting failed in planta (Lim et al., 2020). A mitochondria-targeted version was reported in cultured adult rat cardiomyocytes (Hu et al., 2021).

The iNap sensor family (NADPH)

To develop the NADPH-sensitive iNap sensors, the SoNar T-Rex domain was subjected to site-directed mutagenesis (Tao et al., 2017). Structurally important residues for NAD(P) binding were identified by comparison of the T-Rex structure with those of other NAD- and NADP-binding proteins. Moreover, NADPH binding to T-Rex was simulated. Finally, the T-Rex domain of SoNar was modified to accumulate positive residues near the predicted NADPH phosphate group and polar residues were enriched in the adenine binding pocket. Additionally, the flexibility of a loop, which was supposed to sterically clash with the phosphate group, was enhanced. The selected SoNar mutations were performed in different combinations, and the resulting variants were screened for NADPH-binding by fluorescence measurements. The resulting constructs were indeed specific for NADPH with K_d values ranging from $\sim 1.3 \mu\text{M}$ to $\sim 29 \mu\text{M}$ (**Figure 1.5G**) (Tao et al., 2017; Zou et al., 2018). The variants with most favorable characteristics regarding affinity and dynamic range were selected and termed iNap1 to iNap4. The NADPH-specific iNap1, iNap2, iNap3 and iNap4 sensors have K_d values of ~ 2.0 , ~ 6.0 , ~ 25 and $\sim 120 \mu\text{M}$ NADPH (**Appendix, Table S1**). Another study reported lower K_d values for iNap1 and iNap4 of $0.29 \mu\text{M}$ and $30 \mu\text{M}$ NADPH, respectively (Lim et al., 2020). The dynamic range of iNap1 is 9-fold (Tao et al., 2017), but the dynamic ranges alter between the different iNap variants (Lim et al., 2020; Zou et al., 2018). The iNap fluorescence spectra correspond to that of SoNar and cpYFP showing two excitation maxima at 420 nm and 490 nm wavelength, as well as an emission peak around 515 nm (**Figure 1.5H**). Going along with the cpYFP spectral properties, also the iNap fluorescence excited at 490 nm is pH-sensitive.

To enable pH-resistant measurements, mC was N-terminally fused to iNap1 (Tao et al., 2017). The resulting mC-iNap1 construct allowed for normalization of the 420 nm fluorescence to the constant red mC fluorescence. As the apparent K_d of iNap1 when excited at 420 nm does not depend on pH, the 420 nm/mC allows robust NADPH readout. Another approach for the correction of pH artifacts includes iNapc, an iNap control sensor that binds neither NADPH nor NADH and thus, it represents the unbound (apo) state and the open sensor conformation (McLaughlin et al., 2010; Tao et al., 2017). It retains the pH sensitivity of the cpYFP moiety at 490 nm excitation. When measured in parallel, it thus allows for the normalization of the iNap signal, to exclude the pH artifacts from the final sensor readout (**Equation 1.1**) (Zou et al., 2018).

Equation 1.1: Normalization of the iNap1 ratio to the iNapc signal for pH-resistant iNap1 measurements.

$$\text{normalized } \frac{420}{490} (iNap1) = \frac{\frac{420}{490} (iNap1)}{\frac{420}{490} (iNapc)}$$

Altogether, the various NADPH-binding properties of iNap1-4 cover a wide range of different NADPH concentrations and therefore allow for dynamic measurements in different cell types and subcellular compartments. So far, the different iNap variants were applied for cytosolic measurements in different cell cultures (Gregor et al., 2019; Tao et al., 2017), zebrafish (Tao et al., 2017), and plants (Lim et al., 2020). The nuclear targeting of iNap was reported for cell culture experiments (Tao et al., 2017). Successful targeting to plastids and peroxisomes was described for plants, whereas the targeting to the mitochondrial matrix failed (Lim et al., 2020).

1.7 Research objectives

Our current knowledge of subcellular NADH/NAD⁺ and NADPH/NADP⁺ dynamics remains incomplete as traditional measurement methodologies suffer from several limitations. For instance, measurement of pyridine nucleotide autofluorescence does not allow for the discrimination between NADH and NADPH or between protein-bound and free pools. Furthermore, NADP⁺ and NAD⁺ are non-fluorescent species. Cell lysis-based techniques cannot differentiate between different subcellular compartments and the possibilities for making dynamic measurements are very limited. Finally, monitoring via coupled enzymatic reactions or FLIM is technically challenging, laborious, and time-consuming.

The recent development of GFIs for the NADH/NAD⁺ ratio (Hung et al., 2011; Zhao et al., 2015) and the NADPH concentration (Tao et al., 2017) open up the possibility to investigate these redox couples in living cells with high specificity at subcellular resolution and in real-time. However, much scope remains for further probe development and optimization. Therefore, the following major research objectives were defined:

1. *Characterization of available NADH/NAD⁺-specific SoNar and Pdx-mC (DS), as well as NADPH-sensing iNap probes in *S. cerevisiae**

2. *Design and development of novel NADPH/NADP⁺-sensitive GFIs*

A rational mutagenesis strategy sought to be applied to develop novel NADPH/NADP⁺ sensors using the NADH/NAD⁺ probe Peredox as a scaffold. Together with collaborators, extensive in vitro characterization of promising probe candidates will be performed, as well as ultimately broad in vivo characterization in yeast, plant, and human model systems.

3. *Application of novel NADPH/NADP⁺ sensors to gain new insights in subcellular NADPH dynamics.*

Working predominantly in the yeast system, which has the advantage of rapid genetic manipulation, as well as relatively simple and well understood redox pathways, the novel sensors will be employed to gain deeper insights into the regulation of NADPH at the subcellular level.

2 Results

Nicotinamide adenine dinucleotide (NAD; oxidized form NAD^+ , reduced form NADH) and NAD phosphate (NADP; oxidized form NADP^+ , reduced form NADPH) are universal and essential redox cofactors involved in cellular metabolism (Rodrigues et al., 2006). Despite their similar chemical structures, they fulfill very distinct functions inside the cell. The cytosolic NAD pool is very oxidized (low NADH/NAD^+ ratio) with NAD^+ being an important electron acceptor in catabolic pathways (Bakker et al., 2001). In contrast, the NADP pool is very reduced (high $\text{NADPH}/\text{NADP}^+$ ratio). This enables NADPH to serve as electron donor for many anabolic reactions and for antioxidant defense. The NAD and NADP metabolites are highly compartmentalized (Fessel and Oldham, 2018). The current knowledge about NAD(P) is primarily based on measurements of whole cell lysates and on autofluorescence imaging (Blacker and Duchen, 2016). Unfortunately, lysis-based methods cannot differentiate between different subcellular compartments, while autofluorescence measurements induce photodamage to the sample and do not allow for the discrimination between NADH and NADPH. Moreover, these methods cannot distinguish between protein-bound and free coenzyme pools. As a result, the cellular NAD and NADP metabolism is still not understood in detail, although it has been investigated for decades. Recently, genetically encoded, fluorescent indicators (GFIs) for NAD and NADP metabolites were developed. These probes overcome the major drawbacks of traditional NAD(P) quantification methods (Kostyuk et al., 2019) enabling for real-time measurements in living organisms with high specificity and at subcellular resolution. Thus, NAD- and NADP-specific GFIs open the opportunity to gain deeper insights into cellular NAD and NADP metabolism.

2.1 Characterization of SoNar and iNap in *S. cerevisiae*

Various NAD- and NADP-specific GFIs have been developed so far, all with their individual advantages and limitations. The SoNar and iNap sensors sense specifically the NADH/NAD^+ ratio and the NADPH concentration, respectively (Tao et al., 2017; Zhao et al., 2015). Since the iNap sensor design is based on SoNar, both GFIs share a common overall structure. Their sensory domains derive from the nucleotide binding domain (NBD) of the dimeric bacterial T-Rex transcription factor. A circularly permuted (cp) yellow fluorescent protein (YFP) was inserted into a T-Rex surface loop to function as reporter domain. In this way, the calculation of the ratio of fluorescence intensities emitted at 520 nm, when excited

either at 420 nm or at 480 nm (420/480 nm ratio) enables the readout of NADH/NAD⁺ (SoNar) or NADPH (iNap).

The SoNar and iNap probes share advantageous features like ratiometric readout, high fluorescence intensity, and small protein size (385 amino acids per monomer). Additionally, the common cpYFP fluorescence spectra allow for a convenient sensor interchangeability and comparability (Zou et al., 2018). Nonetheless, since the cpYFP fluorescence is strongly pH-sensitive (Schwarzländer et al., 2014), the parallel measurement of a GFI control, iNapc, is recommended for critical experimental setups (Tao et al., 2017; Zhao et al., 2015).

2.1.1 SoNar and iNap are functional in *S. cerevisiae*

Since the SoNar and iNap sensors were reported to have great advantages over other GFIs, SoNar, iNap1, and iNapc were chosen for characterization in *S. cerevisiae*. The cpYFP-based, pH-responsive SypHer probe was employed to monitor pH fluctuations (Poburko et al., 2011). SoNar, iNap1, iNapc, and SypHer were expressed in a BY4742 wild type (WT) strain. The GFI expression was confirmed by the measurement of cpYFP fluorescence spectra of intact, probe expressing cells using a fluorescence plate reader (**Figure 2.1A-D**). All probes showed characteristic cpYFP spectra with a single excitation peak at 420 nm and an emission maximum at 510 nm. A second excitation maximum at 480 nm has been reported for SoNar in its NAD⁺-bound and unbound states (Zhao et al., 2015), as well as for iNap1 in its unbound conformation (Tao et al., 2017). Interestingly, this second excitation maximum was absent in any of excitation spectra of yeast-expressed probes. The excitation spectrum of SypHer also has a second peak at 490 nm at pH values ≥ 7.44 , suggesting the cytosolic pH being below this value (Poburko et al., 2011).

The fluorescence excitation ratio 420/480 nm of SoNar and iNap probes, recorded at 520 nm emission, reflects in a proportional manner either the NADH/NAD⁺ ratio or the NADPH concentration (Tao et al., 2017; Zhao et al., 2015). To verify the reversibility of ligand binding and to determine the maximal changes in the sensor readouts, a calibration method was performed (Tao et al., 2017). To this end, the plasma membrane was semipermeabilized by the application of low digitonin concentrations. Cell semipermeabilization decreased the 420/480 nm ratio of SoNar from ~9 to ~5, and that of iNap1 from ~9 to ~3 (**Figure 2.1E,F**). This implicates a decline in both, NADH/NAD⁺ ratio and NADPH concentration, presumably due to oxidation. The subsequent application of high ligand concentrations (1 mM NADH or NADPH) led to a 420/480 nm ratio increase to values marginally exceeding those observed in intact cells. Both, SoNar and iNap1 were shown to

have very high NADH and NADPH affinities *in vitro* (Tao et al., 2017; Zhao et al., 2015) and are thus expected to be present in their NADH- and NADPH-bound states under these conditions.

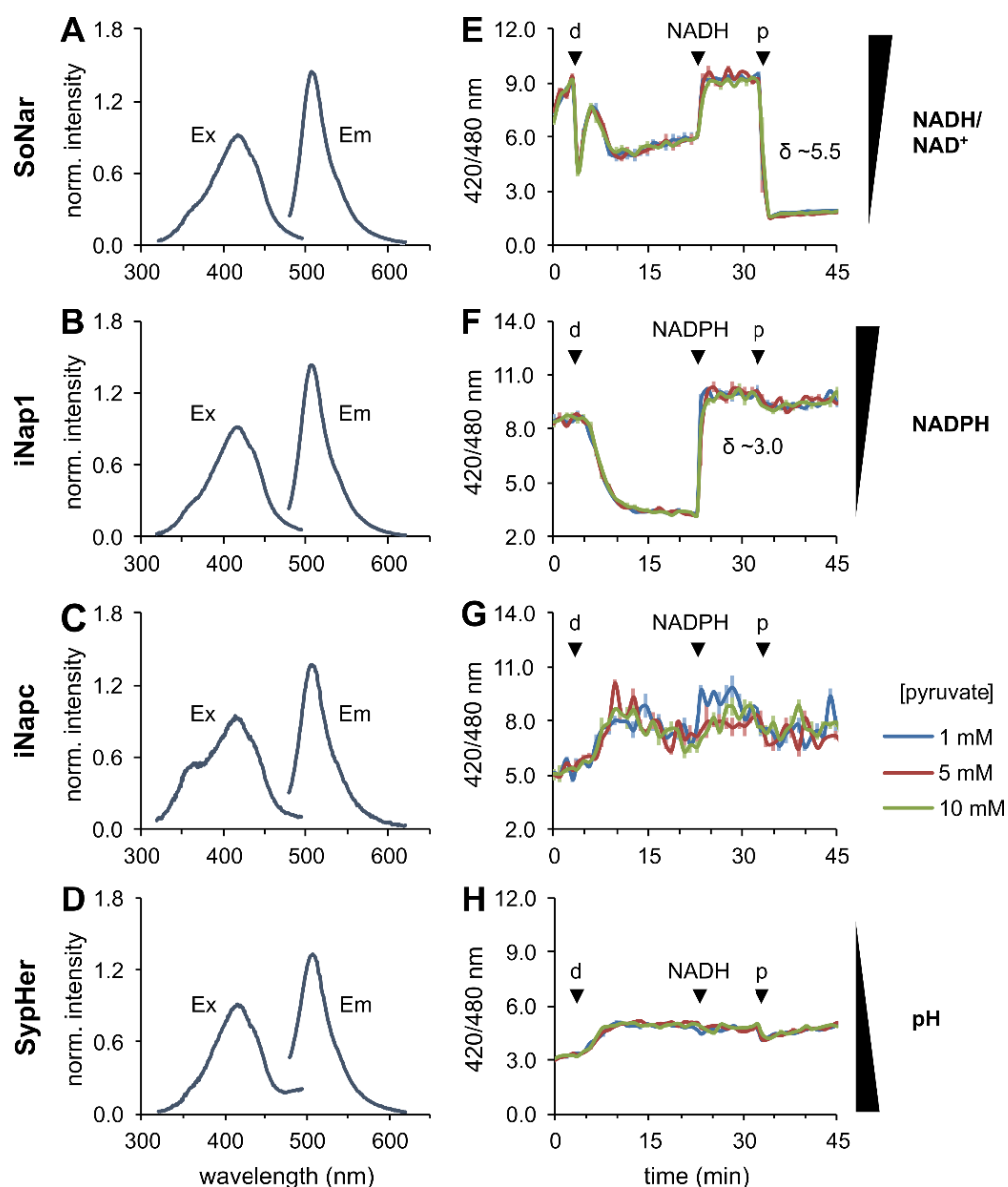


Figure 2.1: Characterization of SoNar and iNap in WT cells.

Excitation (Ex) and emission spectra (Em) of intact WT cells expressing SoNar, iNap1, iNapc, or SypHer (A-D). Intensities were normalized to the emission at 520 nm. SoNar, iNap1, iNapc, or SypHer expressing WT cells were sequentially treated at the indicated time points (\blacktriangledown) with 0.1% (w/v) digitonin (d), 1 mM NADH or NADPH and different concentrations of pyruvate (p) (E-H). Fluorescence was recorded using a plate reader. Dynamic ranges (δ) were calculated by division of average 420/480 nm ratios at ~ 30 min and ~ 35 min (SoNar) or ~ 25 min and ~ 20 min (iNap1). For SypHer calibration curve, refer to **Appendix, Figure S1A**.

To decrease the NADH/NAD⁺ ratio in the next step, pyruvate was added. In the course of alcoholic fermentation, pyruvate is decarboxylated to acetaldehyde (by pyruvate decarboxylase, Pdc) followed by an NADH-dependent reduction to ethanol (by alcohol dehydrogenase, Adh), producing NAD⁺ (Bakker et al., 2001). Indeed, the addition of 1 mM pyruvate decreased the fluorescence ratio of SoNar from ~9 to ~1.5 (**Figure 2.1E**). Higher pyruvate concentrations up to 10 mM did not lead to further ratio decline and the low 420/480 nm ratio remained stable in all the conditions, implying SoNar being present in its NAD⁺-bound state. Oppositely, pyruvate is not expected to influence cellular NADPH levels. Indeed, the fluorescence ratio of iNap1 was barely affected by the different pyruvate concentrations (**Figure 2.1F**). In addition, the fluorescence readout of iNapc and SypHer controls was barely affected (**Figure 2.1G,H**). Hence, the established semipermeabilization-based assay can be employed to investigate the reversible responses of NADH/NAD⁺-specific SoNar and NADPH-sensing iNap probes in a cellular environment.

SoNar and iNap1 dynamic ranges of $\delta_{\text{SoN}} \sim 5.5$ and $\delta_{\text{iN1}} \sim 3.0$ were calculated based on the maximum and minimum fluorescence ratios reached throughout the experiment. These values fall below those reported *in vitro* ($\delta_{\text{SoN}} \sim 15$; $\delta_{\text{iN1}} \sim 9$) and *in vivo* ($\delta_{\text{SoN}} \sim 8$) (Tao et al., 2017; Zhao et al., 2015). Nonetheless, minimum and maximum 420/480 nm ratios enable to calculate the proportion of sensor that is occupied with NAD(P)H at cellular equilibrium, resulting in 81% sensor occupancy with NADH for SoNar and 78% sensor occupancy with NADPH for iNap1.

In contrast to SoNar, iNap1 or SypHer, the time-dependent 420/480 nm ratio of iNapc was marked by strong fluctuations (**Figure 2.1G**), most likely deriving from its low fluorescence intensity (**Section 2.3.4**). On the one hand, these fluctuations hamper the exact monitoring of pH alterations and on the other hand, they impede the normalization of the SoNar and iNap signals to exclude artifacts from their final readouts. Oppositely, the SypHer control conveniently reported the cytosolic pH throughout the experiment. Based on a pH calibration curve (**Appendix, Figure S1A**), the cytosolic pH was determined to be ~7.12, ~6.86, and ~6.95 at cellular steady state, after digitonin, and after pyruvate treatment, respectively.

2.1.2 Fluorescence of SoNar and iNap strongly depends on pH

The reported dynamic ranges of SoNar and iNap1 sensors were not reached in semipermeabilized yeast cells and the reported 480 nm excitation peak (B-band) was not observed, even following semipermeabilization (data not shown). The B-band of cpYFP is extremely pH-sensitive (Meyer and Dick, 2010; Schwarzländer et al., 2014) and shows

strong increase in fluorescence intensity at pH values above 7.0 (Poburko et al., 2011; Schwarzländer et al., 2014). The yeast cytosol is rather acidic (pH 6.5 to 7.4) and its pH is less stable than that of mammalian cells (Dodd and Kralj, 2017; Karagiannis and Young, 2001; Orij et al., 2009). This effect potentially causes the alterations in the SoNar and iNap fluorescence spectra when expressed in the yeast cytosol. Hence, the pH dependencies of cpYFP-based GFIs were further investigated. To this end, GFI expressing WT cells were semipermeabilized in different pH buffers, ranging from pH 6.0 to pH 9.0. Since the fluorescence spectra alter in dependency of the sensors ligand binding state (Tao et al., 2017; Zhao et al., 2015), they were recorded in presence and absence of 2 mM NADH or NADPH. The intensities when separately excited at 420 nm or 480 nm were plotted against the pH. As expected, the 480 nm excitation maxima of all the investigated cpYFP-based GFIs were strongly pH-dependent, dramatically increasing at pH 8 and pH 9, in the absence and presence of additional ligand (**Figure 2.2A-D**). As the cytosolic pH of *S. cerevisiae* is rather acidic, the excitation maximum at 480 nm remains weak in cpYFP-based GFIs expressed in the yeast cytosol. In contrast, the 420 nm fluorescence maximum was more robust towards pH changes, especially for iNap1, iNapc, and SypHer (**Figure 2.2A-C**). In the absence of NADH, the SoNar fluorescence intensity increased at pH values above 7.5 to the fluorescence intensity observed in presence of 2 mM NADH (**Figure 2.2D**), indicating pH-dependent NADH-binding or conformational changes of SoNar.

To determine to what extent the pH sensitivity influences the sensor readout, 420/480 nm ratios were calculated and plotted against the pH. The fold difference in fluorescence ratio between the control condition and the addition of 2 mM NAD(P)H was considered to reflect the dynamic sensor range at this pH and was therefore referred to as the 'apparent' dynamic range. SoNar and iNap1 demonstrated stable fluorescence ratios and apparent dynamic ranges between pH 6.0 and pH 7.0 (**Figure 2.2E,F**). In this range, the 420/480 nm changes of iNapc and SypHer controls were also minor (**Figure 2.2G,H**). Further pH increase led to a strong decline in the 420/480 nm ratio for all the sensors, due to the increase in the fluorescence intensity excited at 480 nm. The apparent dynamic range of SoNar was strongly decreased at pH ≥ 8.0 due to the conformational alterations described above. In contrast, the apparent dynamic range of iNap1 increased at pH 8.0 and pH 9.0 to ~ 5.6 , but was still lower than the reported dynamic range of $\delta_{iN1} \sim 9$ in vitro (Tao et al., 2017). The pH dependencies of iNapc and SypHer controls largely corresponded those of SoNar and iNap1 sensors, confirming that the observed alterations can be largely attributed to the pH dependency of the cpYFP moiety. Altogether, this data indicates that the acidic environment in the yeast cytosol influences the spectral characteristics of cpYFP-based GFIs.

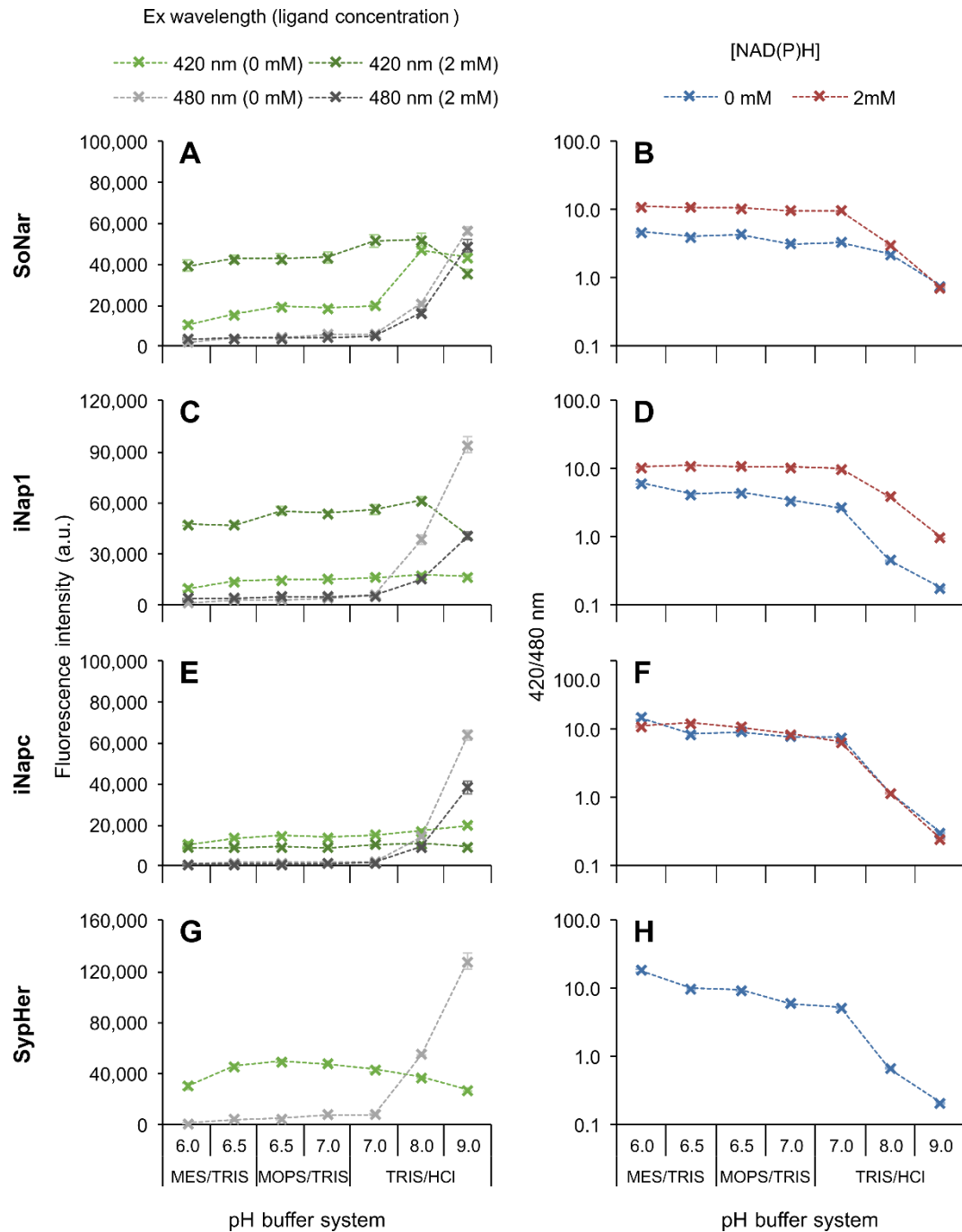


Figure 2.2: pH dependencies of SoNar and iNap in semipermeabilized WT cells.

WT cells expressing SoNar (A,B), iNap1 (C,D), iNapc (E,F), or SypHer (G,H) were semipermeabilized in the indicated buffer solution with 0.1% (w/v) digitonin. Excitation and emission spectra of cpYFP were recorded by a fluorescence plate reader in absence (0 mM) and presence of 2 mM ligand (NADH for SoNar, NADPH for iNap sensors). Fluorescence intensities measured at 420 nm and 480 nm excitation (left) or respective 420/480 nm ratios (right) were plotted against the pH. a.u., arbitrary units; Ex, Excitation.

Construction of mSI-SoNar and mSI-iNap sensors

To design an improved, NADPH-specific GFI with a pH-robust fluorescence readout, mCherry (mC) was N-terminally fused to iNap1, resulting in the mC-iNap1 sensor (Tao et al., 2017). The cpYFP fluorescence of mC-iNap1 excited at 420 nm remains responsive on the NADPH concentration, whereas the mC fluorescence intensity is stable and not affected by NADPH. In this way, the 420 nm excitation channel of cpYFP can be normalized to the constant mC signal, resulting in the 420 nm/mC ratio, which is proportional to the NADPH concentration. In this way, the pH-sensitive cpYFP fluorescence excited at 480 nm is avoided and thus, the intensimetric readout of mC-iNap1 reflects the NADPH concentration independent of pH.

In the slightly acidic environment of the yeast cytosol, the 480 nm fluorescence of SoNar and iNap probes is lost, turning the ratiometric cpYFP readout basically into an intensimetric mode. Intensimetric GFIs require a second FP with constant fluorescence intensity for signal normalization. Hence, inspired by the previously published mC-iNap1 sensor (Tao et al., 2017), red fluorescent protein (RFP) fusions of iNap and SoNar probes were generated. Instead of mC, the fast maturing, bright RFP mScarlet-I (mSI) (Bindels et al., 2017) was N-terminally fused to iNap1-4, iNapc, and SoNar.

2.1.3 SoNar and mSI-SoNar respond to NAD(P)H in semipermeabilized cells

SoNar has been reported to have high affinities for NADH and NAD⁺ with K_d (NADH) \sim 0.2 μ M and K_d (NAD⁺) \sim 5.0 μ M (**Table 1.2**) (Zhao et al., 2015). In contrast, its affinity for NADPH is much lower with K_d (NADPH) \sim 150 μ M (Tao et al., 2017). To verify the reported (mSI-) SoNar specificity, the GFI responses to different concentrations of exogenously added NADH and NADPH were followed in SoNar expressing, semipermeabilized cells. As expected, the supplementation of NADH immediately increased the 420/480 nm ratio in a concentration-dependent manner (**Figure 2.3A**). However, the sensor surprisingly responded to a very similar extent to NADPH (**Figure 2.3B**). The same effect was observed for the mSI-SoNar probe (**Figure 2.3C,D**). The maximum ratio changes (δ') upon NADH treatment were similar for SoNar ($\delta'_{\text{SoN}} \sim$ 2.3) and mSI-SoNar ($\delta'_{\text{mSI-SoN}} \sim$ 2.5), suggesting that mSI-SoNar is an appropriate probe control. To determine the pH alterations during the experiment, the SypHer sensor was employed. Exogenous supplementation of 2 mM NAD(P)H led to a concentration-dependent alkalization from pH \sim 6.88 to pH \sim 6.95 (NADH) and pH \sim 7.05 (NADPH) (**Figure 2.3E,F**). This mild pH change is not expected to influence (mSI-) SoNar or (mSI-) iNap readouts (**Section 2.1.2**).

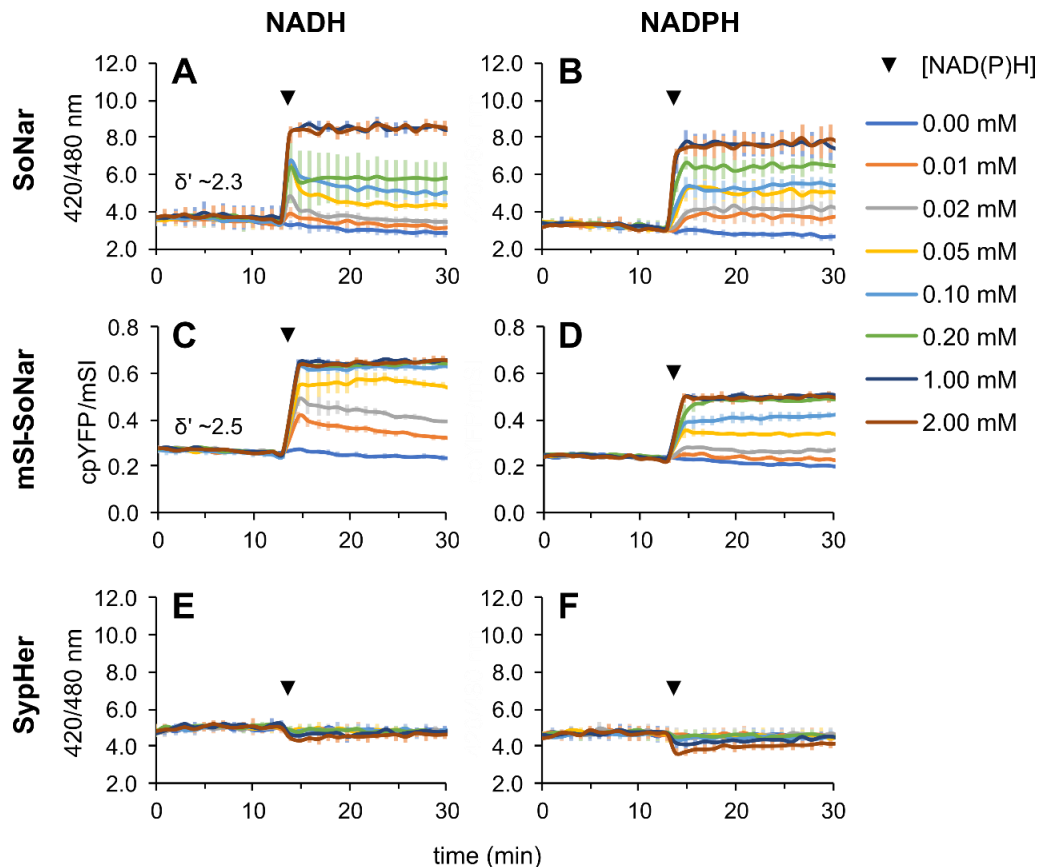


Figure 2.3: NADH and NADPH titration to semipermeabilized WT cells expressing (mSI-) SoNar.

WT cells expressing SoNar (A,B), mSI-SoNar (C,D), or SypHer (E,F) were semipermeabilized prior to fluorescence plate reader measurement. At the indicated time point (▼), cells were treated with different concentrations of NADH (left) or NADPH (right). Maximum ratio changes (δ') were calculated by division of average fluorescence ratios at ~15 min reached with 2 mM NADH by the value in absence of NADH. For SypHer calibration curve, refer to **Appendix, Figure S1A**.

2.1.4 iNap and mSI-iNap respond to NADPH in semipermeabilized cells

The iNap sensor family consists of five members, iNap1-4 and the iNapc control (Tao et al., 2017). They were generated by site-directed mutagenesis of the NBD of SoNar to switch its specificity from NADH/NAD⁺ to NADPH. The individual NADPH affinities of the iNap sensors decrease with increasing number, resulting in *in vitro* K_d (NADPH) values of ~2 μ M, ~6 μ M, ~25 μ M, and ~120 μ M for iNap1, -2, -3 and -4. The iNapc variant binds neither NADPH, nor NADH, and was designed for control measurements. Moreover, it was reported that the above-mentioned N-terminal mC fusion does not influence the binding properties of iNap1. To verify the different NADPH binding affinities of the iNap and mSI-iNap probes, GFI expressing, semipermeabilized cells were supplemented with different concentrations of NADPH. Semipermeabilization of iNap expressing WT yeast cells

resulted in similar 420/480 nm baseline values of ~ 3 for iNap1-3 (**Figure 2.4A-C**). The baseline values of iNap4 and iNapc were higher (~ 6) (**Figure 2.4D,E**). NADPH addition to iNap1-4 immediately elevated the 420/480 nm ratios to ~ 10 in a concentration-dependent manner, whereas the fluorescence of iNapc was not affected. According to their responses to the different NADPH concentrations in semipermeabilized yeast cells, iNap2 showed the highest NADPH affinity, followed by iNap1, -3 and -4. The fluorescence ratio responses of mSI-iNap1-4 to NADPH suggested that the probe affinities corresponded to that of their unfused counterparts (**Figure 2.4F-J**). Further, the NADPH specificity of the (mSI-) iNap sensors was validated by the application of NADH to semipermeabilized, GFI expressing cells. No changes in fluorescence readout were observed for (mSI-) iNap3, -4, or -c (**Appendix, Figure S2C-E,H-J**). High concentrations of 1 mM and 2 mM NADH led to a minor increase in the fluorescence ratio of (mSI-) iNap1 and (mSI-) iNap2 (**Appendix, Figure S2A,B,F,G**). Overall, these results validate the differing NADPH affinities and the specificity of (mSI-) iNap sensors.

Despite their different affinities for NADPH, iNap1-3, as well as iNap4 and -c, demonstrated similar 420/480 nm ratios after semipermeabilization. In addition, lower fluorescence ratios were not detected for the individual sensors throughout this study. This suggests the probes being in their NADPH-unbound state under this condition. Moreover, taking the different K_d (NADPH) values into account, the iNap sensors should be saturated with NADPH after application of 2 mM ligand. Based on the 420/480 nm ratios after the semipermeabilization and after addition of 2 mM NADPH, dynamic ranges δ between 1.8 and 3.2 result for iNap1-4 (**Figure 2.4A-D**). The fusion to mSI affected the dynamic ranges marginally, mSI-iNap1-4 demonstrated dynamic ranges δ between 2.3 and 3.6 (**Figure 2.4F-I**). Overall, the properties of the iNap probes and their mSI fusions were very similar in semipermeabilized yeast cells, suggesting the mSI fusions being appropriate iNap controls. Nonetheless, the pH dependency (**Section 2.3.3**), the low overall fluorescence intensities (**Section 2.3.4**), as well as the loss of the ratiometric readout and dynamic range represent relevant drawbacks of SoNar and iNap probes. These limitations can largely be attributed to the FP used for the sensor design, cpYFP. Enhanced intensities and improved pH stabilities are required to ensure a reliable fluorescence readout for many experimental approaches, such as measurements in medium, or when the probe expression level is low. Moreover, a GFI that specifically reports the important NADPH/NADP⁺ ratio instead of the NADPH concentration is highly desirable for redox process analyses. Due to these manifold disadvantages of iNap probes, alternative NAD(P)-sensitive redox sensors moved into focus.

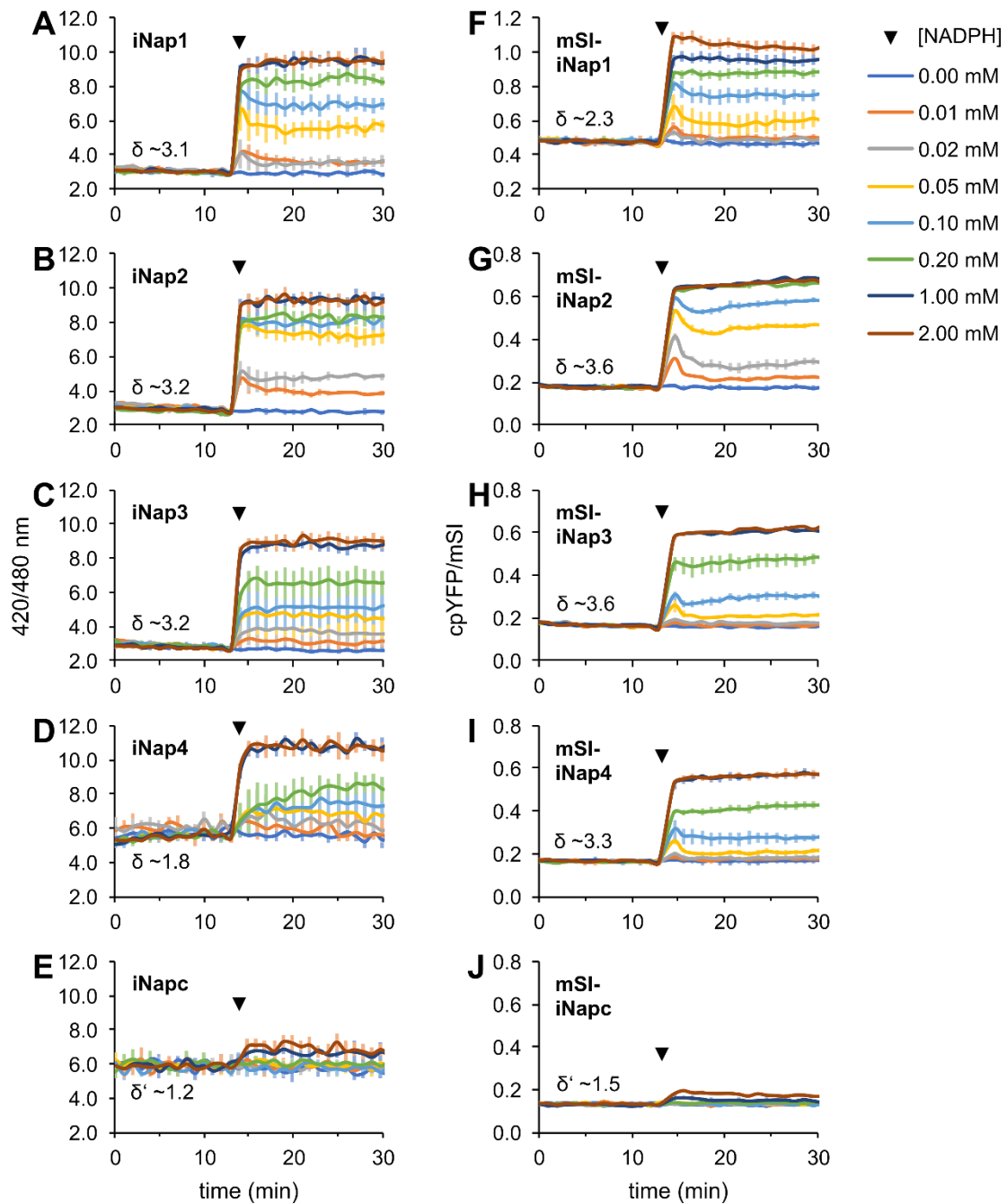


Figure 2.4: NADPH titration to semipermeabilized WT cells expressing (mSI-) iNap.

WT cells expressing iNap1 (A), iNap2 (B), iNap3 (C), iNap4 (D), iNapc (E), or respective mSI fusion constructs (F-J) were semipermeabilized prior to fluorescence plate reader measurement. At the indicated time point (▼), cells were treated with different concentrations of NADPH. Dynamic ranges (δ) were calculated by division of average fluorescence ratios at ~15 min reached with 2 mM NADPH by the value in absence of NADPH. δ' , maximum ratio change.

2.2 Characterization of Pdx-mC and Pdx-mC DS in *S. cerevisiae*

The NADH/NAD⁺ sensor Peredox (Pdx) was constructed as a tandem fusion of two complete T-Rex proteins (Hung et al., 2011). In between, a cpT-Sapphire (cpTS) was inserted to generate the intensimetric Pdx probe. An mC domain has been linked to the C-terminus, resulting in the final Pdx-mC sensor. The cpTS fluorescence intensity of Pdx-mC reflects the NADH/NAD⁺ ratio, whereas the mC fluorescence intensity remains stable. Thus, the cpTS/mC ratio displays the NADH/NAD⁺ ratio in an intensimetric manner. The D112S mutation of both Pdx-mC T-Rex domains increased K_d (NADH) from ~1.2 μ M to ~31.4 μ M, generating the Pdx-mC DS probe with decreased NADH/NAD⁺ affinity (**Table 1.2**) (Steinbeck et al., 2020).

2.2.1 Pdx-mC (DS) are functional in *S. cerevisiae*

Pdx-mC and Pdx-mC DS were chosen for the expression and characterization in the *S. cerevisiae* BY4742 WT strain. First, the correct sensor expression was confirmed by the determination of cpTS and mC fluorescence spectra of intact, probe expressing cells (**Figure 2.5A,B**). To validate the reversible sensor responses of Pdx-mC (DS), the already established, semipermeabilization-based calibration method (**Section 2.1.1**) was utilized. At the start of the measurement (at 'cellular equilibrium' or 'steady state'), the cpTS/mC ratios of Pdx-mC and Pdx-mC DS were similar (~1.2) (**Figure 2.5C,D**). As observed earlier for SoNar, cell semipermeabilization by digitonin decreased the fluorescence ratio to ~1.1 for Pdx-mC and to ~0.6 for Pdx-mC DS, corresponding to a decline in NADH/NAD⁺. The ratio decrease of the DS variant to lower values thereby reflects its lower NADH binding affinity. Cell semipermeabilization was apparently sufficient to drive Pdx-mC DS to the lowest cpTS/mC ratio possible, as lower values were not observed throughout the studies. Since the K_d value of Pdx-mC DS for NAD⁺, as well as the ambient NAD⁺ concentration, are unknown, it is uncertain whether the probe is present in its NAD⁺-bound or unbound state under these conditions. Hence, the respective probe conformation, represented by the lowest fluorescence ratio possible, will be referred to as 'open' sensor state. In contrast to Pdx-mC DS, the cpTS/mC of Pdx-mC remained at a higher level after cell semipermeabilization, suggesting that the probe remains partially bound to NADH. Hence, pyruvate was applied to drive further NADH oxidation to reduce the cpTS/mC of Pdx-mC. Indeed, the cpTS/mC ratio of Pdx-mC fell in a concentration-dependent manner confirming its responsiveness to the NADH/NAD⁺ ratio (**Figure 2.5C**). Treatment with high boluses of 5 mM and 10 mM pyruvate lowered cpTS/mC to ~0.7, corresponding to the cpTS/mC of Pdx-mC DS in its open state. Under these conditions, Pdx-mC was most likely present in

its NAD⁺-bound form, represented by the lowest cpTS/mC value. The addition of 1 mM NADH to Pdx-mC led to a cpTS/mC increase to ~1.4 in the presence of 1 mM pyruvate. The same amount of NADH was not able to completely increase the cpTS/mC ratio in the presence of higher pyruvate concentrations. Likewise, the addition of NADH to the semipermeabilized Pdx-mC DS culture increased the cpTS/mC ratio to ~1.4 (**Figure 2.5D**). The supplementation of 5 mM and 10 mM pyruvate quickly reduced the cpTS/mC of NADH-bound Pdx-mC DS ratio back to ~0.6. In the presence of 1 mM NADH, 1 mM and 2 mM pyruvate did not influence the cpTS/mC ratio of Pdx-mC DS, reflecting its lowered NAD⁺ binding affinity. Overall, the Pdx-mC (DS) sensors responded as expected on the various treatments, indicating that they are responsive to the NADH/NAD⁺ ratio.

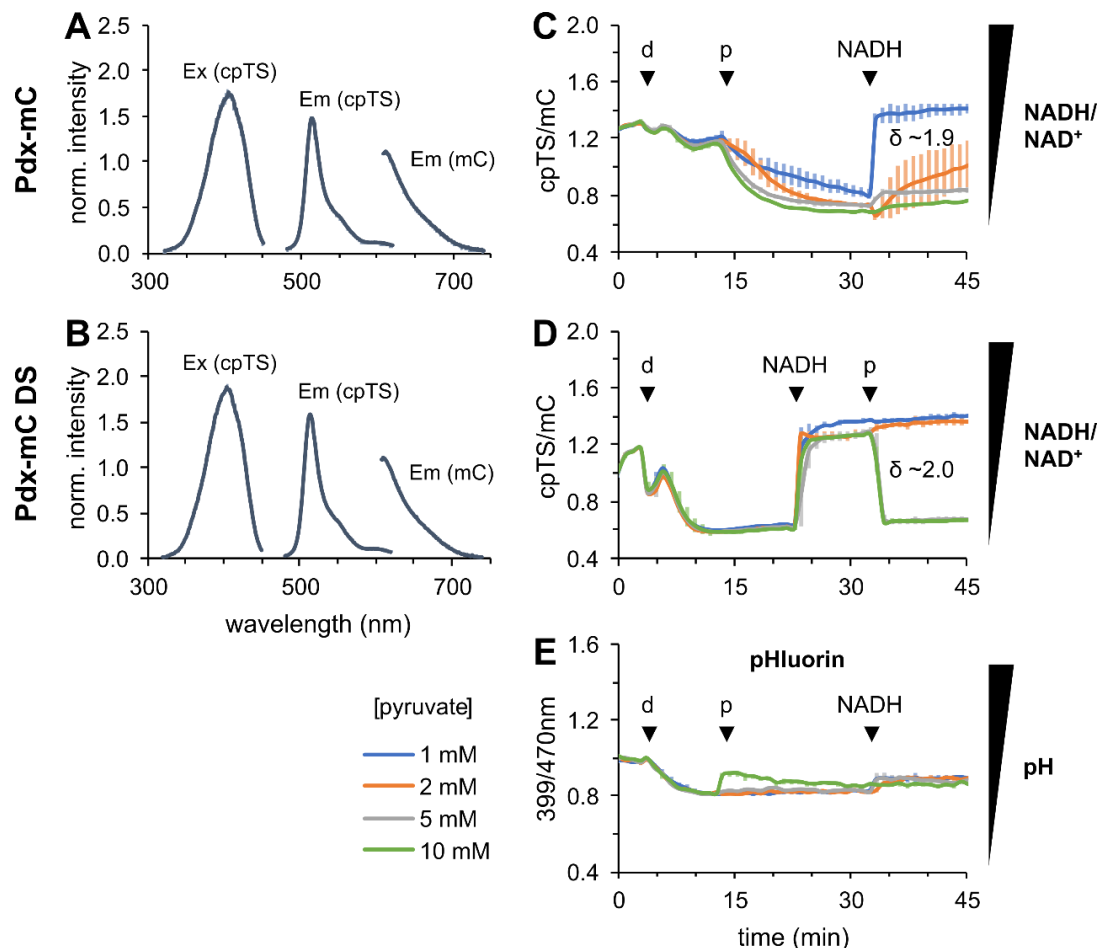


Figure 2.5: Characterization of Pdx-mC (DS) in WT cells.

Excitation (Ex) and emission spectra (Em) of cpTS and mC of intact WT cells expressing Pdx-mC (**A**) or Pdx-mC DS (**B**). Intensities were normalized to the mC emission at 619 nm. WT cells expressing Pdx-mC (**C**), Pdx-mC DS (**D**) or pHluorin (**E**) were sequentially treated at the indicated time points (\blacktriangledown) with 0.1% (w/v) digitonin (d), 1 mM NADH and the indicated concentration of pyruvate (p). Measurements were performed using a fluorescence plate reader. Dynamic ranges (δ) were calculated by division of average cpTS/mC ratio at ~40 min, 1 mM pyruvate, by the value reached with 10 mM pyruvate. For pHluorin calibration curve, refer to **Appendix, Figure S1B**.

It can be expected that minimum and maximum fluorescence ratios were achieved by this method, resulting in dynamic ranges of $\delta_{\text{Pdx}} \sim 1.9$ and $\delta_{\text{DS}} \sim 2.0$. These values are in the range of those reported from in vitro analyses ($\delta_{\text{Pdx}} \sim 2.2$ - and $\delta_{\text{DS}} \sim 2.9$) (Steinbeck et al., 2020). Further, the calculated NADH occupancy at cellular steady state was 82% for Pdx-mC and 62% for Pdx-mC DS. This additionally confirms the lowered NADH/NAD⁺ affinity of the DS variant and indicates that this probe should be preferred over Pdx-mC for dynamic measurements in intact cells to avoid sensor saturation with NADH.

The pH-sensitive SypHer sensor has been employed to monitor the pH-induced alterations of the cpYFP fluorescence (**Section 2.1**). In analogy, the green fluorescent pHluorin was employed as pH control for the fluorescence of cpTS of the Pdx-mC (DS) probes (Miesenböck et al., 1998). Based on a calibration curve (**Appendix, Figure S1B**), the pH at cellular steady state was determined to be ~ 7.03 (**Figure 2.5E**). Digitonin application led to an acidification to pH ~ 6.74 , whereas subsequent pyruvate treatment did not further alter pH, except for the highest concentration of 10 mM, increasing the pH to ~ 6.88 . These results correspond to those obtained with the SypHer sensor. Hence, the pHluorin sensor represents a reliable, green fluorescent pH control sensor.

2.2.2 Pdx-mC (DS) show minor pH dependency

The pH dependency is critical for the GFI application in vivo limiting the application of SoNar and iNap sensors in the yeast cytosol. The Pdx-mC (DS) readouts have been reported to be robust in a broad pH range (Höhne, 2020; Hung et al., 2011; Steinbeck et al., 2020). To validate these reports in the yeast system, sensor expressing cells were semipermeabilized in different pH buffers and the fluorescence spectra of cpTS and mC were recorded. The pH-sensitive pHluorin sensor was used to validate the adaptation of the cytosolic pH to the buffer pH after semipermeabilization. Indeed, its 399/450 nm ratio increased with increasing pH (**Figure 2.6C**). Three different conditions were examined for Pdx-mC (DS): the addition of either 2 mM NADH or 5 mM pyruvate, to transfer the probes into their NADH-bound and open conformation, respectively, and the control condition in absence of any additional compound. The resulting Pdx-mC (DS) readouts were rather pH stable when GFIs were bound to NADH demonstrating only moderate increase in cpTS/mC with increasing pH values (**Figure 2.6A,B**). In the presence of pyruvate, the Pdx-mC readout was stable up to pH 7.0 (**Figure 2.6A**). At pH 8.0 and pH 9.0, cpTS/mC adopted values of the NADH-bound state. As expected, the fluorescence ratio in the control condition was between those observed in the presence of NADH and pyruvate. For all the tested conditions, the cpTS/mC values recorded in the control condition and in presence of

pyruvate were very similar for Pdx-mC DS (**Figure 2.6B**). With rising pH values, cpTS/mC increased. Overall, this data hints on pH-dependent NADH-binding of the Pdx-mC (DS) probes at higher pH values, narrowing down the apparent dynamic range as observed for the SoNar sensor (**Section 2.1.2**).

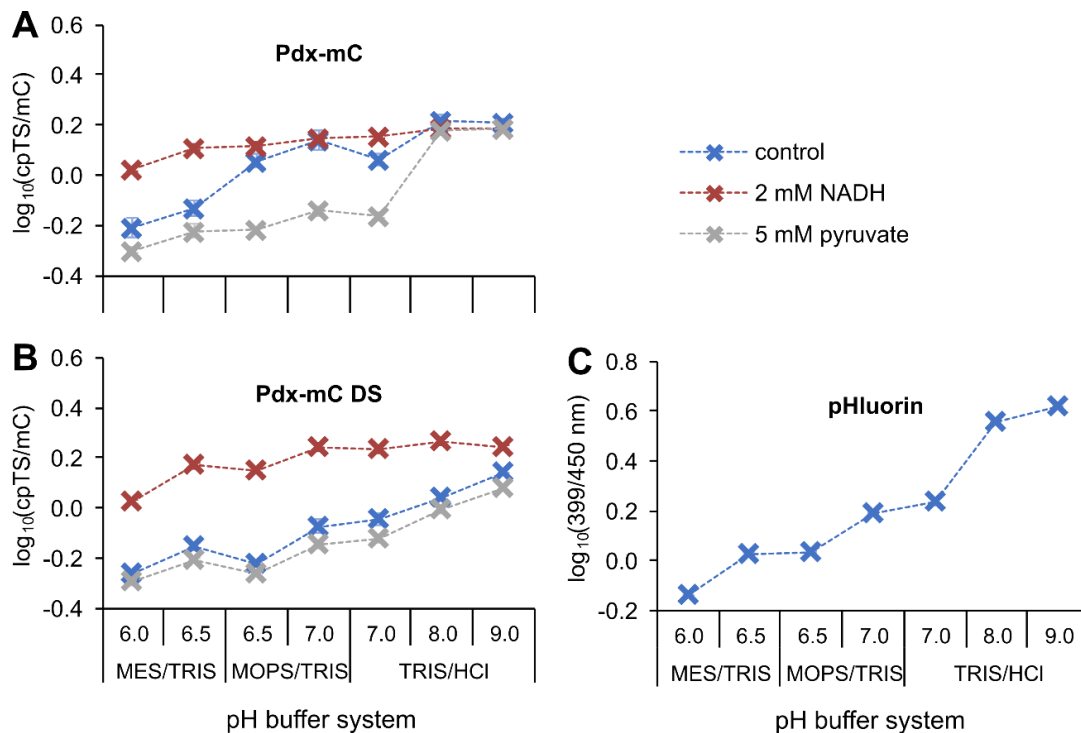


Figure 2.6: pH dependencies of Pdx-mC (DS) sensors in semipermeabilized WT cells.

WT cells expressing Pdx-mC (**A**), Pdx-mC DS (**B**), or pHluorin (**C**) were semipermeabilized in the indicated buffer solution with 0.1% (w/v) digitonin. Excitation and emission spectra of cpTS and mC were recorded in absence (control) and presence of NADH or pyruvate. Fluorescence intensities were normalized to the mC emission at 619 nm for Pdx sensors. Emission of cpTS at 510 nm was plotted against the pH as $\log_{10}(\text{cpTS}/\text{mC})$. For pHluorin, 399/450 nm ratio was calculated without normalization. Measurements were performed using a fluorescence plate reader.

2.2.3 Maturation time discrepancies between cpTS and mC are minor

The maturation of FPs requires correct protein folding and complex chromophore formation, including an oxidation reaction (Craggs, 2009). In living organisms, exogenously expressed FPs compete with other reactions and cellular processes, such as respiration, for the available molecular oxygen. Therefore, the relative fluorescence intensity of slow maturing FPs is under oxygen-limited conditions dimmer than that of FPs with faster maturation rates. Moreover, this phenomenon is observed in fast-growing cultures, where the fluorescence intensities of slow maturing FPs lack behind the growth rate. Hence, the

discrepancy in fluorescence intensities between fast and slow maturing FPs is expected to be less pronounced in well-aerated and slow growing cultures. Discrepancies in maturation time could limit the application of GFIs containing two FPs, such as Pdx-mC. A shorter cpTS than mC maturation time was reported to bias the Pdx-mC readout of fast growing *Ustilago maydis* cultures (Hartmann et al., 2018).

To investigate the differences in maturation rate between cpTS and mC in *S. cerevisiae*, the Pdx-mC DS expression was induced in BY4742 WT using the GAL promoter. Single fluorescence intensities were subsequently followed over time. Similar to reports from *U. maydis*, cpTS seemed to reach full intensity earlier than mC (**Figure 2.7A**). But when cpTS and mC intensities were plotted against each other, all data points matched a fitted line (**Figure 2.7B**), indicating similar maturation rates. The acquirement of further data points up to full fluorescence intensity would provide worthy information to assess actual maturation time discrepancies. Nonetheless, the discrimination between the influences deriving from altered maturation time from those caused by a changed NADH/NAD⁺ ratio is impossible. Hence, a cpTS- and mC-containing sensor that is unresponsive to NAD(P)H or NAD(P)⁺, such as NAPstarC (**Section 2.3**), is desired to control for actual maturation artifacts. The presented results suggest that the differences in cpTS and mC maturation do not affect Pdx-mC (DS) measurements when the probes are expressed in WT strain. Therefore, Pdx-mC-based probes were considered suitable for the use in *S. cerevisiae*.

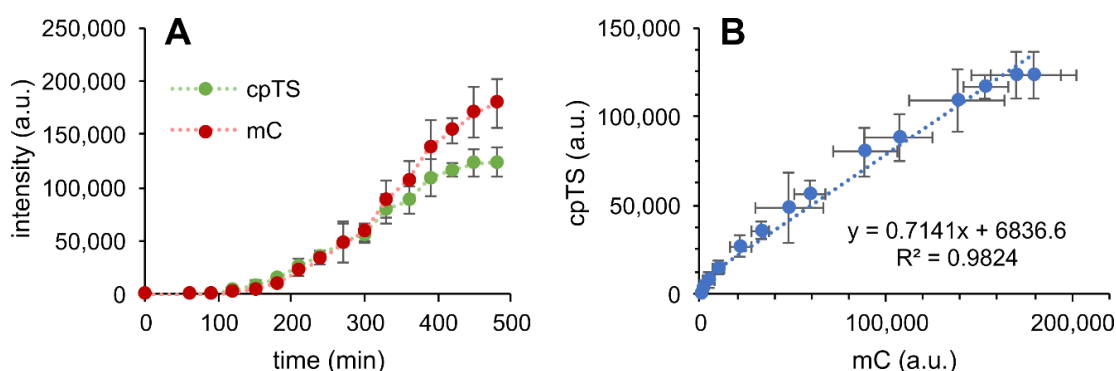


Figure 2.7: Maturation of cpTS and mC after induction of Pdx-mC DS expression.

WT cells were transformed with p415 GAL Pdx-mC DS plasmid. During exponential phase, gene expression was induced by addition of galactose ($t = 0$ min). Fluorescence intensities of cpTS and mC were subsequently measured by the plate reader in 60 min time intervals. Intensities were blank corrected and plotted in arbitrary units (a.u.) over time (**A**) or against each other (**B**).

2.2.4 Pdx-mC (DS) respond to NAD(P)H in semipermeabilized cells

The NADH affinity of Pdx-mC was lowered by site-directed mutagenesis, resulting in the DS variant. Thereby the K_d (NADH) was shifted from $\sim 1.2 \mu\text{M}$ to $\sim 31.4 \mu\text{M}$ and the K_d (NADPH) from $\sim 531 \mu\text{M}$ to $\sim 324 \mu\text{M}$ (**Table 1.2**) (Steinbeck et al., 2020). To verify the different Pdx-mC (DS) affinities for NADH, sensor expressing WT cells were semipermeabilized and treated with increasing amounts of NADH. Both, Pdx-mC and Pdx-mC DS, readily responded with a concentration-dependent increase in the cpTS/mC ratio (**Figure 2.8A,B**). Although a significant proportion of Pdx-mC was NADH-bound when additional ligand was added, Pdx-mC reacted readily, even to low NADH concentrations, demonstrating its high NADH affinity. In contrast, at least 0.05 mM NADH were necessary to induce an increase in the cpTS/mC of Pdx-mC DS. Consequently, the different NADH affinities of Pdx-mC (DS) could be qualitatively validated using the semipermeabilization-based NADH titration assay.

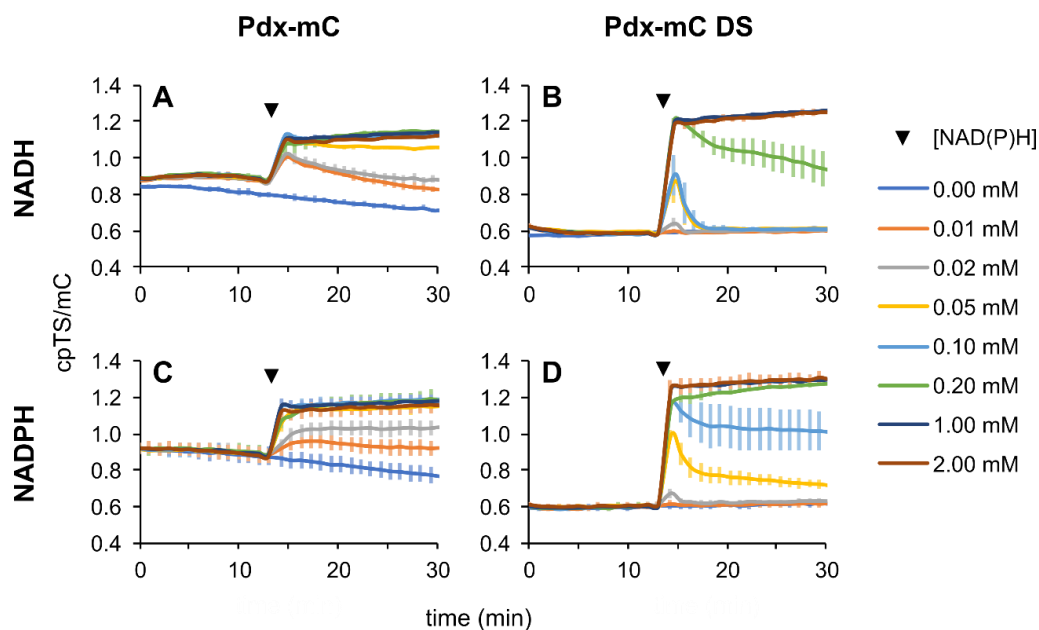


Figure 2.8: NADH and NADPH titration to semipermeabilized WT cells expressing Pdx-mC (DS).

Pdx-mC (**A,B**) and Pdx-mC DS (**C,D**) expressing, semipermeabilized WT cells (0.1% [w/v] digitonin) were treated at indicated time points (▼) with different concentrations of NADH (top) or NADPH (bottom) during fluorescence plate reader measurement.

In semipermeabilized cells, the NADH/NAD⁺-sensitive SoNar sensor responded to both NADH, and NADPH. This effect is either caused by the conversion of exogenous NADPH to NADH, or unspecific sensor binding. *S. cerevisiae* lacks a bona fide NAD(P) transhydrogenase and a mechanism underlying the potential NADPH → NADH conversion

has not been identified so far. In relation to SoNar, Pdx-mC and Pdx-mC DS possess 3.5- and 2.2-fold lowered NADPH affinities (**Table 1.2**). Thus, the Pdx-mC (DS) sensors should be less responsive to the supplementation of NADPH to semipermeabilized cells. But in fact, the Pdx-mC cpTS/mC increase upon NADPH addition resembled that observed for NADH (**Figure 2.8C**), while the response of the Pdx-mC DS fluorescence ratio to exogenous NADPH was even stronger than that to NADH (**Figure 2.8D**). Overall, the responses of the three different NADH/NAD⁺-sensing GFIs, Pdx-mC, Pdx-mC DS, and SoNar, to exogenous NADPH in semipermeabilized *S. cerevisiae* cells were much stronger than it would have been expected from their in vitro K_d values. This strongly suggests the conversion of NADPH to NADH under these conditions by a yet unknown mechanism.

2.3 Design of novel NADPH/NADP⁺-responsive NAPstar sensors

The cpYFP-based SoNar and iNap probes are restricted by their low fluorescence intensity and pH sensitivity of the cpYFP moiety when expressed in *S. cerevisiae*. In contrast, Pdx-mC (DS) demonstrated increased fluorescence intensities (**Section 2.3.4**) as well as improved pH stability in vitro (Hartmann et al., 2018; Steinbeck et al., 2020; Tao et al., 2017; Zhao et al., 2015) and in semipermeabilized yeast cells (**Section 2.3.3**). With this, the Pdx-mC (DS) sensors overcome the general limitations of cpYFP-based SoNar and iNap probes. In addition, the NADPH-responsive iNap probes are insensitive to NADP⁺ and thus not able to monitor the crucial NADPH/NADP⁺ redox poise, which is more important for NADPH-dependent redox reactions than the NADPH concentration. The iNap sensors were designed based on the NADH/NAD⁺-sensitive SoNar probe using structure-guided, site-directed mutagenesis of the T-Rex NBD (**Figure 2.9A**) (Tao et al., 2017). By the combination of different mutations, a range of various iNap probes with varying NADPH affinities was produced (**Table 2.1**). Since the NBDs of both, the Pdx and SoNar sensors, derive from the T-Rex protein, they exhibit a high degree of similarity (Hung et al., 2011; Sickmier et al., 2005; Zhao et al., 2015). Thus, it was hypothesized that the mutation site transfer from the various iNap family members to the Pdx-mC probe would transform Pdx-mC into NADP-specific sensors with different NADPH affinities (**Figure 2.9A,B**). These novel GFIs were generated by the application of the individual iNap mutations simultaneously on both Pdx-mC T-Rex domains (**Table 2.1**). The resulting constructs were termed NAPstar1-4 and NAPstarC, corresponding to the iNap nomenclature. Due to the modified NBDs, the novel NAPstar sensors are supposed to have NADPH affinities that decrease with increasing variant number. Moreover, they are expected to report either the NADPH concentration or – if NADP⁺ competes with NADPH for binding to the sensors – the

NADPH/NADP⁺ ratio. At the same time, the NAPstar probes should retain the advantageous fluorescence properties of Pdx-mC (**Figure 2.9C**). In addition, their fluorescence readout is performed by the determination of the cpTS/mC ratio, such as for the Pdx-mC progenitor. Overall, the novel NAPstar sensors have the potential to outperform the already established NADPH-sensitive iNap probes regarding fluorescence intensity, pH resistance, and responsiveness to NADPH/NADP⁺.

Table 2.1: Mutations and in vitro NADPH binding affinities of NAPstar and iNap variants.

NAPstar in vitro analysis was performed by the group of Prof. Dr. Markus Schwarzländer (WWU Münster). The amino acids are numbered according to the native T-Rex sequence (UniProt-AC Q9X2V5). 'Additional mutations' of the first and second T-Rex domain (from N' to C') are separated by a slash. References: ^A Steinbeck et al., 2020; ^B Hung et al., 2011; ^C Mai et al., manuscript in preparation; ^D Tao et al., 2017; ^E Zhao et al., 2015.

Variant name or number (K _d [NADPH] in ~μM)		Position 112-116	Additional mutations
Pdx-mC (531) ^{A,B}	—	DVDPG	—
Pdx-mC DS (324) ^A	—	SVDPG	—
—	SoNar (150) ^{D,E}	DVDPE	—
NAPstar1 (0.7) ^C	iNap1 (2.0) ^D	SRSAQ	—
NAPstar2 (1.5) ^C	iNap2 (6.4) ^D	SRSAE	V130T
NAPstar3 (5.4) ^C	iNap3 (25.2) ^D	SRKAE	V130Y
NAPstar4 ^C	iNap4 (120.2) ^D	SRSAQ	R90D
NAPstarC ^C	iNapc (∞) ^D	SVSPE	R90D, V148A
—	33 (3.6) ^D	SRSAQ	V130Y
—	37 (12.6) ^D	SRSAQ	V148A
—	38 (7.8) ^D	SRSAQ	V148T
NAPstar5	—	SRSAQ	R90L
NAPstar6 (12) ^C	—	SRKAE	V148A
NAPstar7 (7) ^C	—	SRKAE	V148T
NAPstar1.4 ^C	—	SRSAQ	— / R90D
NAPstar2.4 ^C	—	SRSAE / SRSAQ	V130T / R90D
NAPstar3.4 ^C	—	SRKAE / SRSAQ	V130Y / R90D
NAPstar4.1 ^C	—	SRSAQ	R90D / —
NAPstar4.2 ^C	—	SRSAQ / SRSAE	R90D / V130T
NAPstar4.3 (53.8) ^C	—	SRSAQ / SRKAE	R90D / V130Y
NAPstar3b (2.7) ^C	—	SRKAE	V126Y / V130Y

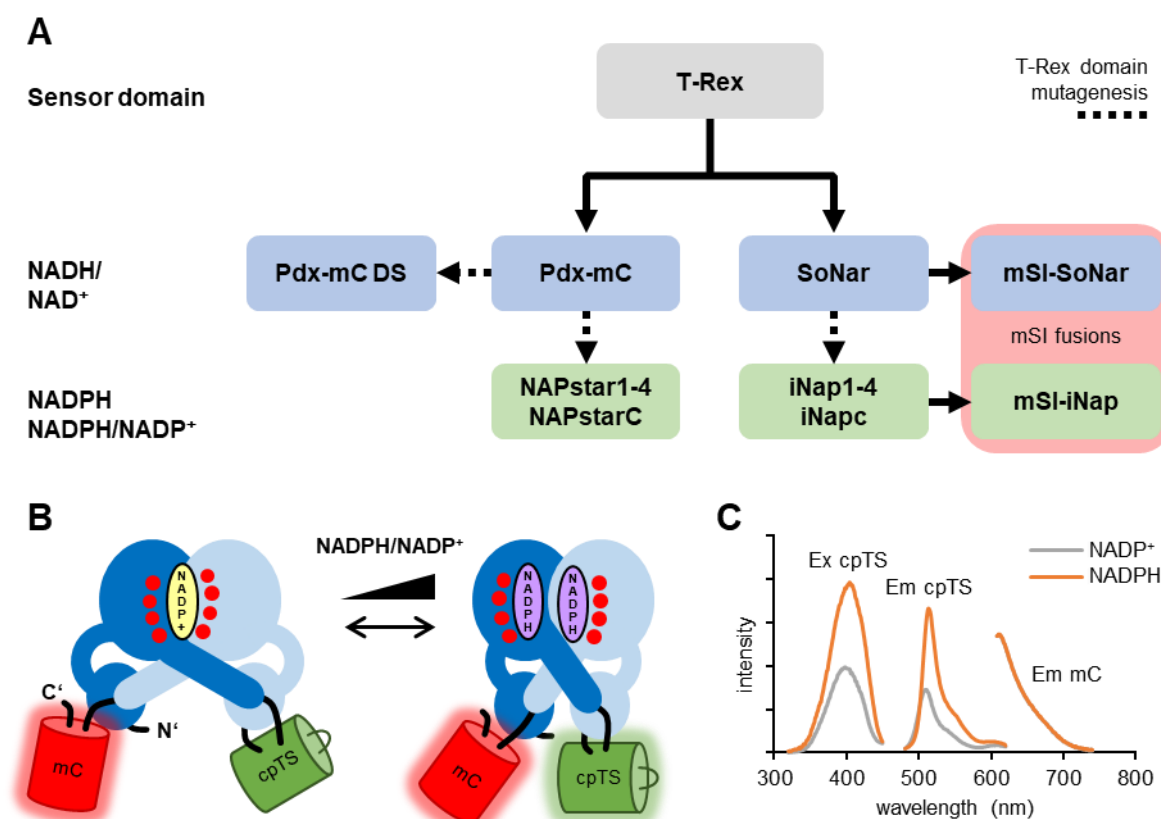


Figure 2.9: Design of novel Pdx-mC-based NADPH/NADP⁺-specific NAPstar sensors.

Based on the bacterial T-Rex protein (grey), various NADH/NAD⁺ ratio sensors were generated (blue) (A). The site-directed mutagenesis of the NADH/NAD⁺-sensing SoNar (Zhao et al., 2015) led to the construction of NADPH-specific iNap sensors (NADP-specific sensors in green) (Tao et al., 2017). The N-terminal fusion of an RFP (e.g., mSI) generates a set of control probes which is supposed to be more pH-robust (red). The mutations performed for iNap generation were applied on the T-Rex domains of Pdx-mC (red dots in B) to develop the novel NADPH/NADP⁺-responsive NAPstar probes. Model of NADPH/NADP⁺-sensing of NAPstar probes (B) that inherit the fluorescence properties from the Pdx-mC ancestor (C).

2.3.1 In vitro characterization of NAPstar probes

For the comprehensive understanding of NAPstar probes, NAPstar1-3 were recombinantly expressed in *E. coli*, purified, and analyzed in vitro by Jan-Ole Niemeyer and colleagues in the laboratory of Prof. Dr. Markus Schwarzländer (WWU Münster). Compared to the Pdx-mC ancestor ($K_d \sim 1.2 \mu\text{M}$ NADH), the NADH affinities of NAPstar1-3 were lowered, with a K_d (NADH) of $\sim 98.2 \mu\text{M}$ for NAPstar3 (Appendix, Table S2) (Mai et al., in preparation). In the presence of $150 \mu\text{M}$ NADP⁺, NAPstar1-3 demonstrated high NADPH binding affinities with K_d (NADPH) of $\sim 0.7 \mu\text{M}$ for NAPstar1, $\sim 1.5 \mu\text{M}$ for NAPstar2, and $\sim 5.5 \mu\text{M}$ for NAPstar3 (Table 2.1). Moreover, NADP⁺ competed with NADPH for NAPstar

binding. When NADP⁺ bound to the probes, the cpTS/mC ratio was decreased. In contrast, NAD⁺ had no effect. In addition, the NAPstar K_d (NADPH/NADP⁺) values were almost unaffected by the total NADP pool size. The various NAPstar sensors were pH-robust in the range between pH 7 and pH 8.5, especially in their NADPH-bound states. The in vitro NAPstar fluorescence signals were not affected by niacin (NA), ADP or AMP. As expected, the NAPstarC control did not respond to NADH, NAD⁺, NADPH, NADP⁺, NA, ADP, or AMP. The addition of 10 mM ATP lowered the cpTS/mC ratio of each of the sensor variants, including NAPstarC. Hence, NAPstarC represents a valuable and necessary control sensor to exclude ATP binding artifacts. Altogether, the in vitro analyses confirm the novel NAPstar probes being largely pH-resistant and specific for the NADPH/NADP⁺ ratio with different NADPH affinities.

2.3.2 NAPstar sensors are functional in *S. cerevisiae*

NAPstar3 was chosen for a first characterization in *S. cerevisiae* BY4742 WT, as it had an intermediate NADPH affinity of K_d ~5.4 μM (**Table 2.1**). The NAPstarC sensor was used as a control. The correct GFI expression was confirmed based on the cpTS and mC fluorescence spectra (**Figure 2.10A,B**). The dynamic NAPstar3 response was validated by cell semipermeabilization, decreasing cpTS/mC from ~1.2 to ~0.4 (**Figure 2.10C**). The subsequent supplementation of 1 mM NADPH did not lead to full cpTS/mC recovery, but to a ~2.5-fold increase to ~1.1. Application of pyruvate did not affect the fluorescence ratio. The NAPstar3 responses resembled those of iNap1, indicating that the sensor is not responsive to NADH/NAD⁺ but to NADPH/(NADP⁺).

The NAPstarC variant carries T-Rex mutations that impede NAD(P)H binding and thus, it represents a sensor control for NAPstar and Pdx-mC (DS) probes. As expected, the cpTS/mC ratio of NAPstarC was barely affected and showed only marginal alterations after digitonin and NADPH addition (**Figure 2.10D**), as observed for SypHer and pHluorin pH controls (**Section 2.1.1** and **Section 2.2.1**). This result demonstrates that NAPstarC is likely a suitable control sensor.

2.3.3 NAPstar sensors show minor pH dependency

Two distinct toolboxes are now available to quantify either the NADPH concentration or the NADPH/NADP⁺ ratio in yeast, the iNap and NAPstar GFIs. The strong pH dependency of the cpYFP fluorescence limits the application of iNap probes in *S. cerevisiae* (**Section 2.1.2**). To check whether the Pdx-mC-derived NAPstar sensors overcome this

downside, the pH sensitivities of NAPstar3 and NAPstarC were investigated in the yeast-based setup. To this end, probe expressing WT cells were semipermeabilized in different pH buffers, in the absence and the presence of 2 mM NADPH, as shown previously (**Section 2.1.2**). NAPstar3 and NAPstarC demonstrated increased robustness towards pH changes (**Figure 2.11A,B**). Only minor cpTS/mC alterations were detected in the range between pH 6.0 and pH 9.0, irrespective of the ligand addition. Since the pH dependencies of NAPstar3 and NAPstarC were very similar to that of Pdx-mC (DS), NAPstarC can be regarded as a suitable pH control for both, NAPstar and Pdx-mC (DS) probes. Moreover, the NAPstarC enables to detect potential maturation time discrepancies between cpTS and mC in critical setups, independent of NAD(P)H (**Section 2.2.3**). Nonetheless, the individual influences of ATP changes, pH fluctuations, and the FP maturation on the NAPstarC readout cannot be clearly separated. Therefore, alterations in the NAPstarC cpTS/mC ratio must be interpreted with caution.

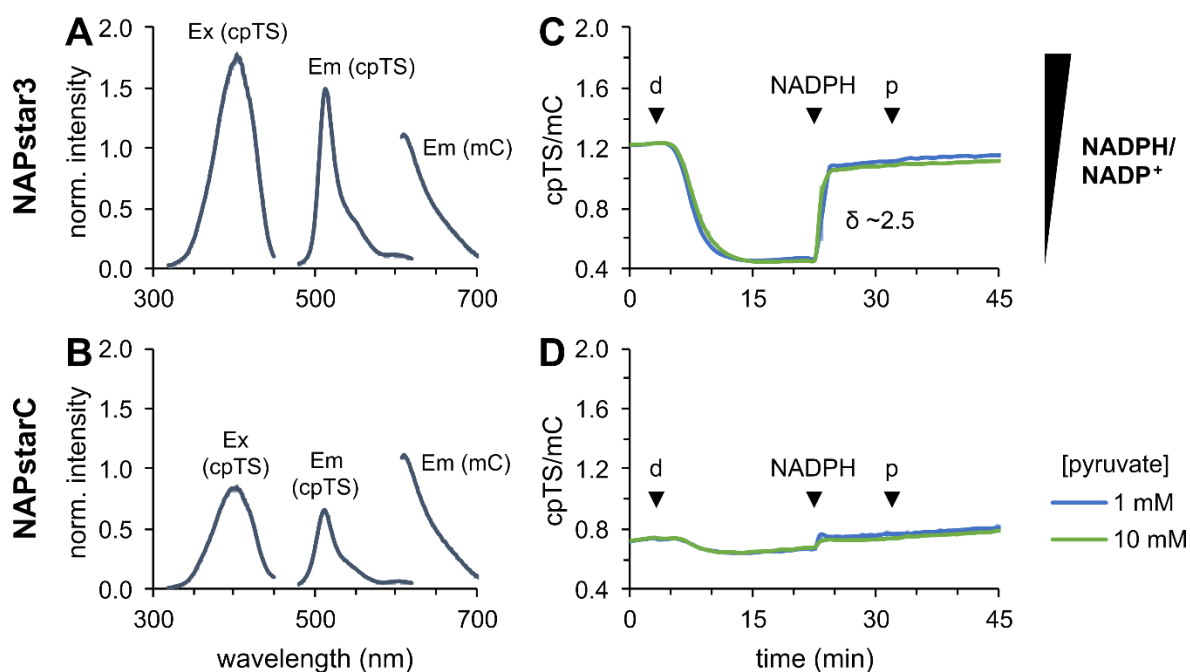


Figure 2.10: Characterization of NAPstar3 and NAPstarC in WT cells.

Excitation (Ex) and emission spectra (Em) of cpTS and mC of intact WT cells expressing NAPstar3 (**A**) or NAPstarC (**B**) were recorded. Fluorescence intensities were normalized to the mC emission at 619 nm. WT cells expressing NAPstar3 (**C**) or NAPstarC (**D**) were sequentially treated at the indicated time points (▼) with 0.1% (w/v) digitonin (d), 1 mM NADPH and different concentrations of pyruvate (p). Measurements were performed using a fluorescence plate reader. Dynamic range (δ) was calculated by division of average cpTS/mC ratio at ~30 min by the cpTS/mC ratio at ~15 min in presence of 1 mM pyruvate.

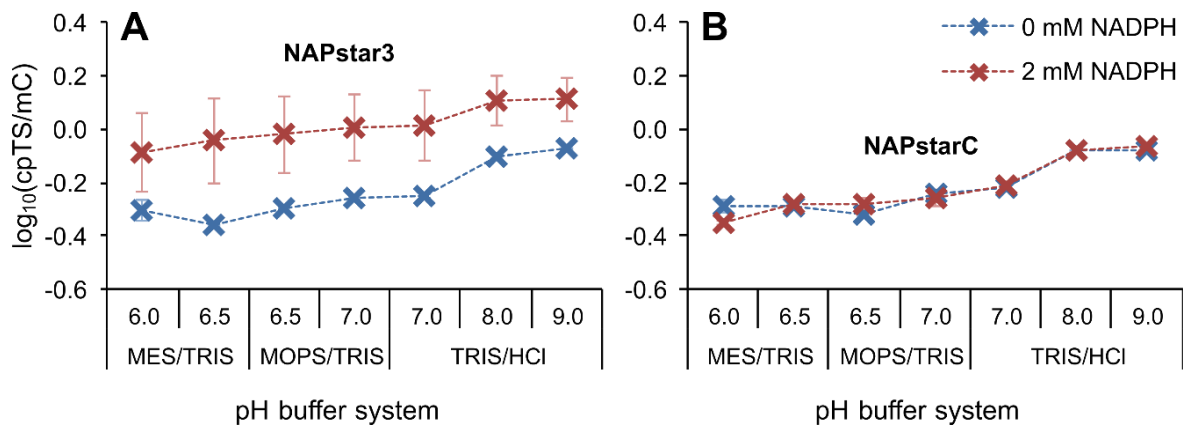


Figure 2.11: pH dependencies of NAPstar3 and NAPstarC in semipermeabilized WT cells.

WT cells expressing NAPstar3 (A) or NAPstarC (B) were semipermeabilized in the indicated buffer solution with 0.1% (w/v) digitonin. Excitation and emission spectra of cpTS and mC were recorded in absence (control) and presence of NADPH. Fluorescence intensities were normalized to the mC emission at 619 nm. Emission of cpTS at 510 nm was plotted against the pH as $\log_{10}(\text{cpTS}/\text{mC})$. Measurements were performed using a fluorescence plate reader.

To allow for the direct comparison of pH dependencies between cpTS- and cpYFP-based probes, the GFI fluorescence ratio changes between pH 6.0 and pH 9.0 in the presence of 2 mM ligand were considered (Table 2.2). The cpTS/mC ratios of Pdx-mC and NAPstar probes demonstrated fold changes in the range of 1.47 to 1.91. The fold changes of SoNar and iNap probes were much bigger, ranging from 10.69 to 45.12. Since also the dynamic ranges of cpYFP-based GFIs is larger under physiological conditions, the pH-dependent fold changes were normalized (norm.) to the respective sensor dynamic ranges to compute a meaningful parameter (Table 2.2). Despite this correction, the norm. fold change values of Pdx-mC (0.8) and NAPstar3 (0.6) probes were clearly lower than those received for SoNar (2.8) and iNap1 (3.6). Consequently, the Pdx-mC and NAPstar probes show improved pH overall stability compared to SoNar and iNap sensors.

Table 2.2: pH-dependent fold change in fluorescence ratio of different NAD(P)-specific GFIs.

The fluorescence ratios were determined in sensor expressing, semipermeabilized cells in the presence of 2 mM ligand, in 0.1 M MES/TRIS, pH 6.0 and in 0.1 M TRIS/HCl, pH 9.0 (**Figure 2.2**, **Figure 2.6**, and **Figure 2.12**). The pH-dependent sensor fold change was calculated by division of the higher fluorescence ratio by the lower value. Further normalization to the dynamic range resulted in norm. pH-dependent fold changes. Dynamic ranges δ : Pdx-mC, 1.9 (**Figure 2.5**); NAPstar3, 2.5 (**Figure 2.10**); SoNar, 5.5 (**Figure 2.1**); iNap1, 3.0 (**Figure 2.1**).

Sensor	pH-dependent fold change	norm. pH-dependent fold change
Pdx-mC	1.47	0.8
NAPstar3	1.49	0.6
NAPstarC	1.91	—
SoNar	15.27	2.8
iNap1	10.69	3.6
iNapc	45.12	—

2.3.4 NAPstar sensors have improved fluorescence intensities

Besides high pH sensitivities, low fluorescence intensities limit the application of SoNar and iNap probes in *S. cerevisiae*. In contrast, Pdx-mC and NAPstar probes showed high fluorescence intensities. To compare the different fluorescence intensities despite deviating plate reader settings, the individual fluorescence intensities were normalized to the respective background (blank) signals deriving from empty vector-transformed cells. The resulting norm. intensity of the red fluorescent mC clearly exceeded those of cpYFP and cpTS by far with values ranging from 277 (Pdx-mC DS) to 974 (NAPstar3) times background intensity (data not shown). A closer look on the green emitting FPs (cpYFP and cpTS) revealed very low norm. fluorescence intensities of the cpYFP-based GFIs when excited at 480 nm, ranging from 1.9 (iNapc) to 4.8 (SypHer) times background signal (**Figure 2.12A**). Norm. fluorescence intensities excited at 420 nm were higher (4.1 to 15.8 times background) but below those of cpTS probes. The norm. cpTS intensities of the Pdx-mC (DS) sensors were lower (20.3 and 15.2) than those of the NAPstar sensors (72.7 and 21.3 for NAPstar3 and NAPstarC). Remarkably, the cpTS fluorescence intensity of NAPstar3 was much higher than that of related probes. Overall, the Pdx-mC (DS) and NAPstar sensors demonstrated enhanced fluorescence intensities when compared to the cpYFP-based GFIs.

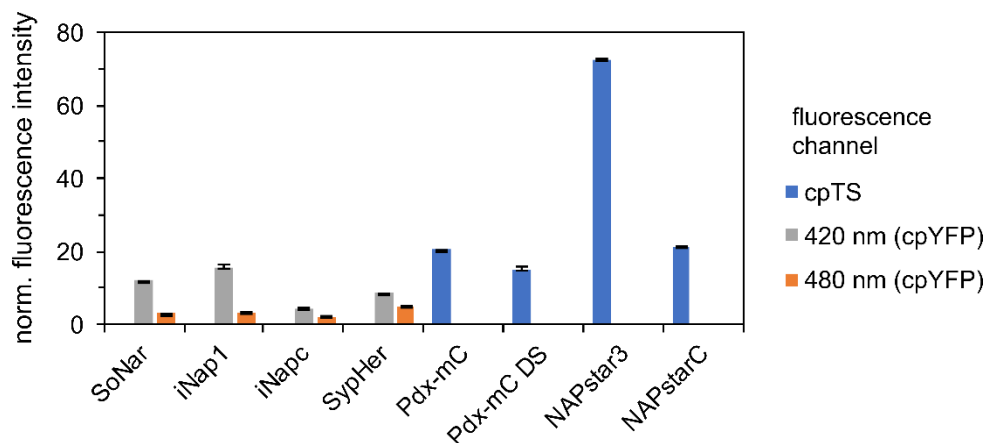


Figure 2.12: Fluorescence intensities of cpYFP- and cpTS-based NAD(P)-specific GFI.

The fluorescence intensities of the indicated fluorescence channels were determined by a fluorescence plate reader for 1.5 OD₆₀₀ units of GFI expressing WT cells in 0.1 M MOPS/TRIS buffer, pH 7. Fluorescence intensities were normalized to the signal of a culture transformed with a p413 TEF empty plasmid (blank) that was measured in parallel.

2.3.5 NAPstar sensors respond to NADPH in semipermeabilized cells

Opposing to their Pdx-mC ancestor, the novel NAPstar sensors are specific reporters of the NADPH/NADP⁺ ratio (Mai et al., in preparation). Corresponding to their iNap counterparts, NAPstar1-4 probes bind NADPH/NADP⁺ with decreasing NADPH affinity, whereas NAPstarC neither binds to NADH nor to NADPH. To confirm the different NADPH affinities of the NAPstar sensors and to exclude NADH binding in the yeast-based setup, the fluorescence ratio responses to exogenous NADPH and NADH were followed in semipermeabilized sensor expressing WT cells. After semipermeabilization, the cpTS/mC ratios of all NAPstar variants adapted a low, stable value between 0.4 and 0.6, indicating open sensor conformations (**Figure 2.13**). The subsequent application of NADPH rapidly increased the cpTS/mC ratios of NAPstar1-3 (**Figure 2.13A-C**), whereas only very high exogenous concentrations of NADH (1 and 2 mM) provoked slow sensor responses (**Figure 2.13F-H**). The NADPH affinity of NAPstar4 was strongly diminished, an increase in cpTS/mC was only observed at 1 mM and 2 mM NADPH (**Figure 2.13D**). Based on the maximum and minimum cpTS/mC values reached throughout the experiment, NAPstar1-4 dynamic ranges of $\delta \sim 2.2$, ~ 2.2 , ~ 2.4 and ~ 1.6 were calculated (**Figure 2.13A-D**). As expected, the NAPstarC fluorescence ratio was not affected by any of the NAD(P)H concentrations tested (**Figure 2.13E,J**). In total, the increase in the NAPstar variant number is connected to a lower NADPH binding affinity, with NAPstarC being unresponsive to NAD(P)H, corresponding to the in vitro data and to the reports on iNap probes (**Table 2.1**).

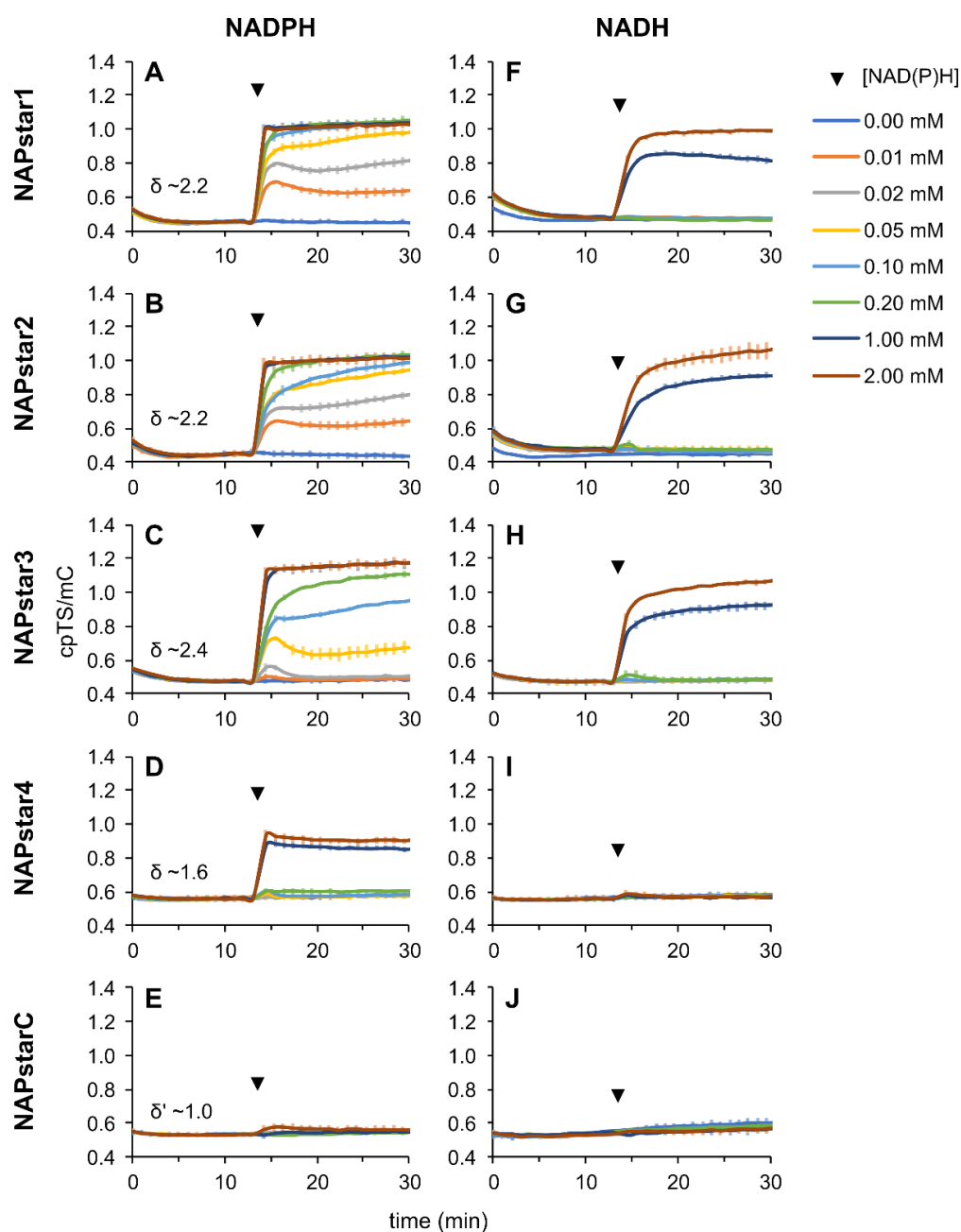


Figure 2.13: NADPH and NADH titration to semipermeabilized WT cells expressing NAPstar1-4 or NAPstarC.

NAPstar1 (A,F), NAPstar2 (B,G), NAPstar3 (C,H), NAPstar4 (D,I), or NAPstarC (E,J) expressing, semipermeabilized WT cells (0.1% [w/v] digitonin) were treated at the indicated time point (▼) with different concentrations of NADPH (left) or NADH (right) during fluorescence plate reader measurements. Dynamic ranges (δ) were calculated by division of cpTS/mC ratios at ~15 min, 2 mM NADPH by the value in absence of NADPH. δ' , maximum ratio change.

2.4 Multiparameter imaging during acute oxidative stress

The activities of antioxidative glutathione (GSH, reduced form; GSSG, oxidized form) and thioredoxin (Trx) -coupled systems rely on NADPH as final electron donor (Netto et al., 2007). In contrast, the involvement of NADH-dependent reactions in the antioxidative defense is rather indirect (Grant et al., 1999). Hence, it was asked in how far acute oxidative stress influences specifically the cytosolic NADP and NAD redox balances. Three different oxidants (H_2O_2 , diamide, and TBHP) were employed in a fluorescence plate reader-based assay to induce different kinds of acute oxidative stress in the BY4742 WT strain. At the same time, various important cytosolic parameters were followed by GFI measurements in parallel:

- (i) roGFP2-Tsa2 ΔC_R is an ultrasensitive H_2O_2 probe which is also oxidized by TBHP and hypochlorite in vitro (Morgan et al., 2016).
- (ii) roGFP2-Grx1 specifically equilibrates with the **GSSG/2GSH ratio** (Gutscher et al., 2008; Morgan et al., 2013).
- (iii) pHluorin and SypHer were used to monitor the **cytosolic pH** (Section 2.2 and Section 2.1).
- (iv) NAPstar probes report the **NADPH/NADP⁺ ratio** (Section 2.3).
- (v) iNap sensors are sensitive for the **NADPH concentration** (Tao et al., 2017). mSI-iNap probes were measured in parallel (Section 2.1).
- (vi) Pdx-mC (DS) and SoNar sensors were utilized to trace the **NADH/NAD⁺ ratio** (Hung et al., 2011; Steinbeck et al., 2020; Zhao et al., 2015). mSI-SoNar was employed as control (Section 2.1).

After four minutes of fluorescence measurement, the oxidant was applied and the sensor responses to the different oxidative challenges were followed in real-time.

2.4.1 Effect of exogenous H_2O_2 on cytosolic NAD(P) redox states

H_2O_2 is a physiological signaling molecule that is primarily detoxified by Tsa1 via the Trx system (Figure 2.14) (Herrero et al., 2008; Winterbourn, 2013; Zimmermann et al., in preparation). Recent data from our laboratory indicates that Tsa1 is also a major producer of cellular GSSG after H_2O_2 treatment (Zimmermann et al., in preparation). The reduction of oxidized Trx and GSSG relies on electrons from NADPH. To investigate the redox fluxes induced by exogenous H_2O_2 , the plate reader-based setup described above was validated. To this end, the H_2O_2 diffusion into the cell was monitored by roGFP2-Tsa2 ΔC_R . The H_2O_2

sensor reported a degree of oxidation (OxD) of 0.4 at cellular steady state and was sensitively oxidized after exogenous H_2O_2 application (**Figure 2.15A**). Yet 0.5 mM extracellular H_2O_2 were enough to fully oxidize the Tsa2 ΔC_R moiety. To further verify the H_2O_2 -induced GSSG formation, roGFP2-Grx1 was employed. GSSG/2GSH was rather robust towards oxidation by exogenous H_2O_2 , showing a concentration-dependent oxidation with a subsequent recovery phase (**Figure 2.15B**). Overall, the chosen roGFP2-based probes confirmed the diffusion of exogenous H_2O_2 into the cytosol and the formation of GSSG.

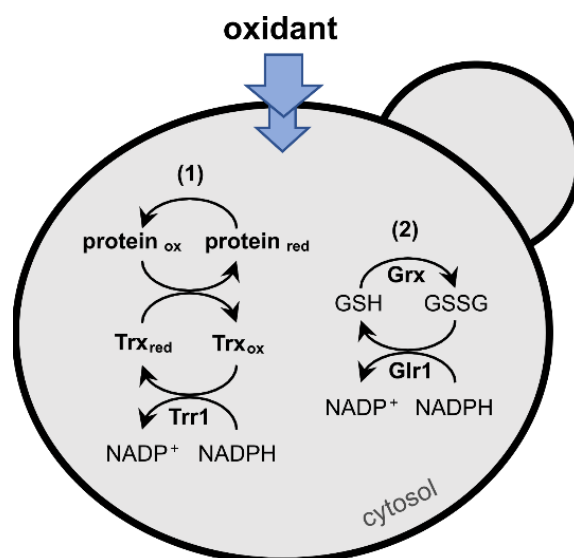


Figure 2.14: Cytosolic mechanisms of NADPH oxidation after exogenous oxidant application to *S. cerevisiae* cells.

Exogenously added oxidant can diffuse through the plasma membrane and the cell wall leading to the oxidation of biological molecules ('oxidative stress') (Grant et al., 1999; Herrero et al., 2008; Toledano et al., 2003). Trx- (1) and GSH-based systems (2) detoxify harmful and damaged molecules via thiol-exchange mechanisms. These systems rely on NADPH as electron source. Glr1, glutathione reductase; Grx, glutaredoxin; ox, oxidized; Prx, peroxiredoxin; red, reduced; Trr1, cytosolic Trx reductase.

Next, the influence of the H_2O_2 treatment on the cytosolic pH was examined. The application of H_2O_2 led to a marginal acidification of the cytosol as reported by pHluorin and SypHer (**Figure 2.15C,D**). The highest H_2O_2 concentration, 5 mM, led to a decrease in pH from ~6.97 to pH ~6.83 (pHluorin) and pH ~6.89 (SypHer). Importantly, the reported changes in pH are not sufficient to interfere with the NAD(P) measurements.

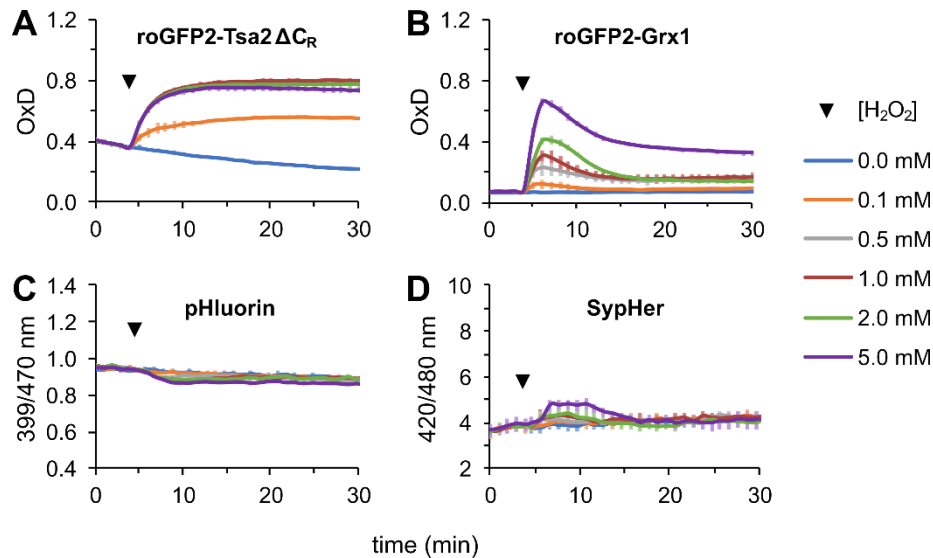


Figure 2.15: Influence of exogenous H_2O_2 on cytosolic roGFP2-Tsa2 ΔC_R , roGFP2-Grx1, and pH in WT strain.

WT cells expressing roGFP2-Tsa2 ΔC_R (A), roGFP2-Grx1 (B), pHluorin (C), or SypHer (D) were treated at the indicated time point (\blacktriangledown) with different concentrations of H_2O_2 during fluorescence plate reader measurement (C and D were adapted from Jakob, 2021). For pHluorin and SypHer calibration curves, refer to **Appendix, Figure S1**.

NADPH is robustly maintained during H_2O_2 challenge

Excess H_2O_2 leads to the accumulation of oxidized Trx and GSSG and the reduction of both depends on NADPH. Consequently, the application of H_2O_2 is expected to reduce the NADPH/NADP⁺ ratio and to lower the cytosolic NADPH concentration. The NAPstar sensors were utilized to validate the response of NADPH/NADP⁺ to exogenous H_2O_2 . NAPstar1, -2 and -3 showed high cpTS/mC ratios throughout the experiment (**Figure 2.16A-C**). The comparison to the fluorescence ratios obtained by the NADPH titration to semipermeabilized cells (**Section 2.3.5**) revealed the saturation of NAPstar1-3 with NADPH at cellular steady state. NAPstar1 and -2 did not respond to any of the H_2O_2 concentrations applied, implicating their NADPH affinities being too high to detect any NADPH oxidation under these conditions. In contrast, the cpTS/mC ratios of NAPstar4 and NAPstarC were constantly low but also robust towards exogenous H_2O_2 (**Figure 2.16D,E**) with values corresponding to those observed in semipermeabilized cells. Hence, NAPstar4 and -C were present in their open conformations and not bound to NADPH. Despite being NADPH-saturated at steady state, NAPstar3 reported an NADPH/NADP⁺ decrease after H_2O_2 treatment (**Figure 2.16C**). At 0.5 mM H_2O_2 , a persistent NADPH/NADP⁺ decrease was observed. Higher concentrations led to a transient NADPH oxidation. The total cpTS/mC changes of NAPstar3 from 1.20 to 1.15 were not pronounced in comparison to the expected

oxidative effect that was visualized by the roGFP2-based sensors (**Figure 2.15A,B**). It is conceivable, that the cytosolic NADPH oxidation is underestimated by NAPstar3 due to its high affinity for NADPH. Overall, the NADPH affinities of NAPstar1, -2, and -4 are not suitable to detect changes in cytosolic NADPH/NADP⁺ ratio after H₂O₂ treatment in the cytosol of WT cells, whereas NAPstar3 registered a decrease in NADPH/NADP⁺.

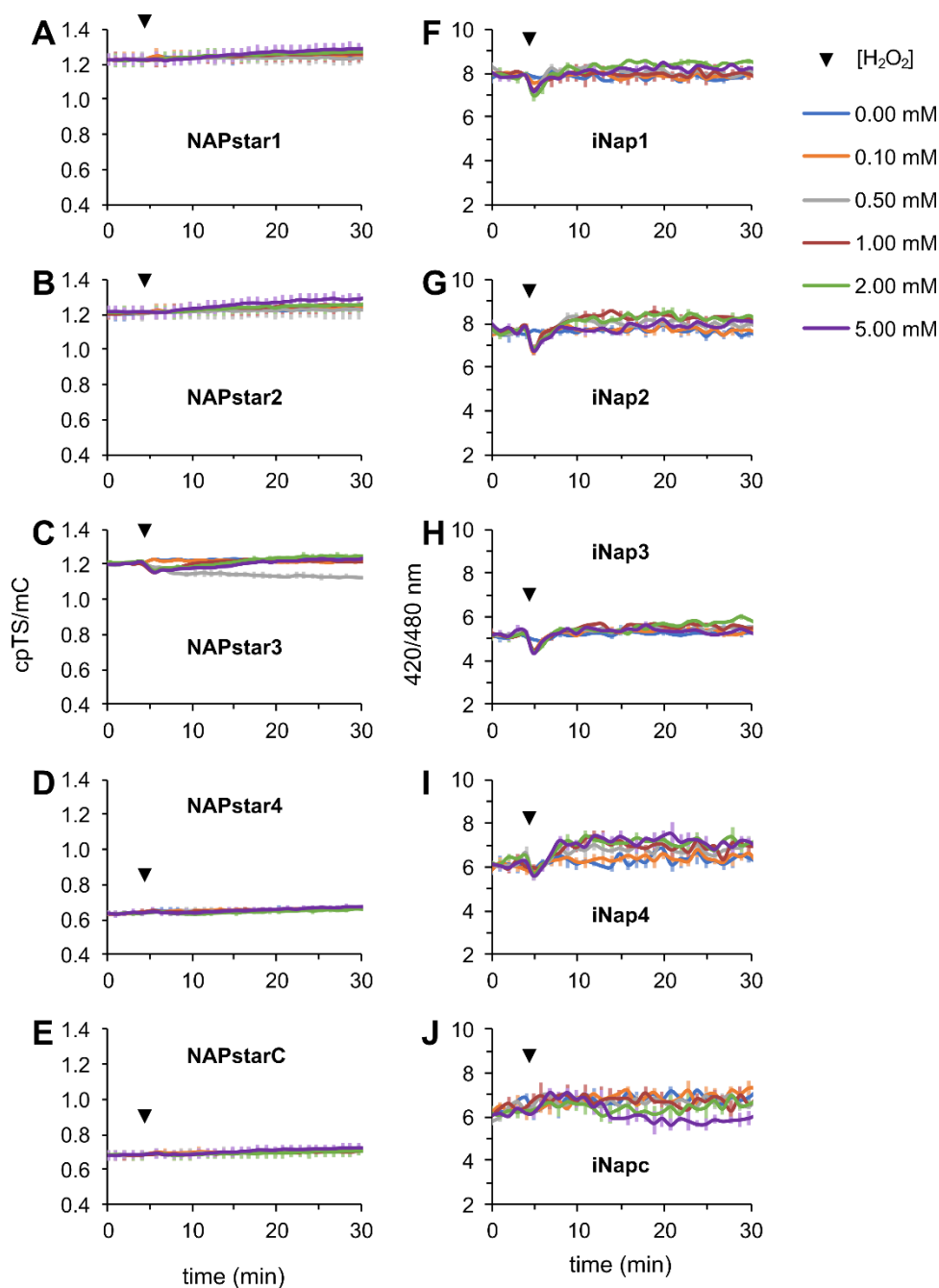


Figure 2.16: Influence of exogenous H₂O₂ on cytosolic NADP in WT strain.

WT cells expressing NAPstar1-4, NAPstarC (A-E were adapted from Jakob, 2021), iNap1-4, or iNapc (F-J) were treated at the indicated time point (▼) with different concentrations of H₂O₂ during fluorescence plate reader measurement.

To monitor the effect of exogenous H_2O_2 on the cytosolic NADPH concentration and to uncover a potential NADPH oxidation, that was overlooked by NAPstar3, the iNap probes were expressed in the WT strain. At cellular equilibrium, the 420/480 nm ratios altered between the different iNap variants according to their NADPH affinities (**Figure 2.16F-I**). By comparison to the NADPH titration data obtained in semipermeabilized cells (**Section 2.1.4**), the different NADPH binding states at cellular equilibrium were calculated. iNap1-4 were NADPH-bound to 78%, 76%, 39%, and 4%, respectively. Although none of the iNap probes was saturated at steady state, led the application of H_2O_2 only to a 2-minute, transient NADPH decline, independent of the applied concentration. This decline was followed by an overshoot in fluorescence ratio of iNap2 and iNap4. Since this overshoot resembled the fluorescence patterns of SypHer and iNapc controls (**Figure 2.15D** and **Figure 2.16J**), and was not registered by iNap3, it is questionable in how far it actually derives from elevated NADPH concentrations. Intriguingly, the mSI-iNap controls did not detect any significant change in the cytosolic NADPH concentration after H_2O_2 treatment due to low reproducibility (**Appendix, Figure S3A-E**) (Bennington, 2019; Schiffmann, 2019). Overall, the results obtained by NAPstar and iNap probes implicate that the cytosolic NADP homeostasis is highly robust against exogenous H_2O_2 -induced oxidation.

NADH/NAD⁺ ratio is transiently reduced by exogenous H_2O_2

The carbon flux, starting from glucose, is divided between glycolysis, producing cytosolic NADH, and the pentose phosphate pathway (PPP), producing cytosolic NADPH (**Figure 2.17A**). H_2O_2 inactivates the glyceraldehyde-3-phosphate dehydrogenase (GAPDH, yeast Tdh3), rerouting the flux from glycolysis to the PPP (Grant et al., 1999; Shenton and Grant, 2003). As a consequence, the cytosolic NADH production decreases to enhance the generation of NADPH to support the antioxidative defense systems. This model would explain the robust NADPH pool observed after the application of H_2O_2 (**Figure 2.16**) and would suggest, that exogenous H_2O_2 leads to a net oxidation of cytosolic NADH resulting from decreased Tdh activity. To check for the influence of H_2O_2 application on the NADH/NAD⁺ balance, the Pdx-mC (DS) and SoNar sensors were expressed in WT strain. In whole cells, Pdx-mC, Pdx-mC DS, and SoNar were occupied with NADH to 82%, 62%, and 81%, as determined by their minimum and maximum fluorescence ratios in semipermeabilized cells (**Section 2.1.1** and **Section 2.2.1**). Due to its high NADH affinity, Pdx-mC showed only a minor and prolonged cpTS/mC decrease from 1.3 to 1.2 after treatment with high H_2O_2 concentrations exceeding 0.5 mM (**Figure 2.17B**). In contrast, the Pdx-mC DS variant demonstrated an initial, transient, and concentration dependent NADH oxidation in all conditions, even after the treatment with buffer (**Figure 2.17C**). At 0.1 mM

and 0.5 mM H₂O₂, an NADH/NAD⁺ recovery was visible after the oxidation leading to a cpTS/mC recovery to the steady state value after ≥ 15 min of measurement time. At 1 mM H₂O₂, a prolonged NADH/NAD⁺ decline was detected. Increase in the H₂O₂ concentration prolonged the phase of low NADH/NAD⁺ ratio. The same effects were observed for SoNar and mSI-SoNar, for which the ratio recovery took longer, indicative for their high NAD⁺ binding affinities (**Figure 2.17D**, **Table 1.2** and **Appendix, Figure S3F**). This data revealed Pdx-mC DS and SoNar being suitable NADH/NAD⁺ ratio sensors in the plate reader-based setup demonstrating that exogenous H₂O₂ leads to a transient and concentration-dependent decrease in the cytosolic NADH/NAD⁺ ratio, possibly via Tdh3 inactivation.

2.4.2 Effect of exogenous diamide on cytosolic NAD(P) redox states

The oxidant tetramethylazodicarboxamide (diamide) is commonly used to induce unspecific thiol oxidation and disulfide formation (Kosower and Kosower, 1995). Due to their high abundance and reactivity, exogenous diamide is expected to primarily oxidize GSH and enzymes of the GSH- and Trx-based systems which in turn require NADPH for reduction. First, the responses of roGFP2-Tsa2ΔC_R and -Grx1 were monitored to confirm the diamide-induced oxidation in the plate reader-based setup. The application of 0.1 mM diamide neither affected roGFP2-Tsa2ΔC_R nor roGFP2-Grx1 (**Figure 2.18A,B**). Higher concentrations up to 2 mM led to a gradual OxD increase of roGFP2-Tsa2ΔC_R. The diamide-induced GSH oxidation, monitored by roGFP2-Grx1, resembled the oxidation mediated by H₂O₂ up to 0.5 mM. Higher diamide concentrations of 1 mM and 2 mM led to a strong sensor oxidation demonstrating massive GSSG/2GSH accumulation with a subsequent recovery phase. The application of 5 and 10 mM diamide led to an immediate and full oxidation of the roGFP2 moieties to OxD 1, indicating the direct oxidation by diamide. Hence, the measurements of roGFP2-based probes confirmed a strong diamide-induced GSH oxidation, especially at high concentrations (≥ 1 mM).

The influence of diamide on the cytosolic pH was imaged using the pHluorin and SypHer probes (**Figure 2.18C,D**). At 2 mM diamide, a mild acidification of the cytosol from pH ~7.03 to pH ~6.86 was observed. 5 and 10 μM diamide persistently acidified the cytosol reaching pH values of ~6.65 (pHluorin) and ~6.54 (SypHer) after 30 min of total measurement time. Hence, high diamide concentrations (≥ 2 mM) strongly decrease the cytosolic pH, potentially leading to artifacts during the following NAD(P) measurements.

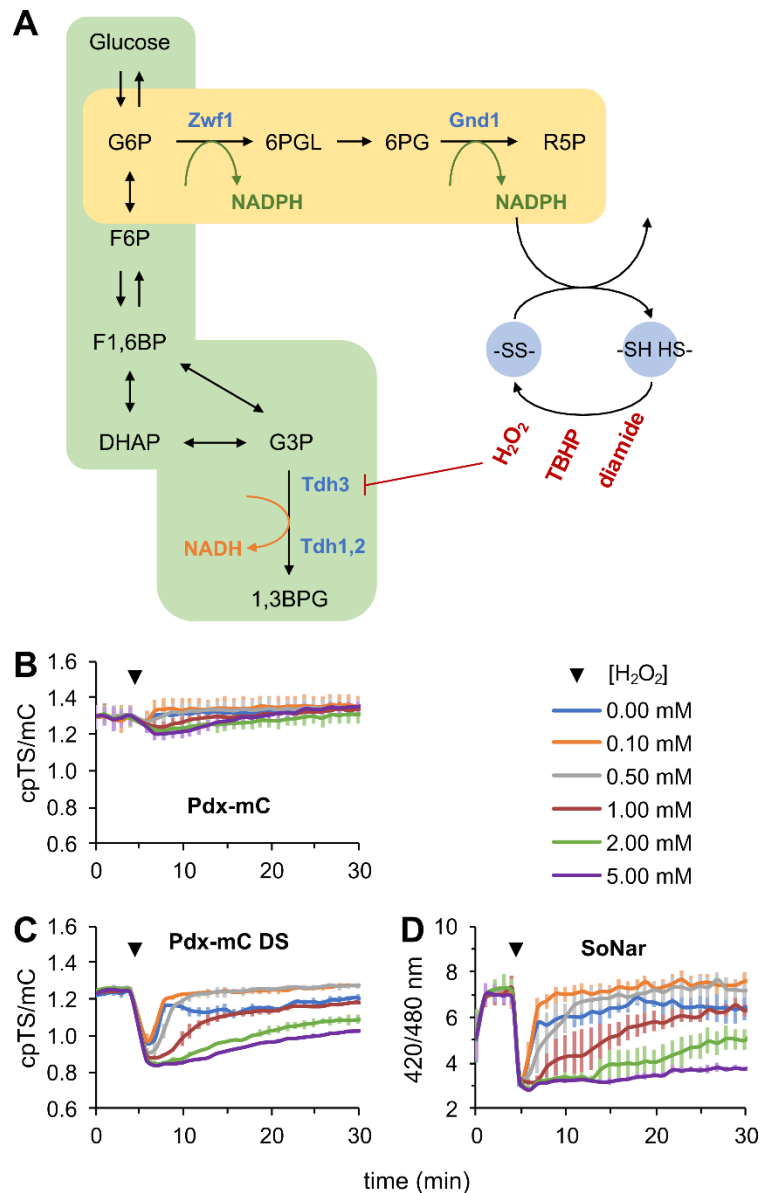


Figure 2.17: Influence of exogenous H_2O_2 on cytosolic NAD in WT strain.

Simplified scheme demonstrating the proposed carbon flux redirection from glycolysis (green) to oxidative PPP (yellow) by H_2O_2 -mediated Tdh3 inactivation (A, adapted from Peralta et al., 2015 and Shenton and Grant, 2003). This enhances the production of NADPH which is required to reduce oxidized thiol groups of the Trx and GSH systems (-SS-). Opposing to H_2O_2 , diamide and TBHP do not influence Tdh3 activity (Grant et al., 1999). WT cells expressing Pdx-mC (B), Pdx-mC DS (C), or SoNar (D) were treated at the indicated time point (\blacktriangledown) with different concentrations of H_2O_2 during fluorescence plate reader measurement (B and C adapted from Jakob, 2021). 1,3BPG, 1,3-bisphosphoglycerate; DHAP, dihydroxyacetone phosphate; F1,6BP, fructose-1,6-bisphosphate; F6P, fructose-6-phosphate; G3P, glyceraldehyde-3-phosphate; G6P, glucose-6-phosphate; 6PG, 6-phosphogluconate; 6PGL, 6-phosphogluconolactone; R5P, ribulose-5-phosphate; -SH, reduced thiol group of proteins or GSH.

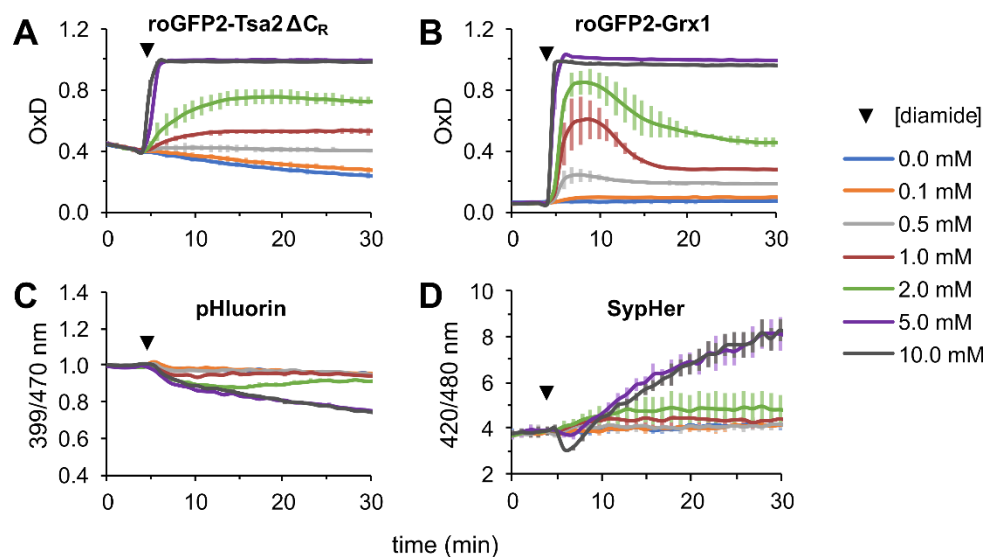


Figure 2.18: Influence of exogenous diamide on cytosolic roGFP2-Tsa2 Δ C_R, roGFP2-Grx1, and pH in WT strain.

WT cells expressing either roGFP2-Tsa2 Δ C_R (A), roGFP2-Grx1 (B), pHluorin (C), or SypHer (D) were treated at the indicated time point (\blacktriangledown) with different concentrations of diamide during fluorescence plate reader measurement (C and D were adapted from Jakob, 2021). For pHluorin and SypHer calibration curves, refer to **Appendix, Figure S1**.

Diamide-induced NADP oxidation resembles cytosolic acidification

The strong oxidative effect of diamide is expected to end up in a high consumption of NADPH, decreasing the cytosolic NADPH/NADP⁺ ratio. To check for NADPH oxidation, NAPstar expressing WT cells were treated with diamide during fluorescence measurements (**Appendix, Figure S4**). At the highest diamide concentrations of 5 mM and 10 mM, the cpTS/mC ratio of the control sensor, NAPstarC, decreased slightly from 0.68 to 0.60 (**Appendix, Figure S4G**), most likely due to the cytosolic acidification. To exclude this artifact from the final NAPstar readout, the cpTS/mC ratios of NAPstar1-4 were normalized to that of NAPstarC. After supplementation of 5 mM and 10 mM diamide, norm. cpTS/mC ratios of NAPstar1 and -2 decreased from 1.72 to 1.50 (**Figure 2.19A,B**). A stronger cpTS/mC response was observed for NAPstar3 (**Figure 2.19C**). The application of 2 mM diamide lowered the norm. cpTS/mC of NAPstar3 from 1.85 to 1.58 and higher diamide concentrations led to an almost complete norm. cpTS/mC decline. Nonetheless, the fluorescence ratio responses of NAPstar1-3 occurred only at very high diamide concentrations and thus possibly derive from pH alterations.

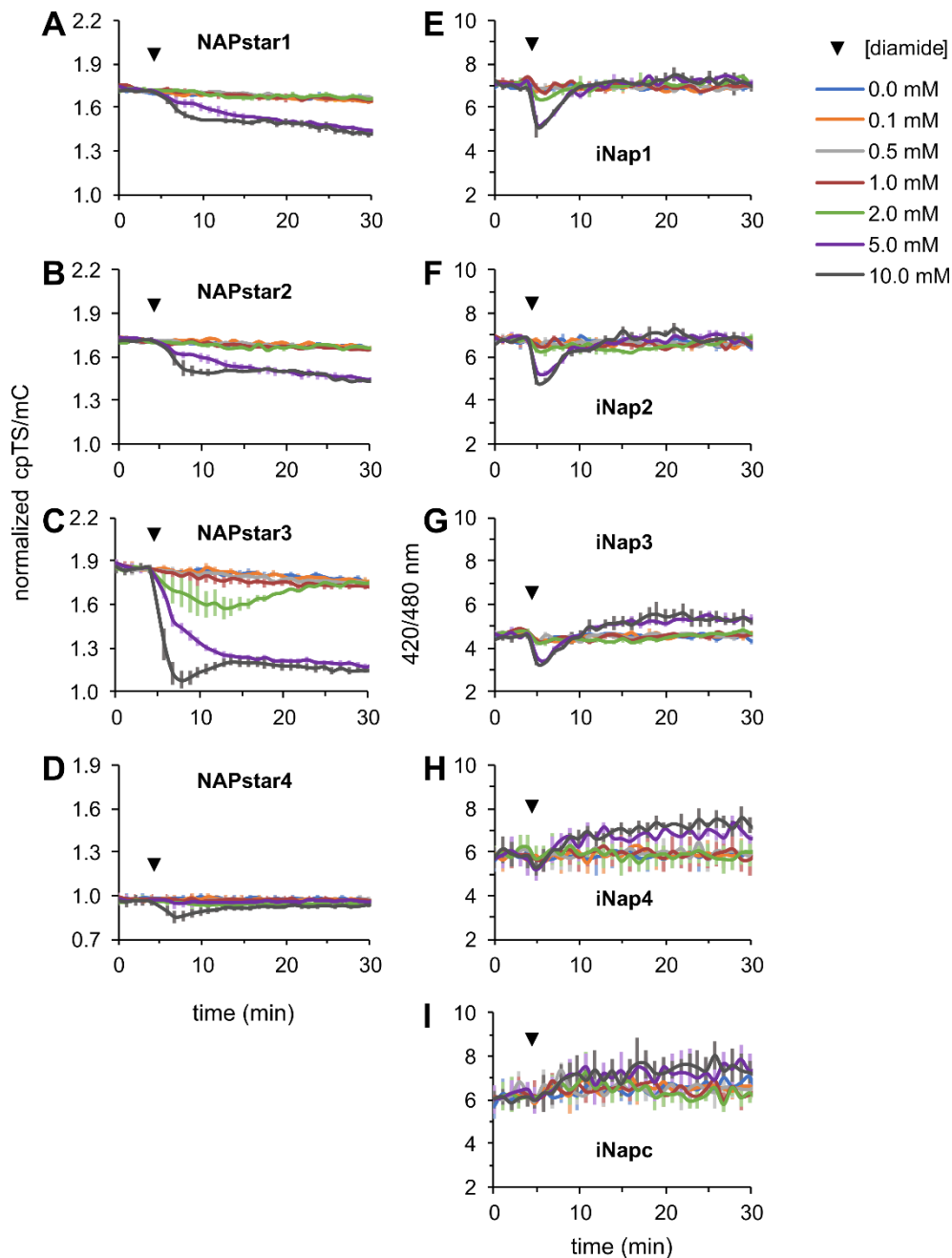


Figure 2.19: Influence of exogenous diamide on cytosolic NADP in WT strain.

WT cells expressing NAPstar1-4, NAPstarC (A-D were adapted from Jakob, 2021), iNap1-4, or iNapc (F-J) were treated at the indicated time point (▼) with different concentrations of diamide during fluorescence plate reader measurement.

To determine the influence of exogenous diamide on the cytosolic NADPH concentration, the iNap sensors were utilized. Similar to the results received for the H₂O₂ treatments (Section 2.4.1), the drop in NADPH, reported by iNap1-3, was transient at 5 mM exogenous diamide (Figure 2.19E-G). Nonetheless, since the 420/480 nm ratio of SypHer strongly and persistently increased after treatment with 5 mM and 10 mM diamide, the

NADPH oxidation is potentially underestimated. The fluorescence of iNap4 and iNapc were barely affected by the different diamide treatments (**Figure 2.19H,I**). In contrast to the iNap sensors, mSI-iNap1-3 demonstrated a prolonged NADPH decrease after treatment with 5 mM and 10 mM diamide and mSI-iNap2 detected a concentration-dependent NADPH oxidation at 1 mM and 2 mM diamide (**Appendix, Figure S5A-C**). The cpYFP/mSI ratios of mSI-iNap4 and -c were not affected by diamide (**Appendix, Figure S5D,E**). Interestingly, the mSI-iNap sensors did not detect an NADPH oxidation upon H₂O₂, but after diamide application. The registered decrease in the fluorescence ratios was very similar to the NADPH/NADP⁺ oxidation kinetics observed by NAPstar3. Overall, these results question in how far the observed GFI responses derive from specific NADPH oxidation and in how far they are caused by measurement artifacts. Nonetheless, they clearly show that cytosolic NADPH is highly robust toward diamide-induced oxidation.

NADH/NAD⁺ ratio is transiently reduced by exogenous diamide

In mammalian cells, the cytosolic NADH/NAD⁺ ratio (determined by SoNar) was reported to be robust towards diamide treatment (Zou et al., 2018), whereas in bacteria, the NADH/NAD⁺ ratio (reported by Pdx-mC) even increased after diamide treatment (Bhat et al., 2016b). Diamide is not expected to influence the cytosolic NADH/NAD⁺ ratio in *S. cerevisiae* as it does not lead to Tdh inactivation (Grant et al., 1999). To determine the influence of exogenous diamide on the cytosolic NAD redox state in *S. cerevisiae*, WT cells expressing either Pdx-mC (DS) or SoNar were subjected to the application of diamide. The Pdx-mC (DS) and NAPstar structures are closely related and expected to be affected by similar artifacts caused by the pH alterations. Hence, the Pdx-mC (DS) cpTS/mC readouts (**Appendix, Figure S4A,B**) were corrected by normalization to the NAPstarC signal. The resulting fluorescence ratio responses of Pdx-mC DS and SoNar to exogenous diamide strongly resembled those observed for H₂O₂ (**Figure 2.20A-C**) with a fast, initial decrease, and a concentration-dependent recovery phase. Intriguingly, these results indicate, contrary to reports in the literature, a diamide-mediated inactivation of Tdh, decreasing NADH/NAD⁺.

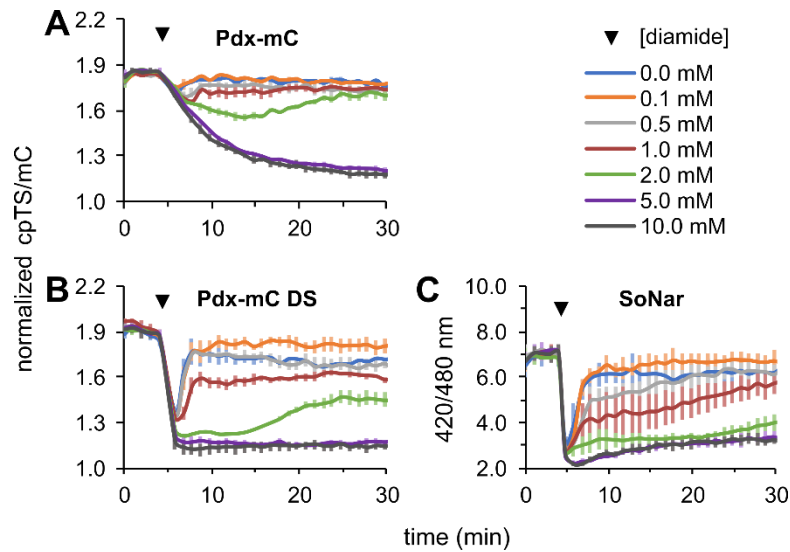


Figure 2.20: Influence of exogenous diamide on cytosolic NAD in WT strain.

WT cells expressing Pdx-mC (A), Pdx-mC DS (B), or SoNar (C) were treated at the indicated time point (▼) with different concentrations of diamide during fluorescence plate reader measurement (A and B were adapted from Jakob, 2021).

2.4.3 Effect of exogenous TBHP on cytosolic NAD(P) redox states

The organic *tert*-butyl hydroperoxide (TBHP) is commonly used as an oxidant during synthetic processes and for disinfection. TBHP is more lipophilic than H_2O_2 and thus expected to produce enhanced amounts of lipid peroxides (Linden et al., 2008; Masaki et al., 1989; Wenz et al., 2018). The detoxification of TBHP is primarily accomplished by NADPH-dependent Trx and GSH systems. In addition, the roGFP2-Tsa2 ΔC_R sensor was shown to be sensitive to the direct oxidation by TBHP in vitro (Morgan et al., 2016). Indeed, 0.1 mM of exogenous TBHP increased the OxD of roGFP2-Tsa2 ΔC_R to 0.5 in WT strain (Figure 2.21A). A 10- and 100-fold increase in extracellular TBHP concentration further elevated the sensor OxD to 0.6. In contrast, the application of 0.1 mM TBHP barely affected the roGFP2-Grx1 oxidation, 1 and 10 mM exogenous TBHP increased the sensor OxD to 0.35 and 0.55, respectively (Figure 2.21B). Altogether, roGFP2-Tsa2 ΔC_R and roGFP2-Grx1 confirmed that TBHP diffuses into the cell leading to the accumulation of GSSG.

The influence of TBHP on the cytosolic pH was monitored using pHluorin and SypHer. Neither the fluorescence ratio of pHluorin nor that of SypHer was affected by any of the tested TBHP concentrations (Figure 2.21C,D). Hence, TBHP-driven pH artifacts are not expected to play a role during GFI-based NAD(P) measurements.

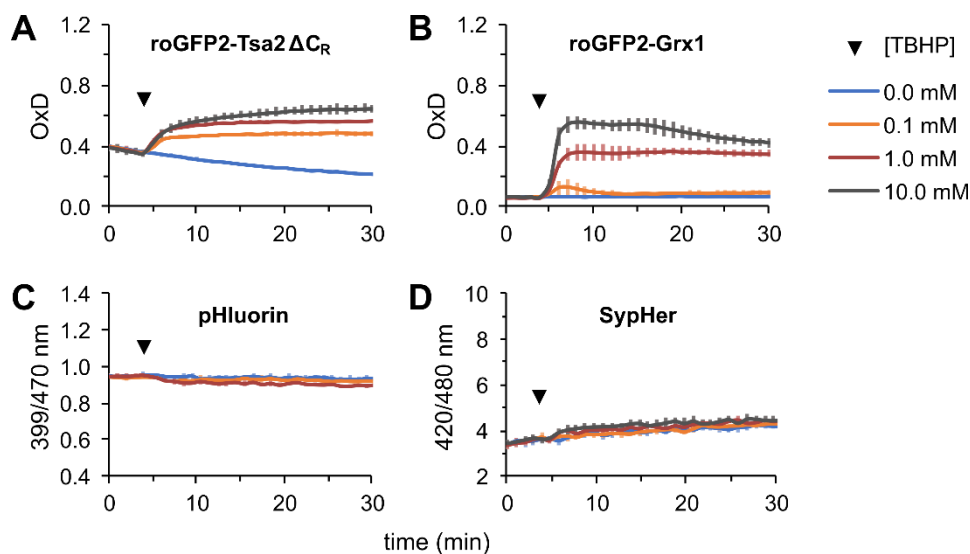


Figure 2.21: Influence of exogenous TBHP on cytosolic roGFP2-Tsa2 Δ C_R, roGFP2-Grx1, and pH in WT strain.

WT cells expressing either roGFP2-Tsa2 Δ C_R (A), roGFP2-Grx1 (B), pHluorin (C), or SypHer (D) were treated at the indicated time point (▼) with different concentrations of TBHP during fluorescence plate reader measurement (C and D were adapted from Jakob, 2021). For pHluorin and SypHer calibration curves, refer to **Appendix, Figure S1**.

NADPH is robustly maintained during TBHP challenge

To investigate the TBHP-induced oxidation of NADPH, the NADPH/NADP⁺ ratio was monitored using the NAPstar sensors. Indeed, the TBHP application decreased NADPH/NADP⁺ as detected by NAPstar3 (**Figure 2.22C**). After the treatment with 0.1 mM TBHP, the NADPH/NADP⁺ oxidation from cpTS/mC 1.20 to 1.11 was partially reversible, whereas 1 mM exogenous TBHP led to an irreversible oxidation. NAPstar1 and -2 were again saturated with NADPH throughout the experiment and did not report any change in the NADPH/NADP⁺ ratio after TBHP application (**Figure 2.22A,B**). In contrast, the addition of 1 mM TBHP induced a strong oxidation artifact in NAPstar4 and NAPstarC (**Figure 2.22D,E**), increasing the cpTS/mC ratios. This effect was apparently not present in NAPstar1-3, indicating that only the open probe conformation was affected. Nevertheless, higher TBHP concentrations were not tested for NAPstar or Pdx-mC (DS) sensors. The cytosolic NADPH concentration determined by iNap1-4 decreased slightly after the TBHP bolus, followed by a prolonged recovery phase (**Figure 2.22F-I**). Opposing to NAPstar4 and -C, the fluorescence ratio of iNapc was not affected by TBHP (**Figure 2.22J**). The control measurements employing the mSI-iNap sensors resembled the TBHP-induced oxidation kinetics of both, NAPstar3 and iNap probes, but interexperimental variations were very high (**Appendix, Figure S6**). Overall, the detected TBHP-induced NADP oxidation was low.

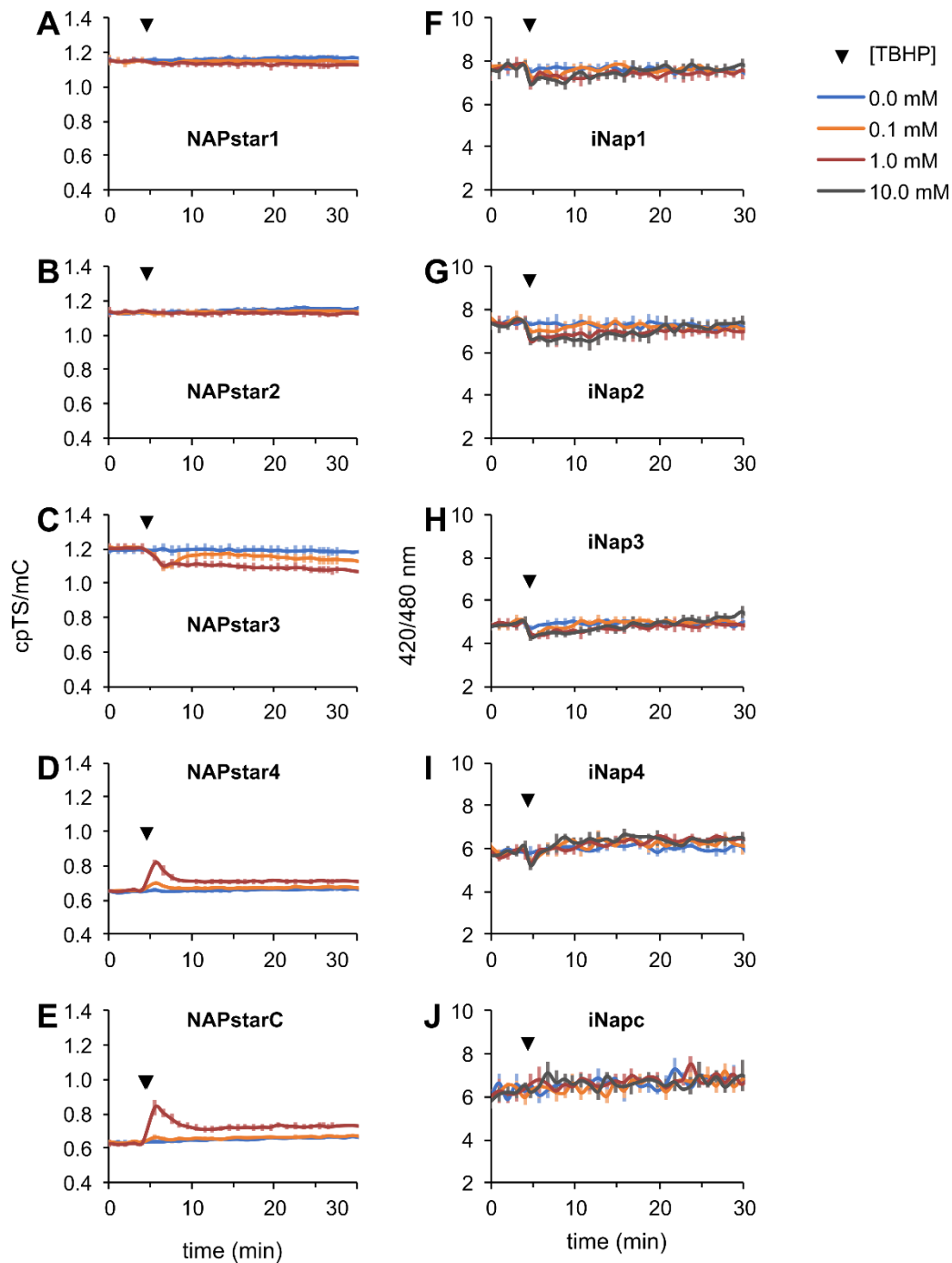


Figure 2.22: Influence of exogenous TBHP on cytosolic NADP in WT strain.

WT cells expressing NAPstar1-4, NAPstarC (A-E were adapted from Jakob, 2021), iNap1-4, or iNapc (F-J) were treated at the indicated time point (▼) with different concentrations of TBHP during fluorescence plate reader measurement.

NADH/NAD⁺ is not affected by exogenous TBHP

The Tdh activity was reported to be robust against TBHP-induced oxidation (Grant et al., 1999; Peralta et al., 2015). Hence, the TBHP application was not expected to affect the cytosolic NADH/NAD⁺ ratio. To confirm this hypothesis, Pdx-mC (DS) and SoNar sensors were expressed in WT cells and subjected to TBHP treatment. Indeed, the Pdx-mC (DS) and SoNar fluorescence ratios were not altered by exogenous TBHP (Figure 2.23A-C), probably due to continuous Tdh activity.

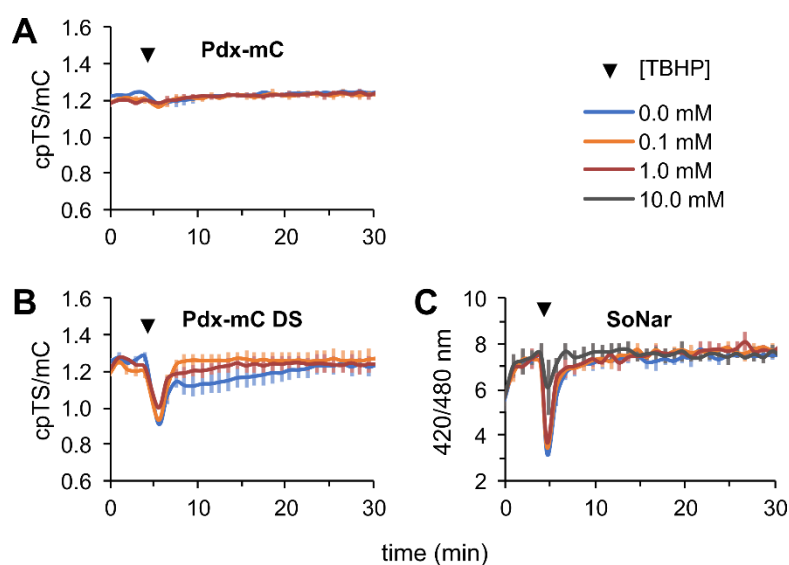


Figure 2.23: Influence of exogenous diamide on cytosolic NAD in WT strain.

WT cells expressing Pdx-mC (A), Pdx-mC DS (B), or SoNar (C) were treated at the indicated time point (▼) with different concentrations of TBHP during fluorescence plate reader measurement (A and B were adapted from Jakob, 2021).

This chapter described the combination of the plate reader-based setup with various GFIs expressed in a WT yeast strain. This approach was shown to provide an excellent platform to investigate the impact of exogenous H₂O₂, diamide, and TBHP on several cytosolic parameters such as GSSG/2GSH, NADPH/NADP⁺, NADPH, and NADH/NAD⁺. Overall, the TBHP- and H₂O₂-induced oxidation of roGFP2-Tsa2ΔC_R, -Grx1 and NADPH corresponded to each other with NADPH being remarkably robust. The diamide-triggered oxidation of roGFP2-Tsa2ΔC_R, -Grx1 and NADPH appeared stronger, but the impact of diamide on the cytosolic pH hampers direct comparisons. Remarkably, H₂O₂ and diamide led to similar NADH/NAD⁺ oxidation kinetics, whereas exogenous TBHP failed to affect the NADH/NAD⁺ ratio, hinting on differential Tdh redox regulation mechanisms.

2.5 Role of the PPP in NADPH production during acute oxidative stress

The cytoplasmic glucose-6-phosphate dehydrogenase (G6PDH, *S. cerevisiae* Zwf1) catalyzes the first, irreversible, and rate-limiting step of the PPP (Nogae and Johnston, 1990). In the presence of glucose, Zwf1 is regarded the main producer of NADPH in the yeast cytosol (Frick and Wittmann, 2005; Grabowska and Chelstowska, 2003; Minard and McAlister-Henn, 2005). The $\Delta zwf1$ strain was reported to be more resilient to low concentrations of H_2O_2 , but more sensitive towards diamide and high doses of H_2O_2 (Larochelle et al., 2006; Ng et al., 2008; Nogae and Johnston, 1990; Yoshikawa et al., 2021). Further, the deletion of *ZWF1* decreases the whole cell NADPH concentration (Hector et al., 2009; Yoshikawa et al., 2021). Due to the reduced NADPH availability, the efficient maintenance of a low GSSG/2GSH ratio via the activity of the glutathione reductase Glr1 is hampered, resulting in increased GSSG/2GSH ratios (Izawa et al., 1998). To determine the contribution of Zwf1 to the NADPH/NADP⁺ balance at cellular equilibrium and during oxidative stress, *ZWF1* was deleted and the cytosolic H_2O_2 and GSSG/2GSH levels, as well as the NADPH/NADP⁺ and NADH/NAD⁺ ratios were monitored by GFI measurements. To this end, a fluorescence plate reader-based assay was performed during which $\Delta zwf1$ cells were treated with either H_2O_2 , diamide or TBHP. First, the cytosolic H_2O_2 levels were determined using roGFP2-Tsa2 ΔC_R . The steady state OxD (**Table 2.3**), as well as the sensor responses to exogenous H_2O_2 and diamide (**Figure 2.24A,B**), were not altered by the *ZWF1* deletion. Interestingly, the roGFP2-Tsa2 ΔC_R sensor was more sensitive to TBHP application in the $\Delta zwf1$ strain (**Figure 2.24C**). Next, the cytosolic GSSG/2GSH ratio was monitored using roGFP2-Grx1. Corresponding to the reports from the literature, the GSSG/2GSH ratio was elevated in $\Delta zwf1$, reflected by an increased OxD value of 0.24 (**Table 2.3**). Further, GSSG/2GSH was sensitively oxidized after H_2O_2 and TBHP applications (**Figure 2.24D,F**). Surprisingly, the GSSG/2GSH robustness towards diamide was slightly increased (**Figure 2.24E**). Overall, the expression of roGFP2-based probes in $\Delta zwf1$ revealed pleiotropic effects after the different oxidant treatments.

To monitor the cytosolic NADPH/NADP⁺ and NADH/NAD⁺ ratios, NAPstar3 and Pdx-mC DS sensors were utilized. For the diamide experiments, the cpTS/mC ratios of NAPstar3 and Pdx-mC DS were normalized to those of NAPstarC to exclude pH artifacts (**Section 2.4.2**). In contrast to diamide, the application of H_2O_2 or TBHP did not affect the NAPstarC readout (data not shown). Steady state norm. cpTS/mC values of 1.89 (NAPstar3) and 1.92 (Pdx-mC DS) implied that the deletion of *ZWF1* does not affect basal cytosolic NADPH/NADP⁺ and NADH/NAD⁺ ratios (**Table 2.3**). Thus, the yeast metabolism is able to compensate for the loss of Zwf1 at cellular equilibrium to maintain physiological

NADP and NAD redox balances. For all oxidants tested, the NADPH/NADP⁺ ratio response detected by NAPstar3 mirrored the oxidation of roGFP2 probes (**Figure 2.24G-I**). The NADPH oxidation after H₂O₂ and TBHP treatments was significantly increased in the $\Delta zwf1$ mutant. Surprisingly, the NADPH/NADP⁺ oxidation kinetics after the application of diamide was similar to that observed in WT cells. The cytosolic, Pdx-mC-DS-sensed NADH/NAD⁺ ratio was hardly affected by the *ZWF1* deletion in any of the tested conditions (**Figure 2.24J-L**). Overall, the *ZWF1* deletion did not affect steady state NAD(P)H/NAD(P)⁺ ratios but rendered the NADP redox state much more sensitive towards H₂O₂ and TBHP. The sensitization of the cytosolic NADPH/NADP⁺ ratio in the $\Delta zwf1$ mutant validates the PPP being an important NADPH producer during acute oxidative stress.

Table 2.3: Steady state readouts of roGFP2-Tsa2 Δ C_R, roGFP2-Grx1, NAPstar3 and Pdx-mC DS expressed in the cytosol of the investigated yeast strains.

Listed is the average readout before oxidant application (steady state). Readouts reflecting increased oxidative or reductive states were marked in orange or blue, respectively. The cpTS/mC values of Pdx-mC DS and NAPstar3 were normalized to that of NAPstarC. Norm. cpTS/mC deviation > 0.05 from WT was considered significant.

	OxD		Norm. cpTS/mC	
	roGFP2-Tsa2 Δ C _R	roGFP2-Grx1	NAPstar3	Pdx-mC DS
WT	0.4	0.07	1.84	1.90
$\Delta zwf1$	0.4	0.24	1.89	1.92
$\Delta glr1$	0.8	0.33	1.95	2.11
$\Delta trx1\Delta trx2$	0.6	0.22	1.82	1.80
$\Delta tsa1\Delta tsa2$	0.7	0.07	2.04	2.10

2.6 Influence of GSH- and Trx-based antioxidant systems on cytosolic NAD(P) redox homeostasis during oxidative stress

The NADPH consumption during oxidative challenge is directly linked to the activity of GSH- and Trx-based systems (**Figure 2.14**). To gain further insights into the underlying redox mechanisms, the electron fluxes through these antioxidative systems were interrupted at various stages by distinct gene deletions. The respective consequences for the cytosolic H_2O_2 concentration (roGFP2-Tsa2 ΔC_R), the GSSG/2GSH (roGFP2-Grx1), NADPH/NADP⁺ (NAPstar3) and NADH/NAD⁺ (Pdx-mC DS) ratios were determined by GFI measurements in the plate reader-based assay. To stimulate the electron flux through the antioxidative pathways, acute oxidative challenge was induced by the application of either H_2O_2 or diamide.

2.6.1 *GLR1* deletion abolishes any detectable H_2O_2 - and diamide-induced NADPH oxidation

Different mechanisms contribute to a reduced cytosolic GSSG/2GSH ratio (Morgan et al., 2013). An important source of GSH, especially during acute oxidative stress, is the NADPH-dependent reduction of GSSG by Glr1 (Collinson and Dawes, 1995). Deletion of *GLR1* decreases the oxidative stress resistance (Outten et al., 2005) and lowers the cytosolic GSH/2GSSG ratio (Morgan et al., 2013) due to insufficient GSH regeneration. To validate the influence of the *GLR1* deletion on the cytosolic redox state and on the sensitivity towards oxidants, roGFP2-Tsa2 ΔC_R was employed. Since this probe depends on GSH for reduction, a consistent shift to higher OxD values in the Δglr1 strain can be expected, irrespective of actual H_2O_2 concentrations. Indeed, basal OxD levels were elevated to 0.8 (**Table 2.3**), but the *GLR1* deletion did apparently not alter the roGFP2-Tsa2 ΔC_R oxidation kinetics after the application of H_2O_2 or diamide (**Figure 2.25A** and **Figure 2.26A**). As reported before, the *GLR1* deletion increased the roGFP2-Grx1 OxD value at cellular steady state to 0.33, validating the oxidized cytosolic GSSG/2GSH ratio (**Table 2.3**) (Morgan et al., 2013). Exogenous H_2O_2 and diamide application led to very strong roGFP2-Grx1 responses in Δglr1 (**Figure 2.25B** and **Figure 2.26B**). Overall, the deletion of *GLR1* elevated the GSSG/2GSH ratio and sensitized GSSG/2GSH to H_2O_2 - and diamide-induced oxidation.

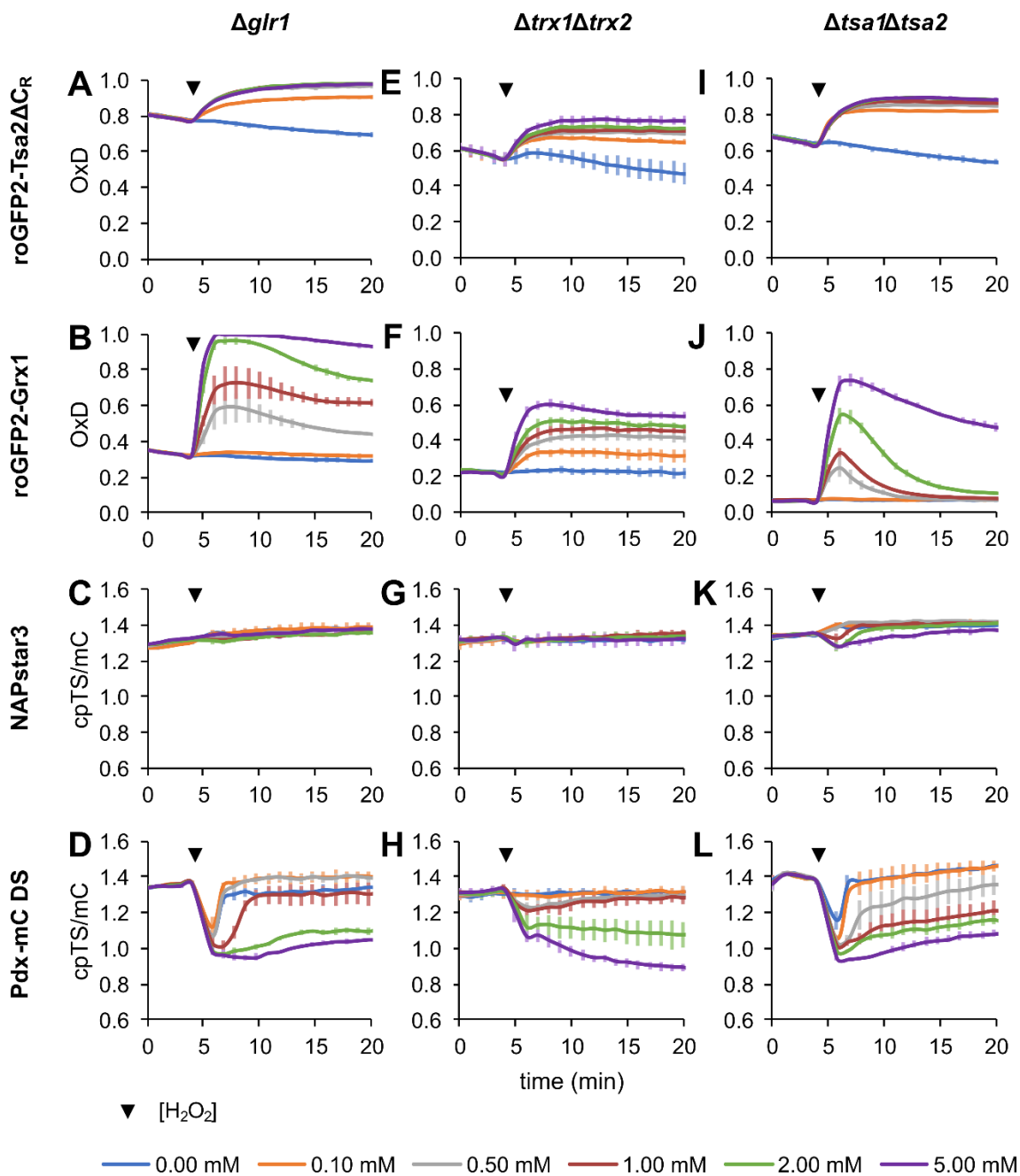


Figure 2.25: Influence of exogenous H₂O₂ on cytosolic roGFP2-Tsa2Δ_{CR}, roGFP2-Grx1, NAPstar3, and Pdx-mC DS in $\Delta glr1$, $\Delta trx1\Delta trx2$, and $\Delta tsa1\Delta tsa2$ strains.

$\Delta glr1$ (A-D), $\Delta trx1\Delta trx2$ (E-H) and $\Delta tsa1\Delta tsa2$ (I-L) strain expressing either roGFP2-Tsa2Δ_{CR} (first), roGFP2-Grx1 (second), NAPstar3 (third) or Pdx-mC DS (fourth row) were treated at the indicated time point (▼) with different concentrations of H₂O₂ during plate reader measurement (C, D, G, and H were adapted from Jakob, 2021).

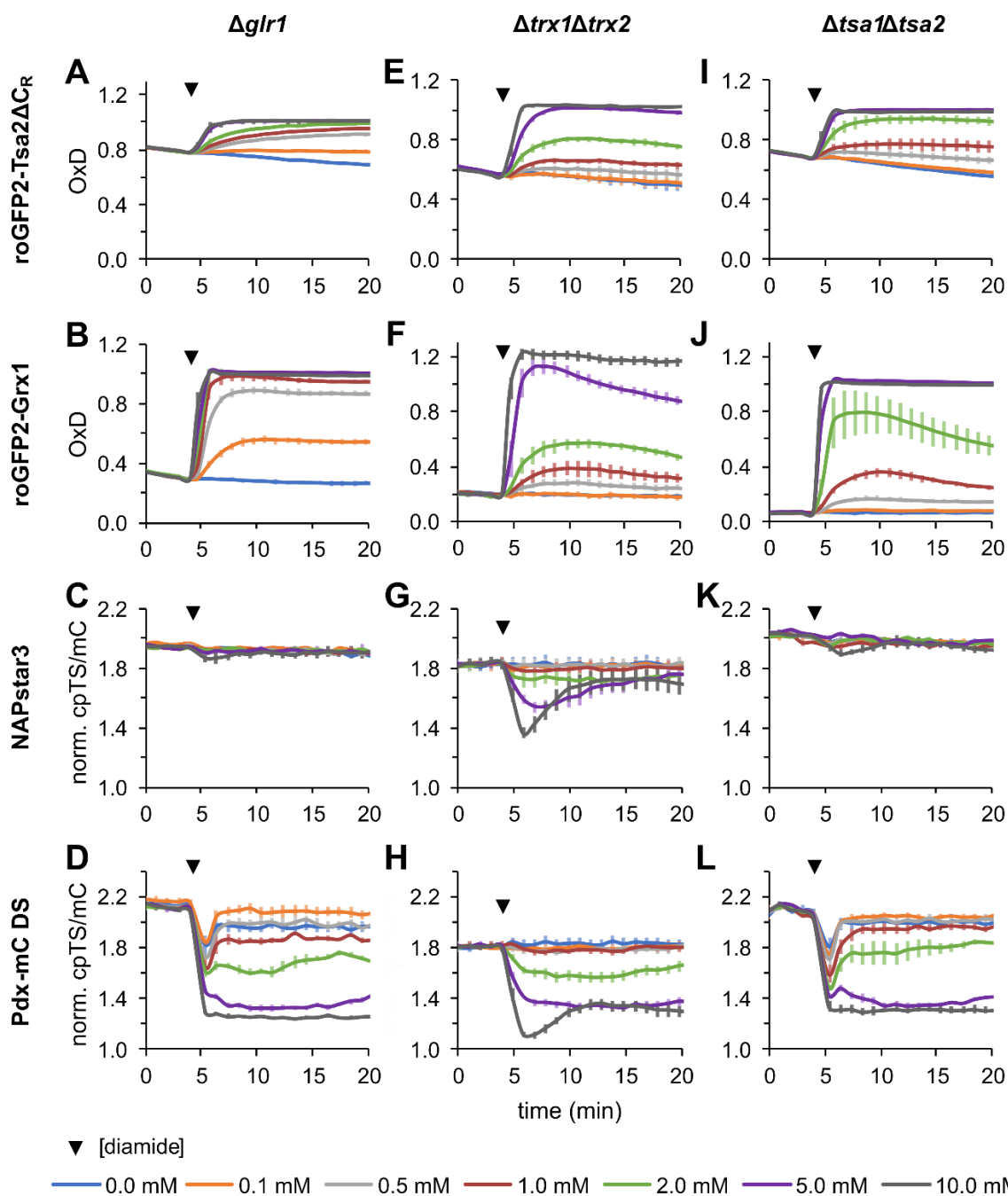


Figure 2.26: Influence of exogenous diamide on cytosolic roGFP2-Tsa2 Δ C_R, roGFP2-Grx1, NAPstar3, and Pdx-mC DS in Δ glr1, Δ trx1 Δ trx2, and Δ tsa1 Δ tsa2 strains.

Δ glr1 (A-D), *Δ trx1 Δ trx2* (E-H) and *Δ tsa1 Δ tsa2* strain expressing either roGFP2-Tsa2 Δ C_R (first), roGFP2-Grx1 (second), NAPstar3 (third) or Pdx-mC DS (fourth row) were treated at the indicated time point (▼) with different concentrations of diamide during plate reader measurement (C, D, G, and H were adapted from Jakob, 2021). NAPstar3 and Pdx-mC DS cpTS/mC ratios were normalized to average cpTS/mC of NAPstarC.

As cytosolic GSSG cannot readily be reduced to GSH in an NADPH-dependent manner in the absence Glr1, the NADPH consumption driven by exogenously added oxidants is expected to be diminished in the *Δ glr1* strain. To verify this hypothesis, NAPstar3

was employed. Further, the Pdx-mC DS probe was utilized to investigate the influence of the deletion on the NADH/NAD⁺ ratio. Respective cpTS/mC ratios were normalized to the signal of NAPstarC for diamide experiments, since high diamide concentrations led to artifacts in the NAPstarC readout (data not shown). This normalization revealed increased basal norm. cpTS/mC ratios of 1.95 for NAPstar3 and 2.11 for Pdx-mC DS and thus increased cytosolic NADPH/NADP⁺ and NADH/NAD⁺ ratios for the $\Delta glr1$ mutant (**Table 2.3**). The application of H₂O₂ and diamide revealed the *GLR1* deletion impeding any detectable decrease in NADPH/NADP⁺ (**Figure 2.25C** and **Figure 2.26C**). In contrast, the response pattern of the NADH/NAD⁺ ratio, measured by Pdx-mC DS, did not seem to be altered in the deletion strain (**Figure 2.25D** and **Figure 2.26D**). These results support the hypothesis that the Glr1 activity contributes significantly to the H₂O₂- and diamide-induced NADPH consumption.

2.6.2 *TRX1 TRX2* double deletion renders NADP and NAD pools more robust towards H₂O₂ and diamide

Glr1 was chosen as target to shut off a central GSH source and NADPH sink of the GSH-based antioxidant system. The cytosolic thioredoxin reductase (Trr1) represents the corresponding counterpart of the Trx system. Since the deletion of *TRR1* is lethal in the BY4742 (S288C) background (Giaever et al., 2002) the genes encoding for the Trr1 substrates, *TRX1* and *TRX2*, were deleted instead (Herrero et al., 2008; Toledano et al., 2003). Basal H₂O₂ levels, determined by roGFP2-Tsa2ΔC_R, were enhanced to OxD 0.6 in the $\Delta trx1\Delta trx2$ double deletion strain (**Table 2.3**), but the sensor oxidation kinetics after H₂O₂ and diamide treatments were apparently not altered (**Figure 2.25E** and **Figure 2.26E**) (Morgan et al., 2016). In addition, the cytosolic GSSG/2GSH ratio was moderately increased in the $\Delta trx1\Delta trx2$ strain at steady state, reflected by a roGFP2-Grx1 OxD of 0.22 (**Table 2.3**). The application of increasing H₂O₂ concentrations stepwise increased the cytosolic GSSG/2GSH ratio, similar to observations made in the WT strain (**Figure 2.25F**). In contrast, the GSSG/2GSH robustness towards exogenous diamide was increased (**Figure 2.26F**), even 2 mM extracellular diamide oxidized the roGFP2-Grx1 sensor only to OxD 0.5. This underlines the great resilience of the *TRX1 TRX2* double deletion strain towards diamide and thus, thiol oxidation stress (Muller, 1996). Interestingly, almost no reduction of oxidized roGFP2 sensor was observed, although the responsible GSH-based system should be functional in the $\Delta trx1\Delta trx2$ strain.

The cytosolic NADPH/NADP⁺ ratio was monitored in the $\Delta trx1\Delta trx2$ mutant by NAPstar3. While the steady state NADPH/NADP⁺ ratio was not affected (**Table 2.3**),

abolished the *TRX1 TRX2* deletion any detectable NADPH/NADP⁺ oxidation after H₂O₂ application (**Figure 2.25G**). Opposing, the NADPH/NADP⁺ resilience towards diamide was increased, but still detectable (**Figure 2.26K**). Pdx-mC DS was employed to monitor the cytosolic NADH/NAD⁺ ratio that was lowered in the $\Delta trx1\Delta trx2$ mutant at steady state (**Table 2.3**). Compared to the WT strain, the NADH/NAD⁺ ratio was much more robust against H₂O₂- and diamide-driven oxidation (**Figure 2.25H** and **Figure 2.26H**). Remarkably, even the initial NADH/NAD⁺ decline after buffer addition was absent. These results suggest that the reduction of Trx1 and Trx2 by Trr1 consumes relevant NADPH amounts during H₂O₂ (and diamide) -induced oxidative challenge. The highly stabilized cytosolic NADH/NAD⁺ ratio indicates metabolic adaptations upon the *TRX1 TRX2* double deletion.

2.6.3 *TSA1 TSA2* double deletion increases the robustness of cytosolic NAD(P) redox states towards diamide, but not H₂O₂

The cytosolic peroxiredoxins Tsa1 and Tsa2 are important for H₂O₂ signal transduction and detoxification (Amponsah et al., 2021; Netto and Antunes, 2016; Toledano et al., 2003). Moreover, recent data from our laboratory indicates that mainly Tsa1 is responsible for the peroxide-induced GSSG accumulation and for the antioxidative capacity of the yeast cytosol (Zimmermann et al., in preparation). The results obtained by the $\Delta glr1$ and $\Delta trx1\Delta trx2$ deletion strains suggest Glr1 and Trr1 being important NADPH consumers during acute oxidative challenge. Thus, it was asked whether the double deletion of *TSA1* and *TSA2* would be sufficient to impede the oxidant-induced NADPH oxidation. Initially, the influence of *TSA1 TSA2* double deletion on the cytosolic H₂O₂ concentration was investigated using roGFP2-Tsa2 Δ C_R. Steady state H₂O₂ levels were increased to OxD 0.7 (**Table 2.3**) and the probe was more sensitive to further H₂O₂ addition than in the WT strain (**Figure 2.25I**) (Morgan et al., 2016), according to the important role of Tsa1 in peroxide scavenging. In contrast, the oxidation kinetics upon diamide treatment were not altered by the *TSA1 TSA2* double deletion (**Figure 2.26I**). The cytosolic GSSG/2GSH ratio, detected by roGFP2-Grx1, was not affected under steady state conditions (**Table 2.3**), but more sensitive to exogenous H₂O₂ than in WT cells (**Figure 2.25J**). Opposing, the GSSG/2GSH stability towards diamide seemed to be increased up to concentrations of 1 mM diamide (**Figure 2.26J**). Altogether, the *TSA1 TSA2* double deletion increases basal H₂O₂ levels. It does not affect the basal GSSG/2GSH ratio but renders it more sensitive to H₂O₂ and more resilient against diamide. The potential compensatory upregulation of alternative redox enzymes in this deletion strain is likely not sufficient to encounter the oxidative stress by H₂O₂ but enables to challenge diamide-induced stress.

To qualitatively quantify the cytosolic NAD(P) redox ratios in the $\Delta tsa1\Delta tsa2$ double mutant, NAPstar3 and Pdx-mC DS were utilized. Norm. cpTS/mC ratios at steady state revealed increased NADPH/NADP⁺ and NADH/NAD⁺ ratios (**Table 2.3**). The NAPstar3 response to the H₂O₂ treatment was shifted to higher cpTS/mC ratios, but the kinetics were similar to those observed for WT cells (**Figure 2.25K**). Interestingly, 0.5 mM H₂O₂ led to a prolonged NADPH oxidation in WT, whereas it did not affect the cytosolic NADPH/NADP⁺ ratio in $\Delta tsa1\Delta tsa2$ strain. This indicates that the NADPH consumption up to 0.5 mM H₂O₂ is mediated by Tsa in WT, whereas higher concentrations (≥ 1 mM) are known to lead to Tsa hyperoxidation and inactivation (Morgan et al., 2016). Hence, alternative redox mechanisms may lead to the NADPH consumption at these high exogenous H₂O₂ concentrations. Surprisingly, the application of diamide did not affect the cytosolic NADPH/NADP⁺ ratio of the $\Delta tsa1\Delta tsa2$ strain, similar to the observations made for $\Delta glr1$ but not $\Delta trx1\Delta trx2$ cells (**Figure 2.26K**). The NADH/NAD⁺ oxidation kinetics after H₂O₂ and diamide applications were apparently not altered by the *TSA1 TSA2* double deletion (**Figure 2.25L** and **Figure 2.26L**).

The results obtained by the cytosolic expression of GFIs in the *GLR1*, *TRX1 TRX2*, and *TSA1 TSA2* deletion strains demonstrated that the GSH- and Trx-based antioxidant systems are important consumers of cytosolic NADPH during oxidative challenge and that we do not yet understand completely the underlying mechanistic details.

2.7 Expanded NAPstar toolbox covers a range of different NAD(P) binding properties

The NAPstar family members monitor the NADPH/NADP⁺ redox ratio with different affinities (**Section 2.3**). The fluorescence plate reader-based analyses of probe expressing yeast strains demonstrated that cytosolic NAPstar1-3 operate at cellular steady state close to saturation with NADPH due to their high NADPH/NADP⁺ affinities. On the contrary, the NADPH binding affinity of NAPstar4 is very low, such that it was exclusively present in the open conformation under the same conditions. To allow for the sensitive detection of increasing and decreasing NADPH/NADP⁺ ratios under physiological conditions, an approximately half-saturated GFI at cellular steady state would be highly beneficial. Consequently, the optimal NAPstar binding affinity lies between those of NAPstar3 and NAPstar4 ($K_d > 5.4$ μ M NADPH).

2.7.1 Responses of novel NAPstar sensors to NADPH resemble that of NAPstar3 in semipermeabilized WT cells

The different Pdx-mC and NAPstar sensor structures vary only in their nucleotide binding site, which is build up by two, most likely interacting, T-Rex subdomains that finally dictate the NAD(P) affinity and specificity (**Figure 2.9B**). The dimeric T-Rex structure and its mechanism of action are well described (McLaughlin et al., 2010; Sickmier et al., 2005). Moreover, with the Pdx-mC and NAPstar sensors, a total of seven different T-Rex sequences with various NAD(P) binding properties are already available and characterized. Further NADPH-binding T-Rex variants were reported in the literature (Tao et al., 2017). Altogether, this provides a valuable platform to engineer the NAD(P) specificities of NAPstar sensors. To design a NAPstar variant with improved NADPH binding properties for the application in the *S. cerevisiae* cytosol, three different optimization approaches were implemented and followed in parallel: (i) the combination of two different T-Rex domains within one sensor protein ('mixed' NAPstar variants), (ii) the rational design and targeted mutagenesis of the NAPstar1 T-Rex domains (NAPstar5), as well as (iii) the selection of alternative NADPH-binding T-Rex variants for NAPstar generation (NAPstar6 and -7).

The 'mixed' NAPstar approach

The T-Rex NBD is localized at the dimer interface and formed by two T-Rex monomers (Sickmier et al., 2005). A C-terminal 'domain-swapped' alpha helix of the NBD interacts with the interdomain cleft of the opposing T-Rex monomer (McLaughlin et al., 2010; Sickmier et al., 2005). This interaction is important to induce the overall conformational change upon NAD⁺-NADH exchange. These interplays are expected to occur in the Pdx-mC and NAPstar sensor proteins as well. Hence, it was speculated that the modification of the NAD(P) binding properties of one of the NAPstar T-Rex domains would alter the overall sensor affinity. The combination of two different T-Rex subdomains should result in a GFI with intermediate binding properties. To generate a NAPstar sensor with the desired NADPH/NADP⁺ binding affinity, a high-affinity T-Rex domain (deriving from NAPstar1, -2, or -3) was merged with the low-affinity T-Rex domain of NAPstar4. The Pdx-mC (DS) and NAPstar structures are not symmetric, as the cpTS sequence is N- and C-terminally flanked by the NBD of the first, and the DNA binding site of the second T-Rex domain. Moreover, the FP position and the linker design are critical determinants of the GFI responsiveness since they mediate the conformational changes between the sensory and reporter domain. Hence, the domain order potentially plays a role in the resulting sensor readout. To cover all possible arrangements, the NAPstar4 T-Rex was either employed as

N-terminal domain (T-Rex 1), or sandwiched in between cpTS and mC (T-Rex 2). The resulting constructs were termed NAPstarX.4 and NAPstar4.X with X = 1, 2, or 3 (**Figure 2.27** and **Table 2.1**).

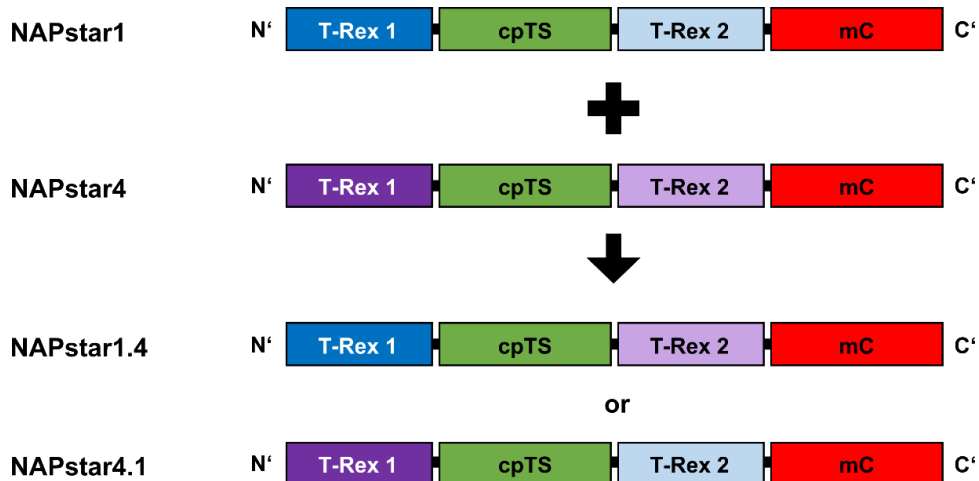


Figure 2.27: Design principle of 'mixed' NAPstar sensors.

The combination of NAPstar1 (blue) and NAPstar4 (purple) T-Rex domains to generate NAPstar1.4 and -4.1 is shown as example. Alternative to the NAPstar1 T-Rex domain, the NAPstar4 T-Rex domain was also combined with those of NAPstar2 or NAPstar3. The 'mixed' NAPstar nomenclature results from the arrangement of the T-Rex domains.

To verify the altered NADPH binding properties of NAPstarX.4 and -4.X constructs, sensor expressing WT yeast cells were semipermeabilized and treated with different amounts of NADPH during fluorescence plate reader measurements. NAPstar3 was carried in parallel to identify sensor variants with lowered NADPH binding affinities. NAPstarC was employed to determine the influence of the changed gain settings on the cpTS/mC readout, but the cpTS/mC of NAPstarC remained unchanged (**Figure 2.28B**). Cell semipermeabilization decreased the cpTS/mC ratio to ~0.5 for all sensor variants (**Figure 2.28A,C-H**), indicating the sensors being in their open conformations. The application of NADPH concentration-dependently increased the cpTS/mC ratios of NAPstarX.4 and -4.X variants, with kinetics similar to that of NAPstar3. After applying 0.1 mM NADPH, NAPstar1.4-3.4 were NADPH occupied to 79%, 84%, and 54%, and NAPstar4.1-4.3 to 74%, 84%, and 60%. In contrast, NAPstar3 was NADPH-bound to 40%, indicating higher NADPH affinities of the novel, 'mixed' NAPstar variants. The orientation of the NAPstar4 T-Rex domain did apparently not affect the NADPH binding due to similar occupancies of the respective variants at 0.1 mM NADPH. Moreover, the apparent NADPH affinity decreased with increasing 'X', according to the affinity of the chosen T-Rex template.

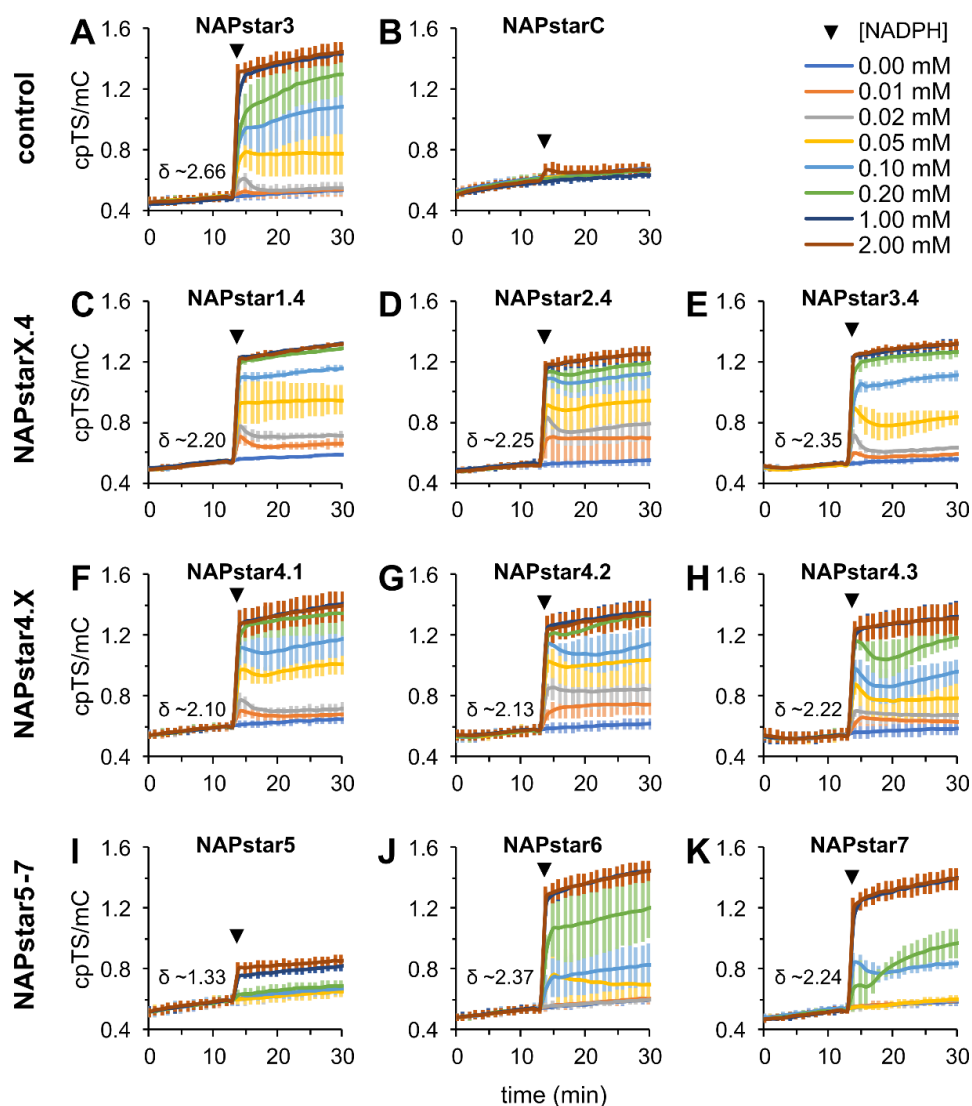


Figure 2.28: NADPH titration to semipermeabilized WT cells expressing novel NAPstar variants.

WT cells expressing NAPstar3 (A), NAPstarC (B), a ‘mixed’ NAPstar variant (C-H), NAPstar5, -6, or NAPstar7 (I-K) were semipermeabilized with 0.1% (w/v) digitonin prior to plate reader measurement. At the indicated time point (▼), cells were treated with different concentrations of NADPH. Gain values were set to 1700.

The dynamic ranges of the novel ‘mixed’ NAPstar variants ranged from 2.10 to 2.35 and were marginally smaller compared to the dynamic range of NAPstar3 (2.66) (Figure 2.28A,C-H). To confirm the NAPstarX.4 and -4.X specificity for NADPH, the sensor responses to NADH were followed in semipermeabilized cells (Appendix, Figure S7A-H). The ‘mixed’ NAPstar sensors only responded to very high NADH concentrations of 1 and 2 mM and the resulting cpTS/mC ratios (~2-fold maximum responses) clearly fell below those observed for the NADPH treatment. The strongest NADH-induced cpTS/mC increase

of 2.4-fold was observed for NAPstar3 (**Appendix, Figure S7A**). Hence, the NADPH specificity seemed to be increased for the ‘mixed’ NAPstar sensors.

Opposing to the observations described in semipermeabilized cells, in vitro analyses of NAPstar4.3 revealed an in vitro K_d (NADPH) of 53.8 μM (Mai et al., in preparation), meaning that the NAPstar3 K_d was lowered about 9.8-fold upon combination with the NAPstar4 T-Rex domain (**Table 2.1**). Further, NAPstar4.3 did not respond to NADH in vitro, as observed for former NAPstar variants (**Appendix, Table S2**). Other in vitro properties, such as pH robustness or sensitivity to ATP, were similar to those of the other NAPstar probes that were investigated in vitro (Mai et al., in preparation). Consequently, the in vitro results demonstrated a successful sensor optimization for NAPstar4.3 regarding NADPH affinity and specificity.

Rational mutagenesis of the iNap1 T-Rex domain

The T-Rex R90 residue is part of a loop of the nucleotide binding site and was shown to be critical for NADH binding (McLaughlin et al., 2010). Since the NADH removal from the recombinantly expressed and purified WT T-Rex protein was not possible, an R90D mutation has been introduced to lower the NADH binding affinity (McLaughlin et al., 2010). In addition, this mutation was introduced for the design of ‘non-binding’ iNapc/ NAPstarC sensor controls (Tao et al., 2017). The R90D mutation of iNap1/ NAPstar1 is associated with a dramatic increase in K_d (NADPH) e.g., from 2 μM to 120 μM for iNap1, leading to the generation of iNap4/ NAPstar4 sensors. It was hypothesized that the charge inversion from the positively charged arginine (R) to the negatively charged aspartic acid (D) hampers the binding of both, NADH and NADPH. To create a NAPstar variant with less impaired NADPH binding, the NAPstar1 R90 residues were exchanged by neutral, lipophilic leucine moieties (L). The resulting NAPstar1 R90L sensor was termed NAPstar5 (**Table 2.1**). To check for NADPH binding of NAPstar5, probe expressing WT cells were semipermeabilized and subjected to fluorescence measurements. The basal cpTS/mC ratio of NAPstar5 in semipermeabilized cells was ~0.5 as observed for other NAPstar variants (**Figure 2.28I**). Subsequent addition of NADPH led to a marginal increase in cpTS/mC to 0.8 at the highest NADPH concentration applied, resulting in a very small dynamic range of ~1.33. Hence, NAPstar5 has unfavorable reduced dynamic range and extremely low NADPH affinity and is expected to be an inappropriate NADP redox probe.

Alternative NADPH-binding T-Rex variants

In the course of iNap development, various T-Rex variants have been screened for their NADPH binding affinities (Tao et al., 2017). Some, but not all, of the analyzed constructs have been chosen to generate the final iNap (and NAPstar) probes. The remaining T-Rex variants were checked for mutations that potentially lower the iNap3/NAPstar3 NADPH binding affinity to gain a NAPstar variant with the desired binding properties. The iNap3 binding site is characterized by a V130Y mutation, but none of the other V130Y variants possessed a higher K_d (NADPH) than iNap3 (see Table S1 in Tao et al., 2017). Variant number 33 harbors a V130Y mutation and the replacement of V130Y with either V148A or V148T (variants number 37 and 38) increases the K_d (NADPH) by 3.5- and 2.2-fold. Hence, it was hypothesized that the exchange of the NAPstar3 V130Y mutation by either V148A or V148T would also increase the sensor K_d for NADPH. Consequently, the NAPstar3 V130 residues were recovered and either the V148A or the V148T mutations were introduced to generate the novel NAPstar6 and NAPstar7 variants (**Table 2.1**).

To investigate the NAPstar6 and NAPstar7 NADPH binding affinities, the sensors were expressed in WT cells, which were then subjected to semipermeabilization and fluorescence measurements. After semipermeabilization, the baseline cpTS/mC ratios were ~0.5, indicating open sensor conformations (**Figure 2.28J,K**). The application of NADPH increased the cpTS/mC ratios of NAPstar6 and NAPstar7 concentration-dependently. At 0.1 mM NADPH, NAPstar3 was NADPH-bound to 40%, whereas NAPstar6 and -7 were bound to 16% and 40%, respectively. Interestingly, further increase in exogenous NADPH to 0.2 mM hardly increased the cpTS/mC ratio of NAPstar7. Hence, NAPstar6 and NAPstar7 have apparently decreased NADPH affinities. The dynamic ranges were slightly diminished to ~2.37 and ~2.24. The GFI specificities were verified by NADH supplementation to sensor expressing, semipermeabilized cells. The sensor readouts were not affected by NADH concentrations up to 1 mM and 2 mM (**Appendix, Figure S7J,K**). Moreover, the maximum responses to NADH were smaller (2.05-fold maximum response) than those on NADPH.

Indeed, *in vitro* analyses showed that NAPstar6 and NAPstar7 have similar properties to NAPstar3 (Mai et al., in preparation) with decreased NADPH affinities of K_d (NADPH) ~12 μ M (NAPstar6) and ~7 μ M (NAPstar7) (**Table 2.1**). Moreover, the NADH affinities were reduced to K_d (NADH) ~353 μ M (NAPstar6) and ~225 μ M (NAPstar7) (**Appendix, Table S2**), suggesting that these sensors have improved NADPH specificities.

Overall, these results demonstrate that the sensor optimization was successful for NAPstar6 and NAPstar7 regarding NADPH affinity and specificity.

2.7.2 Novel NAPstar sensors show minor pH dependency

To verify the *in vitro* results that revealed similar pH dependencies between the novel NAPstar variants, NAPstar4.2, -4.3, -6 and -7 were chosen to be subjected to the plate reader-based pH dependency assay as described before (**Section 2.2.2** and **Section 2.3.3**). These novel NAPstar variants clearly inherited their pH sensitivities from Pdx-mC, demonstrating stable cpTS/mC readouts in the presence of 2 mM NADPH (**Figure 2.29**). In the absence of additional NADPH, the cpTS/mC ratios of the NAPstar variants was low and stable in the range between pH 6.0 and pH 7.0. At pH 8.0 and 9.0, the cpTS/mC values increased. Overall, NAPstar4.2, -4.3, -6 and -7 showed similar mild pH dependencies, corresponding to the Pdx-mC ancestor and to the results obtained *in vitro*.

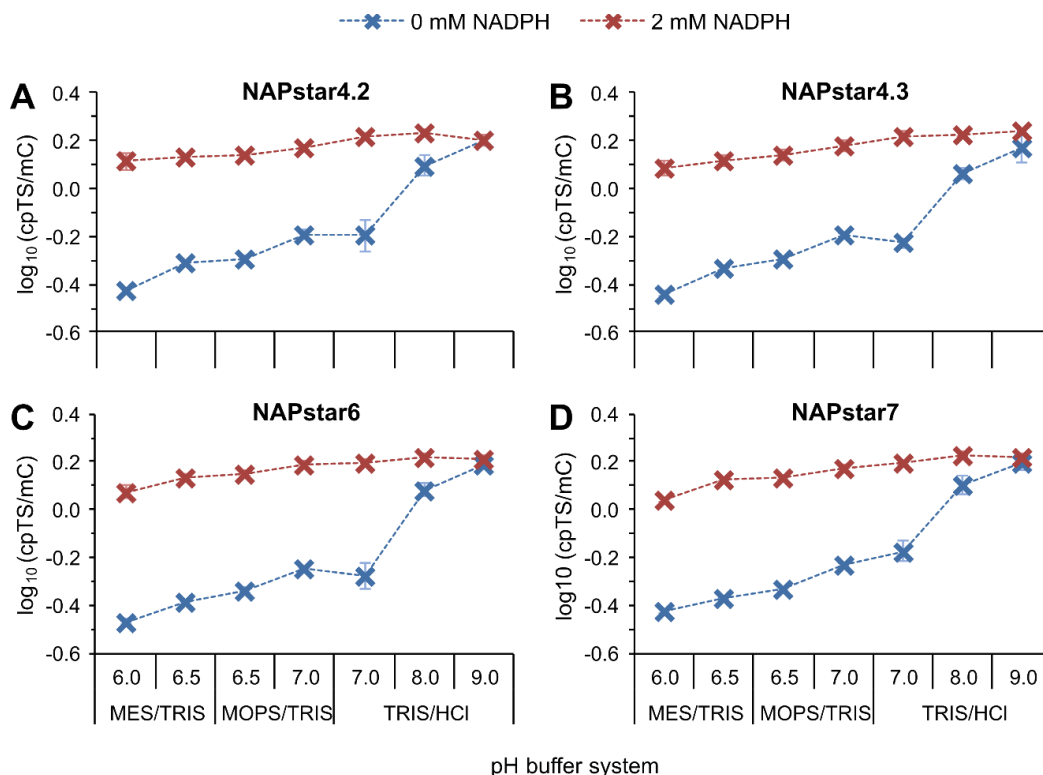


Figure 2.29: pH dependencies of novel NAPstar variants in semipermeabilized WT cells.

WT cells expressing NAPstar4.2 (A), NAPstar4.3 (B), NAPstar6 (C), or NAPstar7 (D) were semipermeabilized in the indicated buffer solution using 0.1% (w/v) digitonin. Excitation and emission spectra of cpTS and mC were recorded in absence and presence of NADPH. Fluorescence intensities were normalized to the mC emission at 619 nm. Emission of cpTS at 510 nm was plotted against the pH as $\log_{10}(\text{cpTS}/\text{mC})$. Measurements were performed using a fluorescence plate reader.

2.7.3 Novel NAPstar sensors possess the desired NADPH/NADP⁺ binding properties

The cytosolic NADPH/NADP⁺ ratio, sensed by NAPstar3, and the cytosolic NADPH concentration, reported by iNap probes, were surprisingly robust towards exogenous H₂O₂ (**Section 2.4.1**). To confirm the altered NADPH binding affinities of the novel NAPstar variants on the one hand, and the robust cytosolic NADPH/NADP⁺ ratio during H₂O₂ challenge on the other hand, WT cells expressing the novel NAPstar variants were subjected to H₂O₂ treatment. For the direct comparison, NAPstar3 was measured in parallel. The calculated sensor occupancies at steady state revealed NAPstar3 to be 98% saturated with NADPH (**Figure 2.30A**). In contrast, the novel NAPstar variants demonstrated decreased sensor occupancies ranging from 47% (NAPstar4.3) to 88% (NAPstar7), confirming the lowered NADPH/NADP⁺ affinities (**Figure 2.30C-K**). NAPstar5 did not bind to NADPH in WT cells (**Figure 2.30I**). The NADPH occupancies of ~50% identified NAPstar4.3, NAPstar6, and NAPstarX.4 variants as most suitable candidates for measurements in the yeast cytosol.

The application of H₂O₂ provoked a reversible NADPH/NADP⁺ oxidation, which was readily detected by all the NAPstar variants, except for NAPstar5 (**Figure 2.30A,C-K**). Interestingly, NAPstar2.4, -4.1, and -4.2 reported an NADPH overshoot after treatment with 1 mM and 2 mM H₂O₂ after 10 min of total measurement time. While the cpTS/mC response dynamics of the 'mixed' NAPstar variants resembled that of NAPstar3, the kinetics of NAPstar6 and -7 were different. Surprisingly, the latter ones registered an initial NADPH/NADP⁺ decrease after the addition of H₂O₂ or buffer, indicating an altered binding behavior of these variants. All novel NAPstar variants (except for NAPstar5) reported dynamically changes in the cytosolic NADPH/NADP⁺ ratio after H₂O₂ treatment during the whole measurement (20 min), whereas NAPstar3 only detected a significant decrease in NADPH/NADP⁺ up to ~10 min of total measurement time. These results validate that the sensor optimization regarding the NADPH/NADP⁺ affinity was successful for the 'mixed' NAPstar (NAPstarX.4, -4.X) and the 'alternative T-Rex domain' (NAPstar6, -7) approaches.

High exogenous diamide decreases the NAPstar cpTS/mC ratio dramatically (**Section 2.4.2**). As novel NAPstar variants demonstrated lowered NADPH/NADP⁺ binding affinities, they should enable for a more sensitive detection of the diamide-induced NADPH oxidation. To this end, WT cells expressing the novel NAPstar probes were subjected to the treatment with diamide (**Figure 2.31**). NAPstar3 and NAPstarC were carried as controls in parallel. NAPstar3 and the novel NAPstar variants, except for NAPstar5, detected a decrease in the NADPH/NADP⁺ ratio after treatment with 2 mM diamide

(Figure 2.31A,C-H). In contrast, NAPstarC was not affected by 2 mM exogenous diamide (Figure 2.31B and Appendix, Figure S4G) and thus, artifacts at this concentration would not be expected. An NADPH oxidation at lower diamide concentrations was not detected by any of the ‘mixed’ NAPstar variants. In contrast, NAPstar6 and -7 reported a prolonged decline in NADPH/NADP⁺ after the treatment with 0.5 and 1.0 mM diamide (Figure 2.31J,K). Hence, NAPstar6 and NAPstar7 seem to be the most sensitive NAPstar variants.

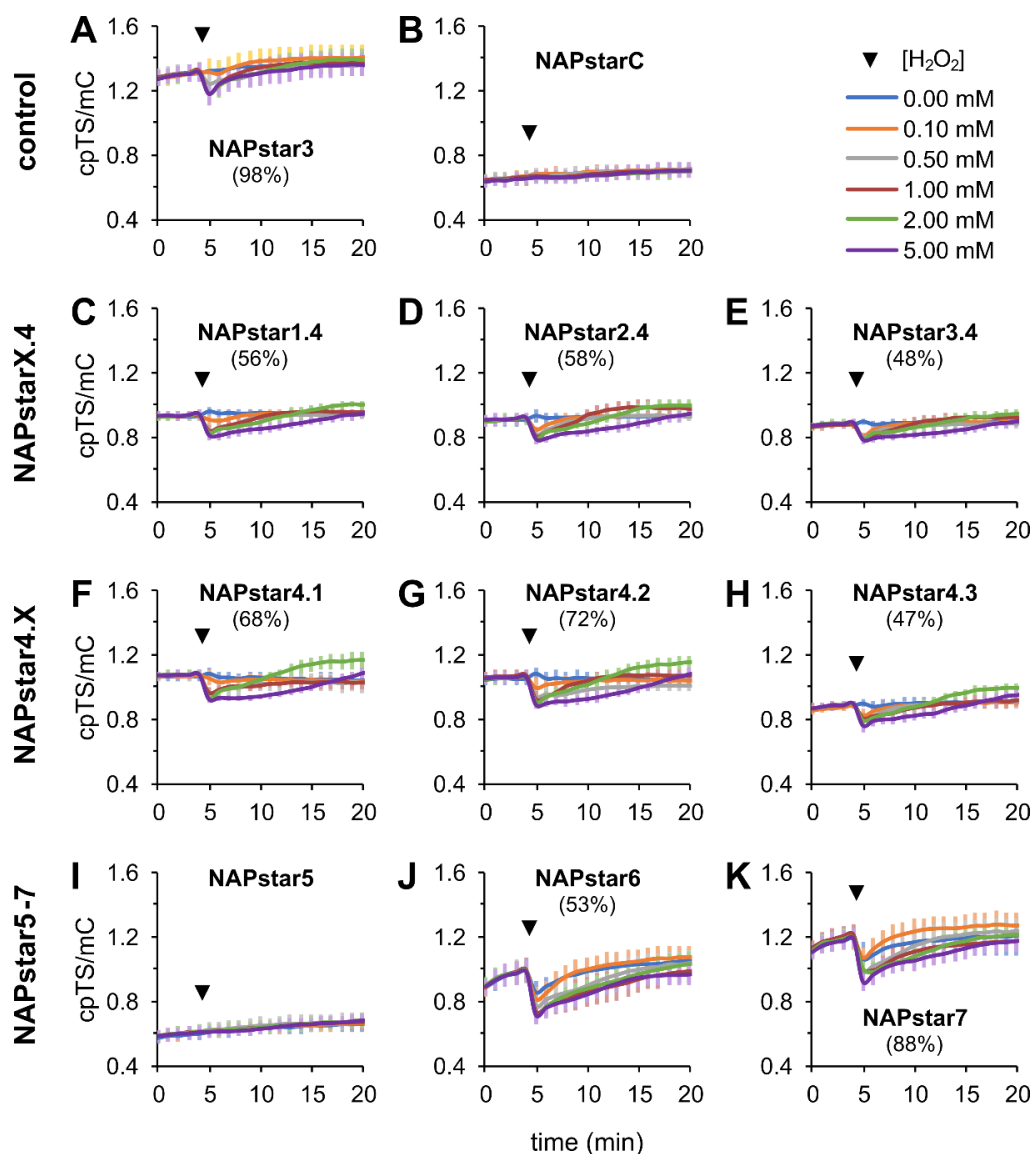


Figure 2.30: H₂O₂ treatment of WT cells expressing novel NAPstar variants.

WT cells expressing NAPstar3 (A), NAPstarC (B), a ‘mixed’ NAPstar variant (C-H), NAPstar5, -6, or NAPstar7 (I-K) were treated at the indicated time point (▼) with different concentrations of H₂O₂ during fluorescence plate reader measurements. Sensor occupancies at steady state are listed in brackets. Gain values were set to 1700.

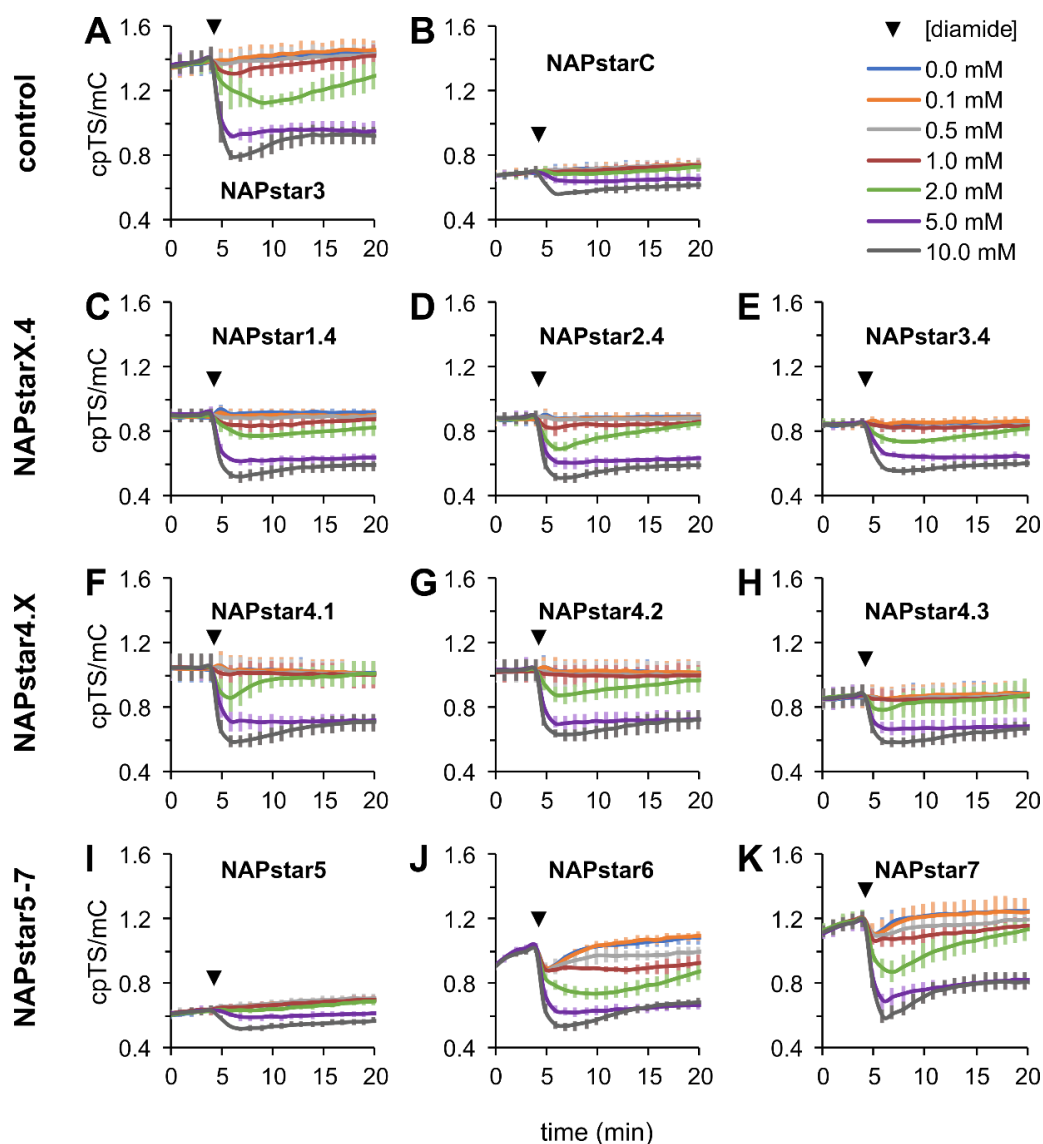


Figure 2.31: Diamide treatment of WT cells expressing novel NAPstar variants.

WT cells expressing NAPstar3 (A), NAPstarC (B), a ‘mixed’ NAPstar variant (C-H), NAPstar5, -6, or NAPstar7 (I-K) were treated at the indicated time point (▼) with different concentrations of diamide during fluorescence plate reader measurements. Gain values were set to 1700.

Overall, the H_2O_2 and diamide treatment of GFI expressing cells confirmed the successful sensor optimization regarding the NADPH/NADP⁺ binding affinity. Thereby, the fluorescence readout responses of the ‘mixed’ NAPstar variants resembled that of NAPstar3. Though sensor NADPH occupancies were in the same range for all the novel NAPstar variants (except for NAPstar5), NADPH seemed to dissociate faster from NAPstar6 and NAPstar7.

2.8 NAD and NADP redox states during the YMC

When yeast is grown under batch culture conditions, the metabolic and cell cycle states alter between single cells (Dodd and Kralj, 2017; Papagiannakis et al., 2017). Under specific continuous culture conditions, where nutrients are limited, the yeast population spontaneously synchronizes its cellular metabolism, including transcriptional and cell cycle programs (Murray et al., 2014; Tu et al., 2007, 2005). This phenomenon is called the yeast metabolic cycle (YMC) and is characterized by periodic changes in the oxygen consumption rate. Synchronized yeast cultures provide deeper insights into the temporal orchestration of cell metabolism, which is usually masked in a diffuse culture due to signal averaging. Most cellular metabolites have been shown to cycle in phase with the YMC, such as the NAD(P)H autofluorescence (Murray et al., 2007). To validate cytosolic metabolite oscillations during the YMC, different GFIs were expressed and measured throughout the cultivation process.

2.8.1 Plasmid-expressed HyPer7 confirms H₂O₂ oscillations

To allow for a stable p413 TEF plasmid transformation of the prototrophic Cen.PK113-1A strain, *HIS3* was deleted from its genome (Amponsah, 2020). To check whether plasmid-expressed *HIS3* influences the YMC cycling, Cen.PK113-1A $\Delta his3$ was transformed with the p413 TEF empty plasmid and the YMC was induced (**Appendix, Figure S8**). The YMC period was shortened to 2.04 h \pm 0.12 (Amponsah et al., 2021) but the strain underwent stable respiratory oscillations.

Recently, cyclic H₂O₂ levels were described during YMC utilizing a genomically-integrated roGFP2-Tsa2 Δ C_R sensor (Amponsah et al., 2021). To check whether the fluorescence signal of a plasmid expressed GFI is sufficient for measurements during the YMC, the bright, cpYFP-based HyPer7 probe was utilized to confirm the described H₂O₂ cycles. To this end, HyPer7 was introduced into the YMC by plasmid transformation. As already reported by the roGFP2-Tsa2 Δ C_R probe, H₂O₂ levels peaked at the start of low oxygen consumption (LOC) phase and continuously decreased during the remaining YMC period (**Figure 2.32A**). Additionally, a sharp drop in H₂O₂ was registered at the start of high oxygen consumption (HOC) phase. The HOC phase was additionally marked by two smaller local maxima in H₂O₂ during early and late HOC phase. The 490/400 nm ratio of the H₂O₂-insensitive HyPer7 C121S sensor control did not alter throughout the measurement (**Figure 2.32B**), confirming the HyPer7-detected H₂O₂ oscillations. Overall, the plasmid-expressed HyPer7 fluorescence signal exceeded that of genomically-integrated roGFP2-Tsa2 Δ C_R (data not shown) and enabled for a high-resolution detection of H₂O₂ oscillations.

To provoke a strong HyPer7 sensor response, excess H_2O_2 or diamide were injected into the fermenter vessel, subsequently leading to strong fluorescence ratio increases to 2.70 and 1.54, respectively (**Figure 2.32B,C**). In contrast, the H_2O_2 supplementation did not influence the fluorescence ratio of HyPer7 C121S (**Figure 2.32E**) and exogenous diamide increased its 490/400 nm ratio to a low extent due to fluorescence quenching at 400 nm excitation (**Figure 2.32F**, data not shown). The application of H_2O_2 led to a dramatic increase in the dissolved oxygen concentration (dO_2) in both experiments caused by the enhanced catalase activity (Amponsah, 2020). After the removal of excess cytosolic H_2O_2 , as reflected by the HyPer7 fluorescence ratio recovery, the culture restarted cycling in HOC phase, as already reported (Amponsah, 2020; Amponsah et al., 2021). Altogether, the HyPer7 expression during the YMC validated the results which were already described using the roGFP2-Tsa2 ΔC_R sensor, demonstrating the high potential of plasmid-expressed GFIs during YMC.

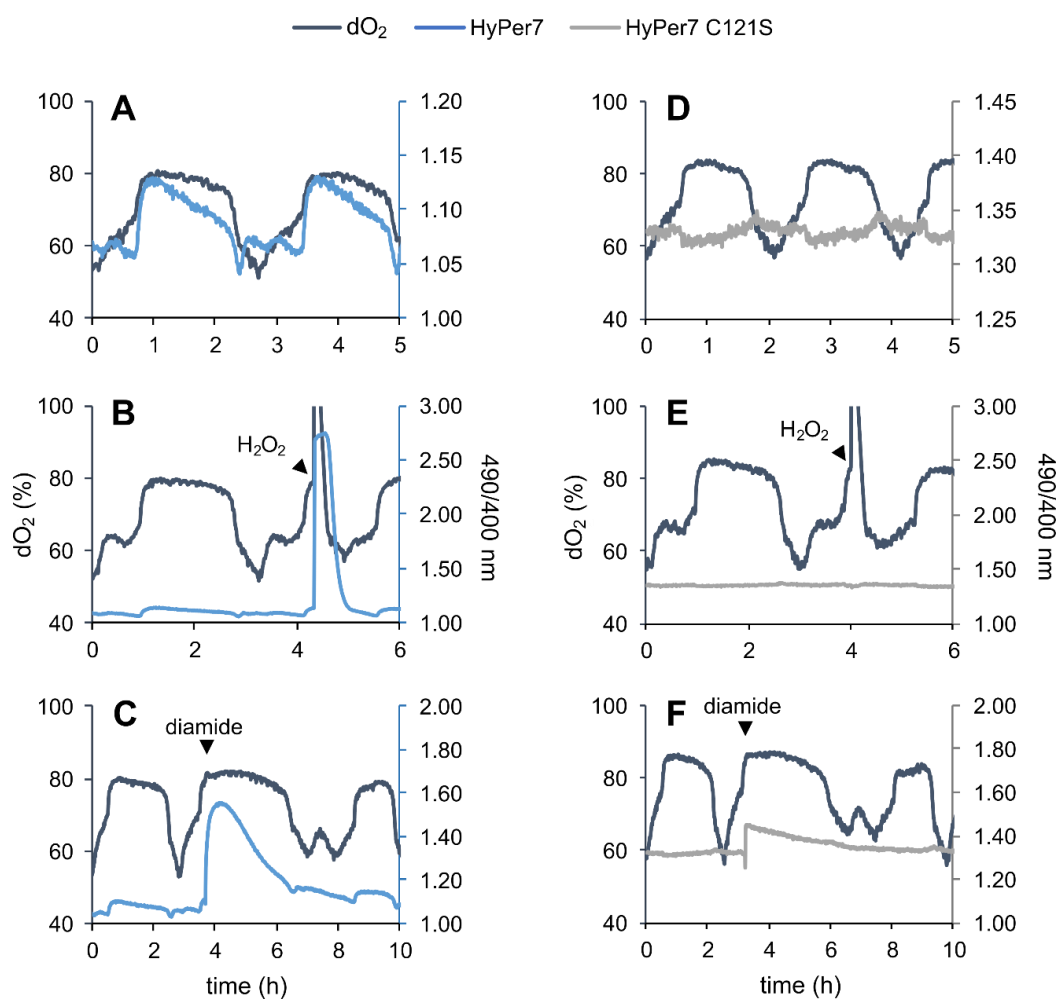


Figure 2.32: Fluorescence ratios of cytosolic HyPer7 and HyPer7 C121S during YMC.

The H_2O_2 sensor HyPer7 (left) and its H_2O_2 -insensitive control C121S (right) were expressed during YMC (**A,D**). Injection of 5 mM H_2O_2 (**B,E**) or 2 mM diamide (**C,F**) into the culture vessel demonstrate specificity and responsiveness of HyPer7.

2.8.2 NADH/NAD⁺ cycles periodically during the YMC

Based on NAD(P)H autofluorescence measurements, NADH has been demonstrated to oscillate during the YMC peaking at the start of the LOC phase (Murray et al., 1999, 1998). A complex output was described which was apparently assembled out of subharmonic components, most likely going back to non-synchronized oscillations on the single-cell level (Murray et al., 2014). To confirm the cyclic NADH pattern with increased subcellular resolution specifically in the yeast cytosol, Pdx-mC (DS) probes were expressed during the YMC via plasmid transformation. To ease the direct phase comparison between different experiments, the YMC start and end, marked by local dO₂ minima, were set to 0° and 360°, respectively. The fluorescence ratio measurements of both, Pdx-mC and Pdx-mC DS revealed NADH/NAD⁺ oscillations that mirrored the dO₂ curve and thus directly correlated to the oxygen consumption rate (**Figure 2.33A,B**). This result hints on the close connection between cellular NADH oxidation and electron transport chain (ETC) activity. At the start of the HOC phase, the NADH/NAD⁺ ratio increased and peaked when dO₂ was lowest. A second local maximum was reached during the late HOC phase. During the LOC phase, the NADH/NAD⁺ ratio was constantly low. These results demonstrate that Pdx-mC (DS) probes act within their dynamic ranges during the YMC. This strongly suggests that the NADH/NAD⁺ ratio is lower during the YMC, when the glucose availability is lower than in the plate reader-based setup, where batch cultures are grown in the presence of high glucose concentrations. This phenomenon could be explained by the relationship between the glycolytic activity and the NADH production. Overall, the detected NADH/NAD⁺ oscillations resemble only partly the reports of NAD(P)H autofluorescence, most probably due to the increased subcellular resolution, specificity, and signal intensity of Pdx-mC (DS).

Oscillations in cytosolic pH trigger cyclic NADH changes during metabolic transitions, such as the diauxic shift (Dodd and Kralj, 2017). Moreover, cytosolic pH oscillations during the YMC were proposed to regulate the activity of the target of rapamycin complex I (TORC1) and thus, the switch between anabolic and catabolic phases (O'Neill et al., 2020). Catabolic processes mainly rely on NAD⁺ as final electron acceptor, producing NADH. Based on these reports, it was hypothesized that the detected cytosolic NADH/NAD⁺ ratio oscillations are accompanied by cyclic changes in cytosolic pH. To verify these pH oscillations by GFI measurements, pHluorin was expressed during the YMC. Similar to former reports (O'Neill et al., 2020), the pH directly correlated with the oxygen consumption rate, reflected by the low 395/475 nm ratio during the LOC phase and higher ratios during the HOC phase (**Figure 2.33C**). The local maxima of the pHluorin ratio were shifted about

-20° to -40° relative to Pdx-mC (DS) maxima i.e., occurred ~8 to ~16 minutes earlier. These results further hint on a close correlation between the cytosolic pH and NAD metabolism.

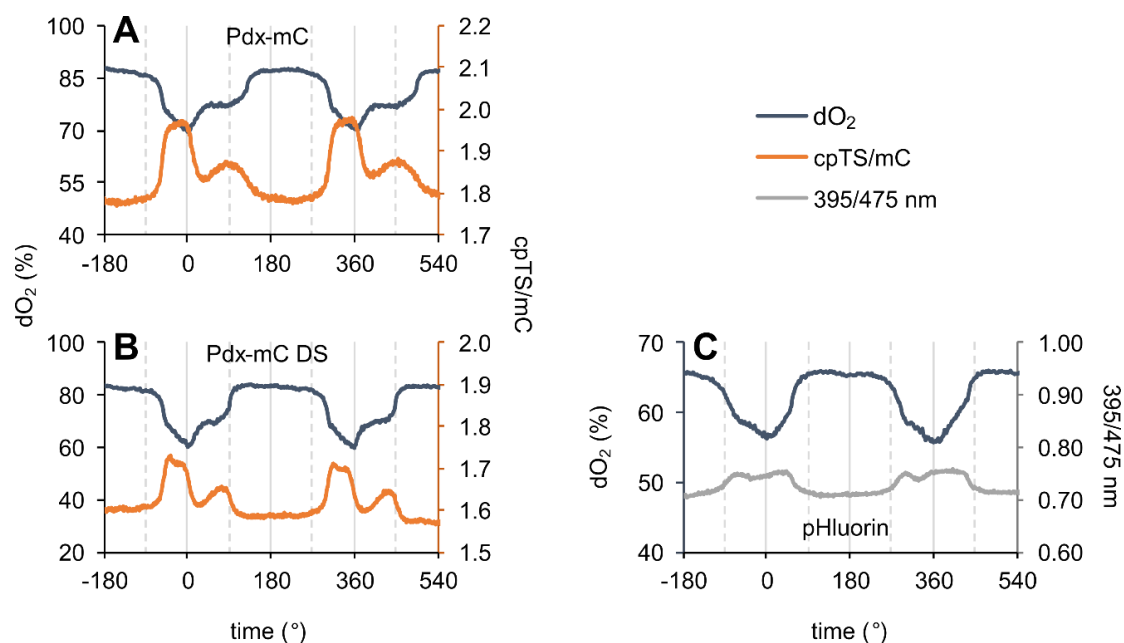


Figure 2.33: Fluorescence ratios of cytosolic Pdx-mC (DS) and pHluorin during YMC. Pdx-mC (A), Pdx-mC DS (B), or pHluorin (C) were expressed during YMC.

2.8.3 NADPH/NADP⁺ oscillations during the YMC could not be clearly detected

Next to the cyclic changes in NADH, oscillations in the whole-cell NADP concentration have been reported during the YMC (Tu et al., 2007). Using a gas chromatography-based technique, a 2.7-fold change in the total NADP level has been detected during a complete YMC period, peaking during the HOC phase. Moreover, the cyclic expression pattern of *UTR1*, *YEF1*, and *POS5* has been reported to be in synchrony with the YMC. Together, these observations hint on the temporal organization of NADP metabolism. To investigate whether the cytosolic NADPH/NADP⁺ ratio oscillates during the YMC, NAPstar probes were expressed via plasmid transformation. Initially, NAPstar3 was chosen to track changes in cytosolic NADPH/NADP⁺. The cpTS/mC ratio of NAPstar3 oscillated peaking towards the end of HOC at ~90° and it was lowest at ~315°, at the start of the HOC phase (**Figure 2.34A**). The cpTS/mC ratio oscillation of NAPstar2, which would be expected to be saturated with NADPH, resembled that of NAPstar3 (**Appendix, Figure S9A**). NAPstarC was used as sensor control demonstrating a similar pattern with a

clear peak in the cpTS/mC ratio at 315° and a local minimum at 120° (**Figure 2.34E**). As NAPstarC is unresponsive to NAD(P)H and its readout did not seem to correspond to the cytosolic pH changes detected by pHluorin, these results indicate changes in the cytosolic ATP concentration (**Section 2.3.1**). Due to the high similarity between the NAPstarC and NAPstar3 (NAPstar2) responses, no clear cycles in the NADPH/NADP⁺ ratio could be identified.

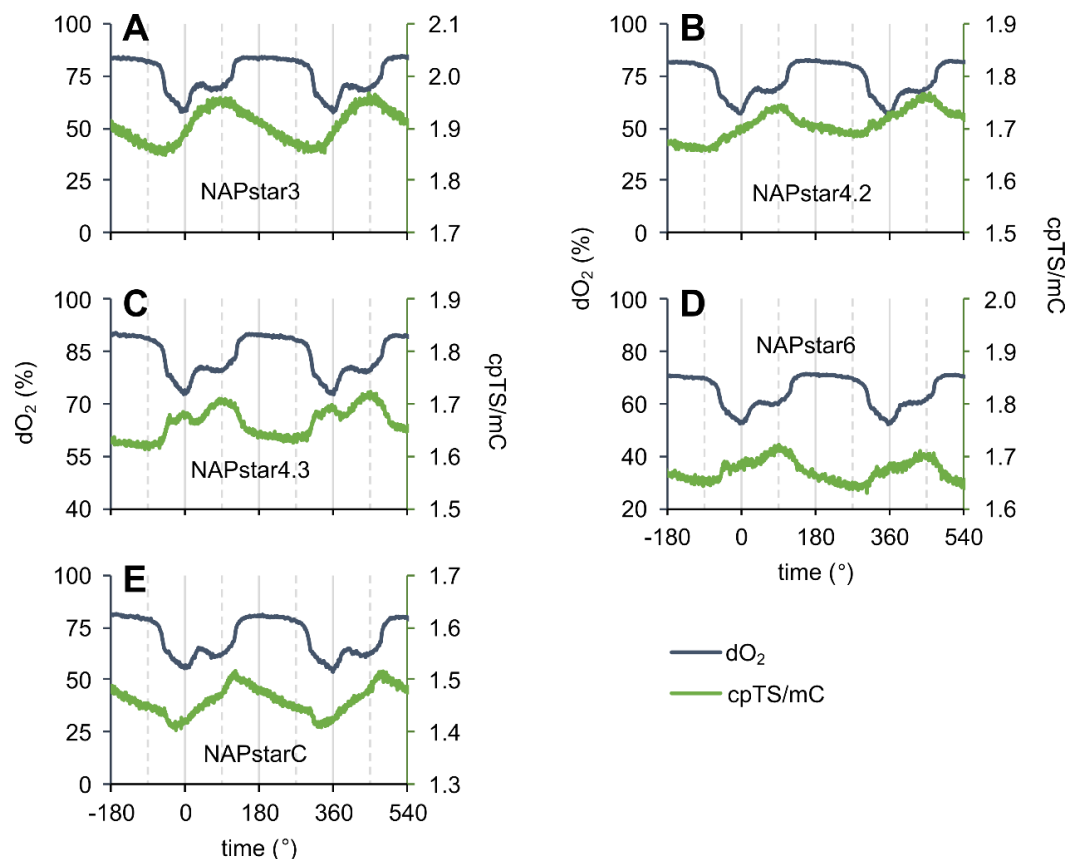


Figure 2.34: Fluorescence ratios of cytosolic NAPstar probes during YMC.

NAPstar3 (**A**), NAPstar4.2 (**B**), NAPstar4.3 (**C**), NAPstar6 (**D**), or NAPstarC (**E**) were expressed during YMC.

To avoid an interference with ATP during the GFI measurements, the mSI-iNap3 probe was expressed during the YMC, but mSI-iNap3 failed to detect any NADPH oscillations due to its low fluorescence intensity (**Appendix, Figure S10**). Although the exact ATP binding affinities of the various NAPstar variants are unknown so far, the most promising candidates, NAPstar4.2, -4.3, -6, and -7 were further screened for alternative cpTS/mC patterns in the YMC setup. The fluorescence ratio of NAPstar7 cycled in a similar manner to that of NAPstar3 (**Appendix, Figure S9B**), whereas the cpTS/mC ratio of NAPstar4.3 clearly demonstrated two local maxima at ~0° and ~90° (**Figure 2.34C**). The

NAPstar4.2 and -6 readouts showed an intermediate pattern (**Figure 2.34B,D**). The distinct cpTS/mC pattern of NAPstar4.3 renders it to the most promising sensor candidate potentially detecting the actual changes in the NADPH/NADP⁺ ratio. Due to the high similarity between the individual NAPstar responses and NAPstarC as well as due to the lack of comprehensive GFI understanding, no clear statements about the NADPH/NADP⁺ ratio cycles are possible.

3 Discussion

The NADH/NAD⁺ and NADPH/NADP⁺ redox couples build the molecular basis of cell metabolism in basically all organisms (Fessel and Oldham, 2018; Pollak et al., 2007). Due to this central role, they are also implicated as signal transducers regulating important cellular processes. NAD⁺ is mainly an electron acceptor in catabolic processes and connected to cellular programs, like autophagy or ageing (Sedlackova and Korolchuk, 2020). On the other hand, NADPH is the major electron donor of anabolic processes, antioxidant defense, and redox signaling (Murray et al., 2011). An altered NAD(P) metabolism has been linked to various pathologies, such as diabetes or the Warburg effect observed in cancer cells (Blacker and Duchon, 2016; Koju et al., 2022). Though intensively investigated for decades, the understanding of cellular NAD(P) metabolism remains incomplete due to the limitations of former measurement techniques and fast turnover rates (Nielsen, 2019). Genetically encoded fluorescent indicators (GFIs) outperform these quantification methods delivering information about NAD(P) in living cells with high specificity and in real-time (Müller-Schüssele et al., 2021).

As one of the best characterized model organisms, with a high similarity to mammalian models and a relevance for biotechnological applications (Parapouli et al., 2020), *S. cerevisiae* represents an ideal system to study NAD(P) homeostasis using GFIs. To the best of my knowledge, this study describes for the first time the establishment and detailed characterization of NAD- and NADP-specific GFIs in *S. cerevisiae* and further, the development of a new NADPH/NADP⁺-specific sensor class, the so-called NAPstar sensors. First, the discrepancies, advantages, and limitations of the various GFIs will be discussed. Afterwards, the mechanisms, which underly the diverse and interesting observations on NAD(P) physiology in *S. cerevisiae*, will be debated.

3.1 T-Rex-based sensor design

The design of all NAD(P)-specific GFIs used in this study is based on the T-Rex protein. Thereby, two different GFI structures can be distinguished (**Figure 1.5**). On the one hand, the ‘tandem’ design of Peredox-mCherry (Pdx-mC) and NAPstar probes, with two complete T-Rex domains within one sensor peptide, and on the other hand the ‘monomeric’ design of SoNar and iNap sensors, containing only one, truncated T-Rex domain per monomer.

3.1.1 Comparison of Pdx-mC (DS) and SoNar probes (NADH/NAD⁺)

The NADH/NAD⁺-specific Pdx-mC (DS) and SoNar probes were intensively characterized *in vitro* (Hung et al., 2011; Steinbeck et al., 2020; Zhao et al., 2015) but the direct comparison between these studies is impeded by the differences in analysis conditions. In contrast, the parallel measurements in *S. cerevisiae* cells in the course of this study created equal prerequisites for comparative investigations. Pdx-mC was reported to have the highest NADH/NAD⁺ affinity of the three GFIs with an average $K_{R'}^{Pdx}$ of ~ 4.5 ($R' = [NADH] \times 1000 / [NAD^+]$) (**Table 1.2**). Pdx-mC DS and SoNar have lower affinities of $K_{R'}^{DS} \sim 63$ and $K_{R'}^{SoN} \sim 36$. Different experiments were performed in yeast cells that enable for the characterization of the NADH/NAD⁺ binding affinities of the various sensors. For instance, the semipermeabilization of sensor expressing cells in measurement buffer led to a marginal decline in the Pdx-mC fluorescence ratio, a $\sim 50\%$ drop in that of SoNar and a full ratio decrease for Pdx-mC DS (**Figure 2.1E** and **Figure 2.5C,D**), reflecting the reported *in vitro* affinities. Additionally, the oxidant application to intact, Pdx-mC expressing cells provoked only small readout changes compared to the Pdx-mC DS and SoNar sensors (**Figure 2.17B-D** and **Figure 2.20**). Interestingly, the Pdx-mC DS and SoNar responses to the various oxidant treatments were almost identical, with the SoNar sensor being slightly more sensitive. These observations may be explained by the high NAD⁺ affinity (and low $K_{R'}$ value) of SoNar that allows for quick nucleotide exchange. Hence, SoNar has the most suitable NADH/NAD⁺ binding properties to monitor rapid NADH/NAD⁺ dynamics in the plate reader-based setup. In contrast, the glucose-limited conditions in the bioreactor dramatically lowered the cytosolic NADH/NAD⁺ ratio during the yeast metabolic cycle (YMC). Therefore, a high-affinity probe is required for this setup. The fluorescence amplitude of Pdx-mC during the YMC measurements was higher (9.3% change) than that of Pdx-mC DS (5.9% change) (**Figure 2.33A,B**). This would correspond to the reported free cytosolic NADH/NAD⁺ ratio of 0.001 to 0.003 ($R' = 1$ to 3) under similar, aerobic and glucose-limited conditions (**Table 1.1**), speaking in favor of the usage of Pdx-mC ($K_{R'}^{Pdx} \sim 4.5$) instead of the DS variant ($K_{R'}^{DS} \sim 63$). Overall, these observations demonstrate that the appropriate GFI affinity for the NADH/NAD⁺ ratio for measurements in *S. cerevisiae* depends on the experimental setup and the culturing conditions. In general, Pdx-mC DS can be utilized for first investigations as it compromises the advantageous features of Pdx-mC and SoNar (see below).

Pdx-mC and Pdx-mC DS have favorable low pH dependency (**Table 2.2**) and bright fluorescence intensity (**Figure 2.13**), whereas SoNar suffers from the pH dependency and weak signal intensity at 480 nm excitation deriving from the circularly permuted yellow fluorescent protein (cpYFP) moiety. For the first time, SoNar has been fused to an RFP to

perform pH-robust readouts. However, the pH did not seem to affect the readout of SoNar in intact cells, since it was almost identical to that of Pdx-mC DS after several oxidant treatments (**Figure 2.17C,D** and **Figure 2.20B,C**). Apart from this, the dynamic range of SoNar is bigger than that of Pdx-mC (DS) in the tested conditions ($\delta_{\text{SoN}} \sim 5.5$, $\delta_{\text{Pdx}} \sim 1.9$, $\delta_{\text{DS}} \sim 2.0$) (**Figure 2.1E** and **Figure 2.5C,D**). Potential factors, which may contribute to the enhanced dynamic range of SoNar, are (i) the cpFP insertion site (ii) the truncation of its T-Rex domain and (iii) the choice of a ratiometric FP for the reporter domain design. To (i): For SoNar design, the cpFP was inserted into a T-Rex surface loop ('monomeric' design) instead of sandwiching it in between two complete T-Rex domains as for Pdx-mC (DS) probes ('tandem' design). This alternative cpFP localization relative to the T-Rex subunit certainly influences its response on the T-Rex conformational change. To (ii): Moreover, the N-terminal T-Rex DNA-binding domain was truncated in SoNar. The T-Rex dimer harbors a C-terminal 'domain swapped' alpha helix that is buried in the interdomain region (between the DNA- and nucleotide binding domain) of the reciprocal subunit (McLaughlin et al., 2010; Sickmier et al., 2005). Due to the truncation of the DNA-binding domain in SoNar, the interaction between the two monomers, which is important for the conformational change of T-Rex, could be influenced, and with this, the SoNar readout. To (iii): Finally, the choice of an intrinsic ratiometric FP (cpYFP) with two changing fluorescence intensities, instead of an intensimetric variant (cpT-Sapphire [cpTS]), also potentially enlarges the dynamic range. Interestingly, the FiNad sensor (T-Rex₁₋₁₈₉ – **G** – cpYFP – **GTG** – T-Rex₁₉₀₋₂₁₁), that differs from SoNar (T-Rex₇₉₋₁₈₉ – **SAG** – cpYFP – **G** – T-Rex₁₉₀₋₂₁₁) only in the linker regions and in the presence of the DNA-binding domain, is responsive to the NAD⁺/AXP ratio (AXP=ATP+ADP+AMP) (Zou et al., 2020). And although it has lost the ratiometric cpYFP readout, it remarkably remains a 7-fold dynamic range. This example clearly demonstrates that a complex interplay between various structural features influences the GFI readout properties.

3.1.2 Comparison of NAPstar (NADPH/NADP⁺) and iNap probes (NADPH)

Based on the iNap mutation sites and the Pdx-mC scaffold, novel, NADPH/NADP⁺-specific sensors were developed, which were termed NAPstar probes (**Figure 2.9**). The NADP-specific sensor families (iNap, NAPstar) inherited their properties from their respective NAD-specific ancestors (SoNar, Pdx-mC). Thus, the NAPstar sensors show average dynamic ranges of $\delta_{\text{Ns}} \sim 2.2$ (**Figure 2.13**), bright fluorescence intensity in the *S. cerevisiae* cytosol (**Figure 2.12**), and increased pH robustness (**Table 2.2**). In contrast, the iNap sensors possess an average dynamic range of $\delta_{\text{iN}} \sim 2.8$ (**Figure 2.4**), suffer from

weak fluorescence intensity (**Figure 2.12**), and increased pH sensitivity (**Table 2.2**). The discrepancies in fluorescence intensities become especially evident in the respective control variants. NAPstarC reliably reports changes in the cpTS/mC readout and based on this highly reproducible data, the Pdx-mC (DS) and NAPstar signals can be normalized using NAPstarC to exclude potential artifacts from the probe readouts. In contrast, the iNapc fluorescence ratio is very noisy impeding any normalizations. These properties render the iNap measurements under conditions of low expression levels or strong pH fluctuations impossible. The pH-dependent, weak-fluorescent 480 nm excitation signal of iNap probes can be bypassed by the generation of RFP fusion constructs (Tao et al., 2017). Hence, the bright monomeric mScarlet-I (mSI) was N-terminally fused to the different iNap probes. For the first time, the RFP fusions of iNap2-4 and iNapc were generated and applied for NADPH measurements. Unfortunately, the results obtained by these novel mSI-iNap probes showed high deviations and resembled overall those of the NAPstar probes (**Appendix, Figure S3, Figure S5 and Figure S6**), rendering the mSI fusions superfluous.

The NADPH binding affinities of the NAPstar sensors exceeded those of the respective iNap counterparts in vitro (**Table 2.1**). The high NADPH binding affinities of NAPstar1-3 were confirmed in intact WT yeast cells. Whereas the NADPH occupancies of iNap1-4 were 78%, 76%, 39%, and 4% (**Figure 2.1F and Figure 2.16F-I**), NAPstar1-3 were fully saturated, and NAPstar4 was not bound to NADPH at all (**Figure 2.10C and Figure 2.16A-D**). Despite the NAPstar affinities hamper the dynamic NADPH/NADP⁺ ratio monitoring in vivo, NAPstar3 was responsive to high amounts of exogenously added oxidants, comparable to iNap1-3 (**Figure 2.16C, Figure 2.19C and Figure 2.22C**). Moreover, the problem of being fully saturated at steady state could be solved by further optimization steps. The NAPstar NADPH binding affinities were optimized for the application in the yeast cytosol using different approaches. The aim was to obtain a NAPstar variant that is ~50% bound to NADPH at steady state. The rational approach to lower the NAPstar1 affinity by an amino acid substitution failed (NAPstar5) (**Figure 2.28I, Figure 2.30I and Figure 2.31I**). However, the combination of a high-affinity with a low-affinity T-Rex domain within one NAPstar protein ('mixed' NAPstar) resulted in six different variants which were 47% to 72% bound to NADPH at steady state (**Figure 2.30C-K**). In addition, the novel T-Rex mutations in NAPstar6 and NAPstar7 led to improved 53% and 88% sensor NADPH occupancies (**Figure 2.30J,K**). Interestingly, the initial NADPH titration to semipermeabilized, sensor expressing cells did not report the lowered NADPH affinity for the 'mixed' NAPstar variants, and also the data received for NAPstar6 and NAPstar7 did not correspond to those obtained in intact cells (**Figure 2.28 and Figure 2.30**). Notably, the NAPstar6 and NAPstar7 kinetics after oxidant application was distinct from those observed

for NAPstar3 or the 'mixed' variants. These deviations could not be attributed to differential pH sensitivities (**Figure 2.29**). Most likely, the GFIs differ in their binding properties, such as the nucleotide specificity (dependency on ATP, ADP etc.), dissociation kinetics, or NADP⁺ affinity. Overall, the 'tandem' and T-Rex-based sensor design enabled the development of a vast variety of NAPstar variants with different binding characteristics. For the detailed understanding and reasonable recommendations, further in vitro analyses of the improved NAPstar variants are required. So far, NAPstar4.3 and NAPstar6 seem to be the most promising candidates for the detection of NADPH/NADP⁺ ratio dynamics in the yeast cytosol using fluorescence plate reader and bioreactor-based setups. For the monitoring of changes in the NADPH concentration under the same conditions, iNap2 or iNap3 are recommended regarding the NADPH binding specificity.

Preliminary in vitro data identified the NAPstar sensors, including NAPstarC, being responsive to ATP (**Section 2.3.1**). Since NAPstarC was analyzed for all conditions in parallel, a significant contribution of ATP changes to the sensor responses can be ruled out. The sensitivity to ATP and analogues is an endogenous feature of Rex and T-Rex-derived GFIs. For instance, the Pdx-mC sensor tends to be dependent on the total ATP+ADP pool due to the large pool size in vivo (Hung et al., 2011). However, this influence was considered not to be relevant under physiological conditions, under which the ATP+ADP concentration should remain relatively constant. In addition, the above mentioned FiNad sensor is specific for the NAD⁺/AXP ratio (Zou et al., 2020). In contrast, the SoNar and iNap sensors were reported not to be affected by the ATP/ADP ratio or the ATP+ADP pool size under similar conditions (Tao et al., 2017; Zhao et al., 2015). The comparison of the *Bacillus subtilis* Rex (B-Rex) structure bound to ATP (B-Rex:ATP) with that of T-Rex:NADH demonstrated that 77% of structural difference in the buried surface area could be attributed to the C-terminal 'domain-swapping' alpha helix (Wang et al., 2008). This helix also forms interactions with the nicotinamide group of the ligand (McLaughlin et al., 2010). As already discussed above, the N-terminal truncation of T-Rex in the 'monomeric' probes likely influences the interaction of the 'domain swapped' helix with the reciprocal subunit and thus the overall conformational change and/ or the nucleotide binding of the sensor. Hence, the N-terminal truncation of the T-Rex domain possibly accounts for the robustness of the SoNar and iNap sensors towards ATP. Interestingly, a detailed in vitro analysis of B-Rex revealed the highest affinity for NADH (24 nM), a ~1,000-fold lower K_d value for ATP (0.07 mM), and the lowest affinity for NAD⁺ (0.49 mM). Further, an allosteric binding was reported for NAD⁺, whereas the B-Rex affinity for ATP was not influenced by the B-Rex conformation. In how far these factors influence the response of the NAPstar probes remains to be shown.

Optimization of iNap3

Despite the beneficial properties of the NAPstar sensors, an intrinsic ratiometric probe is desired due to the potentially increased dynamic range, the smaller protein size, and other favorable characteristics connected to single-FP sensors (Kostyuk et al., 2019). Since the major limitations of the SoNar and iNap probes derive from the cpYFP moiety, it was hypothesized that the cpYFP exchange would confer the desired properties. The improved, pH-independent, cpYFP-based HyPer7 probe displays bright fluorescence in *S. cerevisiae* (**Figure 2.32**) (Kritsiligkou et al., 2021b) which would be required for the iNap sensors. Hence, the cpYFP domain of iNap3 was replaced by the cpYFP domain of HyPer7 to improve its fluorescence properties. Unfortunately, this exchange resulted in a diminished dynamic range ($\delta_{iNap3} \sim 1.2$), low fluorescence intensity, and NADPH binding affinity (data not shown). Further optimization attempts failed. This example illustrates that the rational design of GFIs is not trivial and a modular exchange of the sensory or the reporter domain is not always possible. Beyond that, the comprehensive procedures to generate novel GFIs such as HyPer7, SoNar, or Pdx-mC (Hung et al., 2011; Pak et al., 2020; Zhao et al., 2015) demonstrate the sensitive and complex interplay between the sensor and reporter domain.

3.1.3 Interim conclusion and outlook for future sensor development

This work expands the palette of GFIs applied in *S. cerevisiae*. It validates the versatility of this organism for GFI characterization, making initial probe purification dispensable. As it has already been shown for roGFP2-based sensors, *S. cerevisiae* provides an excellent platform for rapid enzyme or sensor screening for candidate selection prior to, or instead of, in vitro characterization (Liedgens et al., 2020; Zimmermann, 2021; Zimmermann et al., 2021). Using *S. cerevisiae*, the novel NADPH/NADP⁺-sensing NAPstar probe family was developed, optimized, and characterized together with the already existing SoNar/ iNap and Pdx-mC (DS) probes. The individual advantages and limitations of these GFIs were discussed, and potential optimizations were described.

Although a wide variety of different NAD(P)-specific probes has already been described (**Appendix, Table S1**), improved GFIs continue to be a major research interest in the field. To construct optimized probes, alternative protein scaffolds should be considered in addition to the T-Rex. The rational concepts for the design of new sensors and their optimization are limited by the available information about potential protein candidates. The acquirement of the structural data is connected to a high investigational and screening effort. In the future, the development of new algorithms for structure simulations will potentially help in solving these problems. Moreover, automated

evolutionary approaches for sensor optimization could minimize the screening effort. For instance, a redox-sensitive NAD(P)-specific GFI according to the roGFP2 sensor model is certainly conceivable as an alternative concept. Moreover, an NAD(P)-specific GFI with red fluorescence would be favorable since it interferes less with autofluorescence signals. This would allow e.g., for deeper tissue penetration, brighter fluorescence signals, and for simultaneous measurements with a green fluorescent GFI or dye (Kostyuk et al., 2019).

3.2 NAD(P) transhydrogenase-like activity of semipermeabilized cells

Membrane-bound NAD(P) transhydrogenases can be found in bacterial plasma membranes or the inner mitochondrial membrane of eukaryotes (Spaans et al., 2015). They couple reversibly the transmembrane proton gradient to the hydride ion transfer between NAD and NADP ($\text{NADH} + \text{NADP}^+ \leftrightarrow \text{NAD}^+ + \text{NADPH}$) and are primarily important for the production of NADPH. A second group of soluble NAD(P) transhydrogenases can be found in bacteria. These enzymes are not energy-coupled and proposed to produce mainly NADH from NADPH. *S. cerevisiae* lacks a bona fide NAD(P) transhydrogenase (Bruinenberg, 1986; Rodrigues et al., 2006). Thus, it was surprising to detect strong fluorescence responses of the NADH/NAD⁺-sensitive SoNar and Pdx-mC (DS) probes to exogenously added NADPH in semipermeabilized *S. cerevisiae* cells (**Figure 2.3A-D** and **Figure 2.8**). Unspecific NADPH binding of the different sensors is highly unlikely since the concentration-dependent responses to exogenous NADPH and NADH were essentially the same, despite of the reported in vitro K_d values for NADPH are ~10- to ~750-fold higher than those for NADH (**Table 1.2**). The observed NADPH → NADH transhydrogenase-like activity was apparently unidirectional in semipermeabilized cells since neither the NADPH-specific iNap nor the NADPH/NADP⁺-specific NAPstar sensors responded to exogenous NADH in semipermeabilized cells (**Appendix, Figure S2** and **Figure 2.13F-I**). As the production of NADPH from NADH requires an energy input (Spaans et al., 2015), and as the cell semipermeabilization reduces the net 'intracellular energy load' (e.g., in form of redox and transmembrane potentials), the observation of unidirectionality seems conclusive. Although the biological relevance to produce cytosolic NADH at the expense of NADPH is not obvious at the first sight, the clearance of overwhelming NAPDH has been proposed for soluble transhydrogenase in several bacteria (Spaans et al., 2015). However, this hypothesis remains a question of debate. Moreover, it cannot be excluded that the NAD(P) transhydrogenase-like activity of semipermeabilized *S. cerevisiae* is reversible in intact cells to provide NADPH e.g., under oxidative stress conditions or for biosynthetic processes. A similar hypothesis is suggested by the observation of the NAD, but not NADP pool, being

strongly sensitive towards H₂O₂- and diamide-induced oxidation (**Section 2.4.1** and **Section 2.4.2**). Nevertheless, a general NADH → NADPH transhydrogenase-like activity during oxidative stress can be excluded because NADPH, but not NADH, is oxidized in a *Δzwf1* strain after TBHP addition (**Figure 2.24I,L**).

In the context of this study, various hypotheses were followed to unravel the NAD(P) transhydrogenase-like mechanism of semipermeabilized cells (data not shown). To this end, various deletion strains expressing Pdx-mC DS (NADH/NAD⁺) were semipermeabilized and treated with different concentrations of either NADH or NADPH. The fluorescence responses were compared to identify a mutant in which the sensor was less responsive to NADPH than to NADH addition, corresponding to the Pdx-mC DS *in vitro* binding properties. None of the deletions abolished the strong sensor response to NADPH. For instance, multiple single and double deletion strains of the dihydroxyacetone (DHA) cycle were checked for their transhydrogenase-like activity (Valtey, 2021). When the requirement for NADPH is high, the DHA cycle was proposed to supply for cytosolic NADPH in an ATP- and NADH-dependent manner (Celton et al., 2012). Further, the NAD⁺-specific Utr1 and Yef1 kinases were checked for a potential NADPH phosphatase activity in semipermeabilized cells. But neither deletion of *UTR1* (**Appendix, Figure S11A,B**) nor that of *YEF1* (Valtey, 2021) impeded the apparent NADPH → NADH conversion. Finally, it was hypothesized, that the NADPH → NADH interconversion takes place via the action of various Ald enzymes. These are specific for either NAD or NADP and were proposed to act as an extension to the ethanol-acetaldehyde shuttle to balance NADPH/NADP⁺ with NADH/NAD⁺ ratios (Bakker et al., 2001; Celton et al., 2012; Murray et al., 2011). Ald6 plays a central role in this mechanism as it represents the only NADP⁺-dependent cytosolic isoform (Meaden et al., 1997) and thus, its deletion was expected to abolish the Pdx-mC DS response to NADPH, but it did not (**Appendix, Figure S11C,D**). Since the generation and the screening of deletion strains is time-intensive, the usage of a yeast deletion library in combination with an automated screening method would be highly beneficial to elucidate the transhydrogenase-like mechanism. Nonetheless, as respective gene deletions may lead to metabolic adaptations, it remains uncertain whether this approach would find potential candidates of the transhydrogenase-like mechanism.

Other possible transhydrogenase-like mechanisms include NAD(P)H shuttles and reactions occurring in the mitochondrial matrix. For instance, a transhydrogenase-like shunt was established in a xylose-producing *S. cerevisiae* strain by the overexpression of cytosolic pyruvate carboxylase (*PYC2*), malate dehydrogenase (*MDH2*), and mitochondrial malic enzyme (*MAE1*) (**Figure 3.1**) (Suga et al., 2013). This mechanism includes the ATP-

dependent conversion of pyruvate to oxaloacetate (Pyc2). The latter is then NADH-dependently reduced to malate (Mdh2). Malate is subsequently shuttled into the mitochondrial matrix, where it is oxidized to pyruvate (Mae1), forming NADPH. The NADPH produced in the mitochondrial matrix can then be shuttled to the cytosol to provide the electrons for xylose production. However, whether this transhydrogenase-like shunt is relevant under respiratory conditions in a WT strain with physiological enzyme levels, remains unknown. To rule out, whether a mitochondrial shuttle plays a role in the transhydrogenase-like mechanism in semipermeabilized cells, the presence of intact mitochondrial membranes should be confirmed using a dye such as tetramethyl rhodamine methyl ester (TMRM).

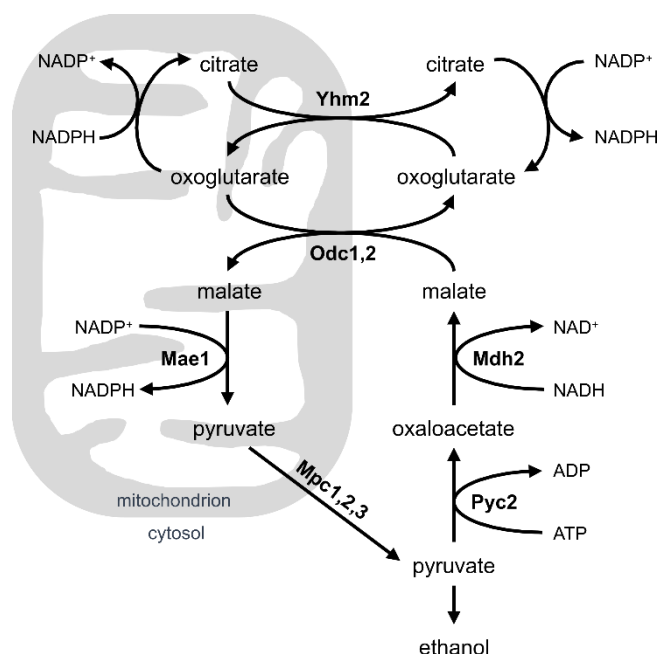


Figure 3.1: Reactions implicated in the reported transhydrogenase-like shunt.

Adapted from Suga et al., 2013. The citrate-oxoglutarate shuttle and the oxodicarboxylate carriers Odc1 and Odc2 were added according to Ferramosca and Zara, 2021.

Interestingly, an NADPH → NADH transhydrogenase activity of a cytosolic fraction of *S. cerevisiae* was already reported in 1985 (Evans et al., 1985). In contrast, no transhydrogenase activity was detected for intact or sonicated mitochondria, suggesting that this mechanism is restricted to the cytosol. Further investigations demonstrated that the cytosolic transhydrogenase activity was mediated by a high-molecular-weight enzyme, most likely fatty acid synthetase (Evans et al., 1985). It was proposed that the enoyl reductase activity is responsible for this effect as it is able to use both, NADPH and NADH, as electron donor (Fox and Lynen, 1980). To the best of my knowledge, further reports on

NAD(P) transhydrogenase activities of fatty acid synthetase do not exist. Hence, it is questionable, in how far it contributes to the NADPH → NADH interconversion observed in semipermeabilized cells. Additional potential transhydrogenase-like shunts, such as cycles between NAD- and NADP-dependent glutamate (Boles et al., 1993; Moreira dos Santos et al., 2004) or isocitrate dehydrogenases (Sazanov and Jackson, 1994) are discussed in detail by Celton et al. (2012). In general, further investigations are required to unravel the transhydrogenase-like activity of semipermeabilized *S. cerevisiae*.

3.3 Redox mechanisms during acute oxidative stress

The influences of three different, exogenously added oxidants (H_2O_2 , diamide, and TBHP) on the cytosolic NAD and NADP redox balances were investigated in the BY4742 WT strain (**Section 2.4**). To gain a deeper insight into the underlying redox mechanisms, roGFP2-Tsa2ΔC_R and roGFP2-Grx1 responses were additionally analyzed in parallel. The exogenous oxidant application led to the oxidation of the roGFP2 probes as expected (**Figure 2.15A,B**, **Figure 2.18A,B** and **Figure 2.21A,B**), whereas the NADPH/NADP⁺ ratio and the NADPH concentration, determined by NAPstar and iNap probes, remained remarkably stable (**Figure 2.16**, **Figure 2.19** and **Figure 2.22**). Since the glutathione (GSH, reduced form) and thioredoxin (Trx) systems rely on NADPH as electron source, a strong oxidation would have been expected. The pentose phosphate pathway (PPP) is the major producer of NADPH when cells are grown in the presence of glucose (Nogae and Johnston, 1990). When the requirement for NADPH is elevated, the flux rate through this pathway increases, inter alia due to its dependency on the NADPH/NADP⁺ ratio (Celton et al., 2012; Frick and Wittmann, 2005; Vaseghi et al., 1999). Hence, the robustness of the cytosolic NADPH concentration and the NADPH/NADP⁺ ratio, even under very strong pro-oxidative conditions, is most likely ensured by the high NADPH production rate of the PPP. This hypothesis is supported by the observation that the deletion of *ZWF1* (encoding for glucose-6-phosphate dehydrogenase, G6PDH) dramatically sensitized the cytosolic NADPH/NADP⁺ ratio towards exogenous H_2O_2 and TBHP (**Figure 2.24G,I**). Surprisingly, it barely affected the sensitivity towards diamide (**Figure 2.24H**), although the PPP was suggested to be central during diamide-induced oxidative stress (Larochelle et al., 2006). In contrast to *S. cerevisiae*, the cytosolic NADPH pool seems to be less robustly maintained in mammalian cells. Diamide reversibly oxidized NADPH in HeLa cells and the additional deletion of the G6PDH abolished the recovery of NADPH (Tao et al., 2017). The fact, that the glucose availability during the cell line cultivation strongly affected the sensitivity of

cytosolic NADPH further underlines the importance of the PPP flux for NADPH homeostasis during oxidative challenge also in mammalian cells.

3.3.1 Relevance of GSH and Trx systems in NAD(P) oxidation

The influence of exogenous H₂O₂ on the *S. cerevisiae* redox systems is well investigated. It can diffuse into the cytosol where H₂O₂-scavenging enzymes produce a steep intracellular H₂O₂ gradient (Calabrese et al., 2019; Zimmermann et al., in preparation). Moreover, the application of H₂O₂ was shown to lead to the intracellular accumulation of glutathione disulfide (GSSG) (Morgan et al., 2013). In contrast, diamide oxidizes thiol groups rather unspecific, in dependency of their nucleophilicity and their accessibility to the oxidant (Kosower and Kosower, 1995). The deletion of the glutathione reductase *GLR1*, which is required for the direct, NADPH-dependent reduction of GSSG, abolished any detectable H₂O₂- and diamide-induced NADPH oxidation in the yeast cytosol (**Figure 2.25C** and **Figure 2.26C**). This result implicates that Glr1 is a major consumer of NADPH during these pro-oxidative injuries. This hypothesis is additionally confirmed by the observations made using the roGFP2-Grx1 and NAPstar3 probes in the $\Delta zwf1$ cytosol, where the low NADPH availability is expected to limit the reduction of GSSG and with this, the GSH production (Izawa et al., 1998; Yoshikawa et al., 2021). Indeed, the oxidation kinetics of the GSSG/2GSH and NADPH/NADP⁺ sensors were mirroring each other (**Figure 2.24D-I**), suggesting that the production of NADPH limits the regeneration of GSH. Similar results were obtained in other eukaryotic organisms. The induction of oxidative stress in NAPstar expressing mammalian or plant cells indicated, that the Glr activities in these organisms also contribute significantly to the consumption of cytosolic NADPH (Mai et al., in preparation). Overall, these results confirm the central role of NADPH-dependent GSH maintenance for eukaryotic cellular antioxidant defense.

Recent data from our laboratory indicates that the Tsa1 activity is central for the peroxide scavenging capacity of the yeast cytosol and that it represents the major source of peroxide-induced cytosolic GSSG (Zimmermann et al., in preparation). Other peroxiredoxins (Prxs) and glutathione peroxidases (Gpxs) may support Tsa1 in H₂O₂ detoxification (Avery and Avery, 2001; Herrero et al., 2008). Most likely, these alternative thiol-exchange mechanisms cause the altered NADPH/NADP⁺ oxidation kinetics upon H₂O₂ application in the $\Delta tsa1\Delta tsa2$ double deletion strain (**Figure 2.25K**). Despite the increased H₂O₂ sensitivity of the roGFP2 probes observed in this mutant, the oxidation kinetics of NADPH did not seem to be accelerated, hinting on the importance of Tsa1 in H₂O₂ detoxification.

The cytosolic Prxs Tsa1 and Tsa2 are primarily reduced by Trx1 and Trx2 which are in turn reduced by the cytosolic NADPH-dependent thioredoxin reductase Trr1 (Grant, 2001). The double deletion of *TRX1* and *TRX2* impeded any measurable, H₂O₂-induced NADPH oxidation highly likely due to the decreased electron flux through Trr1 (**Figure 2.25G**). This suggests, together with the observations made for the $\Delta glr1$ deletion strain, that the Trx- and GSH- based systems contribute significantly to the NADPH consumption after H₂O₂ treatment. In contrast, the cytosolic NADPH oxidation after diamide treatment was diminished in the $\Delta trx1\Delta trx2$ mutant, but still detectable (**Figure 2.26G**), implying that the Trx system consumes less NADPH than the GSH system under these conditions. Interestingly, the double deletion of *TSA1* and *TSA2* apparently impeded completely the decrease in the NADPH/NADP⁺ ratio after diamide application, similar to observations made using the $\Delta glr1$ strain (**Figure 2.26K**). To the best of my knowledge, an implication of Tsa in diamide scavenging has not been described. Hence, these results indicate that a crosstalk between the Trx- and GSH-based systems takes place that finally result in the different NADPH oxidation kinetics observed in the various yeast deletion strains.

Besides the discrepancies in NAD(P) oxidation kinetics, the cellular steady states of the cytosolic NADPH/NADP⁺ ratio were altered in the $\Delta tsa1\Delta tsa2$ and $\Delta trx1\Delta trx2$ deletion strains (**Table 2.3**). These alterations are potentially caused by differential metabolic adaptations upon the different gene deletions (**Section 3.3.2**). To avoid these compensatory mechanisms, chemical interventions can be performed to inhibit the enzyme activities during the experiment. Nonetheless, these agents tend to be unspecific, induce global metabolic alterations, and have produced conflicting results according to previous literature (Saccoccia et al., 2014).

Despite the exact, diamide-induced redox mechanism remains unclear, different exciting observations were made during this study. (i) Although diamide was not reported to lead to the inactivation of Tdh (Grant et al., 1999), the NAD oxidation induced by exogenous diamide was almost equal to that of H₂O₂ (**Figure 2.17**, **Figure 2.20** and **Section 3.3.2**). (ii) The deletion of *ZWF1* marginally influenced the oxidation of cytosolic NADP by exogenous diamide (**Figure 2.24H**). (iii) The *TSA1 TSA2* double deletion completely abolished any detectable NADP oxidation (**Figure 2.26K**). To understand these observations, further experiments have to be performed including important controls. For instance, the metabolic adaptations (including the ATP metabolism) of the different deletion strains have to be considered (**Section 3.3.2**). Since the NAPstarC fluorescence ratio decreased upon high diamide boluses, it would be interesting to resolve the individual

influences of altered cytosolic pH and ATP concentration to draw conclusions about e.g., pH-dependent regulation of enzymatic activities.

Recent data from our laboratory show that the addition of 0.1 mM exogenous TBHP is sufficient to hyperoxidize a matrix-localized roGFP2-Tsa2 Δ C_R sensor (Zimmermann et al., in preparation). Opposing, treatment with 0.1 and 1 mM TBHP clearly led to a prolonged cytosolic NADPH oxidation in the WT and $\Delta zwf1$ strains in this study (**Figure 2.22C** and **Figure 2.24I**), indicating that the cytosolic antioxidant defense mechanisms are, at least partially, functional under these conditions.

3.3.2 Regulation of NAD metabolism during acute oxidative stress

The metabolic carbon flux, starting with glucose, is divided between the NADH-producing glycolysis and the NADPH-producing PPP. This partitioning is regulated by, inter alia, the glyceraldehyde-3-phosphate dehydrogenase (GAPDH) activity (Shenton and Grant, 2003). It has been shown that H₂O₂ oxidizes GAPDH which is followed by S-glutathionylation, and enzymatic inactivation, rerouting the carbon flux from glycolysis to the PPP, thereby increasing the NADPH generation at the expense of NADH. *S. cerevisiae* harbors three GAPDH isoforms, Tdh1-3 (Bouchérié et al., 1995; Delgado et al., 2001). Tdh2 and Tdh3 represent the major isoforms during exponential growth (McAlister and Holland, 1985). Only Tdh3 was shown to be glutathionylated and inactivated in an H₂O₂-dependent manner (Grant et al., 1999). Opposing to H₂O₂, the treatment with diamide or TBHP was not reported to lead to Tdh3 glutathionylation. Thus, it was surprising that the cytosolic NADH/NAD⁺ ratio was reversibly oxidized in the WT strain after addition of diamide up to 1 mM extracellular concentration as observed for H₂O₂ (**Figure 2.17C,D** and **Figure 2.20B,C**). In contrast, TBHP did not affect NADH/NAD⁺ (**Figure 2.23**). These data suggest an inactivation of Tdh by both, H₂O₂ and diamide. The H₂O₂-induced oxidation kinetics were not altered between strains in which endogenous Tdh1-3 were replaced by either WT Tdh3 or H₂O₂-resistant Tdh3 variants (**Appendix, Figure S12**). The same effect was observed using the respective human GAPDH isoforms (Jakob, 2021). This indicates that the Tdh3/ GAPDH oxidation mechanism is unspecific under the conditions at which the NAD oxidation was observed i.e., most likely the oxidant concentrations were too high to detect kinetic differences between the different Tdh or GAPDH mutants. Overall, the data suggest an inactivation of Tdh by H₂O₂ and diamide, but not TBHP. Whether and to what extent Tdh activity is inhibited upon diamide application remains to be revisited in the described experimental setup to confirm the connection between Tdh activity and the observed oxidation of cytosolic NADH.

Interestingly, the double deletion of *TRX1* and *TRX2* rendered the cytosolic NADH/NAD⁺ ratio remarkably robust against exogenous H₂O₂ and diamide (**Figure 2.25H** and **Figure 2.26H**). A direct implication of Trxs in the oxidation of NADH appears unlikely. But intriguingly, the deletion of *TRR1* was reported to increase the intracellular levels of NAD by the upregulation of NAD⁺ biosynthesis (Picazo et al., 2018). Similar effects potentially occur in the $\Delta trx1\Delta trx2$ strain causing the robust cytosolic NADH/NAD⁺ ratio.

Some of the observations made in this study are certainly caused by cellular adaptations in order to compensate for the loss of important genes implicated in NADPH production, H₂O₂ signaling, or in the GSH- and Trx-based antioxidant systems. The connection network between ROS signaling and NAD(P) metabolism is very complex and far from being completely understood. Only a few mechanisms, which are part of this network, will be mentioned in the following, since a detailed discussion with respect to the results obtained in the course of this study would require further intensive experimental support. (i) Pnc1 catalyzes the production of nicotinic acid (NA) from nicotinamide (NAM) and is part of the NA/NAM salvage pathway. This pathway is the major source of NAD⁺ under common growth conditions. The expression of *PNC1* is regulated by the stress-responsive transcriptional factors Msn2 and Msn4, connecting the NAD⁺ biosynthesis to the cellular stress response (Medvedik et al., 2007). Moreover, Msn2/4 regulate 66% of all yeast genes, making concrete predictions about the consequences for the metabolism of NAD and NADP almost impossible (Causton et al., 2001). (ii) The Stb5 transcription factor regulates the expression of genes involved in the production of NADPH but its exact regulation mechanism is unknown (Larochelle et al., 2006; Ouyang et al., 2018). (iii) The activity of the Yap1 transcription factor is highly likely upregulated in all of the tested deletion strains, resulting in increased NADPH and GSH production, upregulation of catalases, Trxs, and Prxs (Lee et al., 1999). (iv) The Skn7 transcription factor cooperates partially with Yap1 for transcriptional regulation, but both are partly differentially regulated. Interestingly, the expression of *TDH2*, but not that of *TDH3*, is upregulated in a Yap1- and Skn7-dependent manner (Venters et al., 2011). This suggests, that the 'oxidant-robust' Tdh2 is required to maintain a high glycolytic rate during oxidative stress. Thus, the differential regulation of *TDH2*, *TDH3*, and potentially *TDH1*, in the various deletion strains discussed above, possibly influences the carbon flux regulation and with this, NAD(P)H generation.

According to most of the literature, NADPH and NAD⁺ are often reduced to their roles as final electron donor and acceptor at the end of cellular redox reactions. The presented study demonstrates that this thinking is an oversimplification caused by the high metabolic flexibility and the lack of suitable measurement techniques. The invention of novel

tools for the quantification of NAD(P) metabolites will surely change our understanding of NAD and NADP as redox coenzymes, which should additionally be considered as central hubs between redox and metabolic processes.

3.4 NAD(P) during the yeast metabolic cycle

During the yeast metabolic cycle (YMC), different GFIs were expressed in the *S. cerevisiae* cytosol and the respective fluorescence signals were monitored using a flow cell. The heterologous expression was achieved by the plasmid transformation of a Cen.PK113-1A $\Delta his3$ strain. Importantly, the fluorescence signals of plasmid-expressed probes remained stable over time (data not shown). Surprisingly, the plasmid-expressed HyPer7 fluorescence signal was much brighter than that of the genomically-integrated roGFP2 probe, although HyPer7 was expressed under the control of a weaker promoter (data not shown). In addition, elaborate genomic integration was circumvented by the usage of a single, genomically modified strain enabling for easy and flexible plasmid transformation. These results demonstrate the advantages of plasmid-expressed GFIs for the investigation of various parameters in the YMC setup. Interestingly, the YMC period of the transformed Cen.PK113-1A $\Delta his3$ culture was shortened. This was consistent between the different experiments and most likely caused by the reduced growth rate of this strain. The dilution rate, not being adapted to the prolonged doubling time, probably shortened the LOC phase and with this, the overall period (Burnetti et al., 2016). Although the cycle time altered slightly between different experimental runs, the unification of a full cycle to 360° enabled the direct comparison between the various parameters which were determined by GFI measurements (**Figure 3.2**).

Remarkably, stable oscillations of the NAPstarC fluorescence ratio were detected throughout the YMC. Preliminary in vitro analyses demonstrated the NAPstarC ratio being sensitive to ATP and to pH in the range of 6 to 7 (**Section 2.3.1**). With a decrease in ATP, or an increase in pH, the cpTS/mC ratio of NAPstarC rises. As the NAPstarC and pHluorin fluorescence signals behaved rather inverse than in phase (**Figure 2.33C** and **Figure 2.34E**), changes in cytosolic pH did not seem to be the cause of the NAPstarC cycles. Hence, it was concluded that the variations in the NAPstarC signal most likely derived from alterations in the cytosolic ATP concentration. Since the exact ATP dependency of NAPstarC is unknown so far, a suitable control, such as the ATP-specific ATeam sensor (Imamura et al., 2009; Papagiannakis et al., 2017), should be considered as confirmation for future experiments. Nonetheless, the NAPstarC cycles were regarded to detect the changes in ATP concentration and plotted as mC/cpTS ratio (**Figure 3.2**) to

obtain a parameter that is directly proportional to the ATP concentration. Moreover, various NAPstar oscillations were observed during the YMC, marginally differing between the individual variants (**Figure 2.34**). Since the NAPstarC background oscillation partially resembled the NAPstar readouts, unequivocal oscillations in NADPH/NADP⁺ were not identified. Yet, the distinct fluorescence pattern of NAPstar4.3, that partly behaved opposing to that of NAPstarC, might indeed reflect oscillations in NADPH/NADP⁺ (**Figure 2.34C,E**). Thus, the NAPstar4.3 cpTS/mC ratio was regarded to discuss potential NADPH/NADP⁺ changes during the YMC (**Figure 3.2**).

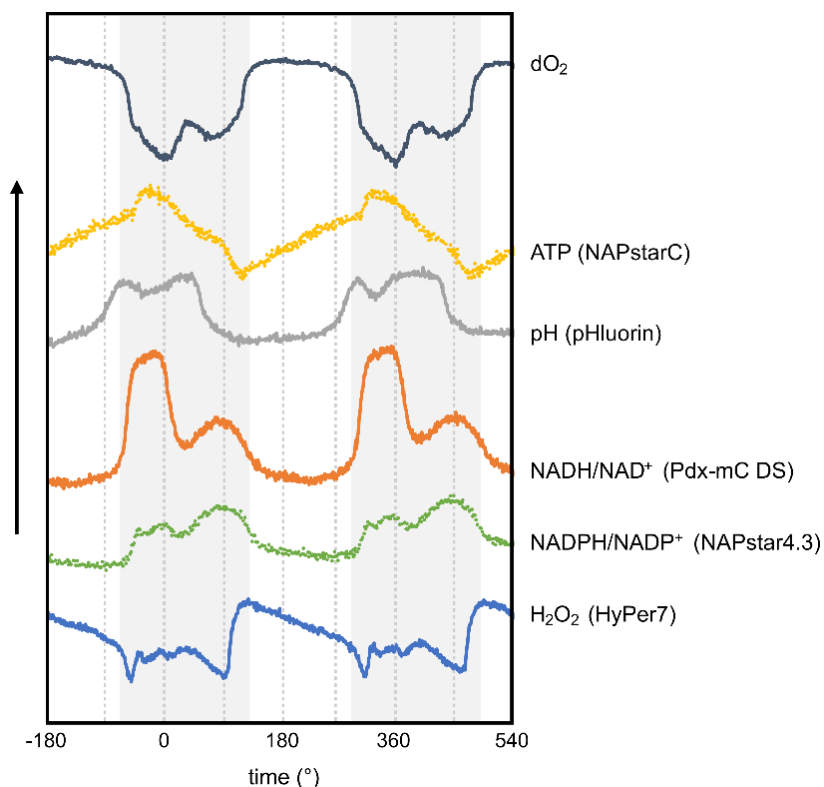


Figure 3.2: Overview over the cytosolic GFI-determined parameters during the YMC.

HOC and LOC phases were marked in grey and white, respectively. mC/cpTS of NAPstarC, 395/475 nm of pHluorin, cpTS/mC of Pdx-mC DS and NAPstar4.3, as well as 490/400 nm of HyPer7 were plotted against the time in degree. Results for ATP and NADPH/NADP⁺ are dotted due to incomplete probe characterization and lack of appropriate controls.

In general, the GFI-determined and -assumed parameters during YMC support the recently proposed model of TORC1 regulation (O'Neill et al., 2020), as will be discussed in the following (for supporting references, please refer to the original publication): The LOC phase is supposed to start with the depletion of the carbohydrate and amino acid storages. The low glucose availability decreases the glycolytic flux, and the respiratory rate, and with this, the oxygen consumption rate and ATP availability. The low ATP level is insufficient to

drive the activity of the plasma-localized H⁺-ATPase Pma1, leading to the acidification of the cytosol. This is supported by the NAPstarC (ATP) and pHluorin (pH) measurements (**Figure 2.33C**, **Figure 2.34E** and **Figure 3.2**). As the pH is marked by a sharp drop during this phase while the ATP concentration seems to decrease rather continuously, an additional regulation mechanism of Pma1 is conceivable e.g., via glucose (Serrano, 1983). At the start of LOC phase, TORC1 is supposed to be inactivated by various mechanisms resulting in the downregulation of protein synthesis and the stimulation of autophagic processes (O'Neill et al., 2020). Thus, the LOC phase represents a quiescent, storage-filling phase.

During the mid-LOC phase, Pma1 was reported to be still inactive due to the low ATP availability (O'Neill et al., 2020). The cytosolic pH is stabilized at pH 6.3. Although the exact pH value cannot be specified using the pHluorin probe, its fluorescence confirms a stable low cytosolic pH (**Figure 2.33C** and **Figure 3.2**). Low pH is assumed to ease the formation of biomolecular condensates, such as stress granules (O'Neill et al., 2020). Thereby, the glycolytic flux is further downregulated, whereas the stress resistance is increased. The low glycolytic rate is reflected by the Pdx-mC fluorescence ratio reporting a low cytosolic NADH/NAD⁺ ratio (**Figure 2.33A** and **Figure 3.2**). This oxidized NAD state persists to the end of LOC phase. As less glucose is consumed by glycolysis, more sugar is available to fill up carbohydrate storages and to produce biosynthetic intermediates via the PPP, the DNA, and the fatty acid synthesis (O'Neill et al., 2020). An increased flux through PPP is expected to rise NADPH/NADP⁺, but NAPstar4.3 reported no alterations in the NADP redox balance (**Figure 2.34C** and **Figure 3.2**). Most likely, the generated NADPH is immediately consumed by the ongoing biosynthetic processes and thus not detected by the GFI. Further, the vacuolar amino acid store is supposed to recharge during this phase (O'Neill et al., 2020).

The entry into HOC is likely initiated by the filled carbohydrate stores, leading to increased glycolytic flux, respiratory rate, and ATP generation (O'Neill et al., 2020). The enhanced ATP availability stimulates the Pma1 activity, increasing the cytosolic pH. This hypothesis is confirmed by a sharp rise in pH, as detected by pHluorin (**Figure 2.33C** and **Figure 3.2**). ATP (NAPstarC) peaks little later during early HOC phase, together with NADH/NAD⁺ (Pdx-mC) and H₂O₂ (HyPer7) (**Figure 2.32A**, **Figure 2.33A** and **Figure 3.2**). The latter is most likely produced by the increased electron flux through the electron transport chain (Ayer et al., 2014). A temporal connection between the glycolytic flux (or NADH/NAD⁺, Pdx-mC) and the ATP production (NAPstarC) detected by the GFIs is not

obvious. Besides other mechanisms, the elevated energy charge in form of ATP is assumed to abrogate the inhibition of TORC1 (O'Neill et al., 2020).

A feed forward mechanism was proposed during early HOC phase which further increases the glycolytic flux and the cytosolic pH to pH 7 (O'Neill et al., 2020). The pH-mediated activation of GTPase Gtr1/2 (Dechant et al., 2014; Saliba et al., 2018) and the subsequent TORC1 activation inhibits autophagy and stimulates translation initiation. The reported elevation in glycolytic flux is mirrored by a rise in NADH/NAD⁺ (**Figure 2.33A** and **Figure 3.2**). During the late HOC phase, the carbohydrate storages are broken down to keep the carbon flux through glycolysis, and the respiratory rate, high (O'Neill et al., 2020). The amino acid storage becomes smaller due to the increased rate in protein synthesis. The reasons, why the protein synthesis may decrease at HOC exit, are discussed in detail by O'Neill and colleagues (2020). The lowered synthetic rate decreases the ATP turnover and thus the oxygen consumption rate. The decreased ATP turnover is accompanied by a rise in ATP as detected by NAPstarC (**Figure 2.34E** and **Figure 3.2**).

Overall, the results obtained by NAPstarC for ATP, pHluorin for pH and Pdx-mC for NADH/NAD⁺ support the proposed model. In addition, a glucose-sensitive GFI, such as the FLIIglu (Bermejo et al., 2010) or Glifon sensors (Mita et al., 2022, 2019), could reveal further insights into the regulation of Pma1 (Serrano, 1983), glucose-mediated TORC1 regulation and the (im)mobilization of carbohydrates.

Changes in NAD(P)H during YMC were so far usually determined by autofluorescence measurements (Murray et al., 2014), but these measurements are imprecise since they mix up different compartments and do not discriminate NADH from NADPH or protein-bound from free coenzyme pools. Nevertheless, the described autofluorescence signals overlap partially with those observed for cytosolic free NADH/NAD⁺ (Pdx-mC) and NADPH/NADP⁺ (NAPstar4.3) (**Figure 3.2**). In contrast to the GFI measurements, the reported major maximum of the NAD(P)H autofluorescence occurs during the late HOC phase (Murray et al., 2014). This circumstance speaks in favor of the shuttling of cytosolic NAD(P)H into the mitochondrial matrix, making it 'invisible' for the probes residing in the cytosol. Indeed, this phase is marked by mitochondria biogenesis (Tu et al., 2005). In how far the mitochondrial shuttle activities are upregulated during this phase remains to be shown. The decrease in the cytosolic ATP concentration (NAPstarC) and the oxygen consumption rate (**Figure 3.2**) during this phase clearly implicate a decreased respiratory rate. Hence, the shuttled NAD(P)H equivalents are most likely required for biosynthetic processes taking place inside the mitochondrial matrix instead of respiration.

As already discussed, the oscillations detected by NAPstar4.3 may reflect the cytosolic NADPH/NADP⁺ ratio during the YMC (see above). Despite this probe being more robust towards NADH (**Section 2.3.1**), its response pattern during the YMC strongly resembled that of NADH/NAD⁺ (**Figure 3.2**). This observation indicates the generally increased carbon flux during the HOC phase, which is partitioned between glycolysis, probably causing the elevated NADH/NAD⁺ ratio, and the PPP, that rises NADPH/NADP⁺. Interestingly, it seems that this flux is differentially regulated during early and late HOC phases. During the early HOC phase, the glycolytic flux (NADH/NAD⁺) seems to be higher than that during the late HOC phase, whereas the reverse pattern is observed for the apparent carbon flux through the PPP (NADPH/NADP⁺). In this context, it would be interesting to investigate the regulatory role of Tdh activity (**Section 3.3.2**). Overall, the results obtained by GFI measurements during YMC could essentially contribute to the refinement of metabolic models for flux determinations.

Moreover, the NADPH/NADP⁺ ratio seems to be connected to the cytosolic H₂O₂ concentration, that shows an inverse pattern (**Figure 3.2**). This connection is most likely mediated via the activities of Trr1 and Glr1. The results for H₂O₂, obtained by the HyPer7 sensor, are in line with the reports from a genomically integrated roGFP2-Tsa2ΔC_R probe (Amponsah et al., 2021). H₂O₂ peaks during HOC entry, and likely couples the YMC to the CDC via a Prx-mediated mechanism (Amponsah et al., 2021). Recently, Tsa1 was shown to regulate the redox modifications of Tpk1, a protein kinase A (PKA) subunit (Roger et al., 2020). Potentially, the H₂O₂ signals help to orchestrate the TORC1 and PKA activities by the mediation of redox modifications, but further investigations are required to support this hypothesis.

3.5 Concluding remarks and outlook

The development of novel NAPstar sensors, together with our collaboration partners, now enables the monitoring of the NADPH/NADP⁺ ratio in yeast, mammalian cells, and plants with high signal intensity (Mai et al., in preparation). Hence, the established GFI toolbox is expected to deepen our comprehension of cellular (redox) metabolism to reveal similarities and discrepancies between numerous organisms. To further elucidate the in vivo electron fluxes in the future, it would be beneficial to develop probes that allow to quantify actual turnover rates instead of ambient redox potentials or concentrations. Furthermore, probes for absolute quantifications are highly desired for accurate kinetic calculations and metabolic models. Ideally, these probes will not overlap in their (spectral) output to allow for simultaneous measurements.

Additionally, this study demonstrated the high potential of NAD(P)-specific GFIs to investigate the cellular metabolism in *S. cerevisiae* during the YMC. The parallel monitoring of various cytosolic parameters gave deep insights into their temporal compartmentation and enabled to draw parallels to an existing model. In combination with metabolic modelling and further Omic approaches, the obtained data will undoubtedly contribute to the understanding of metabolic fluxes during the YMC. This knowledge is of high interest for the fields of biotechnology and cell physiology.

Finally, the investigation of mitochondrial NAD(P) homeostasis was not addressed in this study. Nonetheless, it is of major interest for the comprehensive understanding of cellular metabolism. GFI targeting to the mitochondrial matrix, or the mitochondrial intermembrane space, would essentially help to understand the compartmentalization of NAD(P) metabolites and NAD(P)-dependent redox processes.

4 Material and Methods

4.1 Key resources

Important chemicals, material, and laboratory equipment used to perform the described experiments are listed in **Table 4.1**.

Table 4.1: Key resources used in this study.

Chemicals		
Product	Supplier, Manufacturer	Comment (Identifier)
Acetic acid	Merck Sigma-Aldrich	99.8% (27225)
Calciumchloride hexahydrate	Carl Roth	≥ 97% (CP89)
Deoxyribonucleic acid, single stranded from salmon testes	Merck Sigma-Aldrich	(D7656)
Diamide	Merck Sigma-Aldrich	(D3648)
Digitonin	Merck Millipore	Calbiochem, high purity (300410)
DTT BioChemica	ITW Reagents	PanReac AppliChem (A1101)
Ethylenediamine tetraacetic acid disodium salt dihydrate (EDTA)	Carl Roth	≥ 99% (X986.2)
Glycerol	Grüssing	99%, anhydrous
Hydrogen peroxide solution (H ₂ O ₂)	Merck Sigma-Aldrich	30% (w/w) in H ₂ O, contains stabilizer (H1009)
Lithium acetate	Merck Sigma-Aldrich	99.95% (517992)
Luperox TBH70X, <i>tert</i> -Butylhydroperoxide solution (TBHP)	Merck Sigma-Aldrich	70% (w/v) in H ₂ O (458139)
MES	Carl Roth	≥ 99% (4259)
MOPS	Merck Sigma-Aldrich	≥ 99.5% (M3183)
NADH disodium salt	Carl Roth	≥ 84% (AE12.1)
NADPH tetrasodium salt	ITW Reagents	PanReac AppliChem (A1395)
Polyethylene glycol (PEG)	Merck Sigma-Aldrich	average Mn 3,350, powder (202444)
Sodium pyruvate	Merck Sigma-Aldrich	ReagentPlus ≥ 99% (P2256)
Trizma base (TRIS)	Merck Sigma-Aldrich	≥ 99.9% (T1503)

Molecular biology		
Product	Supplier, Manufacturer	Comment (Identifier)
Biozym dNTP Mix	Biozym Scientific	10 mM each (331520)
Biozym LE Agarose	Biozym Scientific	(840001)
Fast-Link DNA Ligation Kit	Lucigen	epicentre (LK6201H)
LightRun Tube	Eurofins Genomics	Barcodes, Sanger sequencing service
Midori Green Advance	Nippon Genetics Europe	DNA Stain (MG04)
NucleoSpin Plasmid EasyPure	Macherey-Nagel	Plasmid DNA purification kit (740727)
NucleoSpin Gel and PCR Clean-up	Macherey-Nagel	DNA fragment purification kit (740609)
One Shot TOP10	Thermo Fisher Scientific	Chemically competent cells, Invitrogen (C404003)
Owl EasyCast B1A	Thermo Fisher Scientific	Mini gel electrophoresis system
PowerPac Basic Power Supply	Bio-Rad Laboratories	Electrophoresis power supply
Purple 1 kb DNA Ladder	New England Biolabs	Quick-Load (N0552)
Restriction enzymes	New England Biolabs	Endonucleases with 100% activity in Cutsmart Buffer
S7 Fusion Polymerase	Biozym Scientific	High-fidelity (MD-S7)
SpectraMax QuickDrop	Molecular Devices	DNA quantification, Spectrophotometer
PTC-200 Thermal Cycler Dual 48	MJ Research	PCR and ligation reactions
ChemiDoc XRS	Bio-Rad Laboratories	Agarose gel imaging
2011 MACROVUE Transilluminator	LKB Bromma	Illumination for gel cutting (2011-002)
Media preparation		
Product	Supplier, Manufacturer	Comment (Identifier)
Adenine hemisulfate salt	Merck Sigma-Aldrich	BioReagent (A3159)
Ampicillin sodium salt	Carl Roth	≥ 97%, BioScience grade (K029)
Bottle top filter	VWR, Avantor	500 mL, 0.2 µm PES (514-0340)
D(+)-Glucose monohydrate	Carl Roth	≥ 99.5% (6780)
D(+)-Raffinose pentahydrate	Merck Sigma-Aldrich	≥ 98.0% (R050)
Difco LB Broth	BD Difco	Miller (Luria-Bertani) (244610)

Difco Yeast Nitrogen Base (YNB)	BD Difco	without amino acids (291920)
G418 disulfate salt solution	Merck Sigma-Aldrich	50 mg/mL in H ₂ O, sterile filtered (G8168)
Hygromycin B solution	Carl Roth	50 mg/mL, BioScience grade, sterile (1287)
L-Arginine	Merck Sigma-Aldrich	98.5 - 101.0% (A8094)
L-Aspartic acid	Merck Sigma-Aldrich	98.5 - 101.0% (A7219)
L-Glutamic acid	Merck Sigma-Aldrich	98.5 - 100.5% (G8415)
L-Histidine monohydrochloride monohydrate	Merck Sigma-Aldrich	98.5 - 101.0% (H5659)
L-Isoleucine	Merck	SAFC ≥ 98.0% (I5281)
L-Leucine	Merck Sigma-Aldrich	98.5 - 101.0% (L8912)
L-Lysine monohydrochloride	Merck Sigma-Aldrich	98.5 - 101.0% (L8662)
L-Methionine	Merck Sigma-Aldrich	98.5 - 101.0% (M5308)
L-Phenylalanine	Merck Sigma-Aldrich	98.5 - 101.0% (P5482)
L-Serine	Merck Sigma-Aldrich	98.5 - 101.0% (S4311)
L-Threonine	Merck Sigma-Aldrich	99.0 - 101.0% (T8441)
L-Tryptophan	Merck Sigma-Aldrich	99.0 - 101.0% (L8941)
L-Tyrosine	Merck Sigma-Aldrich	≥ 99.0% (T8566)
L-Valine	Merck Sigma-Aldrich	98.5 - 101.0% (V0513)
Nourseothricin solution (NTC, cloNAT)	Jena Bioscience	100 mg/mL, sterile (AB-101)
Tryptone	Carl Roth	enzymatic digest from casein (95039)
Uracil	Merck Sigma-Aldrich	BioReagent (U1128)

Continuous culturing in bioreactor

Product	Supplier, Manufacturer	Comment (Identifier)
Ammonium sulfate	Merck Sigma-Aldrich	≥ 99.0% (A4418)
Antifoam 204	Merck Sigma-Aldrich	(A8311)
Biostat A bioreactor	Sartorius Stedim Systems	UniVessel Glass, 1 L
Calcium chloride dihydrate	Merck Supelco	Emsure (102382)
Cary Eclipse Fluorescence Spectrophotometer	Agilent Technologies	
Copper(II) sulfate pentahydrate	Merck Supelco	Emsure (102790)
Flow cell	Starna	71-F/Q/10

Iron(II) sulfate heptahydrate	Omnilab	Honeywell Fluka (31236)
Magnesium sulfate monohydrate	Merck Sigma-Aldrich	97% (434183)
Manganese(II) chloride tetrahydrate	Merck Sigma-Aldrich	meets USP testing specifications (M8054)
Potassium dihydrogen phosphate	Merck Supelco	Emsure (104873)
Sodium metabisulfite	Merck Sigma-Aldrich	(71932)
Sulfuric acid	Bernd Kraft	95-97% (07060)
Yeast extract SERVIBACTER	SERVA Electrophoresis	(24540)
Zinc sulfate heptahydrate	Merck Sigma-Aldrich	BioReagent (Z0251)

4.2 Molecular biological methods

4.2.1 Oligonucleotides

DNA oligonucleotides were obtained from Eurofins Genomics Germany (**Table 4.2**). Salt-free, lyophilized products were solved and stored as 100 μ M stock solutions at -20°C .

Table 4.2: Oligonucleotides used in this study.

Molecular cloning		
Primer	Sequence 5' -> 3'	Comment
mScarlet_XbaI_fw	GGTGGTTCTAGAACCATGGGATCCGTGAG CAAGGGCGAGGCAGT	N-terminal fusion of mSI to SoNar/ iNap via SpeI cutting site to generate mSI-SoNar and -iNap constructs
mScarlet_SpeI_rv	ACCACCACTAGTCTTGTACAGCTCGTCCAT GC	
iNap_SpeI_fw	GGTGGTACTAGTGGTGGTTCAGGTGGTGG TGGTTCAGGTGGTGGTGGTTCAGGTGGAG GAGGATCAGGAGGAAACAGAAAGTGGGGT TTGTG	
iNap_XhoI_rv	ACCACCCTCGAGTTAACCCATCATTTC	
QC_Perodox_D117S_fw	GAATTGAGAGGTTTCTTTTCCGTTGATCCA GGCATGGTTGGTAGACC	Mutagenesis of Pdx-mC to generate Pdx-mC DS
QC_Perodox_D117S_rv	GGTCTACCAACCATGCCTGGATCAACGGA AAAGAAACCTCTCAATTC	
QC_Perodox_D574S_fw	CATTTGAATTAAGAGGTTTCTTTTCCGTTGA TCCAGGCATGGTCCG	
QC_Perodox_D574S_rv	CCGACCATGCCTGGATCAACGGAAAAGAA ACCTCTTAATTCAAATG	

QC_iNap3b_L366P_fw	CATAAATTGGAATACAACGGTCCAGCAGGT TTGACAAGATTATCC	Mutagenesis of iNap3b linker region to generate iNap3c
QC_iNap3b_L366P_rv	GGATAATCTTGTCAAACCTGCTGGACCGTT GTATTCCAATTTATG	
Sequencing		
Primer	Sequence 5' -> 3'	Comment
Seq_TEF_fw	TTTCTCTTTTCGATGACCTC	binds in <i>TEF1</i> promoter
Seq_TEF_rv	ACTTCAGGTTGTCTAACTC	binds in <i>CYC1</i> terminator
Seq_GAL_fw	ACCTCTATACTTTAACGTC	binds in <i>GAL1</i> promoter
Seq_GPD_fw	GACGGTAGGTATTGATTG	binds in <i>GPD</i> promoter
Seq_promoter_fw	CCGGCTCCTATGTTGTG	Promoter sequencing
Seq_mSI-Spel_fw	GCTGTACAAGACTAGTGG	binds in <i>mSI</i> region
Seq_cpTS_fw	ACATGGTCAGCTGCAGG	binds in <i>cpTS</i> region
Seq_mC_rv	CCATGTTATCTTCTTCACC	binds in <i>mC</i> region
Homologous recombination		
Primer	Sequence 5' -> 3'	Comment
Conf_glr1_fw	GATAGTTTAATTCATTTGCACGGCG	Confirmation of <i>GLR1</i> deletion
Conf_glr1_rv	CTTCTTTGAAGGCTTAAAGTTAGAAAGCAG	
Conf_trx1_fw	AACAAGCTAAGTTGACTGCTG	Confirmation of <i>TRX1</i> deletion
Conf_trx1_rv	TCTCTAAAATTGTGCGTTGC	
Conf_trx2_fw	CGGAACCAACGTATTTAGAG	Confirmation of <i>TRX2</i> deletion
Conf_trx2_rv	AATGTTCCAGTTGAAGCAAG	
Conf_tsa1_fw	CCTATGTGAAGGAGAAGCTG	Confirmation of <i>TSA1</i> deletion
Conf_tsa1_rv	CAATAAGTAGCCCGAAACAG	
Conf_tsa2_fw	TTAGTAAGCGCTACGACGAC	Confirmation of <i>TSA2</i> deletion
Conf_tsa2_rv	GACTATGCCAATTGAGATGC	
S1_zwf1	AGTAAATCCAATAGAATAGAAAACACATA AGGCAAGATGCGTACGCTGCAGGTCGAC	Deletion of <i>ZWF1</i>
S2_zwf1	AGTGACTTAGCCGATAAATGAATGTGCTTG CATTTTTCTAATCGATGAATTCGAGCTCG	
Conf_zwf1_fw	GTCTTACGCGGAGATACAAG	Confirmation of <i>ZWF1</i> deletion
Conf_zwf1_rv	AGTGGATAAGACGCATAACG	
Conf_ald6_rv	TCCACGTTAGTTTTCTTTGG	Confirmation of <i>ALD6</i> deletion
Conf_ald6_fw	AAAGAAAACGACCGAAAAG	

Conf_natNT2_fw	GCGCTCTACATGAGCATGCC	Confirmation of genomic <i>natNT2</i> integration
Conf_natNT2_rv	CATCCAGTGCCTCGATG	
Conf_kanMX4_fw	TGATTTTGGATGACGAGCGTAAT	Confirmation of genomic <i>kanMX4</i> integration
Conf_kanMX4_rv	CTGCAGCGAGGAGCCGTAAT	

4.2.2 Plasmids

All plasmids used in this study are listed in **Table 4.3**. All genes were codon-optimized for expression in *S. cerevisiae*. Indicated plasmids were constructed by either direct subcloning via restriction and ligation or polymerase chain reaction (PCR) was performed for targeted mutagenesis. Newly synthesized products were provided by GenScript Biotech (Netherlands). Open reading frames were usually flanked by the unique restriction sites XbaI (**TCT AGA**) at 5', and XhoI (**CTC GAG**) at 3' terminus. The start codon (**ATG**) was embedded in an ACC **ATG GGA TCC** sequence right after the XbaI cutting site. The generated BamHI cutting site (**GGA TCC**) can be optionally used for the insertion of the Su9 mitochondrial targeting sequence (Westermann and Neupert, 2000).

Table 4.3: Plasmids used in this study.

All plasmids harbor an ampicillin resistance cassette for selection of transformed *E. coli*. p413 and p415 plasmids encode for His3 and Leu2 selection markers, respectively, to enable for selection of transformed *S. cerevisiae*. Plasmids were generated by molecular cloning via ^A PCR-based modification, and/ or ^B restriction digest and ligation. The mSI gene sequence was kindly provided by Prof. Dr. Maya Schuldiner (Department of Molecular Genetics, Weizmann Institute of Science, Rehovot, Israel). The DNA sequences encoding for SoNar, iNap, Pdx-mC (DS) and NAPstar probes are listed in the appendix.

GFI expression		
Plasmid	Source	Reference
p413 TEF empty	—	Mumberg et al., 1995
p413 GPD empty	Molecular cloning ^B	
p415 GAL empty		
p413 TEF SoNar	Genscript Biotech	Zhao et al., 2015
p413 TEF iNap1	Genscript Biotech	Tao et al., 2017
p413 TEF iNap2		
p413 TEF iNap3		
p413 TEF iNap4		
p413 TEF iNapc		

p413 GPD mScarlet-I-SoNar	Molecular cloning ^{A,B}	This study
p413 GPD mScarlet-I-iNap1		
p413 GPD mScarlet-I-iNap2		
p413 GPD mScarlet-I-iNap3		
p413 GPD mScarlet-I-iNap4		
p413 GPD mScarlet-I-iNapc		
p413 TEF Peredox-mCherry	Genscript Biotech	Hung et al., 2011
p413 TEF Peredox-mCherry DS	Molecular cloning ^{A,B}	Steinbeck et al., 2020
p415 GAL Peredox-mCherry DS	Molecular cloning ^B	
p413 TEF NAPstar1	Genscript Biotech	This study
p413 TEF NAPstar2		
p413 TEF NAPstar3		
p413 TEF NAPstar4		
p413 TEF NAPstarC		
p413 TEF NAPstar1.4	Molecular cloning ^B	This study
p413 TEF NAPstar2.4		
p413 TEF NAPstar3.4		
p413 TEF NAPstar4.1		
p413 TEF NAPstar4.2		
p413 TEF NAPstar4.3		
p413 TEF NAPstar5	Genscript Biotech	This study
p413 TEF NAPstar6	Genscript Biotech	
p413 TEF NAPstar7	Genscript Biotech	
p413 TEF roGFP2-Tsa2 Δ C _R	Molecular cloning ^B	Morgan et al., 2016
p413 TEF roGFP2-Grx1	Molecular cloning ^B	Gutscher et al., 2008
p413 TEF pHluorin	Molecular cloning ^B	Miesenböck et al., 1998
p413 TEF SypHer	Molecular cloning ^B	Poburko et al., 2011
Resistance cassette amplification		
Plasmid	Source	Reference
pFA6 α natNT2	—	Janke et al., 2004
pFA6 α hphNT1	—	Janke et al., 2004
pFA6 α kanMX4	—	Goldstein and McCusker, 1999

4.2.3 DNA quantification

The DNA concentration of purified DNA was determined using a micro-volume spectrophotometer measuring the absorption at 260 nm. DNA purity was controlled by calculation of the 260/280 nm ratio.

4.2.4 DNA sequencing

Plasmid sequences were confirmed with appropriate sequencing primers (**Table 4.2**) using the *LightRun Tube* Sanger sequencing service offered by Eurofins Genomics Germany.

4.2.5 Agarose gel electrophoresis

For separation of DNA fragments, samples were supplemented with *6X Purple Loading Dye* (New England Biolabs). Gel electrophoresis was performed in TAE buffer (40 mM Tris, 20 mM acetic acid, 1 mM EDTA) using 1% (w/v) agarose gels supplemented with 40 µL/L DNA stain. The length of fragments was estimated by comparison to a 1 kb ladder which was loaded next to the samples.

4.2.6 Restriction and ligation

Plasmids were subcloning by restriction and ligation. Restriction endonucleases were applied for enzymatic DNA digest according to the manufacturer's protocol in a total volume of 50 µL for 1 h at 37°C. Fragments were separated by agarose gel electrophoresis and subsequently purified using a gel clean-up kit. A ligation kit was used according to manufacturer information. The ligation reaction was performed in a thermo cycler (**Table 4.4**) with a molar insert:vector ratio of 3:1 to 5:1. After transformation of 7 µL ligation mix in *E. coli* and selection on LB_{amp} plates, single colonies were picked for plasmid DNA preparation. Correct ligation was confirmed by test digest (20 µL total volume) and agarose gel electrophoreses prior to sequencing.

4.2.7 Polymerase chain reaction

For all PCR methods, *S7 Fusion polymerase* was used according to the manufacturer's instructions for 50 µL reactions.

Table 4.4: Ligation reaction program.

Step	Command	Time
1	16°C	15 min
2	20°C	15 min
3	70°C	15 min
4	4°C	for ever
5	End	

DNA modification for subcloning

To modify the 5' and/ or 3' regions of a target gene e.g., to add or exchange restriction sites, PCR was performed with respectively designed primer pairs. Next to terminal restriction sites, 3 to 6 base pairs overhangs were created to ensure high restriction efficiency. The PCR program was adapted according to the manufacturer information and primer annealing temperatures. Successful amplification was confirmed by separation of 2 μ L reaction utilizing agarose gel electrophoresis. PCR products were purified from the reaction mix using a PCR clean-up kit according to the manufacturer's protocol prior to further subcloning.

Site-directed mutagenesis

Mutagenesis primers were designed, and PCR program was adapted according to the *QuickChange site-directed mutagenesis protocol* (Agilent Technologies). After PCR (**Table 4.5**), the mix was incubated with 1 μ L DpnI at 37°C for at least 1 h to digest template DNA. Subsequently, *E. coli* cells were transformed with 1 to 10 μ L digested reaction mix and selected on LB_{amp} plates. Single colonies were picked for plasmid DNA isolation. Plasmid integrity was verified by restriction digest and agarose gel electrophoresis. Successful mutagenesis was confirmed by sequencing.

Resistance cassette amplification

For targeted gene deletion, the selected resistance cassette was PCR amplified from a pFA6 α plasmid (**Table 4.3** and **Table 4.6**). Primer pairs were designed to generate 40 base pairs overhangs being homologue to the 5' and 3' untranslated regions of the target gene (Janke et al., 2004). Successful cassette amplification was confirmed by separation of 2 μ L reaction mix via agarose gel electrophoresis prior to homologous recombination.

Table 4.5: PCR program for site-directed mutagenesis.

Step	Command	Time
1	98°C	30 s
2	98°C	30 s
3	55°C	1 min
4	68°C	1 min/kb of plasmid length
5	Go to 2; 12 to 18 times	
6	72°C	10 min
7	4°C	for ever
8	End	

Confirmation PCR

To confirm the correct resistance cassette integration site after homologous recombination, genomic DNA was extracted. To this end, *S. cerevisiae* cells from selected colonies were dissolved in 30 μ L 0.2% SDS, boiled at 95°C for 10 min and thoroughly mixed. Cell debris was pelleted at maximum speed for 1 min and 1 μ L of the supernatant was employed as template for PCR. For confirmation PCR of genomically integrated *kanMX4* and *hphNT1* cassettes, HF buffer was preferred, whereas for amplification of *natNT2* cassette, GC buffer was used. The PCR program is described in **Table 4.6**. The target region was PCR amplified using primers binding in the 5' and 3' regions of the deleted gene (~100 base pairs up- and downstream). A control containing genomic WT DNA was carried as control in parallel. To identify correct PCR product sizes, 20 μ L to 50 μ L PCR mix was subjected to agarose gel electrophoresis.

Table 4.6: PCR program for resistance cassette confirmation.

Step	Command	Time
1	97°C	3 min
2	97°C	30 s
3	60°C	1 min
4	72°C	2 min 40 s
5	Go to 2; 30 times	
6	72°C	10 min
7	4°C	for ever
8	End	

4.3 Bacteriological methods

4.3.1 Bacteria handling

Plasmid DNA was amplified using transformed TOP10 *E. coli* cultures. Cultivation was performed in liquid Luria-Bertani (LB) medium at 37°C and 140 RPM. For short-term storage, *E. coli* cultures were grown on agar plates (2% [w/v] agar) at 37°C overnight and kept at 4°C up to four weeks. Plasmid-transformed cells were selected in liquid LB medium or on plates supplemented with 100 µg/mL ampicillin (amp). For long-time storage, a glycerol stock was prepared by addition of 0.6 mL 80% (w/v) glycerol to 1 mL of *E. coli* culture. Glycerol stocks were kept at -80°C. Stocked cultures were recovered on LB plates.

4.3.2 Preparation of chemically competent *E. coli* cells

An *E. coli* preculture was grown in a test tube to density. The main culture was inoculated 1:100 in 200 mL fresh LB medium in a 2 L chicane flask. When the culture had grown at 220 RPM, 37°C to an optical density (OD₆₀₀) of 0.4, it was cooled down on ice for 10 min. Cells were harvested at 4°C, 3200 RCF, 10 min and taken up in 100 mL ice cold, sterile 0.1 M CaCl₂ solution. Cells were chilled further 30 min on ice and regularly mixed. After final cell harvest (4°C, 3200 RCF, 10 min), competent cells were taken up in 3 mL ice cold storage buffer (0.1 M CaCl₂, 15% [w/v] glycerol), aliquoted to 100 µL, shock frozen and stored at -80°C.

4.3.3 Heat-shock transformation

Chemically competent *E. coli* were thawed on ice and incubated with 0.5 ng plasmid DNA for 30 min on ice. After heat shock at 45°C for 1 min, the cells were chilled on ice for 1 min. Recovery was performed by addition of 1 mL fresh LB and incubation at 37°C for 1 h. Cells were plated in different dilutions on LB_{amp} plates to enable for single colony picking.

4.3.4 Plasmid DNA isolation

For plasmid preparation, a single transformed *E. coli* colony was picked from a LB_{amp} plate and inoculated in 5 mL liquid LB_{amp} medium. After growth at 37°C, shaking, overnight, the plasmid was purified using a DNA purification kit according to the manufacturer's instructions.

4.4 Yeast methods

4.4.1 Yeast strains

The *S. cerevisiae* strains used in this study are listed in **Table 4.7**.

Table 4.7: *S. cerevisiae* strains used in this study.

Strain	Genotype	Source
BY4742 WT	<i>MATα his3Δ1 leu2Δ0 ura3Δ0</i>	Euroscarf
Δ <i>glr1</i>	BY4742 <i>glr1Δ::kanMX4</i>	Morgan et al., 2012
Δ <i>trx1Δtrx2</i>	BY4742 <i>trx1Δ::kanMX4 trx2Δ::natNT2</i>	Morgan et al., 2016
Δ <i>tsa1Δtsa2</i>	BY4742 <i>tsa1Δ::kanMX4 tsa2Δ::natNT2</i>	Morgan et al., 2016
Δ <i>zwf1</i>	BY4742 <i>zwf1Δ::natNT2</i>	This study
Δ <i>ald6</i>	BY4742 <i>ald6Δ::kanMX4</i>	Euroscarf
Δ <i>tdh1Δtdh2Δtdh3</i>	BY4742 <i>tdh3Δ::kanMX4 tdh1Δ::natNT2 tdh2Δ::hphNT1 p415 TEF Tdh3 WT (C149S/ C153S)</i>	Peralta et al., 2015
Cen.PK113-1A Δ <i>his3</i>	Cen.PK113-1A <i>his3Δ::hphNT1</i>	Amponsah, 2020

4.4.2 Yeast culture handling

Liquid yeast cultures were grown in 100 ml Erlenmeyer flasks at 30°C, 140 RPM, in either yeast peptone dextrose (YPD) or Hartwell's Complete (HC) medium. For short-term storage, yeast cultures were grown at 30°C on agar plates (2% [w/v] agar) and kept at 4°C up to four weeks. Long-time storage was performed at -80°C in glycerol stocks. Glycerol stocks were prepared by supplementation of 0.6 mL 80% (w/v) glycerol to 1 mL of dense YPD culture. Stocked cultures were recovered on YPD plates.

Yeast peptone dextrose medium and antibiotics

For preparation of YPD medium, a yeast peptone (YP) stock solution was prepared by solving 1% (w/v) yeast extract, 2% (w/v) peptone, and subsequent pH adjustment by HCl titration to pH 5.5. To sterilize the stock solutions, YP was autoclaved, and 40% [w/v] glucose was sterile filtered prior to medium preparation. YPD medium was produced by the supplementation of 2% (w/v) glucose to the YP solution. To select for genetically integrated resistance cassettes *natNT2*, *kanMX4* and *hphNT1*, YPD plates were supplemented with either 100 μ g/mL nourseothricin, 150 μ g/mL G418 or 200 μ g/mL hygromycin B.

Hartwell's complete medium

Plasmid-transformed yeast cultures were grown on HC medium lacking histidine (p413) or leucine (p415) for plasmid selection (**Table 4.8** and **Table 4.9**). The individual stock solutions were prepared separately and sterile filtered before usage.

Table 4.8: Composition of HC medium.

The 10X YNB stock solution was prepared according to the manufacturer's information as 6.7% (w/v) solution.

Compound	Stock concentration	Final concentration
HC dropout mix	10X	1X
YNB	10X	1X
Glucose	40% (w/v)	2% (w/v)
Uracil	1 g/L	35 mg/L
Adenine	1 g/L	20 mg/L
Lysine	10 g/L	120 mg/L
Tryptophan	10 g/L	80 mg/L
Leucine	20 g/L	80 mg/L
Histidine	10 g/L	20 mg/L

Table 4.9: Composition of 10X dropout mix.

Compound	Concentration in 10X stock
Methionine	0.2 g/L
Tyrosine	0.6 g/L
Isoleucine	0.8 g/L
Phenylalanine	0.5 g/L
Glutamic acid	1.0 g/L
Threonine	2.0 g/L
Aspartic acid	1.0 g/L
Valine	1.5 g/L
Serine	4.0 g/L
Arginine	0.2 g/L

4.4.3 Gene deletion via homologous recombination

A yeast was grown in YPD to log phase. After cell harvest of 1 mL culture at 900 RCF for 3 min, cells were washed in 1 mL of sterile water. After centrifugation at 900 RCF for 3 min, the cell pellet was resuspended in 200 μ L one-step transformation buffer (0.2 M lithium acetate, 40% [w/v] PEG, 100 mM DTT) and kept on ice. 10 μ L single stranded DNA was boiled at 95°C for 5 min and cooled down on ice for 1 min prior to supplementation to the transformation mix. Finally, 5 to 10 μ L PCR mix containing the resistance cassette was added to the transformation mix and thoroughly mixed. The transformation mix was incubated at 45°C for 30 min at 750 RPM. After a short centrifugation step at 500 RCF for 30 s, the buffer was removed, and cells were transferred to and cultivated in 5 mL YPD overnight. The whole culture, and a 1:10 dilution thereof, were plated on two separate antibiotic YPD plates to select for recombined yeast. After incubation for 2 to 3 days at 30°C, single colonies were picked and restreaked on a fresh selective plate. After another day of incubation, the culture was restreaked and grown a third time on an antibiotic plate. Correct cassette integration was validated by confirmation PCR prior to usage.

4.4.4 One-step transformation of plasmids

For plasmid transformation, a yeast culture was grown in YPD to late log or stationary phase. 1 mL of culture was harvested at 900 RPM for 3 min and washed in 1 mL sterile water. After centrifugation at 900 RCF for 3 min, the cell pellet was resuspended in 100 μ L one-step transformation buffer (0.2 M lithium acetate, 40% [w/v] PEG, 100 mM DTT) and kept on ice. 5 μ L single stranded DNA was boiled at 95°C for 5 min and cooled down on ice for 1 min before supplementation to the transformation mix. Finally, 500 ng of plasmid DNA were added to the transformation mix and thoroughly mixed prior to incubation at 45°C for 30 min, 750 RPM. Afterwards, the mix was plated on a selective HC plate and incubated at 30°C for at least 40 h. To obtain more cell material for experiments, multiple colonies were streaked together and grown on a fresh selective plate.

4.5 Multiwell plate reader-based fluorescence spectroscopy

Fluorometric analyzes were performed in 96 well imaging plates (Falcon, Corning Life Science, Identifier 353219) using a multi-mode CLARIOstar plate reader (BMG Labtech). GFI expression was achieved by plasmid transformation of respective yeast strains. For blank correction, a culture transformed with an empty vector was always carried in parallel. Transformed yeast strains were grown in a preculture in selective HC medium

to density. After inoculation of the main culture, cells were grown for at least 16 h to an OD_{600} of 3 to 5. After cell harvest at 900 RCF for 3 min, cells were resuspended in measurement buffer and transferred to the designated wells of the measurement plate with 1.5 OD_{600} units in 200 μ L buffer per well. If not stated otherwise, 0.1 M MOPS/TRIS buffer, pH 7, was used for measurements. After plate centrifugation at 15 RCF for 5 min, fluorescence signals were analyzed in the plate reader using bottom optic, 10 to 20 flashes per well and cycle and appropriate wavelength and gain settings (**Table 4.10**). Treatments during kinetic measurements were performed by addition of 20 μ L 10X stock solution using a multichannel pipette. Treatment stock solutions were prepared in measurement buffer, freshly the same day, except for NADH and NADPH dilutions, which were prepared in advance, kept in dark and stored at -20°C up to eight weeks.

Table 4.10: Plate reader settings for fluorescence measurements.

Kinetic measurements were recorded with 60 s cycle time. Fluorescence spectra were determined at 1 nm resolution.

Kinetic measurements				
GFI		Excitation (nm)	Emission (nm)	Gain
SoNar, iNap, SypHer		420-10	520-10	2000
		480-10	520-10	2000
mSI-SoNar, mSI-iNap		418-10	516-10	2000
		560-10	610-10	2000
roGFP2-Tsa2 Δ C _R , roGFP2-Grx1		400-15	520-20	60% full plate
		480-15	520-20	80% full plate
Pdx-mC (DS), NAPstar		399-10	510-10	2000
		578-15	619-15	2000
pHluorin		399-10	510-10	2000
		470-10	510-10	2000
Fluorescence spectra				
GFI		Excitation (nm)	Emission (nm)	Gain
SoNar, iNap, SypHer		320-10 to 495-10	520-10	2000
		420-10	480-10 to 620-10	2000
Pdx-mC (DS), NAPstar	cpTS	320-10 to 450-10	510-10	1700
		399-10	480-10 to 620-10	1700
	mC	420-15 to 589-15	619-15	1700
		578-15	608-15 to 740-15	1700

4.5.1 NAD(P)H titration and pH dependency experiments

Permeabilization of yeast cells for NAD(P)H titration experiments was achieved by addition of 20 μ L 1% digitonin per well prior to culture addition. Digitonin was solved at 60°C in the respective buffer, shaking, and prepared freshly each day. For pH dependency experiments, all remaining components were solved in buffer (0.1 M MES/TRIS pH 6.0 and 6.5; 0.1 M MOPS/TRIS pH 6.5 and 7.0; 0.1 M TRIS/HCl pH 7.0, 8.0, and 9.0) with a final volume of 180 μ L per well. All components were pipetted into the designated wells, which were already prepared with digitonin, and the plate was incubated for 25 min at room temperature to ensure for sensor equilibration before the spectra were recorded.

4.5.2 roGFP2 measurements

Calibration of roGFP2 probes was performed by addition of 20 μ L 0.2 M diamide and 1 M DTT to separate wells before GFI expressing culture was added to the plate. This allowed for fluorescence measurement of fully oxidized and reduced sensor states (Morgan et al., 2011).

4.5.3 Induction of Peredox-mCherry DS expression

To determine the maturation rate discrepancies between cpTS and mC fluorescent proteins of the Pdx-mC DS sensor, BY4742 WT was transformed with either p415 GAL empty (blank) or p415 GAL Pdx-mC DS. Resulting strains were precultured to density in HC -Leu medium containing glucose. The main culture was inoculated 0.004 OD₆₀₀/mL in HC -Leu supplemented with 2% raffinose and 0.1% total glucose and grown for 18 h to OD₆₀₀ 1. For induction of gene expression, 2% galactose (from 40% [w/v] stock) were added to the culture and 1.5 OD₆₀₀ were immediately harvested for fluorescence measurements in the CLARIOstar plate reader (t = 0 min). The cultures were instantly further incubated at 30°C to allow for optimal growth. Samples were rapidly taken at the indicated time points for fluorescence intensity measurements. Plate reader measurements were performed using 1.5 OD₆₀₀ cells in 200 μ L buffer (0.1 M MES/TRIS, pH 6.0) per well with gain settings of 1700 and 2300 for cpTS and mC channels, respectively.

4.5.4 Calculations

Unless otherwise stated, the obtained blank values were subtracted prior to further calculations. All experiments were performed at least three times. For Figure generation, the average was plotted together with the standard error.

Calculation of OxD value (roGFP2 sensors)

For calibration of roGFP2 probes, a diamide and a DTT treated sample was always carried in parallel. These calibration samples were prepared separately for each sensor-strain combination. The mean of fluorescence intensities of diamide- and DTT-treated samples was calculated for the first five cycles and employed for computing the OxD of roGFP2 (**Equation 4.1**) (Meyer and Dick, 2010; Morgan et al., 2013).

Equation 4.1: OxD calculation of roGFP2-based GFI.

$$OxD_{roGFP2} = \frac{(400_{sample} \times 480_{DTT}) - (400_{DTT} \times 480_{sample})}{(400_{sample} \times 480_{DTT} - 400_{sample} \times 480_{diamide}) + (400_{diamide} \times 480_{sample} - 400_{DTT} \times 480_{sample})}$$

Calculation of 420/480 nm (SypHer, SoNar, iNap) and 399/470 nm ratios (pHluorin)

The cpYFP-based sensors SypHer, SoNar and iNap, as well as the GFP-derived pHluorin sensor, possess intrinsically excitation-ratiometric fluorescence spectra. To detect sensitively fluorescence ratio changes, the ratio of respective fluorescence intensities was calculated separately for each time point of the measurement.

Calculation of (norm.) cpTS/mC (Pdx, NAPstar) and 420 nm/mSI ratios (mSI-iNap, -SoNar)

The RFPs mC and mSI were partly quenched at high oxidant concentrations. Hence, a mean red signal was calculated for mC and mSI for the measurement points prior to compound addition. The cpTS signal was then divided by the mean for mC or mSI for each time point. Normalization of cpTS/mC of Pdx-mC and NAPstar sensors was achieved by division of the sensor ratios of individual experiments by the mean cpTS/mC obtained for NAPstarC (**Equation 4.2**).

Equation 4.2: Normalization of cpTS/mC ratio.

$$norm. \frac{cpTS}{mC} (sensor) = \frac{\frac{cpTS}{mC} (sensor)}{\frac{cpTS}{mC} (NAPstarC)}$$

Calculation of sensor occupancy

To calculate relative sensor occupancies with NAD(P)H, calibration points for completely NAD(P)H dissociated (y_{\min}) and associated (y_{\max}) sensors were determined. These were assumed to be reached during NADPH titration experiments for iNap, NAPstar sensors by buffer (y_{\min}) or 2 mM NADPH addition (y_{\max}) at $t = 15$ min. For SoNar and Pdx-mC (DS) probes, minimum (y_{\min}) and maximum (y_{\max}) fluorescence ratios were achieved after pyruvate and NADH supplementation, respectively. To compute sensor occupancy at steady state, the fluorescence ratio was averaged for the first 4 min of the measurement (steady state), giving y . Sensor occupancy was calculated as displayed in **Equation 4.3**.

Equation 4.3: Determination of NAD(P)H sensor occupancy.

$$\text{occupancy} = \frac{(y - y_{\min})}{(y_{\max} - y_{\min})}$$

4.6 YMC in continuous culture

4.6.1 YMC establishment in the bioreactor

Continuous yeast culturing was performed in a Biostat A bioreactor as described by Amponsah et al., 2021. For media preparation, 25 g ammonium sulfate, 10 g potassium dihydrogen phosphate, 2.5 g magnesium sulfate monohydrate, 0.5 g calcium chloride dihydrate and 5 g yeast extract were solved in 4.5 L distilled water and autoclaved (**Table 4.11**). 2.5 mL 70% (w/v) sulfuric acid and 500 mL 10% (w/v) glucose were autoclaved and added to the medium. 5 mL sterile filtered 1000X trace metal stock solution, 10 mL filtered iron(II) sulfate solution and 2.5 mL antifoam were finally supplemented. The media working volume was constantly kept at 800 mL and the temperature was fixed to 30°C. The media pH value was automatically adjusted to 3.4 by titration of 10% (w/v) NaOH. The culture was permanently stirred at 530 RPM and constantly aerated with atmospheric air at 1 L/min. The oxygen electrode was slope calibrated to the aerated and oxygen saturated medium prior to culture injection. A plasmid transformed Cen.PK113-A1 $\Delta his3$ starter culture was grown to density in selective HC medium in a shaking flask. 20 mL were injected into the bioreactor. After the culture was grown to stationary phase, cells started starving. After a starvation phase of 5 to 6 h, fresh culture medium was supplemented with a constant dilution rate of 0.05 h⁻¹.

Table 4.11: Fermenter medium for yeast continuous culture.

Compound	Stock concentration	Final concentration
Glucose	10% (w/v)	10 g/L
(NH ₄) ₂ SO ₄	–	5 g/L
KH ₂ PO ₄	–	2 g/L
Yeast extract	–	1 g/L
MgSO ₄ · H ₂ O	–	0.5 g/L
H ₂ SO ₄	70% (w/v)	0.35 g/L
CaCl ₂ · 2 H ₂ O	–	0.1 g/L
FeSO ₄ · 7 H ₂ O	10 g/L	0.02 g/L
ZnSO ₄ · 7 H ₂ O	1000X	0.01 g/L
CuSO ₄ · 5 H ₂ O	1000X	0.005 g/L
MnCl ₂ · 4 H ₂ O	1000X	0.001 g/L
Antifoam 204	–	0.5 mL/L

4.6.2 Online fluorimetry during chemostat cultivation

Cen.PK113-A1 $\Delta his3$ strain was transformed with a p413-based vector enabling for GFI expression (Amponsah, 2020). During cultivation in the bioreactor, the culture was permanently pumped through a flow cell that was placed in a fluorescence spectrophotometer (Amponsah et al., 2021). The fluorescence signals were detected with a photomultiplier voltage of 600 V and a simple collect timing every 10 s. Excitation and emission wavelengths were adjusted as listed in **Table 4.12** using a slit width of 10 nm each. The ratio of fluorescence intensities was calculated based on the obtained raw data for each time point of the measurement and plotted together with the dissolved oxygen (pO₂).

Table 4.12: Spectrophotometer settings for fluorescence measurements during continuous culture.

GFI	Excitation (nm)	Emission (nm)
Pdx-mC (DS), NAPstar	399	510
	578	619
pHluorin	395	510
	475	510
HyPer7	400	520
	490	520

5 References

- Amponsah, P.S., 2020. Peroxiredoxins: Novel mediators of cellular timekeeping (Dissertation). TU Kaiserslautern, Kaiserslautern.
- Amponsah, P.S., Yahya, G., Zimmermann, J., Mai, M., Mergel, S., Mühlhaus, T., Storchova, Z., Morgan, B., 2021. Peroxiredoxins couple metabolism and cell division in an ultradian cycle. *Nat Chem Biol* 17, 477–484. <https://doi.org/10.1038/s41589-020-00728-9>
- Avery, A.M., Avery, S.V., 2001. *Saccharomyces cerevisiae* expresses three phospholipid hydroperoxide glutathione peroxidases. *J Biol Chem* 276, 33730–33735. <https://doi.org/10.1074/jbc.M105672200>
- Ayer, A., Gourlay, C.W., Dawes, I.W., 2014. Cellular redox homeostasis, reactive oxygen species and replicative ageing in *Saccharomyces cerevisiae*. *FEMS Yeast Res* 14, 60–72. <https://doi.org/10.1111/1567-1364.12114>
- Bakker, B.M., Bro, C., Kötter, P., Luttk, M.A., van Dijken, J.P., Pronk, J.T., 2000. The mitochondrial alcohol dehydrogenase Adh3p is involved in a redox shuttle in *Saccharomyces cerevisiae*. *J Bacteriol* 182, 4730–4737. <https://doi.org/10.1128/JB.182.17.4730-4737.2000>
- Bakker, B.M., Overkamp, K.M., van Maris, A.J., Kötter, P., Luttk, M.A., van Dijken, J.P., Pronk, J.T., 2001. Stoichiometry and compartmentation of NADH metabolism in *Saccharomyces cerevisiae*. *FEMS Microbiol Rev* 25, 15–37. <https://doi.org/10.1111/j.1574-6976.2001.tb00570.x>
- Bedalov, A., Hirao, M., Posakony, J., Nelson, M., Simon, J.A., 2003. NAD⁺-dependent deacetylase Hst1p controls biosynthesis and cellular NAD⁺ levels in *Saccharomyces cerevisiae*. *Mol Cell Biol* 23, 7044–7054. <https://doi.org/10.1128/MCB.23.19.7044-7054.2003>
- Belousov, V.V., Fradkov, A.F., Lukyanov, K.A., Staroverov, D.B., Shakhbazov, K.S., Terskikh, A.V., Lukyanov, S., 2006. Genetically encoded fluorescent indicator for intracellular hydrogen peroxide. *Nat Methods* 3, 281–286. <https://doi.org/10.1038/nmeth866>
- Bennington, K., 2019. Characterisation of novel genetically encoded NAD(P)⁺/NAD(P)H sensors in *Saccharomyces cerevisiae* (Bachelor thesis). Saarland University, Haute Ecole Léonard de Vinci, Saarbrücken.
- Bermejo, C., Haerizadeh, F., Takanaga, H., Chermak, D., Frommer, W.B., 2010. Dynamic analysis of cytosolic glucose and ATP levels in yeast using optical sensors. *Biochem J* 432, 399–406. <https://doi.org/10.1042/BJ20100946>
- Bhat, S.A., Iqbal, I.K., Kumar, A., 2016a. Imaging the NADH:NAD⁺ homeostasis for understanding the metabolic response of Mycobacterium to physiologically relevant stresses. *Front Cell Infect Microbiol* 6. <https://doi.org/10.3389/fcimb.2016.00145>
- Bhat, S.A., Iqbal, I.K., Kumar, A., 2016b. Imaging the NADH/NAD⁺ homeostasis for understanding the metabolic response of mycobacterium to physiologically relevant stresses. *Front Cell Infect Microbiol* 6, 145. <https://doi.org/10.3389/fcimb.2016.00145>
- Bieganowski, P., Brenner, C., 2004. Discoveries of nicotinamide riboside as a nutrient and conserved NRK genes establish a Preiss-Handler independent route to NAD⁺ in fungi and humans. *Cell* 117, 495–502. [https://doi.org/10.1016/s0092-8674\(04\)00416-7](https://doi.org/10.1016/s0092-8674(04)00416-7)
- Bieganowski, P., Pace, H.C., Brenner, C., 2003. Eukaryotic NAD⁺ synthetase Qns1 contains an essential, obligate intramolecular thiol glutamine amidotransferase domain related to nitrilase. *J Biol Chem* 278, 33049–33055. <https://doi.org/10.1074/jbc.M302257200>
- Bieganowski, P., Seidle, H.F., Wojcik, M., Brenner, C., 2006. Synthetic lethal and biochemical analyses of NAD and NADH kinases in *Saccharomyces cerevisiae* establish separation of cellular functions. *J Biol Chem* 281, 22439–22445. <https://doi.org/10.1074/jbc.M513919200>
- Bilan, D.S., Belousov, V.V., 2017. New tools for redox biology: From imaging to manipulation. *Free Radic Biol Med* 109, 167–188. <https://doi.org/10.1016/j.freeradbiomed.2016.12.004>

References

- Bilan, D.S., Pase, L., Joosen, L., Gorokhovatsky, A.Y., Ermakova, Y.G., Gadella, T.W.J., Grabher, C., Schultz, C., Lukyanov, S., Belousov, V.V., 2013. HyPer-3: A genetically encoded H₂O₂ probe with improved performance for ratiometric and fluorescence lifetime imaging. *ACS Chem Biol* 8, 535–542. <https://doi.org/10.1021/cb300625g>
- Bindels, D.S., Haarbosch, L., van Weeren, L., Postma, M., Wiese, K.E., Mastop, M., Aumonier, S., Gotthard, G., Royant, A., Hink, M.A., Gadella, T.W.J., 2017. mScarlet: A bright monomeric red fluorescent protein for cellular imaging. *Nat Methods* 14, 53–56. <https://doi.org/10.1038/nmeth.4074>
- Bird, J.G., Basu, U., Kuster, D., Ramachandran, A., Grudzien-Nogalska, E., Towheed, A., Wallace, D.C., Kiledjian, M., Temiakov, D., Patel, S.S., Ebright, R.H., Nickels, B.E., 2018. Highly efficient 5' capping of mitochondrial RNA with NAD⁺ and NADH by yeast and human mitochondrial RNA polymerase. *Elife* 7, e42179. <https://doi.org/10.7554/eLife.42179>
- Blacker, T.S., Duchen, M.R., 2016. Investigating mitochondrial redox state using NADH and NADPH autofluorescence. *Free Radic Biol Med* 100, 53–65. <https://doi.org/10.1016/j.freeradbiomed.2016.08.010>
- Blacker, T.S., Mann, Z.F., Gale, J.E., Ziegler, M., Bain, A.J., Szabadkai, G., Duchen, M.R., 2014. Separating NADH and NADPH fluorescence in live cells and tissues using FLIM. *Nat Commun* 5, 3936. <https://doi.org/10.1038/ncomms4936>
- Blinova, K., Carroll, S., Bose, S., Smirnov, A.V., Harvey, J.J., Knutson, J.R., Balaban, R.S., 2005. Distribution of mitochondrial NADH fluorescence lifetimes: Steady-state kinetics of matrix NADH interactions. *Biochemistry* 44, 2585–2594. <https://doi.org/10.1021/bi0485124>
- Bodvard, K., Peeters, K., Roger, F., Romanov, N., Igbaria, A., Welkenhuysen, N., Palais, G., Reiter, W., Toledano, M.B., Käll, M., Molin, M., 2017. Light-sensing via hydrogen peroxide and a peroxiredoxin. *Nat Commun* 8, 14791. <https://doi.org/10.1038/ncomms14791>
- Boles, E., Lehnert, W., Zimmermann, F.K., 1993. The role of the NAD-dependent glutamate dehydrogenase in restoring growth on glucose of a *Saccharomyces cerevisiae* phosphoglucose isomerase mutant. *Eur J Biochem* 217, 469–477. <https://doi.org/10.1111/j.1432-1033.1993.tb18266.x>
- Botstein, D., Fink, G.R., 2011. Yeast: An experimental organism for 21st Century biology. *Genetics* 189, 695–704. <https://doi.org/10.1534/genetics.111.130765>
- Bouchérié, H., Bataille, N., Fitch, I.T., Perrot, M., Tuite, M.F., 1995. Differential synthesis of glyceraldehyde-3-phosphate dehydrogenase polypeptides in stressed yeast cells. *FEMS Microbiol Lett* 125, 127–133. <https://doi.org/10.1111/j.1574-6968.1995.tb07348.x>
- Brekasis, D., Paget, M.S.B., 2003. A novel sensor of NADH/NAD⁺ redox poise in *Streptomyces coelicolor* A3(2). *EMBO J* 22, 4856–4865. <https://doi.org/10.1093/emboj/cdg453>
- Bruinenberg, P.M., 1986. The NADP(H) redox couple in yeast metabolism. *Antonie Van Leeuwenhoek* 52, 411–429. <https://doi.org/10.1007/BF00393469>
- Bücher, T., Brauser, B., Conze, A., Klein, F., Langguth, O., Sies, H., 1972. State of oxidation-reduction and state of binding in the cytosolic NADH-system as disclosed by equilibration with extracellular lactate-pyruvate in hemoglobin-free perfused rat liver. *Eur J Biochem* 27, 301–317. <https://doi.org/10.1111/j.1432-1033.1972.tb01840.x>
- Burnetti, A.J., Aydin, M., Buchler, N.E., 2016. Cell cycle Start is coupled to entry into the yeast metabolic cycle across diverse strains and growth rates. *Mol Biol Cell* 27, 64–74. <https://doi.org/10.1091/mbc.E15-07-0454>
- Calabrese, G., Peker, E., Amponsah, P.S., Hoehne, M.N., Riemer, T., Mai, M., Bienert, G.P., Deponte, M., Morgan, B., Riemer, J., 2019. Hyperoxidation of mitochondrial peroxiredoxin limits H₂O₂-induced cell death in yeast. *EMBO J* 38, e101552. <https://doi.org/10.15252/embj.2019101552>
- Cameron, W.D., Bui, C.V., Hutchinson, A., Loppnau, P., Gräslund, S., Rocheleau, J.V., 2016. Apollo-NADP⁺: A spectrally tunable family of genetically encoded sensors for NADP⁺. *Nat Methods* 13, 352–358. <https://doi.org/10.1038/nmeth.3764>

- Canelas, A.B., van Gulik, W.M., Heijnen, J.J., 2008. Determination of the cytosolic free NAD/NADH ratio in *Saccharomyces cerevisiae* under steady-state and highly dynamic conditions. *Biotechnol Bioeng* 100, 734–743. <https://doi.org/10.1002/bit.21813>
- Castegna, A., Scarcia, P., Agrimi, G., Palmieri, L., Rottensteiner, H., Spera, I., Germinario, L., Palmieri, F., 2010. Identification and functional characterization of a novel mitochondrial carrier for citrate and oxoglutarate in *Saccharomyces cerevisiae*. *J Biol Chem* 285, 17359–17370. <https://doi.org/10.1074/jbc.M109.097188>
- Causton, H.C., Ren, B., Koh, S.S., Harbison, C.T., Kanin, E., Jennings, E.G., Lee, T.I., True, H.L., Lander, E.S., Young, R.A., 2001. Remodeling of yeast genome expression in response to environmental changes. *Mol Biol Cell* 12, 323–337. <https://doi.org/10.1091/mbc.12.2.323>
- Cavero, S., Vozza, A., del Arco, A., Palmieri, L., Villa, A., Blanco, E., Runswick, M.J., Walker, J.E., Cerdán, S., Palmieri, F., Satrustegui, J., 2003. Identification and metabolic role of the mitochondrial aspartate-glutamate transporter in *Saccharomyces cerevisiae*. *Mol Microbiol* 50, 1257–1269. <https://doi.org/10.1046/j.1365-2958.2003.03742.x>
- Celton, M., Goelzer, A., Camarasa, C., Fromion, V., Dequin, S., 2012. A constraint-based model analysis of the metabolic consequences of increased NADPH oxidation in *Saccharomyces cerevisiae*. *Metab Eng* 14, 366–379. <https://doi.org/10.1016/j.ymben.2012.03.008>
- Chance, B., Cohen, P., Jobsis, F., Schoener, B., 1962. Intracellular oxidation-reduction states in vivo: The microfluorometry of pyridine nucleotide gives a continuous measurement of the oxidation state. *Science* 137, 499–508. <https://doi.org/10.1126/science.137.3529.499>
- Chance, B., Thorell, B., 1959. Localization and kinetics of reduced pyridine nucleotides in living cells by microfluorometry. *J Biol Chem* 234, 3044–3050.
- Chang, M., Li, L., Hu, H., Hu, Q., Wang, A., Cao, X., Yu, X., Zhang, S., Zhao, Y., Chen, J., Yang, Y., Xu, J., 2017. Using fractional intensities of time-resolved fluorescence to sensitively quantify NADH/NAD⁺ with genetically encoded fluorescent biosensors. *Sci Rep* 7, 4209. <https://doi.org/10.1038/s41598-017-04051-7>
- Chen, C., Hao, X., Lai, X., Liu, L., Zhu, J., Shao, H., Huang, D., Gu, H., Zhang, T., Yu, Z., Xie, L., Zhang, X., Yang, Y., Xu, J., Zhao, Y., Lu, Z., Zheng, J., 2021. Oxidative phosphorylation enhances the leukemogenic capacity and resistance to chemotherapy of B cell acute lymphoblastic leukemia. *Sci Adv* 7, eabd6280. <https://doi.org/10.1126/sciadv.abd6280>
- Chugunova, A., Loseva, E., Mazin, P., Mitina, A., Navalayeu, T., Bilan, D., Vishnyakova, P., Marey, M., Golovina, A., Serebryakova, M., Pletnev, P., Rubtsova, M., Mair, W., Vanyushkina, A., Khaitovich, P., Belousov, V., Vysokikh, M., Sergiev, P., Dontsova, O., 2019. *LINC00116* codes for a mitochondrial peptide linking respiration and lipid metabolism. *Proc Natl Acad Sci U S A* 116, 4940–4945. <https://doi.org/10.1073/pnas.1809105116>
- Collinson, E.J., Grant, C.M., 2003. Role of yeast glutaredoxins as glutathione S-transferases. *J Biol Chem* 278, 22492–22497. <https://doi.org/10.1074/jbc.M301387200>
- Collinson, L.P., Dawes, I.W., 1995. Isolation, characterization and overexpression of the yeast gene, *GLR1*, encoding glutathione reductase. *Gene* 156, 123–127. [https://doi.org/10.1016/0378-1119\(95\)00026-3](https://doi.org/10.1016/0378-1119(95)00026-3)
- Covarrubias, A.J., Perrone, R., Grozio, A., Verdin, E., 2021. NAD⁺ metabolism and its roles in cellular processes during ageing. *Nat Rev Mol Cell Biol* 22, 119–141. <https://doi.org/10.1038/s41580-020-00313-x>
- Craggs, T.D., 2009. Green fluorescent protein: Structure, folding and chromophore maturation. *Chem. Soc. Rev.* 38, 2865. <https://doi.org/10.1039/b903641p>
- Croft, T., Venkatakrishnan, P., Lin, S.-J., 2020. NAD⁺ metabolism and regulation: Lessons from yeast. *Biomolecules* 10, E330. <https://doi.org/10.3390/biom10020330>
- Culotta, V.C., Yang, M., O'Halloran, T.V., 2006. Activation of superoxide dismutases: Putting the metal to the pedal. *Biochim Biophys Acta* 1763, 747–758. <https://doi.org/10.1016/j.bbamcr.2006.05.003>

References

- de Smidt, O., du Preez, J.C., Albertyn, J., 2012. Molecular and physiological aspects of alcohol dehydrogenases in the ethanol metabolism of *Saccharomyces cerevisiae*. *FEMS Yeast Res* 12, 33–47. <https://doi.org/10.1111/j.1567-1364.2011.00760.x>
- Dechant, R., Saad, S., Ibáñez, A.J., Peter, M., 2014. Cytosolic pH regulates cell growth through distinct GTPases, Arf1 and Gtr1, to promote Ras/PKA and TORC1 activity. *Mol Cell* 55, 409–421. <https://doi.org/10.1016/j.molcel.2014.06.002>
- Delaunay, A., Pflieger, D., Barrault, M.B., Vinh, J., Toledano, M.B., 2002. A thiol peroxidase is an H₂O₂ receptor and redox-transducer in gene activation. *Cell* 111, 471–481. [https://doi.org/10.1016/s0092-8674\(02\)01048-6](https://doi.org/10.1016/s0092-8674(02)01048-6)
- Delgado, M.L., O'Connor, J.E., Azori N, I., Renau-Piqueras, J., Gil, M.L., Gozalbo, D., 2001. The glyceraldehyde-3-phosphate dehydrogenase polypeptides encoded by the *Saccharomyces cerevisiae* *TDH1*, *TDH2* and *TDH3* genes are also cell wall proteins. *Microbiology (Reading)* 147, 411–417. <https://doi.org/10.1099/00221287-147-2-411>
- Deponte, M., 2013. Glutathione catalysis and the reaction mechanisms of glutathione-dependent enzymes. *Biochim Biophys Acta* 1830, 3217–3266. <https://doi.org/10.1016/j.bbagen.2012.09.018>
- Díaz-García, C.M., Mongeon, R., Lahmann, C., Koveal, D., Zucker, H., Yellen, G., 2017. Neuronal stimulation triggers neuronal glycolysis and not lactate uptake. *Cell Metab* 26, 361–374.e4. <https://doi.org/10.1016/j.cmet.2017.06.021>
- Dilova, I., Easlou, E., Lin, S.-J., 2007. Calorie restriction and the nutrient sensing signaling pathways. *Cell Mol Life Sci* 64, 752–767. <https://doi.org/10.1007/s00018-007-6381-y>
- Dodd, B.J.T., Kralj, J.M., 2017. Live cell imaging reveals pH oscillations in *Saccharomyces cerevisiae* during metabolic transitions. *Sci Rep* 7, 13922. <https://doi.org/10.1038/s41598-017-14382-0>
- Dooley, C.T., Dore, T.M., Hanson, G.T., Jackson, W.C., Remington, S.J., Tsien, R.Y., 2004. Imaging dynamic redox changes in mammalian cells with green fluorescent protein indicators. *J Biol Chem* 279, 22284–22293. <https://doi.org/10.1074/jbc.M312847200>
- Draculic, T., Dawes, I.W., Grant, C.M., 2000. A single glutaredoxin or thioredoxin gene is essential for viability in the yeast *Saccharomyces cerevisiae*. *Mol Microbiol* 36, 1167–1174. <https://doi.org/10.1046/j.1365-2958.2000.01948.x>
- Eckers, E., Bien, M., Stroobant, V., Herrmann, J.M., Deponte, M., 2009. Biochemical characterization of dithiol glutaredoxin 8 from *Saccharomyces cerevisiae*: The catalytic redox mechanism redux. *Biochemistry* 48, 1410–1423. <https://doi.org/10.1021/bi801859b>
- Emanuelli, M., Amici, A., Carnevali, F., Pierella, F., Raffaelli, N., Magni, G., 2003. Identification and characterization of a second NMN adenyllyltransferase gene in *Saccharomyces cerevisiae*. *Protein Expr Purif* 27, 357–364. [https://doi.org/10.1016/s1046-5928\(02\)00645-9](https://doi.org/10.1016/s1046-5928(02)00645-9)
- Emanuelli, M., Carnevali, F., Lorenzi, M., Raffaelli, N., Amici, A., Ruggieri, S., Magni, G., 1999. Identification and characterization of *YLR328W*, the *Saccharomyces cerevisiae* structural gene encoding NMN adenyllyltransferase: Expression and characterization of the recombinant enzyme. *FEBS Lett* 455, 13–17. [https://doi.org/10.1016/s0014-5793\(99\)00852-2](https://doi.org/10.1016/s0014-5793(99)00852-2)
- Evans, T.C., Mackler, B., Grace, R., 1985. Pyridine nucleotide transhydrogenations in yeast. *Arch Biochem Biophys* 243, 492–503. [https://doi.org/10.1016/0003-9861\(85\)90526-0](https://doi.org/10.1016/0003-9861(85)90526-0)
- Ezeriņa, D., Morgan, B., Dick, T.P., 2014. Imaging dynamic redox processes with genetically encoded probes. *J Mol Cell Cardiol* 73, 43–49. <https://doi.org/10.1016/j.yjmcc.2013.12.023>
- Ferramosca, A., Zara, V., 2021. Mitochondrial carriers and substrates transport network: A lesson from *Saccharomyces cerevisiae*. *Int J Mol Sci* 22, 8496. <https://doi.org/10.3390/ijms22168496>
- Fessel, J.P., Oldham, W.M., 2018. Pyridine dinucleotides from molecules to man. *Antioxidants & Redox Signaling* 28, 180–212. <https://doi.org/10.1089/ars.2017.7120>
- Finkel, T., 2011. Signal transduction by reactive oxygen species. *J Cell Biol* 194, 7–15. <https://doi.org/10.1083/jcb.201102095>

- Fox, J.L., Lynen, F., 1980. Characterization of the flavoenzyme enoyl reductase of fatty acid synthetase from yeast. *Eur J Biochem* 109, 417–424. <https://doi.org/10.1111/j.1432-1033.1980.tb04810.x>
- Frick, O., Wittmann, C., 2005. Characterization of the metabolic shift between oxidative and fermentative growth in *Saccharomyces cerevisiae* by comparative ¹³C flux analysis. *Microb Cell Fact* 4, 30. <https://doi.org/10.1186/1475-2859-4-30>
- Gan, Z.R., 1991. Yeast thioredoxin genes. *J Biol Chem* 266, 1692–1696.
- Ghaemmaghani, S., Huh, W.-K., Bower, K., Howson, R.W., Belle, A., Dephoure, N., O'Shea, E.K., Weissman, J.S., 2003. Global analysis of protein expression in yeast. *Nature* 425, 737–741. <https://doi.org/10.1038/nature02046>
- Ghislain, M., Talla, E., François, J.M., 2002. Identification and functional analysis of the *Saccharomyces cerevisiae* *Saccharomyces cerevisiae* gene, *PNC1*. *Yeast* 19, 215–224. <https://doi.org/10.1002/yea.810>
- Giaever, G., Chu, A.M., Ni, L., Connelly, C., Riles, L., Véronneau, S., Dow, S., Lucau-Danila, A., Anderson, K., André, B., Arkin, A.P., Astromoff, A., El-Bakkoury, M., Bangham, R., Benito, R., Brachat, S., Campanaro, S., Curtiss, M., Davis, K., Deutschbauer, A., Entian, K.-D., Flaherty, P., Foury, F., Garfinkel, D.J., Gerstein, M., Gotte, D., Güldener, U., Hegemann, J.H., Hempel, S., Herman, Z., Jaramillo, D.F., Kelly, D.E., Kelly, S.L., Kötter, P., LaBonte, D., Lamb, D.C., Lan, N., Liang, H., Liao, H., Liu, L., Luo, C., Lussier, M., Mao, R., Menard, P., Ooi, S.L., Revuelta, J.L., Roberts, C.J., Rose, M., Ross-Macdonald, P., Scherens, B., Schimmack, G., Shafer, B., Shoemaker, D.D., Sookhai-Mahadeo, S., Storms, R.K., Strathern, J.N., Valle, G., Voet, M., Volckaert, G., Wang, C., Ward, T.R., Wilhelmy, J., Winzeler, E.A., Yang, Y., Yen, G., Youngman, E., Yu, K., Bussey, H., Boeke, J.D., Snyder, M., Philippsen, P., Davis, R.W., Johnston, M., 2002. Functional profiling of the *Saccharomyces cerevisiae* genome. *Nature* 418, 387–391. <https://doi.org/10.1038/nature00935>
- Goffeau, A., Barrell, B.G., Bussey, H., Davis, R.W., Dujon, B., Feldmann, H., Galibert, F., Hoheisel, J.D., Jacq, C., Johnston, M., Louis, E.J., Mewes, H.W., Murakami, Y., Philippsen, P., Tettelin, H., Oliver, S.G., 1996. Life with 6000 genes. *Science* 274, 546, 563–567. <https://doi.org/10.1126/science.274.5287.546>
- Goldstein, A.L., McCusker, J.H., 1999. Three new dominant drug resistance cassettes for gene disruption in *Saccharomyces cerevisiae*. *Yeast* 15, 1541–1553. [https://doi.org/10.1002/\(SICI\)1097-0061\(199910\)15:14<1541::AID-YEA476>3.0.CO;2-K](https://doi.org/10.1002/(SICI)1097-0061(199910)15:14<1541::AID-YEA476>3.0.CO;2-K)
- Grabowska, D., Chelstowska, A., 2003. The *ALD6* gene product is indispensable for providing NADPH in yeast cells lacking glucose-6-phosphate dehydrogenase activity. *J Biol Chem* 278, 13984–13988. <https://doi.org/10.1074/jbc.M210076200>
- Grant, C.M., 2001. Role of the glutathione/glutaredoxin and thioredoxin systems in yeast growth and response to stress conditions. *Mol Microbiol* 39, 533–541. <https://doi.org/10.1046/j.1365-2958.2001.02283.x>
- Grant, C.M., Quinn, K.A., Dawes, I.W., 1999. Differential protein S-thiolation of glyceraldehyde-3-phosphate dehydrogenase isoenzymes influences sensitivity to oxidative stress. *Mol Cell Biol* 19, 2650–2656. <https://doi.org/10.1128/MCB.19.4.2650>
- Gregor, C., Pape, J.K., Gwosch, K.C., Gilat, T., Sahl, S.J., Hell, S.W., 2019. Autonomous bioluminescence imaging of single mammalian cells with the bacterial bioluminescence system. *Proc Natl Acad Sci U S A* 201913616. <https://doi.org/10.1073/pnas.1913616116>
- Gu, H., Chen, C., Hao, X., Su, N., Huang, D., Zou, Y., Lin, S.-H., Chen, X., Zheng, D., Liu, L., Yu, Z., Xie, L., Zhang, Y., He, X., Lai, X., Zhang, X., Chen, G.-Q., Zhao, Y., Yang, Y., Loscalzo, J., Zheng, J., 2020. MDH1-mediated malate-aspartate NADH shuttle maintains the activity levels of fetal liver hematopoietic stem cells. *Blood* 136, 553–571. <https://doi.org/10.1182/blood.2019003940>
- Gutscher, M., Pauleau, A.-L., Marty, L., Brach, T., Wabnitz, G.H., Samstag, Y., Meyer, A.J., Dick, T.P., 2008. Real-time imaging of the intracellular glutathione redox potential. *Nat Methods* 5, 553–559. <https://doi.org/10.1038/nmeth.1212>

References

- Hanson, G.T., Aggeler, R., Oglesbee, D., Cannon, M., Capaldi, R.A., Tsien, R.Y., Remington, S.J., 2004. Investigating mitochondrial redox potential with redox-sensitive green fluorescent protein indicators. *J Biol Chem* 279, 13044–13053. <https://doi.org/10.1074/jbc.M312846200>
- Hao, X., Gu, H., Chen, C., Huang, D., Zhao, Y., Xie, L., Zou, Y., Shu, H.S., Zhang, Y., He, X., Lai, X., Zhang, X., Zhou, B.O., Zhang, C.C., Chen, G.-Q., Yu, Z., Yang, Y., Zheng, J., 2019. Metabolic imaging reveals a unique preference of symmetric cell division and homing of leukemia-initiating cells in an endosteal niche. *Cell Metab* 29, 950-965.e6. <https://doi.org/10.1016/j.cmet.2018.11.013>
- Hartmann, S.K., Stockdreher, Y., Wandrey, G., Tehrani, H., Zambanini, T., Meyer, A.J., Büchs, J., Blank, L.M., Schwarzländer, M., Wierckx, N., 2018. Online in vivo monitoring of cytosolic NAD redox dynamics in *Ustilago maydis*. *Biochim Biophys Acta Bioenerg* 1859, 1015–1024. <https://doi.org/10.1016/j.bbabi.2018.05.012>
- Hashimoto, F., Hayashi, H., 1990. Significance of catalase in peroxisomal fatty acyl-CoA beta-oxidation: NADH oxidation by acetoacetyl-CoA and H₂O₂. *J Biochem* 108, 426–431. <https://doi.org/10.1093/oxfordjournals.jbchem.a123217>
- Hector, R.E., Bowman, M.J., Skory, C.D., Cotta, M.A., 2009. The *Saccharomyces cerevisiae* *YMR315W* gene encodes an NADP(H)-specific oxidoreductase regulated by the transcription factor *Stb5p* in response to NADPH limitation. *N Biotechnol* 26, 171–180. <https://doi.org/10.1016/j.nbt.2009.08.008>
- Herrero, E., Ros, J., Bellí, G., Cabisco, E., 2008. Redox control and oxidative stress in yeast cells. *Biochim Biophys Acta* 1780, 1217–1235. <https://doi.org/10.1016/j.bbagen.2007.12.004>
- Höhne, P.R., 2020. Applying novel genetically encoded sensors to investigate subcellular NAD(P)H homeostasis (Bachelor thesis). Saarland University, Saarbrücken.
- Hoseki, J., Oishi, A., Fujimura, T., Sakai, Y., 2016. Development of a stable ERroGFP variant suitable for monitoring redox dynamics in the ER. *Biosci Rep* 36, e00316. <https://doi.org/10.1042/BSR20160027>
- Hu, Q., Wu, D., Walker, M., Wang, P., Tian, R., Wang, W., 2021. Genetically encoded biosensors for evaluating NAD⁺/NADH ratio in cytosolic and mitochondrial compartments. *Cell Rep Methods* 1, 100116. <https://doi.org/10.1016/j.crmeth.2021.100116>
- Hu, Q., Zhang, H., Gutiérrez Cortés, N., Wu, D., Wang, P., Zhang, J., Mattison, J.A., Smith, E., Bettcher, L.F., Wang, M., Lakatta, E.G., Sheu, S.-S., Wang, W., 2020. Increased Drp1 acetylation by lipid overload induces cardiomyocyte death and heart dysfunction. *Circ Res* 126, 456–470. <https://doi.org/10.1161/CIRCRESAHA.119.315252>
- Huang, G., Zhang, Y., Shan, Y., Yang, S., Chelliah, Y., Wang, H., Takahashi, J.S., 2016. Circadian oscillations of NADH redox state using a heterologous metabolic sensor in mammalian cells. *J Biol Chem* 291, 23906–23914. <https://doi.org/10.1074/jbc.M116.728774>
- Hung, Y.P., Albeck, J.G., Tantama, M., Yellen, G., 2011. Imaging cytosolic NADH/NAD⁺ redox state with a genetically encoded fluorescent biosensor. *Cell Metab* 14, 545–554. <https://doi.org/10.1016/j.cmet.2011.08.012>
- Hung, Y.P., Teragawa, C., Kosaisawe, N., Gillies, T.E., Pargett, M., Minguet, M., Distor, K., Rocha-Gregg, B.L., Coloff, J.L., Keibler, M.A., Stephanopoulos, G., Yellen, G., Brugge, J.S., Albeck, J.G., 2017. Akt regulation of glycolysis mediates bioenergetic stability in epithelial cells. *Elife* 6, e27293. <https://doi.org/10.7554/eLife.27293>
- Hung, Y.P., Yellen, G., 2014. Live-cell imaging of cytosolic NADH/NAD⁺ redox state using a genetically encoded fluorescent biosensor. *Methods Mol Biol* 1071, 83–95. https://doi.org/10.1007/978-1-62703-622-1_7
- Imai, S., Armstrong, C.M., Kaeberlein, M., Guarente, L., 2000. Transcriptional silencing and longevity protein Sir2 is an NAD-dependent histone deacetylase. *Nature* 403, 795–800. <https://doi.org/10.1038/35001622>
- Imamura, H., Nhat, K.P.H., Togawa, H., Saito, K., Iino, R., Kato-Yamada, Y., Nagai, T., Noji, H., 2009. Visualization of ATP levels inside single living cells with fluorescence resonance

- energy transfer-based genetically encoded indicators. *Proc Natl Acad Sci U S A* 106, 15651–15656. <https://doi.org/10.1073/pnas.0904764106>
- Irokawa, H., Tachibana, T., Watanabe, T., Matsuyama, Y., Motohashi, H., Ogasawara, A., Iwai, K., Naganuma, A., Kuge, S., 2016. Redox-dependent regulation of gluconeogenesis by a novel mechanism mediated by a peroxidatic cysteine of peroxiredoxin. *Sci Rep* 6, 33536. <https://doi.org/10.1038/srep33536>
- Ishikawa, M., Tanaka, Y., Suzuki, R., Kimura, K., Tanaka, K., Kamiya, K., Ito, H., Kato, S., Kamachi, T., Hori, K., Nakanishi, S., 2017. Real-time monitoring of intracellular redox changes in *Methylococcus capsulatus* (Bath) for efficient bioconversion of methane to methanol. *Bioresour Technol* 241, 1157–1161. <https://doi.org/10.1016/j.biortech.2017.05.107>
- Izawa, S., Maeda, K., Miki, T., Mano, J., Inoue, Y., Kimura, A., 1998. Importance of glucose-6-phosphate dehydrogenase in the adaptive response to hydrogen peroxide in *Saccharomyces cerevisiae*. *Biochem J* 330 (Pt 2), 811–817. <https://doi.org/10.1042/bj3300811>
- Jakob, J., 2021. Charakterisierung neuartiger genetisch codierter Sensoren zur Untersuchung der NAD(P)H-Homöostase (Master thesis). Saarland University, Saarbrücken.
- Jang, H.H., Lee, K.O., Chi, Y.H., Jung, B.G., Park, S.K., Park, J.H., Lee, J.R., Lee, S.S., Moon, J.C., Yun, J.W., Choi, Y.O., Kim, W.Y., Kang, J.S., Cheong, G.-W., Yun, D.-J., Rhee, S.G., Cho, M.J., Lee, S.Y., 2004. Two enzymes in one: Two yeast peroxiredoxins display oxidative stress-dependent switching from a peroxidase to a molecular chaperone function. *Cell* 117, 625–635. <https://doi.org/10.1016/j.cell.2004.05.002>
- Janke, C., Magiera, M.M., Rathfelder, N., Taxis, C., Reber, S., Maekawa, H., Moreno-Borchart, A., Doenges, G., Schwob, E., Schiebel, E., Knop, M., 2004. A versatile toolbox for PCR-based tagging of yeast genes: New fluorescent proteins, more markers and promoter substitution cassettes. *Yeast* 21, 947–962. <https://doi.org/10.1002/yea.1142>
- Ji, Y., Yang, C., Tang, Z., Yang, Y., Tian, Y., Yao, H., Zhu, X., Zhang, Z., Ji, J., Zheng, X., 2017. Adenylate kinase hCINAP determines self-renewal of colorectal cancer stem cells by facilitating LDHA phosphorylation. *Nat Commun* 8, 15308. <https://doi.org/10.1038/ncomms15308>
- Kakhniashvili, D., Mayor, J.A., Gremse, D.A., Xu, Y., Kaplan, R.S., 1997. Identification of a novel gene encoding the yeast mitochondrial dicarboxylate transport protein via overexpression, purification, and characterization of its protein product. *J Biol Chem* 272, 4516–4521. <https://doi.org/10.1074/jbc.272.7.4516>
- Karagiannis, J., Young, P.G., 2001. Intracellular pH homeostasis during cell-cycle progression and growth state transition in *Schizosaccharomyces pombe*. *J Cell Sci* 114, 2929–2941. <https://doi.org/10.1242/jcs.114.16.2929>
- Kato, M., Lin, S.-J., 2014. Regulation of NAD⁺ metabolism, signaling and compartmentalization in the yeast *Saccharomyces cerevisiae*. *DNA Repair (Amst.)* 23, 49–58. <https://doi.org/10.1016/j.dnarep.2014.07.009>
- Kawai, S., Suzuki, S., Mori, S., Murata, K., 2001. Molecular cloning and identification of *UTR1* of a yeast *Saccharomyces cerevisiae* as a gene encoding an NAD kinase. *FEMS Microbiol Lett* 200, 181–184. <https://doi.org/10.1111/j.1574-6968.2001.tb10712.x>
- Kim, W., Deik, A., Gonzalez, C., Gonzalez, M.E., Fu, F., Ferrari, M., Churchhouse, C.L., Florez, J.C., Jacobs, S.B.R., Clish, C.B., Rhee, E.P., 2019. Polyunsaturated fatty acid desaturation is a mechanism for glycolytic NAD⁺ recycling. *Cell Metab* 29, 856-870.e7. <https://doi.org/10.1016/j.cmet.2018.12.023>
- Knudsen, J.D., Carlquist, M., Gorwa-Grauslund, M., 2014. NADH-dependent biosensor in *Saccharomyces cerevisiae*: Principle and validation at the single cell level. *AMB Express* 4, 81. <https://doi.org/10.1186/s13568-014-0081-4>
- Koju, N., Qin, Z.-H., Sheng, R., 2022. Reduced nicotinamide adenine dinucleotide phosphate in redox balance and diseases: A friend or foe? *Acta Pharmacol Sin.* <https://doi.org/10.1038/s41401-021-00838-7>

References

- Kosower, N.S., Kosower, E.M., 1995. Diamide: An oxidant probe for thiols. *Methods Enzymol* 251, 123–133. [https://doi.org/10.1016/0076-6879\(95\)51116-4](https://doi.org/10.1016/0076-6879(95)51116-4)
- Kostyuk, A.I., Demidovich, A.D., Kotova, D.A., Belousov, V.V., Bilan, D.S., 2019. Circularly permuted fluorescent protein-based indicators: History, principles, and classification. *Int J Mol Sci* 20, 4200. <https://doi.org/10.3390/ijms20174200>
- Kritsiligkou, P., Nowicki-Osuch, K., Carter, Z., Kershaw, C.J., Creamer, D.R., Weids, A.J., Grant, C.M., 2021a. Tolerance to nascent protein misfolding stress requires fine-tuning of the cAMP/PKA pathway. *J Biol Chem* 296, 100690. <https://doi.org/10.1016/j.jbc.2021.100690>
- Kritsiligkou, P., Shen, T.K., Dick, T.P., 2021b. A comparison of Prx- and OxyR-based H₂O₂ probes expressed in *S. cerevisiae*. *J Biol Chem* 297, 100866. <https://doi.org/10.1016/j.jbc.2021.100866>
- Larochelle, M., Drouin, S., Robert, F., Turcotte, B., 2006. Oxidative stress-activated zinc cluster protein Stb5 has dual activator/repressor functions required for pentose phosphate pathway regulation and NADPH production. *Mol Cell Biol* 26, 6690–6701. <https://doi.org/10.1128/MCB.02450-05>
- Le Moan, N., Clement, G., Le Maout, S., Tacnet, F., Toledano, M.B., 2006. The *Saccharomyces cerevisiae* proteome of oxidized protein thiols: Contrasted functions for the thioredoxin and glutathione pathways. *J Biol Chem* 281, 10420–10430. <https://doi.org/10.1074/jbc.M513346200>
- Lee, J., Godon, C., Lagniel, G., Spector, D., Garin, J., Labarre, J., Toledano, M.B., 1999. Yap1 and Skn7 control two specialized oxidative stress response regulons in yeast. *J Biol Chem* 274, 16040–16046. <https://doi.org/10.1074/jbc.274.23.16040>
- Li, W., Sun, L., Liang, Q., Wang, J., Mo, W., Zhou, B., 2006. Yeast AMID homologue Ndi1p displays respiration-restricted apoptotic activity and is involved in chronological aging. *Mol Biol Cell* 17, 1802–1811. <https://doi.org/10.1091/mbc.e05-04-0333>
- Liedgens, L., Zimmermann, J., Wäschenbach, L., Geissel, F., Laporte, H., Gohlke, H., Morgan, B., Deponte, M., 2020. Quantitative assessment of the determinant structural differences between redox-active and inactive glutaredoxins. *Nat Commun* 11, 1725. <https://doi.org/10.1038/s41467-020-15441-3>
- Lim, S.-L., Voon, C.P., Guan, X., Yang, Y., Gardeström, P., Lim, B.L., 2020. In planta study of photosynthesis and photorespiration using NADPH and NADH/NAD⁺ fluorescent protein sensors. *Nat Commun* 11, 3238. <https://doi.org/10.1038/s41467-020-17056-0>
- Linden, A., Gülden, M., Martin, H.-J., Maser, E., Seibert, H., 2008. Peroxide-induced cell death and lipid peroxidation in C6 glioma cells. *Toxicol In Vitro* 22, 1371–1376. <https://doi.org/10.1016/j.tiv.2008.02.003>
- Liu, Y., Landick, R., Raman, S., 2019. A regulatory NADH/NAD⁺ redox biosensor for bacteria. *ACS Synth Biol* 8, 264–273. <https://doi.org/10.1021/acssynbio.8b00485>
- Lloyd, D., 2019. *Saccharomyces cerevisiae*: Oscillatory orchestration of growth, in: Satyanarayana, T., Deshmukh, S.K., Deshpande, M.V. (Eds.), *Advancing Frontiers in Mycology and Mycotechnology*. Springer Singapore, Singapore, pp. 181–214. https://doi.org/10.1007/978-981-13-9349-5_7
- Lu, S.-P., Lin, S.-J., 2011. Phosphate-responsive signaling pathway is a novel component of NAD⁺ metabolism in *Saccharomyces cerevisiae*. *J Biol Chem* 286, 14271–14281. <https://doi.org/10.1074/jbc.M110.217885>
- Luikenhuis, S., Perrone, G., Dawes, I.W., Grant, C.M., 1998. The yeast *Saccharomyces cerevisiae* contains two glutaredoxin genes that are required for protection against reactive oxygen species. *Mol Biol Cell* 9, 1081–1091. <https://doi.org/10.1091/mbc.9.5.1081>
- Luttik, M.A., Overkamp, K.M., Kötter, P., de Vries, S., van Dijken, J.P., Pronk, J.T., 1998. The *Saccharomyces cerevisiae* *NDE1* and *NDE2* genes encode separate mitochondrial NADH dehydrogenases catalyzing the oxidation of cytosolic NADH. *J Biol Chem* 273, 24529–24534. <https://doi.org/10.1074/jbc.273.38.24529>

- Markvicheva, K.N., Bilan, D.S., Mishina, N.M., Gorokhovatsky, A.Y., Vinokurov, L.M., Lukyanov, S., Belousov, V.V., 2011. A genetically encoded sensor for H₂O₂ with expanded dynamic range. *Bioorg Med Chem* 19, 1079–1084. <https://doi.org/10.1016/j.bmc.2010.07.014>
- Masaki, N., Kyle, M.E., Farber, J.L., 1989. *tert*-Butyl hydroperoxide kills cultured hepatocytes by peroxidizing membrane lipids. *Arch Biochem Biophys* 269, 390–399. [https://doi.org/10.1016/0003-9861\(89\)90122-7](https://doi.org/10.1016/0003-9861(89)90122-7)
- Masia, R., McCarty, W.J., Lahmann, C., Luther, J., Chung, R.T., Yarmush, M.L., Yellen, G., 2018. Live cell imaging of cytosolic NADH/NAD⁺ ratio in hepatocytes and liver slices. *Am J Physiol Gastrointest Liver Physiol* 314, G97–G108. <https://doi.org/10.1152/ajpgi.00093.2017>
- Masselot, M., De Robichon-Szulmajster, H., 1975. Methionine biosynthesis in *Saccharomyces cerevisiae*. (I) Genetical analysis of auxotrophic mutants. *Mol Gen Genet* 139, 121–132. <https://doi.org/10.1007/BF00264692>
- McAlister, L., Holland, M.J., 1985. Isolation and characterization of yeast strains carrying mutations in the glyceraldehyde-3-phosphate dehydrogenase genes. *J Biol Chem* 260, 15013–15018.
- McLaughlin, K.J., Strain-Damerell, C.M., Xie, K., Brekasis, D., Soares, A.S., Paget, M.S.B., Kielkopf, C.L., 2010. Structural basis for NADH/NAD⁺ redox sensing by a Rex family repressor. *Mol Cell* 38, 563–575. <https://doi.org/10.1016/j.molcel.2010.05.006>
- Meaden, P.G., Dickinson, F.M., Mifsud, A., Tessier, W., Westwater, J., Bussey, H., Midgley, M., 1997. The *ALD6* gene of *Saccharomyces cerevisiae* encodes a cytosolic, Mg²⁺-activated acetaldehyde dehydrogenase. *Yeast* 13, 1319–1327. [https://doi.org/10.1002/\(SICI\)1097-0061\(199711\)13:14<1319::AID-YEA183>3.0.CO;2-T](https://doi.org/10.1002/(SICI)1097-0061(199711)13:14<1319::AID-YEA183>3.0.CO;2-T)
- Medvedik, O., Lamming, D.W., Kim, K.D., Sinclair, D.A., 2007. *MSN2* and *MSN4* link calorie restriction and TOR to sirtuin-mediated lifespan extension in *Saccharomyces cerevisiae*. *PLoS Biol* 5, e261. <https://doi.org/10.1371/journal.pbio.0050261>
- Meyer, A.J., Dick, T.P., 2010. Fluorescent protein-based redox probes. *Antioxid Redox Signal* 13, 621–650. <https://doi.org/10.1089/ars.2009.2948>
- Miesenböck, G., De Angelis, D.A., Rothman, J.E., 1998. Visualizing secretion and synaptic transmission with pH-sensitive green fluorescent proteins. *Nature* 394, 192–195. <https://doi.org/10.1038/28190>
- Milev, N.B., Rhee, S.-G., Reddy, A.B., 2018. Cellular timekeeping: It's redox o'clock. *Cold Spring Harb Perspect Biol* 10, a027698. <https://doi.org/10.1101/cshperspect.a027698>
- Minard, K.I., McAlister-Henn, L., 2005. Sources of NADPH in yeast vary with carbon source. *J Biol Chem* 280, 39890–39896. <https://doi.org/10.1074/jbc.M509461200>
- Minard, K.I., McAlister-Henn, L., 1991. Isolation, nucleotide sequence analysis, and disruption of the *MDH2* gene from *Saccharomyces cerevisiae*: Evidence for three isozymes of yeast malate dehydrogenase. *Mol Cell Biol* 11, 370–380. <https://doi.org/10.1128/mcb.11.1.370-380.1991>
- Mita, M., Ito, M., Harada, K., Sugawara, I., Ueda, H., Tsuboi, T., Kitaguchi, T., 2019. Green fluorescent protein-based glucose indicators report glucose dynamics in living cells. *Anal Chem* 91, 4821–4830. <https://doi.org/10.1021/acs.analchem.9b00447>
- Mita, M., Sugawara, I., Harada, K., Ito, M., Takizawa, M., Ishida, K., Ueda, H., Kitaguchi, T., Tsuboi, T., 2022. Development of red genetically encoded biosensor for visualization of intracellular glucose dynamics. *Cell Chem Biol* 29, 98–108.e4. <https://doi.org/10.1016/j.chembiol.2021.06.002>
- Miyagi, H., Kawai, S., Murata, K., 2009. Two sources of mitochondrial NADPH in the yeast *Saccharomyces cerevisiae*. *J Biol Chem* 284, 7553–7560. <https://doi.org/10.1074/jbc.M804100200>
- Mongeon, R., Venkatachalam, V., Yellen, G., 2016. Cytosolic NADH/NAD⁺ redox visualized in brain slices by two-photon fluorescence lifetime biosensor imaging. *Antioxid Redox Signal* 25, 553–563. <https://doi.org/10.1089/ars.2015.6593>
- Moreira dos Santos, M., Raghevendran, V., Kötter, P., Olsson, L., Nielsen, J., 2004. Manipulation of malic enzyme in *Saccharomyces cerevisiae* for increasing NADPH production capacity

References

- aerobically in different cellular compartments. *Metab Eng* 6, 352–363. <https://doi.org/10.1016/j.ymben.2004.06.002>
- Morgan, B., Ezeriņa, D., Amoako, T.N.E., Riemer, J., Seedorf, M., Dick, T.P., 2013. Multiple glutathione disulfide removal pathways mediate cytosolic redox homeostasis. *Nat Chem Biol* 9, 119–125. <https://doi.org/10.1038/nchembio.1142>
- Morgan, B., Sobotta, M.C., Dick, T.P., 2011. Measuring E_{GSH} and H_2O_2 with roGFP2-based redox probes. *Free Radic Biol Med* 51, 1943–1951. <https://doi.org/10.1016/j.freeradbiomed.2011.08.035>
- Morgan, B., Van Laer, K., Owusu, T.N.E., Ezeriņa, D., Pastor-Flores, D., Amponsah, P.S., Tursch, A., Dick, T.P., 2016. Real-time monitoring of basal H_2O_2 levels with peroxiredoxin-based probes. *Nat Chem Biol* 12, 437–443. <https://doi.org/10.1038/nchembio.2067>
- Muller, E.G., 1996. A glutathione reductase mutant of yeast accumulates high levels of oxidized glutathione and requires thioredoxin for growth. *Mol Biol Cell* 7, 1805–1813. <https://doi.org/10.1091/mbc.7.11.1805>
- Müller-Schüssele, S.J., Schwarzländer, M., Meyer, A.J., 2021. Live monitoring of plant redox and energy physiology with genetically encoded biosensors. *Plant Physiol* 186, 93–109. <https://doi.org/10.1093/plphys/kiab019>
- Mumberg, D., Müller, R., Funk, M., 1995. Yeast vectors for the controlled expression of heterologous proteins in different genetic backgrounds. *Gene* 156, 119–122. [https://doi.org/10.1016/0378-1119\(95\)00037-7](https://doi.org/10.1016/0378-1119(95)00037-7)
- Munhoz, D.C., Netto, L.E.S., 2004. Cytosolic thioredoxin peroxidase I and II are important defenses of yeast against organic hydroperoxide insult: Catalases and peroxiredoxins cooperate in the decomposition of H_2O_2 by yeast. *J Biol Chem* 279, 35219–35227. <https://doi.org/10.1074/jbc.M313773200>
- Murray, D.B., Amariei, C., Sasidharan, K., Machné, R., Aon, M.A., Lloyd, D., 2014. Temporal partitioning of the yeast cellular network, in: Aon, M.A., Saks, V., Schlattner, U. (Eds.), *Systems Biology of Metabolic and Signaling Networks*, Springer Series in Biophysics. Springer Berlin Heidelberg, Berlin, Heidelberg, pp. 323–349. https://doi.org/10.1007/978-3-642-38505-6_12
- Murray, D.B., Beckmann, M., Kitano, H., 2007. Regulation of yeast oscillatory dynamics. *Proc Natl Acad Sci U S A* 104, 2241–2246. <https://doi.org/10.1073/pnas.0606677104>
- Murray, D.B., Engelen, F., Lloyd, D., Kuriyama, H., 1999. Involvement of glutathione in the regulation of respiratory oscillation during a continuous culture of *Saccharomyces cerevisiae*. *Microbiology (Reading)* 145 (Pt 10), 2739–2745. <https://doi.org/10.1099/00221287-145-10-2739>
- Murray, D.B., Engelen, F.A.A., Keulers, M., Kuriyama, H., Lloyd, D., 1998. NO^+ , but not NO^- , inhibits respiratory oscillations in ethanol-grown chemostat cultures of *Saccharomyces cerevisiae*. *FEBS Letters* 431, 297–299. [https://doi.org/10.1016/S0014-5793\(98\)00777-7](https://doi.org/10.1016/S0014-5793(98)00777-7)
- Murray, D.B., Haynes, K., Tomita, M., 2011. Redox regulation in respiring *Saccharomyces cerevisiae*. *Biochim Biophys Acta* 1810, 945–958. <https://doi.org/10.1016/j.bbagen.2011.04.005>
- Nagai, T., Sawano, A., Park, E.S., Miyawaki, A., 2001. Circularly permuted green fluorescent proteins engineered to sense Ca^{2+} . *Proc Natl Acad Sci U S A* 98, 3197–3202. <https://doi.org/10.1073/pnas.051636098>
- Nakamura, A., Sosa, A., Komori, H., Kita, A., Miki, K., 2007. Crystal structure of TTHA1657 (AT-rich DNA-binding protein; p25) from *Thermus thermophilus* HB8 at 2.16 Å resolution. *Proteins* 66, 755–759. <https://doi.org/10.1002/prot.21222>
- Netto, L.E.S., Antunes, F., 2016. The roles of peroxiredoxin and thioredoxin in hydrogen peroxide sensing and in signal transduction. *Mol Cells* 39, 65–71. <https://doi.org/10.14348/molcells.2016.2349>

- Netto, L.E.S., de Oliveira, M.A., Monteiro, G., Demasi, A.P.D., Cussioli, J.R.R., Discola, K.F., Demasi, M., Silva, G.M., Alves, S.V., Faria, V.G., Horta, B.B., 2007. Reactive cysteine in proteins: Protein folding, antioxidant defense, redox signaling and more. *Comp Biochem Physiol C Toxicol Pharmacol* 146, 180–193. <https://doi.org/10.1016/j.cbpc.2006.07.014>
- Ng, C.-H., Tan, S.-X., Perrone, G.G., Thorpe, G.W., Higgins, V.J., Dawes, I.W., 2008. Adaptation to hydrogen peroxide in *Saccharomyces cerevisiae*: The role of NADPH-generating systems and the SKN7 transcription factor. *Free Radic Biol Med* 44, 1131–1145. <https://doi.org/10.1016/j.freeradbiomed.2007.12.008>
- Nielsen, J., 2019. Yeast systems biology: Model organism and cell factory. *Biotechnol J* 14, e1800421. <https://doi.org/10.1002/biot.201800421>
- Nogae, I., Johnston, M., 1990. Isolation and characterization of the *ZWF1* gene of *Saccharomyces cerevisiae*, encoding glucose-6-phosphate dehydrogenase. *Gene* 96, 161–169. [https://doi.org/10.1016/0378-1119\(90\)90248-p](https://doi.org/10.1016/0378-1119(90)90248-p)
- Ocón-Garrido, E., Grant, C.M., 2002. Role of thioredoxins in the response of *Saccharomyces cerevisiae* to oxidative stress induced by hydroperoxides. *Mol Microbiol* 43, 993–1003. <https://doi.org/10.1046/j.1365-2958.2002.02795.x>
- Oestreicher, J., Morgan, B., 2019. Glutathione: Subcellular distribution and membrane transport. *Biochem Cell Biol* 97, 270–289. <https://doi.org/10.1139/bcb-2018-0189>
- Okabe, K., Yaku, K., Tobe, K., Nakagawa, T., 2019. Implications of altered NAD metabolism in metabolic disorders. *J Biomed Sci* 26, 34. <https://doi.org/10.1186/s12929-019-0527-8>
- Oldham, W.M., Clish, C.B., Yang, Y., Loscalzo, J., 2015. Hypoxia-mediated increases in L-2-hydroxyglutarate coordinate the metabolic response to reductive stress. *Cell Metab* 22, 291–303. <https://doi.org/10.1016/j.cmet.2015.06.021>
- O'Neill, J.S., 2021. Redox-coupled rhythm and brews. *Nat Chem Biol* 17, 373–374. <https://doi.org/10.1038/s41589-021-00777-8>
- O'Neill, J.S., Hoyle, N.P., Robertson, J.B., Edgar, R.S., Beale, A.D., Peak-Chew, S.Y., Day, J., Costa, A.S.H., Frezza, C., Causton, H.C., 2020. Eukaryotic cell biology is temporally coordinated to support the energetic demands of protein homeostasis. *Nat Commun* 11, 4706. <https://doi.org/10.1038/s41467-020-18330-x>
- Orij, R., Postmus, J., Ter Beek, A., Brul, S., Smits, G.J., 2009. In vivo measurement of cytosolic and mitochondrial pH using a pH-sensitive GFP derivative in *Saccharomyces cerevisiae* reveals a relation between intracellular pH and growth. *Microbiology (Reading)* 155, 268–278. <https://doi.org/10.1099/mic.0.022038-0>
- Outten, C.E., Culotta, V.C., 2004. Alternative start sites in the *Saccharomyces cerevisiae* *GLR1* gene are responsible for mitochondrial and cytosolic isoforms of glutathione reductase. *J Biol Chem* 279, 7785–7791. <https://doi.org/10.1074/jbc.M312421200>
- Outten, C.E., Falk, R.L., Culotta, V.C., 2005. Cellular factors required for protection from hyperoxia toxicity in *Saccharomyces cerevisiae*. *Biochem J* 388, 93–101. <https://doi.org/10.1042/BJ20041914>
- Ouyang, L., Holland, P., Lu, H., Bergenholm, D., Nielsen, J., 2018. Integrated analysis of the yeast NADPH-regulator Stb5 reveals distinct differences in NADPH requirements and regulation in different states of yeast metabolism. *FEMS Yeast Res* 18. <https://doi.org/10.1093/femsyr/foy091>
- Pak, V.V., Ezeriņa, D., Lyublinskaya, O.G., Pedre, B., Tyurin-Kuzmin, P.A., Mishina, N.M., Thauvin, M., Young, D., Wahni, K., Martínez Gache, S.A., Demidovich, A.D., Ermakova, Y.G., Maslova, Y.D., Shokhina, A.G., Eroglu, E., Bilan, D.S., Bogeski, I., Michel, T., Vríz, S., Messens, J., Belousov, V.V., 2020. Ultrasensitive genetically encoded indicator for hydrogen peroxide identifies roles for the oxidant in cell migration and mitochondrial function. *Cell Metab* 31, 642–653.e6. <https://doi.org/10.1016/j.cmet.2020.02.003>
- Palmieri, L., Vozza, A., Agrimi, G., De Marco, V., Runswick, M.J., Palmieri, F., Walker, J.E., 1999. Identification of the yeast mitochondrial transporter for oxaloacetate and sulfate. *J Biol Chem* 274, 22184–22190. <https://doi.org/10.1074/jbc.274.32.22184>

References

- Pang, Y., Zhang, H., Ai, H.-W., 2021. Genetically encoded fluorescent redox indicators for unveiling redox signaling and oxidative toxicity. *Chem Res Toxicol* 34, 1826–1845. <https://doi.org/10.1021/acs.chemrestox.1c00149>
- Papagiannakis, A., Niebel, B., Wit, E.C., Heinemann, M., 2017. Autonomous metabolic oscillations robustly gate the early and late cell cycle. *Mol Cell* 65, 285–295. <https://doi.org/10.1016/j.molcel.2016.11.018>
- Parapouli, M., Vasileiadis, A., Afendra, A.-S., Hatziloukas, E., 2020. *Saccharomyces cerevisiae* and its industrial applications. *AIMS Microbiol* 6, 1–31. <https://doi.org/10.3934/microbiol.2020001>
- Park, S.G., Cha, M.K., Jeong, W., Kim, I.H., 2000. Distinct physiological functions of thiol peroxidase isoenzymes in *Saccharomyces cerevisiae*. *J Biol Chem* 275, 5723–5732. <https://doi.org/10.1074/jbc.275.8.5723>
- Pedrajas, J.R., Kosmidou, E., Miranda-Vizuete, A., Gustafsson, J.A., Wright, A.P., Spyrou, G., 1999. Identification and functional characterization of a novel mitochondrial thioredoxin system in *Saccharomyces cerevisiae*. *J Biol Chem* 274, 6366–6373. <https://doi.org/10.1074/jbc.274.10.6366>
- Peralta, D., Bronowska, A.K., Morgan, B., Dóka, É., Van Laer, K., Nagy, P., Gräter, F., Dick, T.P., 2015. A proton relay enhances H₂O₂ sensitivity of GAPDH to facilitate metabolic adaptation. *Nat Chem Biol* 11, 156–163. <https://doi.org/10.1038/nchembio.1720>
- Picazo, C., Matallana, E., Aranda, A., 2018. Yeast thioredoxin reductase Trr1p controls TORC1-regulated processes. *Sci Rep* 8, 16500. <https://doi.org/10.1038/s41598-018-34908-4>
- Poburko, D., Santo-Domingo, J., Demarex, N., 2011. Dynamic regulation of the mitochondrial proton gradient during cytosolic calcium elevations. *J Biol Chem* 286, 11672–11684. <https://doi.org/10.1074/jbc.M110.159962>
- Pollak, N., Dölle, C., Ziegler, M., 2007. The power to reduce: Pyridine nucleotides - small molecules with a multitude of functions. *Biochem J* 402, 205–218. <https://doi.org/10.1042/BJ20061638>
- Pronk, J.T., Yde Steensma, H., Van Dijken, J.P., 1996. Pyruvate metabolism in *Saccharomyces cerevisiae*. *Yeast* 12, 1607–1633. [https://doi.org/10.1002/\(sici\)1097-0061\(199612\)12:16<1607::aid-yea70>3.0.co;2-4](https://doi.org/10.1002/(sici)1097-0061(199612)12:16<1607::aid-yea70>3.0.co;2-4)
- Ralser, M., Wamelink, M.M., Kowald, A., Gerisch, B., Heeren, G., Struys, E.A., Klipp, E., Jakobs, C., Breitenbach, M., Lehrach, H., Krobitsch, S., 2007. Dynamic rerouting of the carbohydrate flux is key to counteracting oxidative stress. *J Biol* 6, 10. <https://doi.org/10.1186/jbiol61>
- Ravcheev, D.A., Li, X., Latif, H., Zengler, K., Leyn, S.A., Korostelev, Y.D., Kazakov, A.E., Novichkov, P.S., Osterman, A.L., Rodionov, D.A., 2012. Transcriptional regulation of central carbon and energy metabolism in bacteria by redox-responsive repressor Rex. *J Bacteriol* 194, 1145–1157. <https://doi.org/10.1128/JB.06412-11>
- Rodrigues, F., Ludovico, P., Leão, C., 2006. Sugar metabolism in yeasts: An overview of aerobic and anaerobic glucose catabolism, in: Péter, G., Rosa, C. (Eds.), *Biodiversity and Ecophysiology of Yeasts*, The Yeast Handbook. Springer-Verlag, Berlin/Heidelberg, pp. 101–121. https://doi.org/10.1007/3-540-30985-3_6
- Roger, F., Picazo, C., Reiter, W., Libiad, M., Asami, C., Hanzén, S., Gao, C., Lagniel, G., Welkenhuysen, N., Labarre, J., Nyström, T., Grøtli, M., Hartl, M., Toledano, M.B., Molin, M., 2020. Peroxiredoxin promotes longevity and H₂O₂-resistance in yeast through redox-modulation of protein kinase A. *Elife* 9, e60346. <https://doi.org/10.7554/eLife.60346>
- Saccoccia, F., Angelucci, F., Boumis, G., Carotti, D., Desiato, G., Miele, A.E., Bellelli, A., 2014. Thioredoxin reductase and its inhibitors. *Curr Protein Pept Sci* 15, 621–646. <https://doi.org/10.2174/1389203715666140530091910>
- Saint-Prix, F., Bönquist, L., Dequin, S., 2004. Functional analysis of the *ALD* gene family of *Saccharomyces cerevisiae* during anaerobic growth on glucose: The NADP⁺-dependent Ald6p and Ald5p isoforms play a major role in acetate formation. *Microbiology (Reading)* 150, 2209–2220. <https://doi.org/10.1099/mic.0.26999-0>

- Saliba, E., Evangelinos, M., Gournas, C., Corrillon, F., Georis, I., André, B., 2018. The yeast H⁺-ATPase Pma1 promotes Rag/Gtr-dependent TORC1 activation in response to H⁺-coupled nutrient uptake. *Elife* 7, e31981. <https://doi.org/10.7554/eLife.31981>
- Sandbichler, A.M., Jansen, B., Peer, B.A., Paulitsch, M., Pelster, B., Egg, M., 2018. Metabolic plasticity enables circadian adaptation to acute hypoxia in zebrafish cells. *Cell Physiol Biochem* 46, 1159–1174. <https://doi.org/10.1159/000489058>
- Satroudinov, A.D., Kuriyama, H., Kobayashi, H., 1992. Oscillatory metabolism of *Saccharomyces cerevisiae* in continuous culture. *FEMS Microbiol Lett* 77, 261–267. [https://doi.org/10.1016/0378-1097\(92\)90167-m](https://doi.org/10.1016/0378-1097(92)90167-m)
- Sazanov, L.A., Jackson, J.B., 1994. Proton-translocating transhydrogenase and NAD- and NADP-linked isocitrate dehydrogenases operate in a substrate cycle which contributes to fine regulation of the tricarboxylic acid cycle activity in mitochondria. *FEBS Lett* 344, 109–116. [https://doi.org/10.1016/0014-5793\(94\)00370-x](https://doi.org/10.1016/0014-5793(94)00370-x)
- Schiffmann, L., 2019. Characterization and application of novel genetically encoded NAD(P)H sensors in *Saccharomyces cerevisiae* (Bachelor thesis). Saarland University, Saarbrücken.
- Schöndorf, D.C., Ivanyuk, D., Baden, P., Sanchez-Martinez, A., De Cicco, S., Yu, C., Giunta, I., Schwarz, L.K., Di Napoli, G., Panagiotakopoulou, V., Nestel, S., Keatinge, M., Pruszek, J., Bandmann, O., Heimrich, B., Gasser, T., Whitworth, A.J., Deleidi, M., 2018. The NAD⁺ precursor nicotinamide riboside rescues mitochondrial defects and neuronal loss in iPSC and fly models of Parkinson's disease. *Cell Rep* 23, 2976–2988. <https://doi.org/10.1016/j.celrep.2018.05.009>
- Schwarzländer, M., Dick, T.P., Meyer, A.J., Morgan, B., 2016. Dissecting redox biology using fluorescent protein sensors. *Antioxid Redox Signal* 24, 680–712. <https://doi.org/10.1089/ars.2015.6266>
- Schwarzländer, M., Wagner, S., Ermakova, Y.G., Belousov, V.V., Radi, R., Beckman, J.S., Buettner, G.R., Demareux, N., Duchon, M.R., Forman, H.J., Fricker, M.D., Gems, D., Halestrap, A.P., Halliwell, B., Jakob, U., Johnston, I.G., Jones, N.S., Logan, D.C., Morgan, B., Müller, F.L., Nicholls, D.G., Remington, S.J., Schumacker, P.T., Winterbourn, C.C., Sweetlove, L.J., Meyer, A.J., Dick, T.P., Murphy, M.P., 2014. The “mitoflash” probe cpYFP does not respond to superoxide. *Nature* 514, E12–14. <https://doi.org/10.1038/nature13858>
- Sedlackova, L., Korolchuk, V.I., 2020. The crosstalk of NAD, ROS and autophagy in cellular health and ageing. *Biogerontology* 21, 381–397. <https://doi.org/10.1007/s10522-020-09864-0>
- Serrano, R., 1983. In vivo glucose activation of the yeast plasma membrane ATPase. *FEBS Lett* 156, 11–14. [https://doi.org/10.1016/0014-5793\(83\)80237-3](https://doi.org/10.1016/0014-5793(83)80237-3)
- Shen, J., Zeng, Y., Zhuang, X., Sun, L., Yao, X., Pimpl, P., Jiang, L., 2013. Organelle pH in the *Arabidopsis* endomembrane system. *Mol Plant* 6, 1419–1437. <https://doi.org/10.1093/mp/sst079>
- Shenton, D., Grant, C.M., 2003. Protein S-thiolation targets glycolysis and protein synthesis in response to oxidative stress in the yeast *Saccharomyces cerevisiae*. *Biochem J* 374, 513–519. <https://doi.org/10.1042/BJ20030414>
- Shi, F., Kawai, S., Mori, S., Kono, E., Murata, K., 2005. Identification of ATP-NADH kinase isozymes and their contribution to supply of NADP(H) in *Saccharomyces cerevisiae*. *FEBS J* 272, 3337–3349. <https://doi.org/10.1111/j.1742-4658.2005.04749.x>
- Shokhina, A.G., Kostyuk, A.I., Ermakova, Y.G., Panova, A.S., Staroverov, D.B., Egorov, E.S., Baranov, M.S., van Belle, G.J., Katschinski, D.M., Belousov, V.V., Bilan, D.S., 2019. Red fluorescent redox-sensitive biosensor Grx1-roCherry. *Redox Biol* 21, 101071. <https://doi.org/10.1016/j.redox.2018.101071>
- Sickmier, E.A., Brekasis, D., Paranawithana, S., Bonanno, J.B., Paget, M.S.B., Burley, S.K., Kielkopf, C.L., 2005. X-Ray structure of a Rex-family repressor/NADH complex: Insights into the mechanism of redox sensing. *Structure* 13, 43–54. <https://doi.org/10.1016/j.str.2004.10.012>

References

- Siedler, S., Schendzielorz, G., Binder, S., Eggeling, L., Bringer, S., Bott, M., 2014. SoxR as a single-cell biosensor for NADPH-consuming enzymes in *Escherichia coli*. *ACS Synth Biol* 3, 41–47. <https://doi.org/10.1021/sb400110j>
- Sinha, A., Maitra, P.K., 1992. Induction of specific enzymes of the oxidative pentose phosphate pathway by glucono-delta-lactone in *Saccharomyces cerevisiae*. *J Gen Microbiol* 138, 1865–1873. <https://doi.org/10.1099/00221287-138-9-1865>
- Spaans, S.K., Weusthuis, R.A., van der Oost, J., Kengen, S.W.M., 2015. NADPH-generating systems in bacteria and archaea. *Front Microbiol* 6, 742. <https://doi.org/10.3389/fmicb.2015.00742>
- Sporty, J., Lin, S.-J., Kato, M., Ognibene, T., Stewart, B., Turteltaub, K., Bench, G., 2009. Quantitation of NAD⁺ biosynthesis from the salvage pathway in *Saccharomyces cerevisiae*. *Yeast* 26, 363–369. <https://doi.org/10.1002/yea.1671>
- Steinbeck, J., Fuchs, P., Negroni, Y.L., Elsässer, M., Lichtenauer, S., Stockdreher, Y., Feitosa-Araujo, E., Kroll, J.B., Niemeier, J.-O., Humbert, C., Smith, E.N., Mai, M., Nunes-Nesi, A., Meyer, A.J., Zottini, M., Morgan, B., Wagner, S., Schwarzländer, M., 2020. In vivo NADH/NAD⁺ biosensing reveals the dynamics of cytosolic redox metabolism in plants. *Plant Cell* 32, 3324–3345. <https://doi.org/10.1105/tpc.20.00241>
- Strand, M.K., Stuart, G.R., Longley, M.J., Graziewicz, M.A., Dominick, O.C., Copeland, W.C., 2003. *POS5* gene of *Saccharomyces cerevisiae* encodes a mitochondrial NADH kinase required for stability of mitochondrial DNA. *Eukaryot Cell* 2, 809–820. <https://doi.org/10.1128/EC.2.4.809-820.2003>
- Suga, H., Matsuda, F., Hasunuma, T., Ishii, J., Kondo, A., 2013. Implementation of a transhydrogenase-like shunt to counter redox imbalance during xylose fermentation in *Saccharomyces cerevisiae*. *Appl Microbiol Biotechnol* 97, 1669–1678. <https://doi.org/10.1007/s00253-012-4298-3>
- Tao, R., Zhao, Y., Chu, H., Wang, A., Zhu, J., Chen, X., Zou, Y., Shi, M., Liu, R., Su, N., Du, J., Zhou, H.-M., Zhu, L., Qian, X., Liu, H., Loscalzo, J., Yang, Y., 2017. Genetically encoded fluorescent sensors reveal dynamic regulation of NADPH metabolism. *Nat Methods* 14, 720–728. <https://doi.org/10.1038/nmeth.4306>
- Tejwani, V., Schmitt, F.-J., Wilkening, S., Zebger, I., Horch, M., Lenz, O., Friedrich, T., 2017. Investigation of the NADH/NAD⁺ ratio in *Ralstonia eutropha* using the fluorescence reporter protein Peredox. *Biochim Biophys Acta Bioenerg* 1858, 86–94. <https://doi.org/10.1016/j.bbabi.2016.11.001>
- Thompson, L.M., Sutherland, P., Steffan, J.S., McAlister-Henn, L., 1988. Gene sequence and primary structure of mitochondrial malate dehydrogenase from *Saccharomyces cerevisiae*. *Biochemistry* 27, 8393–8400. <https://doi.org/10.1021/bi00422a015>
- Titov, D.V., Cracan, V., Goodman, R.P., Peng, J., Grabarek, Z., Mootha, V.K., 2016. Complementation of mitochondrial electron transport chain by manipulation of the NAD⁺/NADH ratio. *Science* 352, 231–235. <https://doi.org/10.1126/science.aad4017>
- Todisco, S., Agrimi, G., Castegna, A., Palmieri, F., 2006. Identification of the mitochondrial NAD⁺ transporter in *Saccharomyces cerevisiae*. *J Biol Chem* 281, 1524–1531. <https://doi.org/10.1074/jbc.M510425200>
- Toledano, M.B., Delaunay, A., Biteau, B., Spector, D., Azevedo, D., 2003. Oxidative stress responses in yeast, in: Hohmann, S., Mager, W.H. (Eds.), *Yeast Stress Responses*, Current Genetics. Springer, Berlin, Heidelberg.
- Troussicot, L., Burmann, B.M., Molin, M., 2021. Structural determinants of multimerization and dissociation in 2-Cys peroxiredoxin chaperone function. *Structure* 29, 640–654. <https://doi.org/10.1016/j.str.2021.04.007>
- Tu, B.P., Kudlicki, A., Rowicka, M., McKnight, S.L., 2005. Logic of the yeast metabolic cycle: Temporal compartmentalization of cellular processes. *Science* 310, 1152–1158. <https://doi.org/10.1126/science.1120499>

- Tu, B.P., McKnight, S.L., 2006. Metabolic cycles as an underlying basis of biological oscillations. *Nat Rev Mol Cell Biol* 7, 696–701. <https://doi.org/10.1038/nrm1980>
- Tu, B.P., Mohler, R.E., Liu, J.C., Dombek, K.M., Young, E.T., Synovec, R.E., McKnight, S.L., 2007. Cyclic changes in metabolic state during the life of a yeast cell. *Proc Natl Acad Sci U S A* 104, 16886–16891. <https://doi.org/10.1073/pnas.0708365104>
- Valtey, M., 2021. Investigating the molecular mechanisms of NADH/NADPH interconversion in yeast (Bachelor thesis). Saarland University, Saarbrücken.
- Vaseghi, S., Baumeister, A., Rizzi, M., Reuss, M., 1999. In vivo dynamics of the pentose phosphate pathway in *Saccharomyces cerevisiae*. *Metab Eng* 1, 128–140. <https://doi.org/10.1006/mben.1998.0110>
- Venters, B.J., Wachi, S., Mavrich, T.N., Andersen, B.E., Jena, P., Sinnamon, A.J., Jain, P., Roller, N.S., Jiang, C., Hemeryck-Walsh, C., Pugh, B.F., 2011. A comprehensive genomic binding map of gene and chromatin regulatory proteins in *Saccharomyces*. *Mol Cell* 41, 480–492. <https://doi.org/10.1016/j.molcel.2011.01.015>
- Villas-Bôas, S.G., Mas, S., Akesson, M., Smedsgaard, J., Nielsen, J., 2005. Mass spectrometry in metabolome analysis. *Mass Spectrom Rev* 24, 613–646. <https://doi.org/10.1002/mas.20032>
- von Jagow, G., Klingenberg, M., 1970. Pathways of hydrogen in mitochondria of *Saccharomyces carlsbergensis*. *Eur J Biochem* 12, 583–592. <https://doi.org/10.1111/j.1432-1033.1970.tb00890.x>
- Wagner, S., Steinbeck, J., Fuchs, P., Lichtenauer, S., Elsässer, M., Schippers, J.H.M., Nietzel, T., Ruberti, C., Van Aken, O., Meyer, A.J., Van Dongen, J.T., Schmidt, R.R., Schwarzländer, M., 2019. Multiparametric real-time sensing of cytosolic physiology links hypoxia responses to mitochondrial electron transport. *New Phytol* 224, 1668–1684. <https://doi.org/10.1111/nph.16093>
- Walters, R.W., Matheny, T., Mizoue, L.S., Rao, B.S., Muhlrad, D., Parker, R., 2017. Identification of NAD⁺ capped mRNAs in *Saccharomyces cerevisiae*. *Proc Natl Acad Sci U S A* 114, 480–485. <https://doi.org/10.1073/pnas.1619369114>
- Wang, E., Bauer, M.C., Rogstam, A., Linse, S., Logan, D.T., von Wachenfeldt, C., 2008. Structure and functional properties of the *Bacillus subtilis* transcriptional repressor Rex. *Mol Microbiol* 69, 466–478. <https://doi.org/10.1111/j.1365-2958.2008.06295.x>
- Wang, E., Ikonen, T.P., Knaapila, M., Svergun, D., Logan, D.T., von Wachenfeldt, C., 2011. Small-angle X-ray scattering study of a Rex family repressor: Conformational response to NADH and NAD⁺ binding in solution. *J Mol Biol* 408, 670–683. <https://doi.org/10.1016/j.jmb.2011.02.050>
- Wenz, C., Faust, D., Linz, B., Turmann, C., Nikolova, T., Bertin, J., Gough, P., Wipf, P., Schröder, A.S., Krautwald, S., Dietrich, C., 2018. *t*-BuOOH induces ferroptosis in human and murine cell lines. *Arch Toxicol* 92, 759–775. <https://doi.org/10.1007/s00204-017-2066-y>
- Westermann, B., Klecker, T., 2022. Vom Bierbrauen zur Forschung im 21. Jahrhundert. *Biospektrum* 28, 11–13. <https://doi.org/10.1007/s12268-022-1687-8>
- Westermann, B., Neupert, W., 2000. Mitochondria-targeted green fluorescent proteins: Convenient tools for the study of organelle biogenesis in *Saccharomyces cerevisiae*. *Yeast* 16, 1421–1427. [https://doi.org/10.1002/1097-0061\(200011\)16:15<1421::AID-YEA624>3.0.CO;2-U](https://doi.org/10.1002/1097-0061(200011)16:15<1421::AID-YEA624>3.0.CO;2-U)
- Williamson, D.H., Lund, P., Krebs, H.A., 1967. The redox state of free nicotinamide-adenine dinucleotide in the cytoplasm and mitochondria of rat liver. *Biochem J* 103, 514–527. <https://doi.org/10.1042/bj1030514>
- Winterbourn, C.C., 2013. The biological chemistry of hydrogen peroxide. *Methods Enzymol* 528, 3–25. <https://doi.org/10.1016/B978-0-12-405881-1.00001-X>
- Winterbourn, C.C., 2008. Reconciling the chemistry and biology of reactive oxygen species. *Nat Chem Biol* 4, 278–286. <https://doi.org/10.1038/nchembio.85>

References

- Xiao, W., Wang, R.-S., Handy, D.E., Loscalzo, J., 2018. NAD(H) and NADP(H) redox couples and cellular energy metabolism. *Antioxid Redox Signal* 28, 251–272. <https://doi.org/10.1089/ars.2017.7216>
- Yoshikawa, Y., Nasuno, R., Takagi, H., 2021. An NADPH-independent mechanism enhances oxidative and nitrosative stress tolerance in yeast cells lacking glucose-6-phosphate dehydrogenase activity. *Yeast* 38, 414–423. <https://doi.org/10.1002/yea.3558>
- Yu, Q., Heikal, A.A., 2009. Two-photon autofluorescence dynamics imaging reveals sensitivity of intracellular NADH concentration and conformation to cell physiology at the single-cell level. *J Photochem Photobiol B* 95, 46–57. <https://doi.org/10.1016/j.jphotobiol.2008.12.010>
- Zhang, J., Sonnenschein, N., Pihl, T.P.B., Pedersen, K.R., Jensen, M.K., Keasling, J.D., 2016. Engineering an NADPH/NADP⁺ redox biosensor in yeast. *ACS Synth Biol* 5, 1546–1556. <https://doi.org/10.1021/acssynbio.6b00135>
- Zhang, J., ten Pierick, A., van Rossum, H.M., Seifar, R.M., Ras, C., Daran, J.-M., Heijnen, J.J., Wahl, S.A., 2015. Determination of the cytosolic NADPH/NADP ratio in *Saccharomyces cerevisiae* using shikimate dehydrogenase as sensor reaction. *Sci Rep* 5, 12846. <https://doi.org/10.1038/srep12846>
- Zhang, Y., Wang, M., Lin, H., 2020. A regulatory cysteine residue mediates reversible inactivation of NAD⁺-dependent aldehyde dehydrogenases to promote oxidative stress response. *ACS Chem Biol* 15, 28–32. <https://doi.org/10.1021/acscchembio.9b00662>
- Zhang, Z., Chen, W., Zhao, Y., Yang, Y., 2018. Spatiotemporal imaging of cellular energy metabolism with genetically-encoded fluorescent sensors in brain. *Neurosci Bull* 34, 875–886. <https://doi.org/10.1007/s12264-018-0229-3>
- Zhang, Z., Cheng, X., Zhao, Y., Yang, Y., 2020. Lighting up live-cell and in vivo central carbon metabolism with genetically encoded fluorescent sensors. *Annual Rev Anal Chem* 13, 293–314. <https://doi.org/10.1146/annurev-anchem-091619-091306>
- Zhao, F.-L., Zhang, Chang, Zhang, Chen, Tang, Y., Ye, B.-C., 2016. A genetically encoded biosensor for in vitro and in vivo detection of NADP⁺. *Biosens and Bioelectron* 77, 901–906. <https://doi.org/10.1016/j.bios.2015.10.063>
- Zhao, Y., Hu, Q., Cheng, F., Su, N., Wang, A., Zou, Y., Hu, H., Chen, X., Zhou, H.-M., Huang, X., Yang, K., Zhu, Q., Wang, X., Yi, J., Zhu, L., Qian, X., Chen, L., Tang, Y., Loscalzo, J., Yang, Y., 2015. SoNar, a highly responsive NAD⁺/NADH sensor, allows high-throughput metabolic screening of anti-tumor agents. *Cell Metab* 21, 777–789. <https://doi.org/10.1016/j.cmet.2015.04.009>
- Zhao, Y., Wang, A., Zou, Y., Su, N., Loscalzo, J., Yang, Y., 2016. In vivo monitoring of cellular energy metabolism using SoNar, a highly responsive sensor for NAD⁺/NADH redox state. *Nat Protoc* 11, 1345–1359. <https://doi.org/10.1038/nprot.2016.074>
- Zhao, Y., Zhang, Z., Zou, Y., Yang, Y., 2018. Visualization of nicotine adenine dinucleotide redox homeostasis with genetically encoded fluorescent sensors. *Antioxid Redox Signal* 28, 213–229. <https://doi.org/10.1089/ars.2017.7226>
- Zimmermann, J., 2021. 'Lab in a cell': Developing yeast-based systems for rapid in vivo characterization of redox enzymes (Dissertation). Saarland University, Saarbrücken.
- Zimmermann, J., Laporte, H., Amponsah, P.S., Michalk, C., Sukmann, T., Oestreicher, J., Tursch, A., Owusu, T.N.E., Prates-Roma, L., Riemer, J., Morgan, B., in preparation. Tsa1 is the dominant peroxide scavenger and a major source of H₂O₂-dependent GSSG production in yeast.
- Zimmermann, J., Morgan, B., 2022. Thiol-based redox probes, in: Alvarez, B., Comini, M.A., Salinas, G., Trujillo, M. (Eds.), *Redox Chemistry and Biology of Thiols*. Elsevier, pp. 373–403. <https://doi.org/10.1016/B978-0-323-90219-9.00024-8>
- Zimmermann, J., Oestreicher, J., Geissel, F., Deponte, M., Morgan, B., 2021. An intracellular assay for activity screening and characterization of glutathione-dependent oxidoreductases. *Free Radic Biol Med* 172, 340–349. <https://doi.org/10.1016/j.freeradbiomed.2021.06.016>

-
- Zimmermann, J., Oestreicher, J., Hess, S., Herrmann, J.M., Deponte, M., Morgan, B., 2020. One cysteine is enough: A monothiol Grx can functionally replace all cytosolic Trx and dithiol Grx. *Redox Biol* 36, 101598. <https://doi.org/10.1016/j.redox.2020.101598>
- Zito, E., 2015. ERO1: A protein disulfide oxidase and H₂O₂ producer. *Free Radic Biol Med* 83, 299–304. <https://doi.org/10.1016/j.freeradbiomed.2015.01.011>
- Zou, Y., Wang, A., Huang, L., Zhu, X., Hu, Q., Zhang, Y., Chen, X., Li, F., Wang, Q., Wang, H., Liu, R., Zuo, F., Li, T., Yao, J., Qian, Y., Shi, M., Yue, X., Chen, W., Zhang, Z., Wang, C., Zhou, Y., Zhu, L., Ju, Z., Loscalzo, J., Yang, Y., Zhao, Y., 2020. Illuminating NAD⁺ metabolism in live cells and in vivo using a genetically encoded fluorescent sensor. *Dev Cell* 53, 240–252.e7. <https://doi.org/10.1016/j.devcel.2020.02.017>
- Zou, Y., Wang, A., Shi, M., Chen, X., Liu, R., Li, T., Zhang, C., Zhang, Z., Zhu, L., Ju, Z., Loscalzo, J., Yang, Y., Zhao, Y., 2018. Analysis of redox landscapes and dynamics in living cells and in vivo using genetically encoded fluorescent sensors. *Nat Protoc* 13, 2362–2386. <https://doi.org/10.1038/s41596-018-0042-5>

Appendix

List of supplementary figures

Figure S1: pH calibration of SypHer and pHluorin.	154
Figure S2: NADH titration to permeabilized WT cells expressing (mSI-) iNap.....	155
Figure S3: H ₂ O ₂ treatment of WT cells expressing mSI-iNap or mSI-SoNar.	156
Figure S4: Raw cpTS/mC values of WT cells expressing Pdx-mC (DS), NAPstar1-4, or NAPstarC during diamide treatment.....	157
Figure S5: Diamide treatment of WT cells expressing mSI-iNap or mSI-SoNar.	158
Figure S6: TBHP treatment of WT cells expressing mSI-iNap or mSI-SoNar.....	159
Figure S7: NADH titration to permeabilized WT cells expressing novel NAPstar variants...	160
Figure S8: Regular YMC of p413 TEF empty-transformed CEN.PK113-1A $\Delta his3$ culture...	161
Figure S9: Fluorescence ratio of cytosolic NAPstar2 and NAPstar7 during YMC.....	162
Figure S10: Fluorescence of mSI-iNap3 during YMC.	162
Figure S11: NADH and NADPH titration to permeabilized $\Delta utr1$ and $\Delta ald6$ cells expressing Pdx-mC DS.....	163
Figure S12: Oxidation of cytosolic NAD and NADP after H ₂ O ₂ treatment of strains expressing either WT Tdh3 or H ₂ O ₂ -resistant variants.	164

List of supplementary tables

Table S1: In vitro properties of different NAD(P)-specific GFIs.	165
Table S2: In vitro NADH binding affinities of Pdx-mC and NAPstar sensors.	167

Supplementary figures

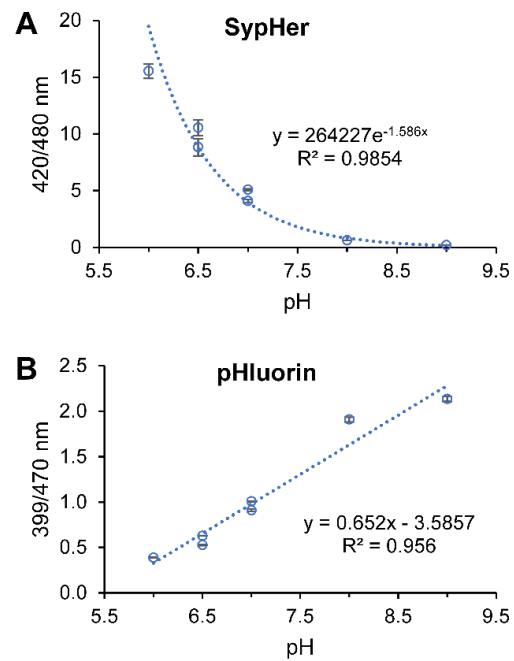


Figure S1: pH calibration of SypHer and pHluorin.

Sensor expressing WT cells were permeabilized in 0.1 M buffer solution (MES/TRIS pH 6.0, 6.5; MOPS/TRIS, pH 6.5, 7.0; TRIS/HCl, pH 7.0, 8.0, 9.0) with 0.1 % (w/v) digitonin. Fluorescence intensities of SypHer (**A**) and pHluorin (**B**) were measured with standard plate reader settings and the fluorescence ratio was plotted against the pH value. The obtained fit was used to calculate the cytosolic pH under different experimental conditions.

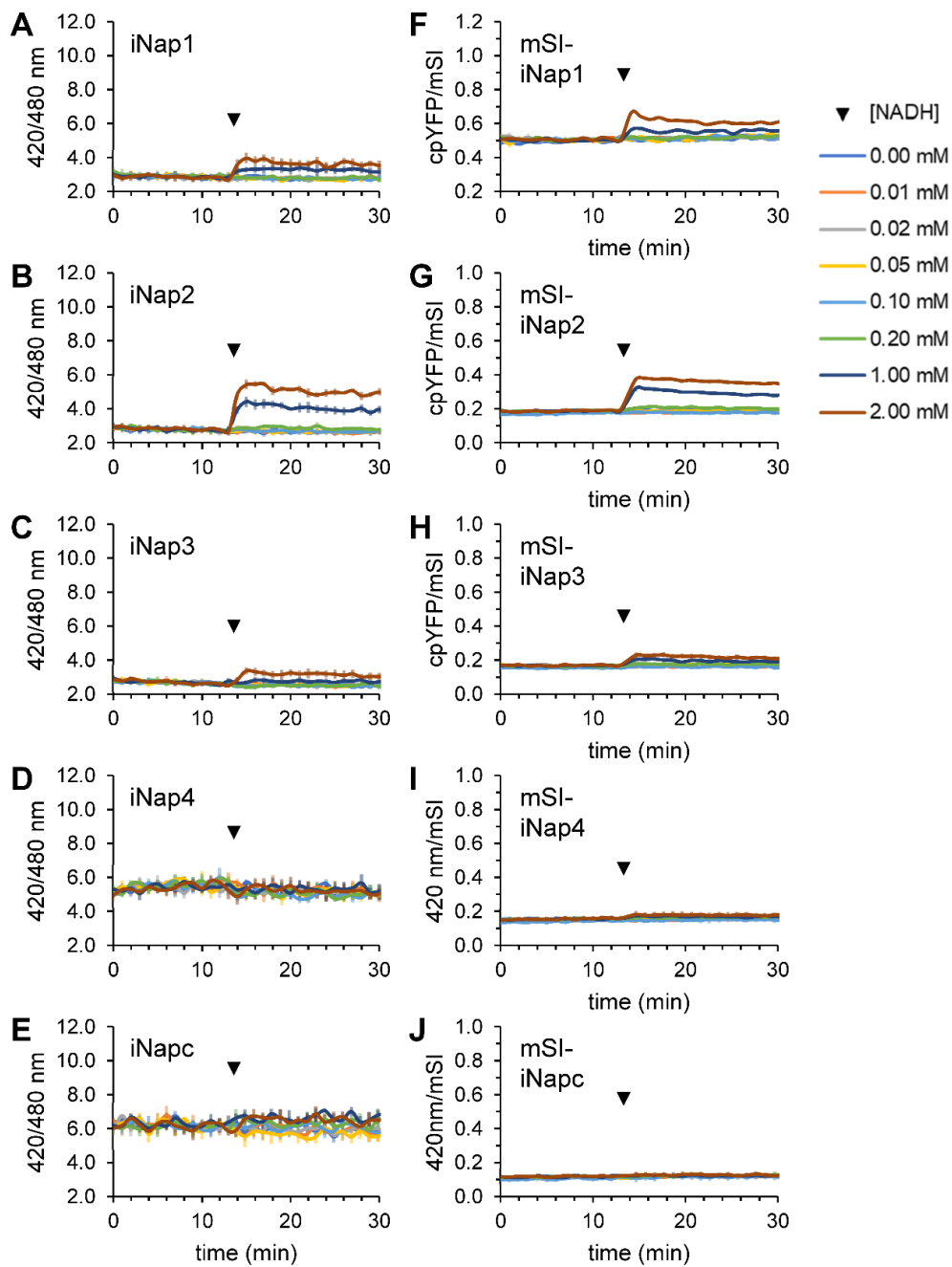


Figure S2: NADH titration to permeabilized WT cells expressing (mSI-) iNap.

iNap1-4 (A-D), iNapc (E), or respective mSI fusion constructs (F-J) were expressed in WT cells. 0.1 % (w/v) digitonin was added before plate reader measurement. At the indicated time point (▼), cells were treated with different concentrations of NADH.

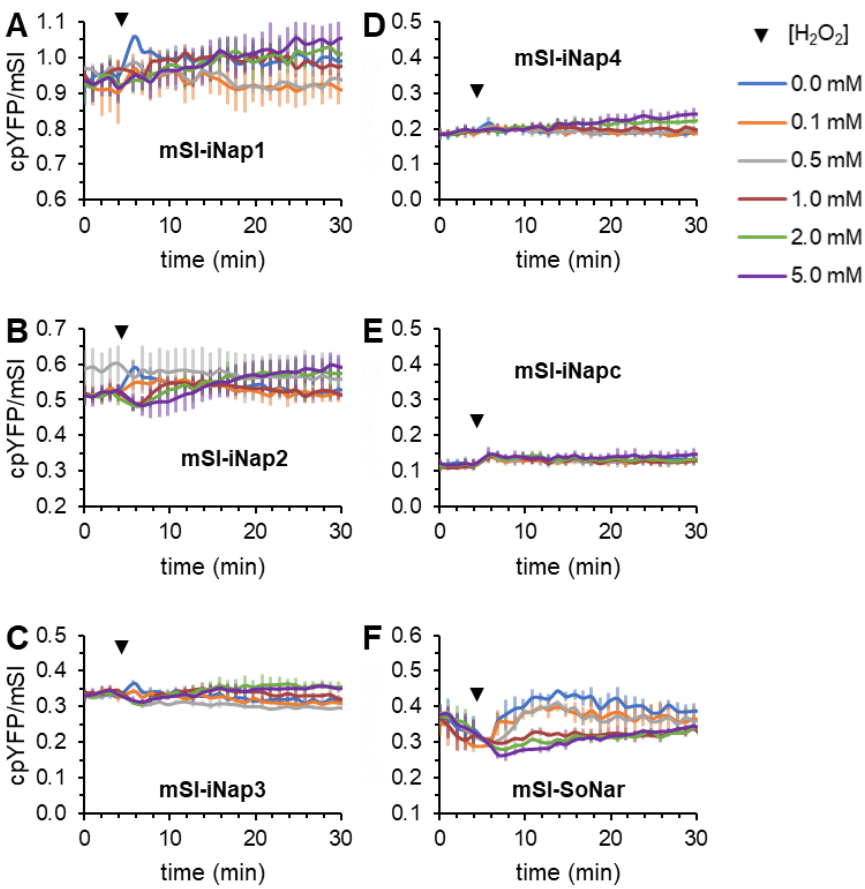


Figure S3: H₂O₂ treatment of WT cells expressing mSI-iNap or mSI-SoNar. WT cells expressing mSI-iNap1-4 (A-D), mSI-iNapc (E) or mSI-SoNar (F) were treated at the indicated time point (▼) with different amounts of H₂O₂ during plate reader measurement.

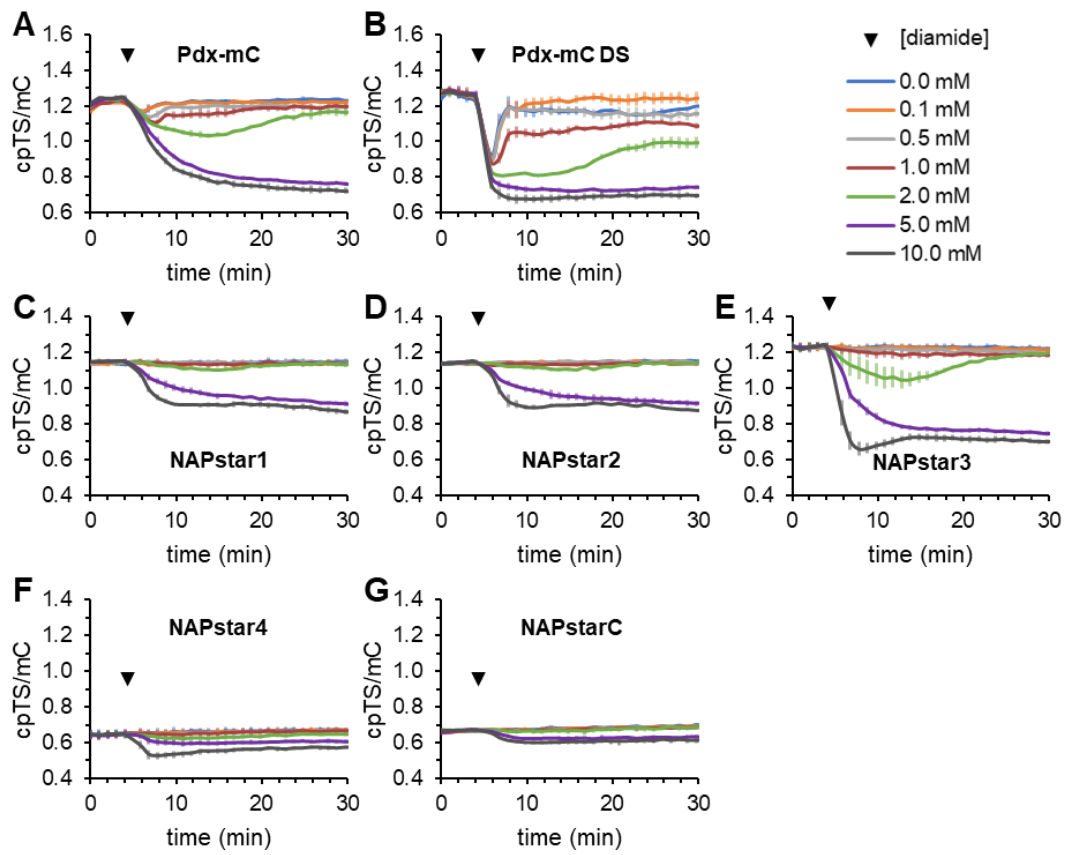


Figure S4: Raw cpTS/mC values of WT cells expressing Pdx-mC (DS), NAPstar1-4, or NAPstarC during diamide treatment.

WT cells expressing either Pdx-mC (A), Pdx-mC DS (B), NAPstar probes (C-G) or pHluorin (H) were treated at the indicated time point (▼) with different concentrations of diamide during plate reader measurement.

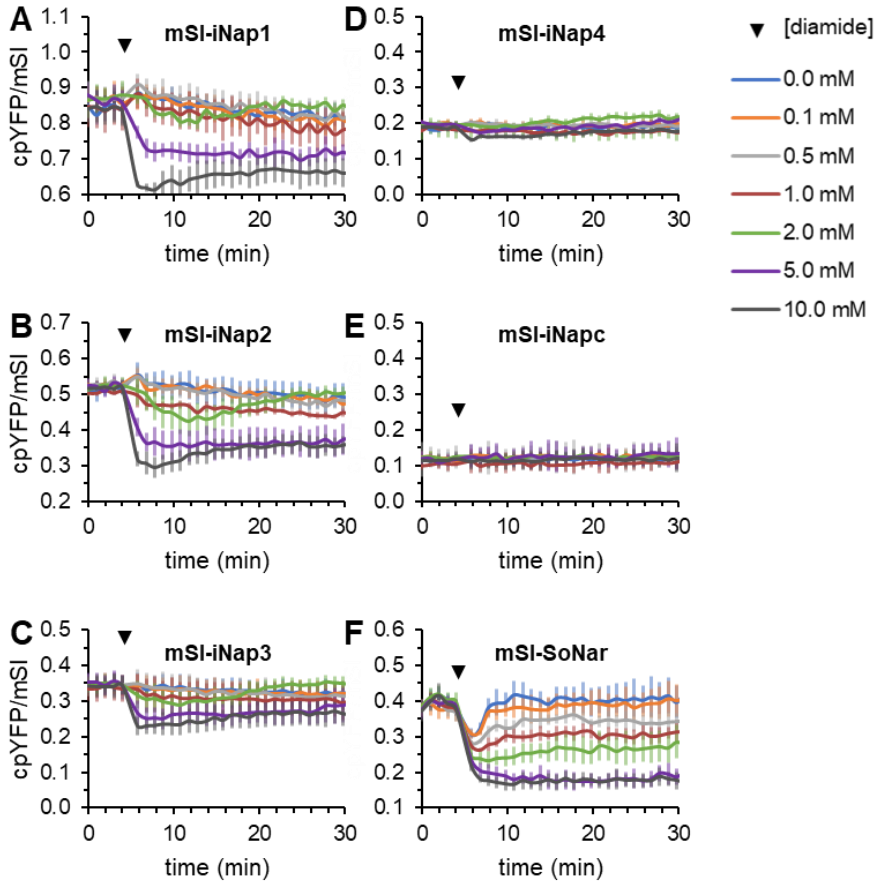


Figure S5: Diamide treatment of WT cells expressing mSI-iNap or mSI-SoNar.
WT cells expressing mSI-iNap sensors (A-E) or mSI-SoNar (F) were treated at indicated time point (▼) with different concentrations of diamide during plate reader measurement.

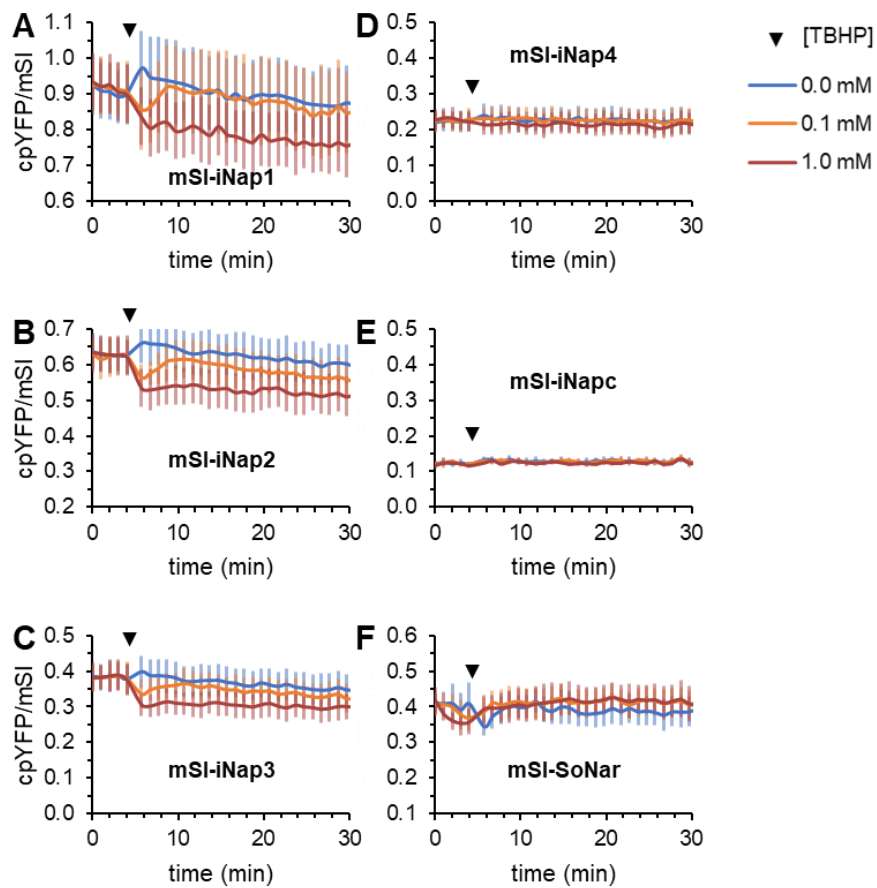


Figure S6: TBHP treatment of WT cells expressing mSI-iNap or mSI-SoNar.

WT cells expressing mSI-iNap sensors (A-E) or mSI-SoNar (F) were treated at indicated time point (▼) with different concentrations of TBHP during plate reader measurement.

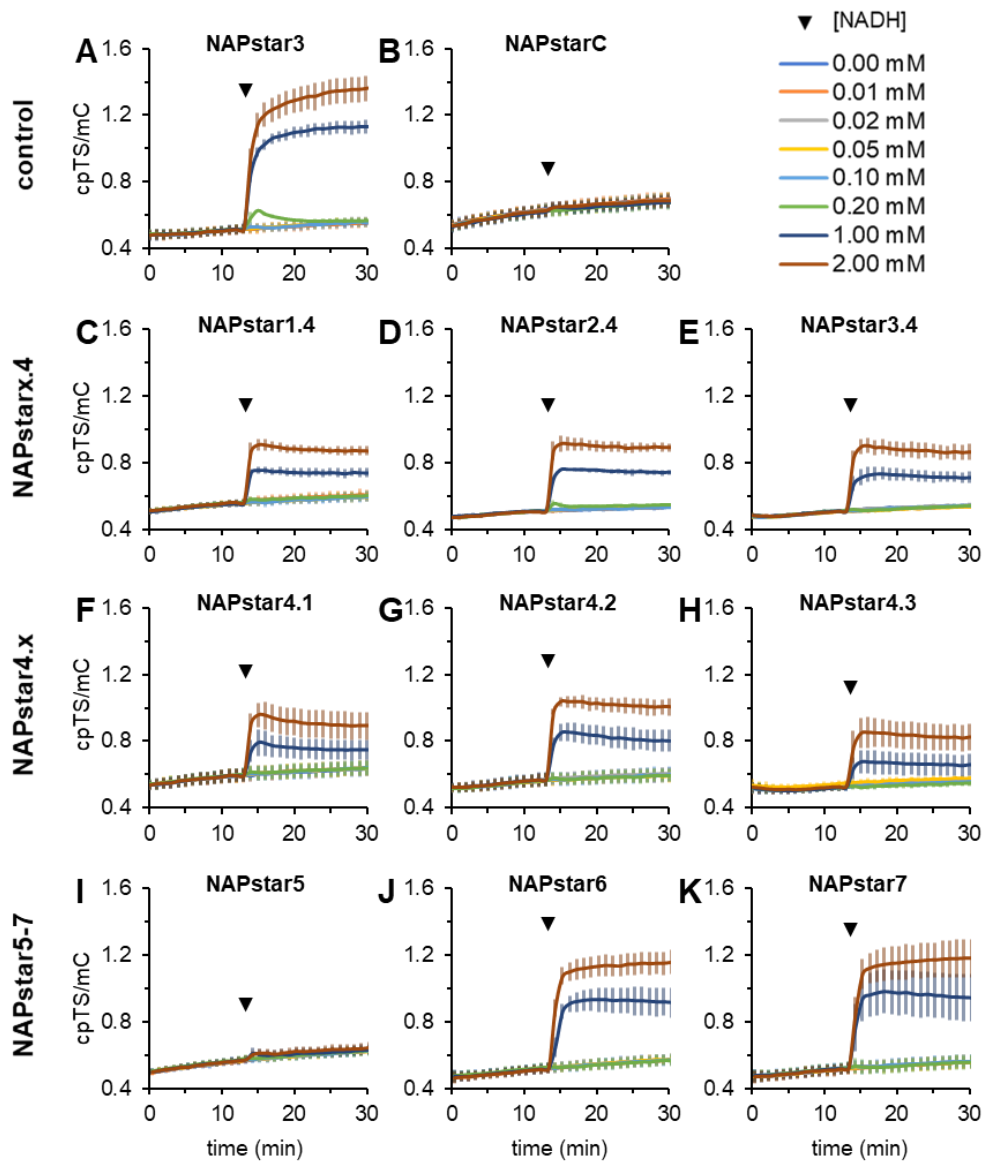


Figure S7: NADH titration to permeabilized WT cells expressing novel NAPstar variants.

WT cells expressing NAPstar3 (A), NAPstarC (B), a 'mixed' NAPstar variant (C-H), NAPstar5, -6, or NAPstar7 (I-K) were permeabilized with 0.1% (w/v) digitonin prior to plate reader measurement. At the indicated time point (▼), cells were treated with different concentrations of NADH. Gain values were set to 1700.

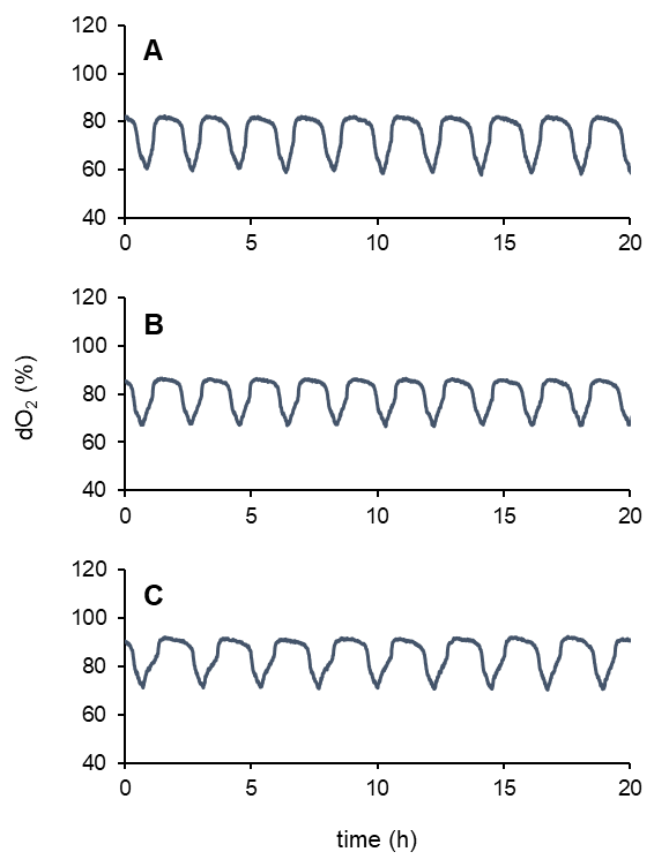


Figure S8: Regular YMC of p413 TEF empty-transformed CEN.PK113-1A $\Delta his3$ culture. CEN.PK113-1A $\Delta his3$ strain transformed with p413 TEF empty control was used to establish YMC. Average period was 2.04 h \pm 0.12 h (\pm standard error).

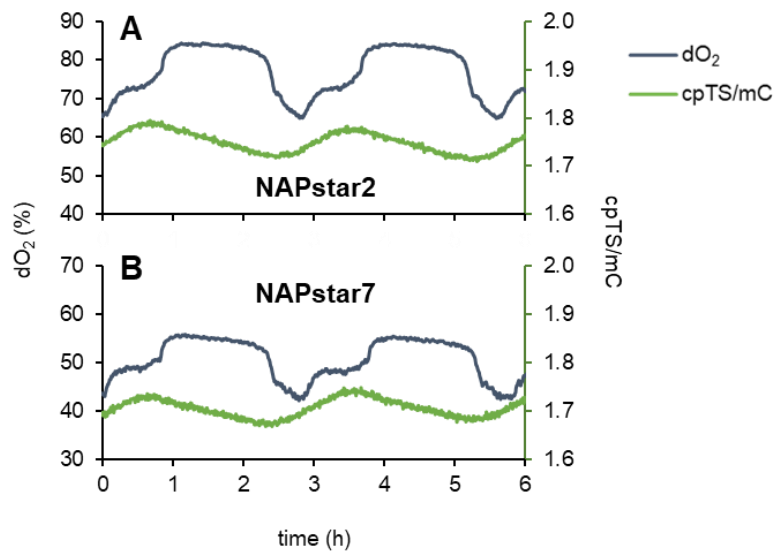


Figure S9: Fluorescence ratio of cytosolic NAPstar2 and NAPstar7 during YMC. NAPstar2 or NAPstar7 were expressed in CEN.PK113-1A $\Delta his3$ during YMC (A,B).

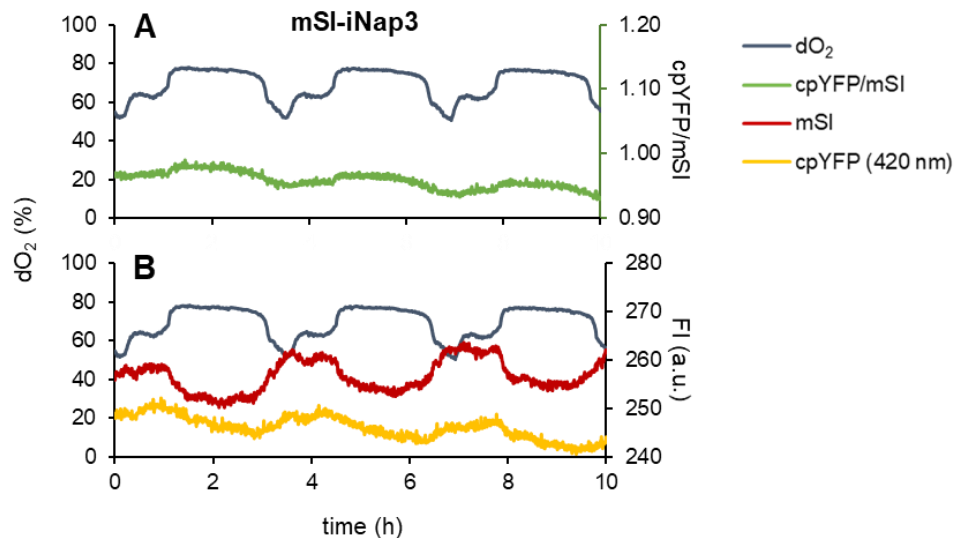


Figure S10: Fluorescence of mSI-iNap3 during YMC.

Fluorescence ratio of mSI-iNap3 expressing CEN.PK113-1A $\Delta his3$ culture was recorded during YMC (A). Single fluorescence intensities of mSI and cpYFP over time (B). FI, fluorescence intensity in arbitrary units (a.u.).

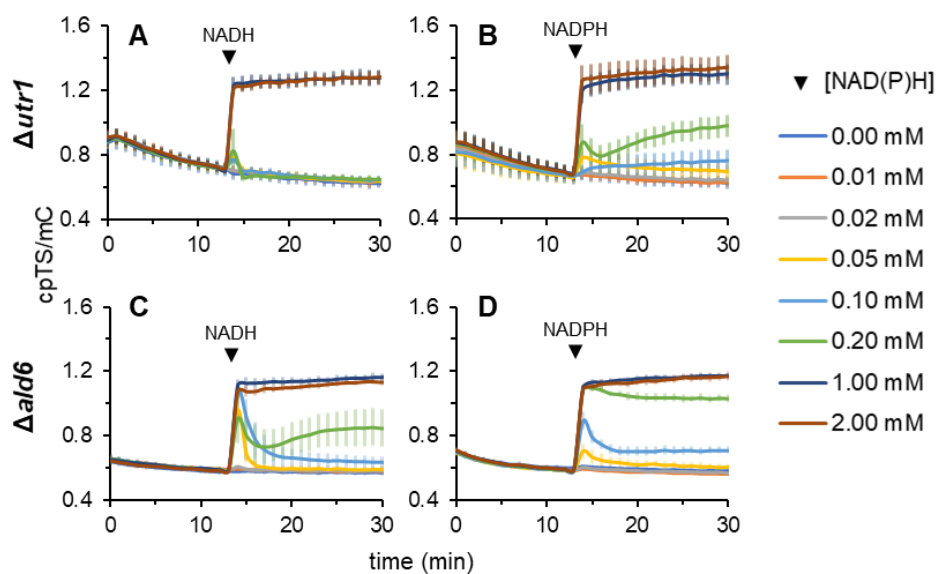


Figure S11: NADH and NADPH titration to permeabilized $\Delta utr1$ and $\Delta ald6$ cells expressing Pdx-mC DS.

Pdx-mC DS expressing, permeabilized $\Delta utr1$ (A,B) and $\Delta ald6$ (C,D) cells (0.1% [w/v] digitonin) were treated at the indicated time point (\blacktriangledown) with different concentrations of NADH (left) or NADPH (right) during plate reader measurement.

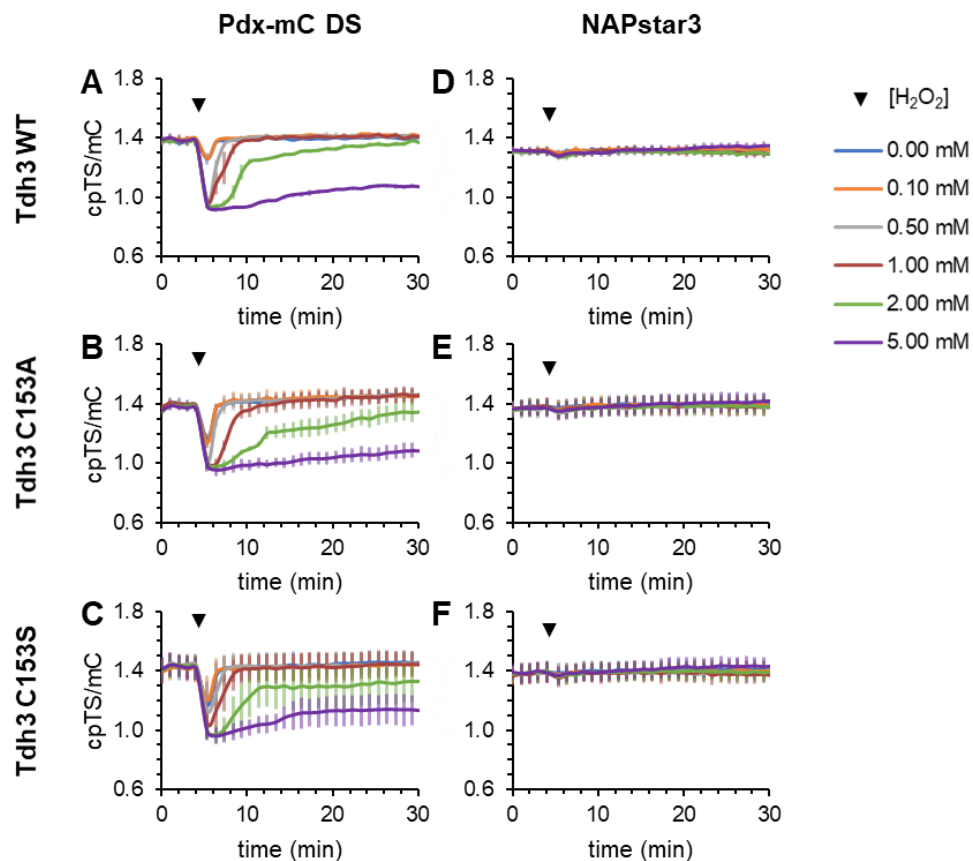


Figure S12: Oxidation of cytosolic NAD and NADP after H_2O_2 treatment of strains expressing either WT Tdh3 or H_2O_2 -resistant variants.

A yeast strain deleted for the three Tdh isoforms, $\Delta tdh1\Delta tdh2\Delta tdh3$ were transformed with a plasmid, encoding for WT Tdh3 (A,D), Tdh3 C153A (B,E) or Tdh3 C153S (C,F) and a second plasmid for sensor expression of Pdx-mC DS (left) or NAPstar3 (right). During plate reader measurement, cells were treated at the indicated time point (▼) with different concentrations of H_2O_2 .

Supplementary tables

Table S1: In vitro properties of different NAD(P)-specific GFIs.

AXP = ATP+ADP+AMP; B-Rex, Rex protein from *B. subtilis*; G6PD, glucose-6-phosphate dehydrogenase; KPR, *E. coli* ketopantoate reductase; LigA, 'bipartite NAD⁺-binding domain' modeled from *Enterococcus faecalis* ligase; N.D., not determined; $R' = [\text{NADH}] \times 1000 / [\text{NAD}^+]$; SPR, human sepiapterin reductase; ^A originally termed NAD⁺ biosensor; ^B detailed information about improved mBFP Y157H variant is not available (Seo et al., 2019); ^C ratiometric readout of Frex probes only possible under high fluorescence intensity conditions.

Sensor [variant]	Sensed species	Affinity	Sensor domain	Reporter domain	Dynamic range δ	Readout type	References
[mC-]Flnad	NAD ⁺ /AXP	$K_d \sim 14 \mu\text{M NAD}^+$ (0 mM AXP), $\sim 1.3 \text{ mM NAD}^+$ (1 mM AXP)	T-Rex	cpYFP [cpYFP, mC]	7-fold [N.D.]	intensiometric	Zou et al., 2020
NAD-Snifit	NAD ⁺	$K_d \sim 63 \mu\text{M NAD}^+$	SPR	variable synthetic labels	8-fold	ratiometric (FRET)	Sallin et al., 2018
NADP-Snifit	NADPH/ NADP ⁺	$K_{\text{NADPH/NADP}^+} \sim 30$	SPR		8.9-fold		Sallin et al., 2018
iNap1-4	NADPH	$K_d \sim 2, \sim 6, \sim 25, \sim 120 \mu\text{M NADPH}$	T-Rex	cpYFP	9-fold (iNap1)	intrinsically ratiometric	Tao et al., 2017; Zou et al., 2018
NADPsor	NADP ⁺	$K_d \sim 2 \text{ mM NADP}^+$	KPR	CFP, YFP	1.3-fold	ratiometric (FRET)	Zhao et al., 2016
LigA-cpVenus ^A	NAD ⁺	$K_d \sim 65 \mu\text{M NAD}^+$	LigA	cpVenus	N.D.	intensiometric	Cambronne et al., 2016
Apollo-NADP ⁺	NADP ⁺	K_d 0.1 to 20 $\mu\text{M NADP}^+$	G6PD	variable	1.2-fold	homoFRET (anisotropy)	Cameron et al., 2016
SoNar	NADH/NAD ⁺	$K_{R'} \sim 36$	T-Rex	cpYFP	15-fold	intrinsically ratiometric	Zhao et al., 2015
RexYFP	NADH/NAD ⁺	$K_d \sim 0.18 \mu\text{M NADH}$, $\sim 6.2 \mu\text{M NADPH}$	T-Rex	cpYFP	N.D.	intensiometric	Bilan et al., 2015
mBFP ^B	NADPH	$K_d \sim 640 \mu\text{M NADPH}$	mBFP	mBFP	7.5-fold (0.5 mM NADPH)	autofluorescence	Hwang et al., 2012; Goldbeck et al., 2018 Seo et al., 2019
Peredox-mC [DS]	NADH/NAD ⁺	$K_{R'} \sim 2$ [63]	T-Rex	cpTS, mC	2.2- [2.9-] fold	intensiometric	Hung et al., 2011; Steinbeck et al., 2020
C3L194K, Frex, FrexH	NADH	$K_d \sim 50, \sim 3.7, \sim 0.04 \mu\text{M NADH}$	B-Rex	cpYFP	4-, 9-, 3-fold	intensiometric ^C	Zhao et al., 2011; Wilkening et al., 2019

Table S2: In vitro NADH binding affinities of Pdx-mC and NAPstar sensors.

The in vitro K_d (NADH) values were determined in the presence of 500 μM NAD⁺.

Sensor	K_d (NADH) in $\sim\mu\text{M}$	Reference
Pdx-mC	1.2	Steinbeck et al., 2020
Pdx-mC DS	31.4	
NAPstar3	98.2	Mai et al., in preparation
NAPstar4.3	∞	
NAPstar6	353	
NAPstar7	225	

Gene sequences

All open reading frames were codon-optimized for expression in *S. cerevisiae*.

Legend: Restriction sites **Start/ Stop codons**

SoNar and iNap sequences

>SoNar

TCTAGAACCATGGGATCCAACAGAAAGTGGGGTTTGTGTATCGTCGGTATGGGTAGATTAGGTTCCGCCTTAGCAGACT
 ATCCTGGTTTTGGTGAAAGTTTTGAATTGAGAGGTTTCTTTGATGTTGATCCAGAAAAAGTTGGTAGACCAGTTAGAGG
 TGGTGTTATTGAACATGTTGATTTGTTGCCACAAAGAGTTCCAGGTAGAATTGAAATTGCTTTGTTAACTGTTCCAAGA
 GAAGCTGCACAAAAAGCTGCAGATTTGTTAGTTGCTGCAGGTATTAAGGTATTTTGAAGTTCTGCACCCAGTTGTTTTAG
 AAGTTCCAAAGGAAGTTGCTGTTGAAAACGTTGATTTCTCAGCAGGTTACAACCTCTGATAACGTTTACATCATGGCTGA
 TAAGCAAAAAGAAATGGTATTAAGCAAACCTTCAAGATCAGACATAATGTTGAAGATGGTTCAGTTCAATTGGCTGATCAT
 TACCAACAAAACACACCAATTGGTGACGGTCCAGTTTTGTTGCCAGATAACCATTACTTGTCTTTTCAATCAGTTTTGT
 CTAAGATCCAAACGAAAAGAGAGATCATATGGTTTTGTTAGAATTCGTTACTGCTGCAGGTATCACATTGGGTATGGA
 TGAATTATACAACGTTGATGGTGGTTCAGGTGGTACTGGTCTAAAGGTGAAGAATTGTTTACAGGTGTTGTTCCAATT
 TTAGTTGAATTGGATGGTGACGTTAATGGTCATAAATTTTCTGTTTTCAGGTGAAGGTGAAGGTGACGCTACTTACGGTA
 AATTGACATTGAAATTGATCTGTACTACTGGTAAATTACCAGTTCATGGCCAACCTTACTTACTACATTGGGTTACGG
 TTTAAAGTGTGTTGCTAGATACCCAGATCATATGAAGCAACATGATTTCTTTAAGTCTGCAATGCCAGAAGGTTACGTT
 CAAGAAAGAACAATTTTCTTTAAAGATGATGGTAACTACAAGACTAGAGCTGAGGTTAAGTTCGAAGGTGACACATTGG
 TTAACAGAATCGAATTAAGGGTATTGGTTTTAAAGAAGATGGTAACATCTTGGGTATAAATTAGAATACAATGGTTT
 GGCAGGTTTGACAAGATTATCCTTTGCTATATTGAATCCTAAGTGGAGAGAAGAAATGATGGGTTAACTCGAG

>iNap1

TCTAGAACCATGGGATCCAACAGAAAGTGGGGTTTGTGTATCGTCGGTATGGGTAGATTAGGTTCCGCCTTAGCAGACT
 ATCCTGGTTTTGGTGAAAGTTTTGAATTGAGAGGTTTCTTTCTAGGTCGGCTCAAAAAGTTGGTAGACCAGTTAGAGG
 TGGTGTTATTGAACATGTTGATTTGTTGCCACAAAGAGTTCCAGGTAGAATTGAAATTGCTTTGTTAACTGTTCCAAGA
 GAAGCTGCACAAAAAGCTGCAGATTTGTTAGTTGCTGCAGGTATTAAGGTATTTTGAAGTTCTGCACCCAGTTGTTTTAG
 AAGTTCCAAAGGAAGTTGCTGTTGAAAACGTTGATTTCTCAGCAGGTTACAACCTCTGATAACGTTTACATCATGGCTGA
 TAAGCAAAAAGAAATGGTATTAAGCAAACCTTCAAGATCAGACATAATGTTGAAGATGGTTCAGTTCAATTGGCTGATCAT
 TACCAACAAAACACACCAATTGGTGACGGTCCAGTTTTGTTGCCAGATAACCATTACTTGTCTTTTCAATCAGTTTTGT
 CTAAGATCCAAACGAAAAGAGAGATCATATGGTTTTGTTAGAATTCGTTACTGCTGCAGGTATCACATTGGGTATGGA
 TGAATTATACAACGTTGATGGTGGTTCAGGTGGTACTGGTCTAAAGGTGAAGAATTGTTTACAGGTGTTGTTCCAATT
 TTAGTTGAATTGGATGGTGACGTTAATGGTCATAAATTTTCTGTTTTCAGGTGAAGGTGAAGGTGACGCTACTTACGGTA
 AATTGACATTGAAATTGATCTGTACTACTGGTAAATTACCAGTTCATGGCCAACCTTACTTACTACATTGGGTTACGG
 TTTAAAGTGTGTTGCTAGATACCCAGATCATATGAAGCAACATGATTTCTTTAAGTCTGCAATGCCAGAAGGTTACGTT
 CAAGAAAGAACAATTTTCTTTAAAGATGATGGTAACTACAAGACTAGAGCTGAGGTTAAGTTCGAAGGTGACACATTGG
 TTAACAGAATCGAATTAAGGGTATTGGTTTTAAAGAAGATGGTAACATCTTGGGTATAAATTAGAATACAATGGTTT
 GGCAGGTTTGACAAGATTATCCTTTGCTATATTGAATCCTAAGTGGAGAGAAGAAATGATGGGTTAACTCGAG

>iNap2

TCTAGAACCATGGGATCCAACAGAAAGTGGGGTTTTGTGTATCGTCGGTATGGGTAGATTAGGTTCCGCCTTAGCAGACT
ATCCTGGTTTTGGTGAAAGTTTTGAATTGAGAGGTTTTCTTTCTAGGTCGGCTGAAAAAGTTGGTAGACCAGTTAGAGG
TGGTGTATTGAACATACAGATTTGTTGCCACAAAGAGTTCCAGGTAGAATTGAAATTGCTTTGTTAACTGTTCCAAGA
GAAGTGCACAAAAAGCTGCAGATTTGTTAGTTGCTGCAGGTATTAAGGATTTTTGAACTTCGCACCAGTTGTTTTAG
AAGTTCCAAAGGAAGTTGCTGTTGAAAACGTTGATTTCTCAGCAGGTTACAACCTCTGATAACGTTTACATCATGGCTGA
TAAGCAAAAAGTGGTATTAAGCAAACCTCAAGATCAGACATAATGTTGAAGATGGTTCAGTTCAATTGGCTGATCAT
TACCAACAAAACACACCAATTGGTGACGGTCCAGTTTTGTTGCCAGATAACCATTACTTGTCTTTTCAATCAGTTTTGT
CTAAAGATCCAAACGAAAAGAGAGATCATATGGTTTTGTTAGAATTCGTTACTGCTGCAGGTATCACATTGGGTATGGA
TGAATTATAACAACGTTGATGGTGGTTCAGGTGGTACTGGTCTAAAGGTGAAGAATTGTTTACAGGTGTTGTTCCAATT
TTAGTTGAATTGGATGGTGACGTTAATGGTCATAAATTTCTGTTTCAGGTGAAGGTGAAGGTGACGCTACTTACGGTA
AATTGACATTGAAATTGATCTGTAATAATTACCAGTTCCATGGCCAACCTTAGTTACTACATTGGGTTACGG
TTTTAAAGTGTGTTGCTAGATACCCAGATCATATGAAGCAACATGATTTCTTTAAGTCTGCAATGCCAGAAGGTTACGTT
CAAGAAAAGAACAATTTCTTTAAAGATGATGTTAACTACAAGACTAGAGCTGAGGTTAAGTTTGAAGGTGACACATTGG
TTAACAGAATCGAATTAAGGGTATTGGTTTTAAAGAAGATGGTAACATCTTGGGTCATAAATTAGAATACAATGGTTT
GGCAGGTTTGACAAGATTATCCTTTGCTATATTGAATCCTAAGTGGAGAGAAGAAATGATGGGTTAACTCGAG

>iNap3

TCTAGAACCATGGGATCCAACAGAAAGTGGGGTTTTGTGTATCGTCGGTATGGGTAGATTAGGTTCCGCCTTAGCAGACT
ATCCTGGTTTTGGTGAAAGTTTTGAATTGAGAGGTTTTCTTTTCGCGTAAGGCAGAAAAAGTTGGTAGACCAGTTAGAGG
TGGTGTATTGAACATTACGATTTGTTGCCACAAAGAGTTCCAGGTAGAATTGAAATTGCTTTGTTAACTGTTCCAAGA
GAAGTGCACAAAAAGCTGCAGATTTGTTAGTTGCTGCAGGTATTAAGGATTTTTGAACTTCGCACCAGTTGTTTTAG
AAGTTCCAAAGGAAGTTGCTGTTGAAAACGTTGATTTCTCAGCAGGTTACAACCTCTGATAACGTTTACATCATGGCTGA
TAAGCAAAAAGTGGTATTAAGCAAACCTCAAGATCAGACATAATGTTGAAGATGGTTCAGTTCAATTGGCTGATCAT
TACCAACAAAACACACCAATTGGTGACGGTCCAGTTTTGTTGCCAGATAACCATTACTTGTCTTTTCAATCAGTTTTGT
CTAAAGATCCAAACGAAAAGAGAGATCATATGGTTTTGTTAGAATTCGTTACTGCTGCAGGTATCACATTGGGTATGGA
TGAATTATAACAACGTTGATGGTGGTTCAGGTGGTACTGGTCTAAAGGTGAAGAATTGTTTACAGGTGTTGTTCCAATT
TTAGTTGAATTGGATGGTGACGTTAATGGTCATAAATTTCTGTTTCAGGTGAAGGTGAAGGTGACGCTACTTACGGTA
AATTGACATTGAAATTGATCTGTAATAATTACCAGTTCCATGGCCAACCTTAGTTACTACATTGGGTTACGG
TTTTAAAGTGTGTTGCTAGATACCCAGATCATATGAAGCAACATGATTTCTTTAAGTCTGCAATGCCAGAAGGTTACGTT
CAAGAAAAGAACAATTTCTTTAAAGATGATGTTAACTACAAGACTAGAGCTGAGGTTAAGTTTGAAGGTGACACATTGG
TTAACAGAATCGAATTAAGGGTATTGGTTTTAAAGAAGATGGTAACATCTTGGGTCATAAATTAGAATACAATGGTTT
GGCAGGTTTGACAAGATTATCCTTTGCTATATTGAATCCTAAGTGGAGAGAAGAAATGATGGGTTAACTCGAG

>iNap4

TCTAGAACCATGGGATCCAACAGAAAGTGGGGTTTTGTGTATCGTCGGTATGGGTGATTTAGGTTCCGCCTTAGCAGACT
ATCCTGGTTTTGGTGAAAGTTTTGAATTGAGAGGTTTTCTTTCTAGGTCGGCTCAAAAAGTTGGTAGACCAGTTAGAGG
TGGTGTATTGAACATGTTGATTTGTTGCCACAAAGAGTTCCAGGTAGAATTGAAATTGCTTTGTTAACTGTTCCAAGA
GAAGTGCACAAAAAGCTGCAGATTTGTTAGTTGCTGCAGGTATTAAGGATTTTTGAACTTCGCACCAGTTGTTTTAG
AAGTTCCAAAGGAAGTTGCTGTTGAAAACGTTGATTTCTCAGCAGGTTACAACCTCTGATAACGTTTACATCATGGCTGA
TAAGCAAAAAGTGGTATTAAGCAAACCTCAAGATCAGACATAATGTTGAAGATGGTTCAGTTCAATTGGCTGATCAT
TACCAACAAAACACACCAATTGGTGACGGTCCAGTTTTGTTGCCAGATAACCATTACTTGTCTTTTCAATCAGTTTTGT
CTAAAGATCCAAACGAAAAGAGAGATCATATGGTTTTGTTAGAATTCGTTACTGCTGCAGGTATCACATTGGGTATGGA
TGAATTATAACAACGTTGATGGTGGTTCAGGTGGTACTGGTCTAAAGGTGAAGAATTGTTTACAGGTGTTGTTCCAATT
TTAGTTGAATTGGATGGTGACGTTAATGGTCATAAATTTCTGTTTCAGGTGAAGGTGAAGGTGACGCTACTTACGGTA
AATTGACATTGAAATTGATCTGTAATAATTACCAGTTCCATGGCCAACCTTAGTTACTACATTGGGTTACGG
TTTTAAAGTGTGTTGCTAGATACCCAGATCATATGAAGCAACATGATTTCTTTAAGTCTGCAATGCCAGAAGGTTACGTT
CAAGAAAAGAACAATTTCTTTAAAGATGATGTTAACTACAAGACTAGAGCTGAGGTTAAGTTTGAAGGTGACACATTGG
TTAACAGAATCGAATTAAGGGTATTGGTTTTAAAGAAGATGGTAACATCTTGGGTCATAAATTAGAATACAATGGTTT
GGCAGGTTTGACAAGATTATCCTTTGCTATATTGAATCCTAAGTGGAGAGAAGAAATGATGGGTTAACTCGAG

>iNapc

TCTAGAACCATGGGATCCAACAGAAAGTGGGGTTTTGTGTATCGTCGGTATGGGTGATTTAGGTTCCGCCTTAGCAGACT
ATCCTGGTTTTGGTGAAAGTTTTGAATTGAGAGGTTTTCTTTTCAGTTTCGCCAGAAAAAGTTGGTAGACCAGTTAGAGG
TGGTGTATTGAACATGTTGATTTGTTGCCACAAAGAGTTCCAGGTAGAATTGAAATTGCTTTGTTAACTGCACCAAGA
GAAGTGCACAAAAAGCTGCAGATTTGTTAGTTGCTGCAGGTATTAAGGATTTTTGAACTTCGCACCAGTTGTTTTAG
AAGTTCCAAAGGAAGTTGCTGTTGAAAACGTTGATTTCTCAGCAGGTTACAACCTCTGATAACGTTTACATCATGGCTGA
TAAGCAAAAAGTGGTATTAAGCAAACCTCAAGATCAGACATAATGTTGAAGATGGTTCAGTTCAATTGGCTGATCAT

TACCAACAAAACACACCAATTGGTGACGGTCCAGTTTTGTTGCCAGATAACCATTACTTGTCTTTTCAATCAGTTTTGTCTAAAGATCCAAACGAAAAGAGAGATCATATGGTTTTGTTAGAATTCGTTACTGCTGCAGGTATCACATTGGGTATGGATGAATTATACAACGTTGATGGTGGTTTCAGGTGGTACTGGTTCTAAAGGTGAAGAATTGTTTACAGGTGTTGTTCCAATTTAGTTGAATTGGATGGTGACGTTAATGGTCATAAATTTCTGTTTCAGGTGAAGGTGAAGGTGACGCTACTTACGGTA AATTGACATTGAAATTGATCTGTACTACTGGTAAATTACCAGTTCATGGCCAACCTTGTACTACATTGGGTACGGTTTAAAGTGTGTTGCTAGATACCCAGATCATATGAAGCAACATGATTTCTTAAAGTCTGCAATGCCAGAAGGTACGTTCAAGAAAGAACAATTTTCTTAAAGATGATGGTAACTACAAGACTAGAGCTGAGGTTAAGTTCGAAGGTGACACATTGGTTAACAGAATCGAATTAAGGGTATTGGTTTTAAAGAAGATGGTAACTCTTGGGTATAAATTAAGAATACAATGGTTTTGGCAGGTTTGACAAGATTATCCTTGGCTATATTGAATCCTAAGTGGAGAGAAGAAATGATGGGT TAACTCGAG

>mSI-iNap1 (all other mSI fusion constructs were constructed in analogy)

TCTAGAACCATGGGATCCGTGAGCAAGGGCGAGGCAGTGATCAAGGAGTTCATGCGTTCAAGGTGCACATGGAGGGCTCCATGAACGGCCACGAGTTCGAGATCGAGGGCGAGGGCGAGGGCCGCCCTACGAGGGCACCCAGACCGCAAGCTGAA GGTGACCAAGGGTGGCCCCCTGCCCTTCTCTGGGACATCCTGTCCCCTCAGTTCATGTACGGCTCCAGGGCCTTCATC AAGCACCCCGCCGACATCCCCGACTACTATAAGCAGTCTTCCCCGAGGGCTTCAAGTGGGAGCGCTGATGAACCTCG AGGACGGCGGCGCGGTGACCGTGACCCAGGACACCTCCCTGGAGGACGGCACCTGATCTACAAGGTGAAGCTCCGCGG CACCAACTTCCCTCCTGACGGCCCCGTAATGCAGAAGAAGACAATGGGTGGGAAGCGTCCACCGAGCGGTTGTACCCC GAGGACGGCGTGTGAAGGGCGACATTAAGATGGCCCTGCGCTGAAGGACGGCGGCGCTACCTGGCGGACTTCAAGA CCACCTACAAGGCCAAGAAGCCCCGTGCAGATGCCCGCGCCTACAACGTGACCGCAAGTTGGACATCACCTCCACAA CGAGGACTACACCGTGGTGAACAGTACGAACGCTCCGAGGGCCGCCACTCCACCGGCGGCATGGACGAGCTGTACAAG ACTAGTGGTGGTTCAGGTGGTGGTGGTTCAGGTGGTGGTGGTTCAGGTGGAGGAGGATCAGGAGGAAACAGAAAGTGGG GTTTTGTGTATCGTCGGTATGGGTAGATTAGGTTCCGCTTAGCAGACTATCCTGGTTTTGGTGAAGTTTTGAATTGAG AGGTTTTCTTTCTAGGTCGGCTCAAAAAGTTGGTAGACCAGTTAGAGGTGGTGTATTGAACATGTTGATTTGTTGCCA CAAAGAGTTCAGGTAGAATTGAAATTGCTTTGTTAACTGTTCCAAGAGAAGCTGCACAAAAAGCTGCAGATTTGTTAG TTGCTGCAGGTATTAAGGTATTTGAACTTCGCACCAGTTGTTTTAGAAGTTCCAAAGGAAGTTGCTGTTGAAAACGT TGATTTCTCAGCAGGTTACAACCTGATAACGTTTACATCATGGCTGATAAGCAAAAAGATGGTATTAAGCAAACCTC AAGATCAGACATAATGTTGAAGATGGTTCAGTTC AATTGGCTGATCATTACCAACAAAACACACCAATTGGTGACGGTC CAGTTTTGTTGCCAGATAACCATTACTTGTCTTTTCAATCAGTTTTGTCTAAAGATCCAAACGAAAAGAGAGATCATAT GGTTTTTGTTAGAATTCGTTACTGCTGCAGGTATCACATTTGGGTATGGATGAATTATACAACGTTGATGGTGGTTCAGGT GGTACTGGTTC AAGGTGAAGAATTGTTTACAGGTGTTGTTCCAATTTTAGTTGAATTGGATGGTGACGTTAATGGTC ATAAATTTCTGTTTCAGGTGAAGGTGAAGGTGACGCTACTTACGGTAAATTGACATTGAAATTGATCTGTACTACTGG TAAATTACCAGTTCATGGCCAACCTTGTACTACATTTGGGTTACGGTTTAAAGTGTGTTGCTAGATACCCAGATCAT ATGAAGCAACATGATTTCTTAAAGTCTGCAATGCCAGAAGGTTACGTTCAAGAAAGAACAATTTCTTAAAGATGATG GTAACTACAAGACTAGAGCTGAGGTTAAGTTCGAAGGTGACACATTTGGTTAACAGAATCGAATTAAGGGTATTGGTTTT TAAAGAAGATGGTAACATCTTGGGTATAAATTAAGAATACAATGGTTTTGGCAGGTTTGACAAGATTATCCTTGGCTATA TTGAATCCTAAGTGGAGAGAAGAAATGATGGGT TAACTCGAG

Pdx-mC and NAPstar sequences

>Pdx-mC

TCTAGAACCATGGGATCCGTGTCCTCAAGGTCCCTGAAGCCGCCATTTCCAGATTGATTACTTATTTGAGAATTTTAG AAGAATTAGAAGCACAAAGGTGCCACAGAACAGCTTCTGAACAATTGGGTGAATTAGCTCAAGTTACTGCATTC AAGT TGATAAGGATTTGTCATACTTTGGTTCCTACGGTACTGATGGTGTGGTTACACAGTTCAGTTTTGAAGAGAGAATTG AGACATATCTTGGGTTTAAACAGAAAAGTGGGGTTTATGTATCGTTGGTATGGGTAGATTAGGTTCTGCTTTGGCAGATT GGCCAGGTTTTGGTGAATCATTGAATTGAGAGGTTCTTTGATGTTGATCCAGGCATGGTTGGTAGACCAGTTAGAGG TGGTGTATTGAACATGTTGATTTGTTGCCACAAAGAGTTCAGGTAGAATTGAAATTGCTTTGTTAACAGTTC AAGA GAAGCTGCACAAAAAGCTGCAGATTTGTTAGTTGCTGCAGGTATTAAGGATTTTTAACTTCGCACCAGTTGTTTTGG AAGTTCCAAAGGAAGTTGCTGTTGAAAACGTTGATATCTTGGCAGGTTTAACTAGATTGCTTTTGTATCTTGAATCC AACATGGTCAGCTGCAGGTGGTCATGGTTTTACTGCTCATAACGTTTACATCATGGCAGATAAGCAAAAAGATGGTATT AAAGCTAACTCAAGATCAGACATAATATTGAAGATGGTGGTGTTC AATTGGCAGATCATTACCAACAAAACACTCCAA TTGGTGACGGTCCAGTTTTGTTACCAGATAACCATTACTTATCTATCCAATCAAATTGCTTAAAGATCCAAACGAAAA GAGAGATCATATGGTTTTGTTAGAATTCGTTACTGCTGCAGGTATCACACACGGTATGGACGAATTGTACAAAGGTGGT ACAGGTGGTCAATGGTTTTCTAAAGGTGAAGAATTGTTTACTGGTGTGTTCCAATTTTAGTTGAATTGGATGGTGACG TTAATGGTCATAAATTTCTGTTTCAGGTGAAGGTGAAGGTGACGCTACTTACGGTAAATTGACATTGAAGTTTATTTG TACTACTGGTAAATTACCAGTTCATGGCCAACATTTGGTACTACATTTTCTTACGGTGTATGGTTTTGCTAGATAC CCAGATCATATGAAGCAACATGATTTCTTAAAGTCAAGCAATGCCAGAAGGTTACGTTCAAGAAAGAAGTATTTCTTTA AAGATGATGGTAACTACAAGACAAGAGCTGAGGTTAAGTTCGAAGGTGACACTTTAGTTAACAGAATCGAATTGAAAGG

TATCGATTTCAAGGAAGATGGTAACATCTTAGGTCTATAAATTGGAATATAATACAAAAGTTCCAGAAGCTGCAATTTCA
 AGATTGATCACTTACTTAAAGATTTTGGGAAGATTAGAAGCTCAAGGTGTTTCATAGAACAGCATCAGAACAATTAGGTG
 AATTAGCTCAAGTCACAGCTTTCCAAGTTGATGAAGATTTGTCATACTTCGGTCTTATGGTACAGACGGTGTGGTTA
 TACTGTCCCTGTCTTAAAAAGAGAATTAAGACACATTTTAGGTTTAAATAGAAAATGGGGTTTATGCATTGTGGTATG
 GGTAGATTGGGTTCTGCTTTGGCAGACTGGCCTGGTTTCGGTGAATCATTTGAATTAAGAGTTTCTTTGACGTTGATC
 CAGGCATGGTCGGTAGACCAGTTAGAGGTGGTGTATTGAGCACGTGATTTGTTACCTCAAAGAGTCCCTGGTAGAAT
 CGAAATCGCCTTATTGACTGTCCCAAGAGAAGCCGCTCAAAGGCCGCTGATTTGTTAGTTGCCGCTGGTATTAAGGT
 ATTTTAAATTTGCTCCTGTGTTTTGGAAGTCCCTAAGGAAGTTCAGTTGAAAACGTTGATTTCTTGGCTGGTTTAA
 CAAGATTGTCTTTTGAATCTTGAACCCAAAGTGGAGAGAAGAAATGATGGGTTCCAGTACTGGTGGTAATGCTTCAGA
 TGGTGGTGGTCTGGTGGTATGGTTTCAAAGGTGAAGAAGATAACATGGCAATTATTAAGGAATTCATGAGATTCAA
 GTTCATATGGAAGGTTCTGTTAACGGTCATGAATTCGAAATCGAAGGTGAAGGTGAAGGTAGACCATATGAAGTACTC
 AAACAGCTAAATTAAGGTTACTAAAGGTGGTCCATTACCATTTGCATGGGATATTTTGTCTCCACAATTCATGTACGG
 TTCAAAGCATATGTTAAGCATCCAGCAGATATCCCAGATTACTTGAAATTATCTTTCCAGAAGGTTTTAAATGGGAA
 AGAGTTATGAACTTCAAGATGGTGGTGTGTTACTGTTACACAAGATTCTTCATTACAAGATGGTGAATTCATATATA
 AAGTTAAATTGAGAGGTACAAATTTCCATCAGATGGTCCAGTTATGCAAAAGAAAACATGGGTTGGGAAGCATCTTC
 TGAAGAATGTACCCAGAAGATGGTGCATTGAAGGGTGAATTAACAAAGATTGAAATTAAGGATGGTGGTCAATAC
 GATGCTGAAGTTAAGACTACATAACAAGGCTAAGAAACCAGTTCAATTACCAGGTGCTTACAACGTTAACATCAAATTGG
 ATATCACTTCTCATAACGAAGATTACACAATGTTGAACAATATGAAAGAGCCGAAGGTAGACACTCAACTGGTGGTAT
 GGATGAATTGTATAAGTAAAGCTTCTCGAG

>Pdx-mC DS

TCTAGACCATGGGATCCGTTGCCTCCAAGTCCCTGAAGCCGCCATTTCCAGATTGATTACTTATTTGAGAATTTTAGA
 AGAATTAGAAGCACAAGGTGCCACAGAACAGCTTCTGAACAATTGGGTGAATTAGCTCAAGTTACTGCATTCGAAGTT
 GATAAGGATTTGTCATACTTTGGTCTTACGGTACTGATGGTGTGGTTACACAGTTCAGTTTTGAAGAGAGAATTGA
 GACATATCTTGGGTTTAAACAGAAAGTGGGTTTATGTATCGTTGGTATGGGTAGATTAGGTTCTGCTTTGGCAGATTG
 GCCAGTTTTTGGTGAATCATTTGAATTGAGAGTTTTCTTTCCGTTGATCCAGGCATGGTTGGTAGACCAGTTAGAGGT
 GGTGTTATTGAACATGTTGATTTGTTGCCACAAAGAGTTCAGGTAGAATTGAAATGCTTTGTTAACAGTTCCAAGAG
 AAGCTGCACAAAAGCTGCAGATTTGTTAGTTGCTGCAGGTATTAAGGTATTTTAACTTCGCACCAGTTGTTTTGGA
 AGTTCCAAAGGAAGTTGCTGTTGAAAACGTTGATATCTTGGCAGGTTTAACTAGATTGTCTTTGCTATCTTGAATCCA
 ACATGGTCAGCTGCAGGTGGTTCATGGTTTTACTGCTCATAACGTTTACATCATGGCAGATAAGCAAAAGAATGGTATTA
 AAGCTAACTTCAAGATCAGACATAATATTGAAGATGGTGGTGTCAATTGGCAGATCATTACCAACAAAACACTCCAAT
 TGGTGACGGTCCAGTTTTGTTACCAGATAACCATTAATCTATCCAATCAAATTTGCTAAAGATCCAACGAAAAG
 AGAGATCATATGGTTTTGTTAGAATTCGTTACTGCTGCAGGTATCACACACGGTATGGACGAATTGTACAAAAGGTGGTA
 CAGGTGGTTCATGGTTTTCAAAGGTGAAGAATTGTTTACTGGTGTGTTCCAATTTTAGTTGAATTGGATGGTGACGT
 TAATGGTCATAAATTTCTGTTTCCAGGTGAAGGTGAAGGTGACGCTACTTACGGTAAATTGACATTGAAGTTTATTTGT
 ACTACTGGTAAATTACCAGTTCCATGGCCAACATTTGGTACTACATTTTCTTACGGTGTATGGTTTTGCTAGATACC
 CAGATCATATGAAGCAACATGATTTCTTTAAGTCAGCAATGCCAGAAGGTTACGTTCAAGAAAAGAACTATTTCTTTAA
 AGATGATGGTAACTACAAGACAAGAGCTGAGGTTAAGTTCGAAGGTGACACTTTAGTTAACAGAATCGAATTGAAAGGT
 ATCGATTTCAAGGAAGATGGTAACATCTTAGGTCTATAAATTGGAATATAATACAAAAGTTCCAGAAGCTGCAATTTCAA
 GATTGATCACTTACTTAAAGATTTTGGGAAGAATTAGAAGCTCAAGGTGTTTCATAGAACAGCATCAGAACAATTAGGTGA
 ATTAGCTCAAGTCACAGCTTTCAAAGTTGATGAAGATTTGTCATACTTCGGTCTTATGGTACAGACGGTGTGGTTAT
 ACTGTCCCTGTCTTAAAAAGAGAATTAAGACACATTTTAGGTTTAAATAGAAAATGGGGTTTATGCATTGTGGTATGG
 GTAGATTGGGTTCTGCTTTGGCAGACTGGCCTGGTTTTCGGTGAATCATTTGAATTAAGAGGTTTTCTTTCCGTTGATCC
 AGGCATGGTCGGTAGACCAGTTAGAGGTGGTGTATTGAGCACGTGATTTGTTACCTCAAAGAGTCCCTGGTGAATC
 GAAATCGCCTTATTGACTGTCCCAAGAGAAGCCGCTCAAAGGCCGCTGATTTGTTAGTTGCCGCTGGTATTAAGGTA
 TTTTAAATTTCTGCTCCTGTGTTTTGGAAGTCCCTAAGGAAGTTGCAGTTGAAAACGTTGATTTCTTGGCTGGTTTAA
 AAGATTGTCTTTTGAATCTTGAACCCAAAGTGGAGAGAAGAAATGATGGTTCCAGTACTGGTGGTAATGCTTCAGAT
 GGTGGTGGTCTGGTGGTATGGTTTCAAAGGTGAAGAAGATAACATGGCAATTATTAAGGAATTCATGAGATTCAAAG
 TTCATATGGAAGGTTCTGTTAACGGTCATGAATTCGAAATCGAAGGTGAAGGTGAAGGTAGACCATATGAAGGTACTCA
 AACAGCTAAATTAAGGTTACTAAAGGTGGTCCATTACCATTTGCATGGGATATTTTGTCTCCACAATTCATGTACGGT
 TCAAAGCATATGTTAAGCATCCAGCAGATATCCCAGATTACTTGAAATTATCTTTCCAGAAGGTTTTAAATGGGAAA
 GAGTTATGAACTTCAAGATGGTGGTGTGTTACTGTTACACAAGATTCTTCATTACAAGATGGTGAATTCATATATA
 AGTTAAATTGAGAGGTACAAATTTCCATCAGATGGTCCAGTTATGCAAAAGAAAACATGGGTTGGGAAGCATCTTCT
 GAAAGAATGTACCCAGAAGATGGTGCATTGAAGGGTGAATTAACAAAGATTGAAATTAAGGATGGTGGTCAATACG
 ATGCTGAAGTTAAGACTACATAACAAGGCTAAGAAACCAGTTCAATTACCAGGTGCTTACAACGTTAACATCAAATTGGA
 TATCACTTCTCATAACGAAGATTACACAATGTTGAACAATATGAAAGAGCCGAAGGTAGACACTCAACTGGTGGTATG
 GATGAATTGTATAAGTAAAGCTTCTCGAG

>NAPstar1

TCTAGAACCATGGGATCCAAAGTACCAGAAGCCGCTATTTCCAGATTGATAACATATTTGAGAATTTT
 AAGCACAAGGTGTCCACAGAACCGCTTCTGAACAATTGGGTGAATTAGCTCAAGTTACAGCATTCCAAGTTGATAAAGA
 TTTGTCATACTTTGGTTCTTACGGTACTGATGGTGTGGTTACACAGTCCAGTTTTGAAGAGAGAATTGAGACATATC
 TTGGGTTTAAACAGAAAGTGGGGTTTATGTATCGTTGGTATGGGTAGATTAGGTTCTGCTTTGGCAGATTGGCCAGGTT
 TTGGTGAATCATTTGAATTGAGAGGTTTCTTTTCAAGATCAGCTCAAAAAGTTGGTAGACCAGTTAGAGGTGGTGTAT
 TGAACATGTTGATTTGTTGCCACAAAGAGTTCCAGGTAGAATTGAAATGCTTTGTTAACTGTTCCAAGAGAAGCTGCA
 CAAAAGCTGCAGATTTGTTAGTTGCTGCAGGTATTAAGGTATTTTAACTTCGCACCAGTTGTTTTGGAAGTTCCAA
 AAGAAGTTGCTGTTGAAAACGTTGATATTTGGCAGGTTTAACTAGATTGCTTTTGTATCTTGAATCCAACATGGTC
 AGCTGCAGGTGGTCATGGTTTTACTGCTCATAACGTTTACATCATGGCAGATAAGCAAAAGAATGGTATTAAGCTAAC
 TTCAAGATCAGACATAATATTGAAGATGGTGGTGTCAATTGGCAGATCATTACCAACAAAACACTCCAATTGGTGACG
 GTCCAGTTTTGTTACCAGATAACCATTACTTATCTATCCAATCAAAATGCTAAAGATCCAAACGAAAAGAGAGATCA
 TATGGTTTTGTTAGAATTTGTTACTGCTGCAGGTATCACACATGGTATGGATGAATTATACAAAGGTGGTACAGGTGGT
 TCAATGGTTTTCTAAAGGTGAAGAATTGTTTACTGGTGTGTTCCAATTTTAGTTGAATTGGATGGTGACGTTAATGGTC
 ATAAATTTCTGTTTCAGGTGAAGGTGAAGGTGACGCTACTTACGGTAAATGACATTGAAGTTATTTGACTACTGG
 TAAATTACCAGTTCCTTGGCCAACATTGGTTACTACATTTTCTTACGGTGTATGGTTTTGCTAGATACCCAGATCAT
 ATGAAGCAACATGATTTCTTTAAGTCAGCAATGCCAGAAGGTTACGTTCAAGAAAGAACTATTTCTTTAAGATGATG
 GTAACTACAAGACAAGAGCTGAGGTTAAGTTTCAAGGTGACACTTTAGTTAACAGAATCGAATTGAAAGGTATCGATTT
 CAAAGAAGATGGTAACATCTTAGGTACAAAATTGGAATATAATACAAAAGTTCCAGAAGCTGCTATTTCAAGATTGATC
 ACTTACTTAAGAATTTTGAAGAATTAGAAGCTCAAGGTGTTTATAGAACAGCATCAGAACAATTAGGTGAATTAGCTC
 AAGTCACTGCATTTCAAGTTGATGAAGATTTGTCATACTTCGGTCTTATGGTACTGACGGTGTCCGGTTATACAGTCC
 AGTCTTAAAAAGAGAATTGAGACACATTTTAGGTTTAAATAGAAAATGGGGTTTATGCATTGTCCGGCATGGGTAGATTA
 GGTCTGCTTTGGCAGACTGGCCTGGTTTCGGCGAATCATTTGAATTGCGTGGTTTTCTTTCAAGATCAGCGCAAAAGG
 TCGGTAGACCAGTTAGAGGTGGTGTATTGAGCACGTTGATTTGTTACCTCAGAGAGTTCCAGGCAGAATCGAAATCGC
 TTTGTTAACAGTTCCAAGAGAAGCCGCTCAAAAGGCCGAGATTTGTTAGTTGCCGCTGGTATTAAGGTATTTTAAAT
 TTCGCTCCTGTCGTTTTGGAAGTTCCAAAAGAAGTTGCGGTTGAAAACGTTGATTTCTTGGCTGGTTTAAACAAGATTGT
 CTTTTGCAATCTGAACCCAAAGTGGAGAGAAGAAATGATGGGTTCCAGTACTGGTGGTAAATGCTTCAGATGGTGGTGG
 TTCTGGTGGTATGGTTTCAAAGGGTGAAGAAGATAACATGGCAATTATTAAGGAGTTTATGAGATTCAAAGTTCATATG
 GAAGGTTCTGTTAACGGTCAATGATTTGAAATCGAAGGTGAAGGTGAAGGTAGACCATATGAAGGTACTCAAACAGCTA
 AATTGAAGTTACTAAAGGTGGTCCATTACCATTTGCATGGGATATTTGCTCCACAATTCATGTACGGTTCAAACAGC
 ATATGTTAAGCATCCAGCAGATATTCAGATTACTTGAATTTATCTTTTCTGAAGTTTTAAATGGGAAAGAGTTATG
 AACTTCAAGATGGTGGTGTGTTACTGTTACACAAGATTTCTTATTACAAGATGGCGAGTTTATATAAAGGTTAAAT
 TGAGAGGTACAAATTTTCCATCAGATGGTCCAGTTATGCAAAAGAAAACATGGGTTGGGAAGCATCTTCTGAAAGAAT
 GTACCCAGAAGATGGTGCATTGAAGGGTGAATTAACAAAGATTGAAATGAAGGATGGTGGTCAATACGATGCTGAA
 GTTAAGACTACATAACAGCTAAGAAACAGTTCAATTACCAGGTGCTTACAACGTTAACATCAAATTTGGATATTACTT
 CTCATAACGAAGATTACACAATTGTTGAACAATATGAAAGAGCCGAAGGTAGACACTCAACAGGTGGTATGGATGAATT
 GTATAAGTAACTCGAG

>NAPstar2

TCTAGAACCATGGGATCCAAAGTACCAGAAGCCGCTATTTCCAGATTGATAACATATTTGAGAATTTT
 AAGCACAAGGTGTCCACAGAACCGCTTCTGAACAATTGGGTGAATTAGCTCAAGTTACAGCATTCCAAGTTGATAAAGA
 TTTGTCATACTTTGGTTCTTACGGTACTGATGGTGTGGTTACACAGTCCAGTTTTGAAGAGAGAATTGAGACATATC
 TTGGGTTTAAACAGAAAGTGGGGTTTATGTATCGTTGGTATGGGTAGATTAGGTTCTGCTTTGGCAGATTGGCCAGGTT
 TTGGTGAATCATTTGAATTGAGAGGTTTCTTTTCAAGATCAGCTGAAAAGTTGGTAGACCAGTTAGAGGTGGTGTAT
 TGAACATACCGATTTGTTGCCACAAAGAGTTCCAGGTAGAATTGAAATGCTTTGTTAACTGTTCCAAGAGAAGCTGCA
 CAAAAGCTGCAGATTTGTTAGTTGCTGCAGGTATTAAGGTATTTTAACTTCGCACCAGTTGTTTTGGAAGTTCCAA
 AAGAAGTTGCTGTTGAAAACGTTGATATTTGGCAGGTTTAACTAGATTGCTTTTGTATCTTGAATCCAACATGGTC
 AGCTGCAGGTGGTCATGGTTTTACTGCTCATAACGTTTACATCATGGCAGATAAGCAAAAGAATGGTATTAAGCTAAC
 TTCAAGATCAGACATAATATTGAAGATGGTGGTGTCAATTGGCAGATCATTACCAACAAAACACTCCAATTGGTGACG
 GTCCAGTTTTGTTACCAGATAACCATTACTTATCTATCCAATCAAAATGCTAAAGATCCAAACGAAAAGAGAGATCA
 TATGGTTTTGTTAGAATTTGTTACTGCTGCAGGTATCACACATGGTATGGATGAATTATACAAAGGTGGTACAGGTGGT
 TCAATGGTTTTCTAAAGGTGAAGAATTGTTTACTGGTGTGTTCCAATTTTAGTTGAATTGGATGGTGACGTTAATGGTC
 ATAAATTTCTGTTTCAGGTGAAGGTGAAGGTGACGCTACTTACGGTAAATGACATTGAAGTTATTTGACTACTGG
 TAAATTACCAGTTCCTTGGCCAACATTGGTTACTACATTTTCTTACGGTGTATGGTTTTGCTAGATACCCAGATCAT
 ATGAAGCAACATGATTTCTTTAAGTCAGCAATGCCAGAAGGTTACGTTCAAGAAAGAACTATTTCTTTAAGATGATG
 GTAACTACAAGACAAGAGCTGAGGTTAAGTTTCAAGGTGACACTTTAGTTAACAGAATCGAATTGAAAGGTATCGATTT
 CAAAGAAGATGGTAACATCTTAGGTACAAAATTGGAATATAATACAAAAGTTCCAGAAGCTGCTATTTCAAGATTGATC
 ACTTACTTAAGAATTTTGAAGAATTAGAAGCTCAAGGTGTTTATAGAACAGCATCAGAACAATTAGGTGAATTAGCTC

AAGTCACTGCATTCCAAGTTGATGAAGATTTGTCATACTTCGGTCTTATGGTACTGACGGTGTTCGGTTATACAGTTCC
 AGTCTTAAAAAGAGAATTGAGACACATTTTAGGTTTAAATAGAAAATGGGGTTTATGCATTGTCGGCATGGGTAGATTA
 GGTTCGCTTTGGCAGACTGGCCTGGTTTCGGCGAATCATTTGAATTGCGTGGTTTCTTTTCAAGATCAGCGAAAAGG
 TCGGTAGACCAGTTAGAGGTGGTGTATTGAGCACACCGATTTGTACCTCAGAGAGTTCAGGCAGAATCGAAATCGC
 TTTGTTAACAGTTCCAAGAGAAGCCGCTCAAAAGGCCGAGATTTGTTAGTTGCCGCTGGTATTAAGGTATTTTAAAT
 TTCGCTCCTGTCGTTTTGGAAGTTCCAAAAGAAGTTGCGGTTGAAAACGTTGATTTCTTGCTGGTTTAAACAAGATTGT
 CTTTTGCAATCTTGAACCCAAAGTGGAGAGAAGAAATGATGGGTTACGGTACTGGTGGTAATGCTTCAGATGGTGGTGG
 TTCTGGTGGTATGGTTTTCAAAGGGTGAAGAAGATAACATGGCAATTATTAAGGAGTTTATGAGATTCAAAGTTCATATG
 GAAGGTTCTGTTAACGGTCATGAATTTGAAATCGAAGGTGAAGGTGAAGGTAGACCATATGAAGGTACTCAAACAGCTA
 AATTGAAGGTTACTAAAGGTGGTCCATTACCATTTGCATGGGATATTTTGTCTCCACAATTCATGTACGGTTCAAAAGC
 ATATGTTAAGCATCCAGCAGATATTCCAGATTACTTGAATTTATCTTTTCTGAAGTTTTAAATGGGAAAAGAGTTATG
 AACTTCGAAGATGGTGGTGTGTTACTGTTACACAAGATTTCTCATTACAAGATGGCGAGTTTATATATAAGGTTAAAT
 TGAGAGGTACAAATTTCCATCAGATGGTCCAGTTATGCAAAAGAAAATATGGGTTGGGAAGCATCTTCTGAAAGAAT
 GTACCCAGAAGATGGTGCATTGAAGGGTGAATTAACAAAGATTGAAATTGAAGGATGGTGGTGCATTACGATGCTGAA
 GTTAAGACTACATACAAGGCTAAGAAACCAGTTCAATTACCAGGTGCTTACAACGTTAAACATCAAATTGGATATTACTT
 CTCATAACGAAGATTACACAATTTGTTGAACAATATGAAAGAGCCGAAGGTAGACACTCAACAGGTGGTATGGATGAATT
 GTATAAGTAACTCGAG

>NAPstar3

TCTAGAACCATGGGATCCAAAGTACCAGAAGCCGCTATTTCCAGATTGATAACATATTTGAGAATTTAGAGAATTAG
 AAGCACAAAGGTGTCCACAGAACCGCTTCTGAACAATTGGGTGAATTAGCTCAAGTTACAGCATTCCAAGTTGATAAAGA
 TTTGTCATACTTTGGTCTTACGGTACTGATGGTGTGGTTACACAGTTCCAGTTTTGAAGAGAGAATTGAGACATATC
 TTGGGTTTAAACAGAAAGTGGGTTTTATGTATCGTTGGTATGGGTAGATTAGGTTCTGCTTTGGCAGATTGGCCAGGTT
 TTGGTGAATCATTTGAATTGAGAGTTTTCTTTCAAGAaagGCTgaaAAAGTTGGTAGACCAGTTAGAGGTGGTGTAT
 TGAACATtacGATTTGTTGCCACAAAGAGTTCCAGGTAGAATTGAAATTGCTTTGTTAACTGTTCCAAGAGAAGCTGCA
 CAAAAAGCTGCAGATTTGTTAGTTGCTGCAGGTATTAAGGTATTTTAAACTTCGCACCAGTTGTTTTGGAAGTTCCAA
 AAGAAGTTGCTGTTGAAAACGTTGATATTTGGCAGGTTAACTAGATTGTCTTTTGTATCTTGAATCCAACATGGTC
 AGCTGCAGGTGGTCATGGTTTTACTGCTCATAACGTTTACATCATGGCAGATAAGCAAAAGAATGGTATTAAGCTAAC
 TTCAAGATCAGACATAATATTGAAGATGGTGGTGTCAATTGGCAGATCATTACCAACAAAACACTCCAATTGGTGACG
 GTCCAGTTTTGTTACCAGATAACCATTACTTATCTATCCAATCAAATTTGTCTAAAGATCCAAACGAAAAGAGAGATCA
 TATGGTTTTGTTAGAATTTGTTACTGCTGCAGGTATCACACATGGTATGGATGAATTATACAAAGGTGGTACAGGTGGT
 TCAATGGTTTTCTAAAGGTGAAGAATTTGTTACTGGTGTGTTCCAATTTTAGTTGAATTGGATGGTGACGTTAATGGTC
 ATAAATTTCTGTTTCAGGTGAAGGTGAAGGTGACGCTACTTACGGTAAATTGACATTGAAGTTTTATTTGTTACTACTGG
 TAAATTACCAGTTCCTTGGCCAACATTGGTTACTACATTTTCTTACGGTGTATGGTTTTTGTAGATACCCAGATCAT
 ATGAAGCAACATGATTTCTTTAAGTCAGCAATGCCAGAAGGTTACGTTCAAGAAAGAACTATTTTCTTTAAAGATGATG
 GTAACACAAGACAAGAGCTGAGGTTAAGTTCGAAGGTGACACTTAGTTAACAGAATCGAATTGAAAGGTATCGATTT
 CAAAGAAGATGGTAACATCTTAGGTACAAAATTGGAATATAATACAAAAGTTCCAGAAGCTGCTATTTCAAGATTGATC
 ACTTACTTAAGAATTTTGGAAAGATTAGAAGCTCAAGGTGTTATAGAACAGCATCAGAACAATTAGGTGAATTAGCTC
 AAGTCACTGCATTCCAAGTTGATGAAGATTTGTCATACTTCGGTCTTATGGTACTGACGGTGTTCGGTTATACAGTTCC
 AGTCTTAAAAAGAGAATTGAGACACATTTTAGGTTTAAATAGAAAATGGGGTTTATGCATTGTCGGCATGGGTAGATTA
 GGTTCGCTTTGGCAGACTGGCCTGGTTTCGGCGAATCATTTGAATTGCGTGGTTTCTTTTCAAGAaagGCGaaAAGG
 TCGGTAGACCAGTTAGAGGTGGTGTATTGAGCACTacGATTTGTTACCTCAGAGAGTTCAGGCAGAATCGAAATCGC
 TTTGTTAACAGTTCCAAGAGAAGCCGCTCAAAAGGCCGAGATTTGTTAGTTGCCGCTGGTATTAAGGTATTTTAAAT
 TTCGCTCCTGTCGTTTTGGAAGTTCCAAAAGAAGTTGCGGTTGAAAACGTTGATTTCTTGCTGGTTTAAACAAGATTGT
 CTTTTGCAATCTTGAACCCAAAGTGGAGAGAAGAAATGATGGGTTACGGTACTGGTGGTAATGCTTCAGATGGTGGTGG
 TTCTGGTGGTATGGTTTTCAAAGGGTGAAGAAGATAACATGGCAATTATTAAGGAGTTTATGAGATTCAAAGTTCATATG
 GAAGGTTCTGTTAACGGTCATGAATTTGAAATCGAAGGTGAAGGTGAAGGTAGACCATATGAAGGTACTCAAACAGCTA
 AATTGAAGGTTACTAAAGGTGGTCCATTACCATTTGCATGGGATATTTTGTCTCCACAATTCATGTACGGTTCAAAAGC
 ATATGTTAAGCATCCAGCAGATATTCCAGATTACTTGAATTTATCTTTTCTGAAGTTTTAAATGGGAAAAGAGTTATG
 AACTTCGAAGATGGTGGTGTGTTACTGTTACACAAGATTTCTCATTACAAGATGGCGAGTTTATATATAAGGTTAAAT
 TGAGAGGTACAAATTTCCATCAGATGGTCCAGTTATGCAAAAGAAAATATGGGTTGGGAAGCATCTTCTGAAAGAAT
 GTACCCAGAAGATGGTGCATTGAAGGGTGAATTAACAAAGATTGAAATTGAAGGATGGTGGTGCATTACGATGCTGAA
 GTTAAGACTACATACAAGGCTAAGAAACCAGTTCAATTACCAGGTGCTTACAACGTTAAACATCAAATTGGATATTACTT
 CTCATAACGAAGATTACACAATTTGTTGAACAATATGAAAGAGCCGAAGGTAGACACTCAACAGGTGGTATGGATGAATT
 GTATAAGTAACTCGAG

>NAPstar4

TCTAGAACCATGGGATCCAAAGTACCAGAAGCCGCTATTTCCAGATTGATAACATATTTGAGAATTTTAGAAGAATTAG
 AAGCACAAAGGTGTCCACAGAACCGCTTCTGAACAATTGGGTGAATTAGCTCAAGTTACAGCATTCCAAGTTGATAAAGA
 TTTGTCATACTTTGGTTCCTACGGTACTGATGGTGTGGTTACACAGTCCAGTTTTGAAGAGAGAATTGAGACATATC
 TTGGGTTTAAACAGAAAGTGGGGTTTATGTATCGTTGGTATGGGTgacTTAGGTTCTGCTTTGGCAGATTGGCCAGGTT
 TTGGTGAATCATTTGAATTGAGAGGTTTCTTTTCAAGATCAGCTCAAAAAGTTGGTAGACCAGTTAGAGGTGGTGTAT
 TGAACATGTTGATTTGTTGCCACAAAGAGTTCCAGGTAGAATTGAAATTGCTTTGTTAACTGTTCCAAGAGAAGCTGCA
 CAAAAGCTGCAGATTTGTTAGTTGCTGCAGGTATTAAGGTATTTTAACTTCGCACCAGTTGTTTTGGAAGTTCCAA
 AAGAAGTTGCTGTTGAAAACGTTGATATTTGGCAGGTTTAACTAGATTGCTTTTGTATCTTGAATCCAACATGGTC
 AGCTGCAGGTGGTCATGGTTTTACTGCTCATAACGTTTACATCATGGCAGATAAGCAAAAGAATGGTATTAAGCTAAC
 TTCAAGATCAGACATAATATTGAAGATGGTGGTGTCAATTGGCAGATCATTACCAACAAAACACTCCAATTGGTGACG
 GTCCAGTTTTGTTACCAGATAACCATTACTTATCTATCCAATCAAAATTGTCTAAAGATCCAAACGAAAAGAGAGATCA
 TATGGTTTTGTTAGAATTTGTTACTGCTGCAGGTATCACACATGGTATGGATGAATTATACAAAGGTGGTACAGGTGGT
 TCAATGGTTTTCTAAAGGTGAAGAATTGTTTACTGGTGTGTTCCAATTTTAGTTGAATTGGATGGTGACGTTAATGGTC
 ATAAATTTCTGTTTCAGGTGAAGGTGAAGGTGACGCTACTTACGGTAAATTGACATTGAAGTTTATTTGACTACTGG
 TAAATTACCAGTTCCTTGGCCAACATTGGTTACTACATTTTCTTACGGTGTATGGTTTTGCTAGATACCCAGATCAT
 ATGAAGCAACATGATTTCTTTAAGTCAGCAATGCCAGAAGGTTACGTTCAAGAAAGAACTATTTCTTTAAAGATGATG
 GTAACTACAAGACAAGAGCTGAGGTTAAGTTCGAAGGTGACACTTTAGTTAACAGAATCGAATTGAAAGGTATCGATTT
 CAAAGAAGATGGTAACATCTTAGGTACAAAATTGGAATATAATACAAAAGTTCCAGAAGCTGCTATTTCAAGATTGATC
 ACTTACTTAAGAATTTTGAAGAATTAGAAGCTCAAGGTGTTTATAGAACAGCATCAGAACAATTAGGTGAATTAGCTC
 AAGTCACTGCATTTCCAAGTTGATGAAGATTTGTCATACTTCGGTCTTATGGTACTGACGGTGTCCGGTTATACAGTTC
 AGTCTTAAAAAGAGAATTGAGACACATTTTAGGTTTAAATAGAAAATGGGGTTTATGCATTGTCCGCATGGGTgacTTA
 GGTCTGCTTTGGCAGACTGGCCTGGTTTCGGCGAATCATTTGAATTGCGTGGTTTTCTTTCAAGATCAGCGCAAAAGG
 TCGGTAGACCAGTTAGAGGTGGTGTATTGAGCACGTTGATTTGTTACCTCAGAGAGTTCCAGGCAGAATCGAAATCGC
 TTTGTTAACAGTTCCAAGAGAAGCCGCTCAAAAGGCCGAGATTTGTTAGTTGCCGCTGGTATTAAGGTATTTTAAAT
 TTCGCTCCTGTCGTTTTGGAAGTTCCAAAAGAAGTTGCGGTTGAAAACGTTGATTTCTTGGCTGGTTTAAACAAGATTGT
 CTTTTGCAATCTTGAACCCAAAGTGGAGAGAAGAAATGATGGGTTCCAGGTACTGGTGGTAATGCTTCAGATGGTGGTGG
 TTCTGGTGGTATGGTTTCAAAGGGTGAAGAAGATAACATGGCAATTATTAAGGAGTTTATGAGATTCAAAGTTCATATG
 GAAGGTTCTGTTAACGGTCATGAATTTGAAATCGAAGGTGAAGGTGAAGGTAGACCATATGAAGGTACTCAAACAGCTA
 AATTGAAGGTTACTAAAGGTGGTCCATTACCATTTGCATGGGATATTTGCTCCACAATTCATGTACGGTTCAAAGC
 ATATGTTAAGCATCCAGCAGATATTCAGATTACTTGAATTTATCTTTTCTGAAGGTTTTAAATGGGAAAGAGTTATG
 AACTTCAAGATGGTGGTGTGTTACTGTTACACAAGATTTCTTATTACAAGATGGCGAGTTTATATAAGGTTAAAT
 TGAGAGGTACAAATTTTCCATCAGATGGTCCAGTTATGCAAAAGAAAACATGGGTTGGGAAGCATCTTCTGAAAGAAT
 GTACCCAGAAGATGGTGCATTGAAGGGTGAATTTAAACAAAGATTGAAATGAAGGATGGTGGTCAATACGATGCTGAA
 GTTAAGACTACATAACAGCTAAGAAACAGTTCAATTACCAGGTGCTTACAACGTTAACATCAAATTTGGATATTACTT
 CTCATAACGAAGATTACACAATTGTTGAACAATATGAAAGAGCCGAAGGTAGACACTCAACAGGTGGTATGGATGAATT
 GTATAAGTAACTCGAG

>NAPstarC

TCTAGAACCATGGGATCCAAAGTACCAGAAGCCGCTATTTCCAGATTGATAACATATTTGAGAATTTTAGAAGAATTAG
 AAGCACAAAGGTGTCCACAGAACCGCTTCTGAACAATTGGGTGAATTAGCTCAAGTTACAGCATTCCAAGTTGATAAAGA
 TTTGTCATACTTTGGTTCCTACGGTACTGATGGTGTGGTTACACAGTCCAGTTTTGAAGAGAGAATTGAGACATATC
 TTGGGTTTAAACAGAAAGTGGGGTTTATGTATCGTTGGTATGGGTGATTTAGGTTCTGCTTTGGCAGATTGGCCAGGTT
 TTGGTGAATCATTTGAATTGAGAGGTTTCTTTTCAAGTGTACCAGGAAAAGTTGGTAGACCAGTTAGAGGTGGTGTAT
 TGAACATGTTGATTTGTTGCCACAAAGAGTTCCAGGTAGAATTGAAATTGCTTTGTTAACTGCGCCAAGAGAAGCTGCA
 CAAAAGCTGCAGATTTGTTAGTTGCTGCAGGTATTAAGGTATTTTAACTTCGCACCAGTTGTTTTGGAAGTTCCAA
 AAGAAGTTGCTGTTGAAAACGTTGATATTTGGCAGGTTTAACTAGATTGCTTTTGTATCTTGAATCCAACATGGTC
 AGCTGCAGGTGGTCATGGTTTTACTGCTCATAACGTTTACATCATGGCAGATAAGCAAAAGAATGGTATTAAGCTAAC
 TTCAAGATCAGACATAATATTGAAGATGGTGGTGTCAATTGGCAGATCATTACCAACAAAACACTCCAATTGGTGACG
 GTCCAGTTTTGTTACCAGATAACCATTACTTATCTATCCAATCAAAATTGTCTAAAGATCCAAACGAAAAGAGAGATCA
 TATGGTTTTGTTAGAATTTGTTACTGCTGCAGGTATCACACATGGTATGGATGAATTATACAAAGGTGGTACAGGTGGT
 TCAATGGTTTTCTAAAGGTGAAGAATTGTTTACTGGTGTGTTCCAATTTTAGTTGAATTGGATGGTGACGTTAATGGTC
 ATAAATTTCTGTTTCAGGTGAAGGTGAAGGTGACGCTACTTACGGTAAATTGACATTGAAGTTTATTTGACTACTGG
 TAAATTACCAGTTCCTTGGCCAACATTGGTTACTACATTTTCTTACGGTGTATGGTTTTGCTAGATACCCAGATCAT
 ATGAAGCAACATGATTTCTTTAAGTCAGCAATGCCAGAAGGTTACGTTCAAGAAAGAACTATTTCTTTAAAGATGATG
 GTAACTACAAGACAAGAGCTGAGGTTAAGTTCGAAGGTGACACTTTAGTTAACAGAATCGAATTGAAAGGTATCGATTT
 CAAAGAAGATGGTAACATCTTAGGTACAAAATTGGAATATAATACAAAAGTTCCAGAAGCTGCTATTTCAAGATTGATC
 ACTTACTTAAGAATTTTGAAGAATTAGAAGCTCAAGGTGTTTATAGAACAGCATCAGAACAATTAGGTGAATTAGCTC

AAGTCACTGCATTCCAAGTTGATGAAGATTTGTCATACTTCGGTCTTATGGTACTGACGGTGTGGTTATACAGTTCC
 AGTCTTAAAAAGAGAATTGAGACACATTTTAGGTTTAAATAGAAAATGGGGTTTATGCATTGTCGGCATGGGTGATTTA
 GGTTCGCTTTGGCAGACTGGCCTGGTTTCGGCGAATCATTTGAATTGCGTGGTTTCTTTTCAGTGTACCAGGAAAAGG
 TCGGTAGACCAGTTAGAGGTGGTGTATTGAGCACGTTGATTTGTTACCTCAGAGAGTTCAGGCAGAATCGAAATCGC
 TTTGTTAACAGCGCCAAGAGAAGCCGCTCAAAAGGCCGAGATTTGTTAGTTGCCGCTGGTATTAAGGTATTTAAAT
 TTCGCTCCTGTCGTTTTGGAAGTTCAAAAGAAGTTGCGGTTGAAAACGTTGATTTCTTGCTGGTTTAAACAAGATTGT
 CTTTTGCAATCTTGAACCCAAAGTGGAGAGAAGAAATGATGGGTTGAGTACTGGTGGTAATGCTTCAGATGGTGGTGG
 TTCTGGTGGTATGGTTTCAAAGGGTGAAGAAGATAACATGGCAATTATTAAGGAGTTTATGAGATTCAAAGTTCATATG
 GAAGGTTCTGTTAACGGTCATGAATTTGAAATCGAAGGTGAAGGTGAAGGTAGACCATATGAAGGTACTCAAACAGCTA
 AATTGAAGGTTACTAAAGGTGGTCCATTACCATTTGCATGGGATATTTGCTCCACAATTCATGTACGGTTCAAAAGC
 ATATGTTAAGCATCCAGCAGATATTCCAGATTACTTGAATTTATCTTTTCTGAAGGTTTTAAATGGGAAAAGAGTTATG
 AACTTCGAAGATGGTGGTGTGTTACTGTTACACAAGATTCTTCATTACAAGATGGCGAGTTTATATATAAGGTTAAAT
 TGAGAGGTACAAATTTCCATCAGATGGTCCAGTTATGCAAAAGAAAATATGGGTTGGGAAGCATCTTCTGAAAGAAT
 GTACCCAGAAGATGGTGCATTGAAGGGTGAATTAACAAAAGATTGAAATTGAAGGATGGTGGTGCATTACGATGCTGAA
 GTTAAGACTACATACAAGGCTAAGAAACCAGTTCAATTACCAGGTGCTTACAACGTTAACATCAAATTGGATATTACTT
 CTCATAACGAAGATTACACAATTTGTTGAACAATATGAAAGAGCCGAAGGTAGACACTCAACAGGTGGTATGGATGAATT
 GTATAAGTAACTCGAG

>NAPstar1.4

TCTAGAACCATGGGATCCAAAGTACCAGAAGCCGCTATTTCCAGATTGATAACATATTTGAGAATTTAGAGAATTAG
 AAGCACAAAGGTGTCCACAGAACCGCTTCTGAACAATTGGGTGAATTAGCTCAAGTTACAGCATTCCAAGTTGATAAAGA
 TTTGTCATACTTTGGTCTTACGGTACTGATGGTGTGGTTACACAGTTCCAGTTTTGAAGAGAGAATTGAGACATATC
 TTGGGTTTAAACAGAAAAGTGGGGTTTATGTATCGTTGGTATGGGTAGATTAGGTTCTGCTTTGGCAGATTGGCCAGGTT
 TTGGTGAATCATTTGAATTGAGAGGTTTCTTTTCAAGATCAGCTCAAAAAGTTGGTAGACCAGTTAGAGGTGGTGTAT
 TGAACATGTTGATTTGTTGCCACAAAGAGTTCCAGGTAGAATTGAAATTGCTTTGTTAACTGTTCCAAGAGAAGCTGCA
 CAAAAAGCTGCAGATTTGTTAGTTGCTGCAGGTATTAAGGTATTTTAAACTTCGCACCAGTTGTTTTGGAAGTTCCAA
 AAGAAGTTGCTGTTGAAAACGTTGATATTTGGCAGGTTTAACTAGATTGCTTTTGTCTATCTTGAATCCAACATGGTC
 AGCTGCAGGTGGTCATGGTTTTACTGCTCATAACGTTTACATCATGGCAGATAAGCAAAAAGAATGGTATTAAGCTAAC
 TTCAAGATCAGACATAATATTGAAGATGGTGGTGTCAATTGGCAGATCATTACCAACAAAACACTCCAATTGGTGACG
 GTCCAGTTTTGTTACCAGATAACCATTACTTATCTATCCAATCAAATTTGCTAAAGATCCAAACGAAAAGAGAGATCA
 TATGGTTTTGTTAGAATTTGTTACTGCTGCAGGTATCACACATGGTATGGATGAATTATACAAAGGTGGTACAGGTGGT
 TCAATGGTTTTCTAAAGGTGAAGAATTGTTTACTGGTGTGTTCCAATTTTAGTTGAATTGGATGGTGACGTTAATGGTC
 ATAAATTTCTGTTTCAGGTGAAGGTGAAGGTGACGCTACTTACGGTAAATTGACATTGAAGTTTATTTGACTACTGG
 TAAATTACCAGTTCCTTGGCCAACATTGGTTACTACATTTTCTTACGGTGTATGGTTTTGCTAGATACCCAGATCAT
 ATGAAGCAACATGATTTCTTTAAGTCAGCAATGCCAGAAGGTTACGTTCAAGAAAGAACTATTTTCTTTAAAGATGATG
 GTAACACAAGACAAGAGCTGAGGTTAAGTTCGAAGGTGACACTTAGTTAACAGAATCGAATTGAAAGGTATCGATTT
 CAAAGAAGATGGTAACATCTTAGGTCACAAATTTGGAATATAATACAAAAGTTCCAGAAGCTGCTATTTCAAGATTGATC
 ACTTACTTAAGAATTTTGGAAAGATTAGAAGCTCAAGGTGTTTATAGAACAGCATCAGAACAATTAGGTGAATTAGCTC
 AAGTCACTGCATTCCAAGTTGATGAAGATTTGTCATACTTCGGTCTTATGGTACTGACGGTGTGGTTATACAGTTCC
 AGTCTTAAAAAGAGAATTGAGACACATTTTAGGTTTAAATAGAAAATGGGGTTTATGCATTGTCGGCATGGGTgacTTA
 GGTTCTGCTTTGGCAGACTGGCCTGGTTTCGGCGAATCATTTGAATTGCGTGGTTTCTTTTCAAGATCAGCGCAAAGG
 TCGGTAGACCAGTTAGAGGTGGTGTATTGAGCACGTTGATTTGTTACCTCAGAGAGTTCAGGCAGAATCGAAATCGC
 TTTGTTAACAGTTCAAAGAGAAGCCGCTCAAAAGGCCGAGATTTGTTAGTTGCCGCTGGTATTAAGGTATTTAAAT
 TTCGCTCCTGTCGTTTTGGAAGTTCAAAAGAAGTTGCGGTTGAAAACGTTGATTTCTTGCTGGTTTAAACAAGATTGT
 CTTTTGCAATCTTGAACCCAAAGTGGAGAGAAGAAATGATGGGTTGAGTACTGGTGGTAATGCTTCAGATGGTGGTGG
 TTCTGGTGGTATGGTTTCAAAGGGTGAAGAAGATAACATGGCAATTATTAAGGAGTTTATGAGATTCAAAGTTCATATG
 GAAGGTTCTGTTAACGGTCATGAATTTGAAATCGAAGGTGAAGGTGAAGGTAGACCATATGAAGGTACTCAAACAGCTA
 AATTGAAGGTTACTAAAGGTGGTCCATTACCATTTGCATGGGATATTTGCTCCACAATTCATGTACGGTTCAAAAGC
 ATATGTTAAGCATCCAGCAGATATTCCAGATTACTTGAATTTATCTTTTCTGAAGGTTTTAAATGGGAAAAGAGTTATG
 AACTTCGAAGATGGTGGTGTGTTACTGTTACACAAGATTCTTCATTACAAGATGGCGAGTTTATATATAAGGTTAAAT
 TGAGAGGTACAAATTTCCATCAGATGGTCCAGTTATGCAAAAGAAAATATGGGTTGGGAAGCATCTTCTGAAAGAAT
 GTACCCAGAAGATGGTGCATTGAAGGGTGAATTAACAAAAGATTGAAATTGAAGGATGGTGGTGCATTACGATGCTGAA
 GTTAAGACTACATACAAGGCTAAGAAACCAGTTCAATTACCAGGTGCTTACAACGTTAACATCAAATTGGATATTACTT
 CTCATAACGAAGATTACACAATTTGTTGAACAATATGAAAGAGCCGAAGGTAGACACTCAACAGGTGGTATGGATGAATT
 GTATAAGTAACTCGAG

>NAPstar2.4

TCTAGAACCATGGGATCCAAAGTACCAGAAGCCGCTATTTCCAGATTGATAACATATTTGAGAATTTT
 AAGCACAAGGTGTCCACAGAACCGCTTCTGAACAATTGGGTGAATTAGCTCAAGTTACAGCATTCCAAGTTGATAAAGA
 TTTGTCATACTTTGGTTCTTACGGTACTGATGGTGTGGTTACACAGTCCAGTTTTGAAGAGAGAATTGAGACATATC
 TTGGGTTTAAACAGAAAGTGGGGTTTATGTATCGTTGGTATGGGTAGATTAGGTTCTGCTTTGGCAGATTGGCCAGGTT
 TTGGTGAATCATTTGAATTGAGAGGTTTCTTTTCAAGATCAGCTGAAAAAGTTGGTAGACCAGTTAGAGGTGGTGTAT
 TGAACATACCGATTTGTTGCCACAAAGAGTTCCAGGTAGAATTGAAATGCTTTGTTAACTGTTCCAAGAGAAGCTGCA
 CAAAAAGCTGCAGATTTGTTAGTTGCTGCAGGTATTAAGGTATTTTAACTTCGCACCAGTTGTTTTGGAAGTTCCAA
 AAGAAGTTGCTGTTGAAAACGTTGATATTTGGCAGGTTAACTAGATTGCTTTTGTATCTTGAATCCAACATGGTC
 AGCTGCAGGTGGTCATGGTTTTACTGCTCATAACGTTTACATCATGGCAGATAAGCAAAAGAATGGTATTAAGCTAAC
 TTCAAGATCAGACATAATATTGAAGATGGTGGTGTCAATTGGCAGATCATTACCAACAAAACACTCCAATTGGTGACG
 GTCCAGTTTTGTTACCAGATAACCATTACTTATCTATCCAATCAAAATGCTAAAGATCCAAACGAAAAGAGAGATCA
 TATGGTTTTGTTAGAATTTGTTACTGCTGCAGGTATCACACATGGTATGGATGAATTATACAAAGGTGGTACAGGTGGT
 TCAATGGTTTTCTAAAGGTGAAGAATTGTTTACTGGTGTGTTCCAATTTTAGTTGAATTGGATGGTGACGTTAATGGTC
 ATAAATTTCTGTTTCAGGTGAAGGTGAAGGTGACGCTACTTACGGTAAATTGACATTGAAGTTTATTTGACTACTGG
 TAAATTACCAGTTCCTTGGCCAACATTGGTTACTACATTTTCTTACGGTGTATGGTTTTTGCTAGATACCCAGATCAT
 ATGAAGCAACATGATTTCTTTAAGTCAGCAATGCCAGAAGGTTACGTTCAAGAAAGAACTATTTCTTTAAAGATGATG
 GTAACTACAAGACAAGAGCTGAGGTTAAGTTTCAAGGTGACACTTTAGTTAACAGAATCGAATTGAAAGGTATCGATTT
 CAAAGAAGATGGTAACATCTTAGGTACAAAATTGGAATATAATACAAAAGTTCCAGAAGCTGCTATTTCAAGATTGATC
 ACTTACTTAAGAATTTTGAAGAATTAGAAGCTCAAGGTGTTTATAGAACAGCATCAGAACAATTAGGTGAATTAGCTC
 AAGTCACTGCATTTCAAGTTGATGAAGATTTGTCATACTTCGGTCTTATGGTACTGACGGTGTCCGGTTATACAGTCC
 AGTCTTAAAAAGAGAATTGAGACACATTTTAGGTTTAAATAGAAAATGGGGTTTATGCATTGTCGGCATGGGTgaCTTA
 GGTCTGCTTTGGCAGACTGGCCTGGTTTCGGCGAATCATTTGAATTGCGTGGTTTTCTTTCAAGATCAGCGCAAAAGG
 TCGGTAGACCAGTTAGAGGTGGTGTATTGAGCACGTTGATTTGTTACCTCAGAGAGTTCCAGGCAGAATCGAAATCGC
 TTTGTTAACAGTTCCAAGAGAAGCCGCTCAAAGGCCGAGATTTGTTAGTTGCCGCTGGTATTAAGGTATTTAAAT
 TTCGCTCCTGTCGTTTTGGAAGTTCCAAAAGAAGTTGCGGTTGAAAACGTTGATTTCTTGGCTGGTTAACAAGATTGT
 CTTTTGCAATCTGAACCCAAAGTGGAGAGAAGAAATGATGGGTTCAAGTACTGGTGGTAAATGCTTCAGATGGTGGTGG
 TTCTGGTGGTATGGTTTCAAAGGGTGAAGAAGATAACATGGCAATTATTAAGGAGTTTATGAGATTCAAAGTTCATATG
 GAAGGTTCTGTTAACGGTCAATGATTTGAAATCGAAGGTGAAGGTGAAGGTAGACCATATGAAGGTACTCAAACAGCTA
 AATTGAAGTTACTAAAGGTGGTCCATTACCATTGTCATGGGATATTTGCTCCACAATTCATGTACGGTTCAAAGC
 ATATGTTAAGCATCCAGCAGATATTCAGATTACTTGAATTTATCTTTTCTGAAGTTTTAAATGGGAAAGAGTTATG
 AACTTCAAGATGGTGGTGTGTTACTGTTACACAAGATTTCTTATTACAAGATGGCGAGTTTATATAAAGGTTAAAT
 TGAGAGGTACAAAATTTCCATCAGATGGTCCAGTTATGCAAAAGAAAACATGGGTTGGGAAGCATCTTCTGAAAGAAT
 GTACCCAGAAGATGGTGCATTGAAGGGTGAATTAACAAAGATTGAAATGAAGGATGGTGGTCAATACGATGCTGAA
 GTTAAGACTACATAACAGCTAAGAAACAGTTCAATTACCAGGTGCTTACAACGTTAACATCAAATTTGGATATTACTT
 CTCATAACGAAGATTACACAATTGTTGAACAATATGAAAGAGCCGAAGGTAGACACTCAACAGGTGGTATGGATGAATT
 GTATAAGTAACTCGAG

>NAPstar3.4

TCTAGAACCATGGGATCCAAAGTACCAGAAGCCGCTATTTCCAGATTGATAACATATTTGAGAATTTT
 AAGCACAAGGTGTCCACAGAACCGCTTCTGAACAATTGGGTGAATTAGCTCAAGTTACAGCATTCCAAGTTGATAAAGA
 TTTGTCATACTTTGGTTCTTACGGTACTGATGGTGTGGTTACACAGTCCAGTTTTGAAGAGAGAATTGAGACATATC
 TTGGGTTTAAACAGAAAGTGGGGTTTATGTATCGTTGGTATGGGTAGATTAGGTTCTGCTTTGGCAGATTGGCCAGGTT
 TTGGTGAATCATTTGAATTGAGAGGTTTCTTTTCAAGAAagGCTgaaAAAGTTGGTAGACCAGTTAGAGGTGGTGTAT
 TGAACATtacGATTTGTTGCCACAAAGAGTTCCAGGTAGAATTGAAATGCTTTGTTAACTGTTCCAAGAGAAGCTGCA
 CAAAAAGCTGCAGATTTGTTAGTTGCTGCAGGTATTAAGGTATTTTAACTTCGCACCAGTTGTTTTGGAAGTTCCAA
 AAGAAGTTGCTGTTGAAAACGTTGATATTTGGCAGGTTAACTAGATTGCTTTTGTATCTTGAATCCAACATGGTC
 AGCTGCAGGTGGTCATGGTTTTACTGCTCATAACGTTTACATCATGGCAGATAAGCAAAAGAATGGTATTAAGCTAAC
 TTCAAGATCAGACATAATATTGAAGATGGTGGTGTCAATTGGCAGATCATTACCAACAAAACACTCCAATTGGTGACG
 GTCCAGTTTTGTTACCAGATAACCATTACTTATCTATCCAATCAAAATGCTAAAGATCCAAACGAAAAGAGAGATCA
 TATGGTTTTGTTAGAATTTGTTACTGCTGCAGGTATCACACATGGTATGGATGAATTATACAAAGGTGGTACAGGTGGT
 TCAATGGTTTTCTAAAGGTGAAGAATTGTTTACTGGTGTGTTCCAATTTTAGTTGAATTGGATGGTGACGTTAATGGTC
 ATAAATTTCTGTTTCAGGTGAAGGTGAAGGTGACGCTACTTACGGTAAATTGACATTGAAGTTTATTTGACTACTGG
 TAAATTACCAGTTCCTTGGCCAACATTGGTTACTACATTTTCTTACGGTGTATGGTTTTTGCTAGATACCCAGATCAT
 ATGAAGCAACATGATTTCTTTAAGTCAGCAATGCCAGAAGGTTACGTTCAAGAAAGAACTATTTCTTTAAAGATGATG
 GTAACTACAAGACAAGAGCTGAGGTTAAGTTTCAAGGTGACACTTTAGTTAACAGAATCGAATTGAAAGGTATCGATTT
 CAAAGAAGATGGTAACATCTTAGGTACAAAATTGGAATATAATACAAAAGTTCCAGAAGCTGCTATTTCAAGATTGATC
 ACTTACTTAAGAATTTTGAAGAATTAGAAGCTCAAGGTGTTTATAGAACAGCATCAGAACAATTAGGTGAATTAGCTC

AAGTCACTGCATTCCAAGTTGATGAAGATTTGTCATACTTCGGTCTTATGGTACTGACGGTGTCCGGTTATACAGTTCC
AGTCTTAAAAAGAGAATTGAGACACATTTTAGGTTTAAATAGAAAATGGGGTTTATGCATTGTCGGCATGGGTgacTTA
GGTTCGCTTTGGCAGACTGGCCTGGTTTCGGCGAATCATTTGAATTGCGTGGTTTCTTTTCAAGATCAGCGCAAAGG
TCGGTAGACCAGTTAGAGGTGGTGTATTGAGCACGTTGATTTGTTACCTCAGAGAGTTCAGGCAGAATCGAAATCGC
TTTGTTAACAGTTCCAAGAGAAGCCGCTCAAAAGGCCGAGATTTGTTAGTTGCCGCTGGTATTAAGGTATTTTAAAT
TTCGCTCCTGTCGTTTTGGAAGTTCCAAAAGAAGTTGCGGTTGAAAACGTTGATTTCTTGCTGGTTTAAACAAGATTGT
CTTTTGAATCTTGAACCCAAAGTGGAGAGAAGAAATGATGGGTTGAGTACTGGTGGTAATGCTTCAGATGGTGGTGG
TTCTGGTGGTATGGTTTTCAAAGGGTGAAGAAGATAACATGGCAATTATTAAGGAGTTTATGAGATTCAAAGTTCATATG
GAAGGTTCTGTTAACGGTCATGAATTTGAAATCGAAGGTGAAGGTGAAGGTAGACCATATGAAGGTACTCAAACAGCTA
AATTGAAGGTTACTAAAGGTGGTCCATTACCATTTGCATGGGATATTTGCTCCACAATTCATGTACGGTTCAAAAGC
ATATGTTAAGCATCCAGCAGATATTCCAGATTACTTGAATTTATCTTTTCTGAAGGTTTTAAATGGGAAAGAGTTATG
AATTCGAAGATGGTGGTGTGTTACTGTTACACAAGATTTCTCATTACAAGATGGCGAGTTTATATATAAGGTTAAAT
TGAGAGGTACAAATTTCCATCAGATGGTCCAGTTATGCAAAAGAAAATATGGGTTGGGAAGCATCTTCTGAAAGAAT
GTACCCAGAAGATGGTGCATTGAAGGGTGAATTAACAAAGATTGAAATTGAAGGATGGTGGTGCATTACGATGCTGAA
GTTAAGACTACATACAAGGCTAAGAAACCAGTTCAATTACCAGGTGCTTACAACGTTAAACATCAAATGGATATTACTT
CTCATAACGAAGATTACACAATTTGTTGAACAATATGAAAGAGCCGAAGGTAGACACTCAACAGGTGGTATGGATGAATT
GTATAAGTAACTCGAG

>NAPstar4.1

TCTAGAACCATGGGATCCAAAGTACCAGAAGCCGCTATTTCCAGATTGATAACATATTTGAGAATTTAGAGAATTAG
AAGCACAAAGGTGTCCACAGAACCGCTTCTGAACAATTGGGTGAATTAGCTCAAGTTACAGCATTCCAAGTTGATAAAGA
TTTGTCACTACTTTGGTCTTACGGTACTGATGGTGTGGTTACACAGTTCCAGTTTTGAAGAGAGAATTGAGACATATC
TTGGGTTTAAACAGAAAGTGGGGTTTATGTATCGTTGGTATGGGTgacTTAGGTTCTGCTTTGGCAGATTGGCCAGGTT
TTGGTGAATCATTTGAATTGAGAGGTTTTCTTTTCAAGATCAGCTCAAAAAGTTGGTAGACCAGTTAGAGGTGGTGTAT
TGAACATGTTGATTTGTTGCCACAAAGAGTTCAGGTAGAATTGAAATTGCTTTGTTAACTGTTCCAAGAGAAGCTGCA
CAAAAAGCTGCAGATTTGTTAGTTGCTGCAGGTATTAAGGTATTTTAAACTTCGCACCAGTTGTTTTGGAAGTTCCAA
AAGAAGTTGCTGTTGAAAACGTTGATATTTGGCAGGTTAACTAGATTGCTTTTGTCTATCTTGAATCCAACATGGTC
AGCTGCAGGTGGTGCATGGTTTTACTGCTCATAACGTTTACATCATGGCAGATAAGCAAAAAGAATGGTATTAAGCTAAC
TTCAAGATCAGACATAATATTGAAGATGGTGGTGTCAATTGGCAGATCATTACCAACAAAACACTCCAATTGGTGACG
GTCCAGTTTTGTTACCAGATAACCATTACTTATCTATCCAATCAAAATTGCTAAAGATCCAAACGAAAAGAGAGATCA
TATGGTTTTGTTAGAATTTGTTACTGCTGCAGGTATCACACATGGTATGGATGAATTATACAAAGGTGGTACAGGTGGT
TCAATGGTTTTCTAAAGGTGAAGAATTTGTTACTGGTGTGTTCCAATTTTAGTTGAATTGGATGGTGACGTTAATGGTC
ATAAATTTTCTGTTTCAGGTGAAGGTGAAGGTGACGCTACTTACGGTAAATTGACATTGAAGTTTTATTTGTTACTACTGG
TAAATTACCAGTTCCTTGGCCAACATTGGTTACTACATTTTCTTACGGTGTATGGTTTTTGTAGATACCCAGATCAT
ATGAAGCAACATGATTTCTTTAAGTCAGCAATGCCAGAAGGTTACGTTCAAGAAAGAACTATTTTCTTTAAAGATGATG
GTAACACAAGACAAGAGCTGAGGTTAAGTTCGAAGGTGACACTTATAGTTAACAGAATCGAATTGAAAGGTATCGATTT
CAAAGAAGATGGTAACATCTTAGGTCACAAATGGAATATAATACAAAAGTTCCAGAAGCTGCTATTTCAAGATTGATC
ACTTACTTAAGAATTTTGGAAAGATTAGAAGCTCAAGGTGTTTATAGAACAGCATCAGAACAATTAGGTGAATTAGCTC
AAGTCACTGCATTCCAAGTTGATGAAGATTTGTCATACTTCGGTCTTATGGTACTGACGGTGTCCGGTTATACAGTTCC
AGTCTTAAAAAGAGAATTGAGACACATTTTAGGTTTAAATAGAAAATGGGGTTTATGCATTGTCGGCATGGGTAGATTA
GGTTCGCTTTGGCAGACTGGCCTGGTTTCGGCGAATCATTTGAATTGCGTGGTTTCTTTTCAAGATCAGCGCAAAGG
TCGGTAGACCAGTTAGAGGTGGTGTATTGAGCACGTTGATTTGTTACCTCAGAGAGTTCAGGCAGAATCGAAATCGC
TTTGTTAACAGTTCCAAGAGAAGCCGCTCAAAAGGCCGAGATTTGTTAGTTGCCGCTGGTATTAAGGTATTTTAAAT
TTCGCTCCTGTCGTTTTGGAAGTTCCAAAAGAAGTTGCGGTTGAAAACGTTGATTTCTTGCTGGTTTAAACAAGATTGT
CTTTTGAATCTTGAACCCAAAGTGGAGAGAAGAAATGATGGGTTGAGTACTGGTGGTAATGCTTCAGATGGTGGTGG
TTCTGGTGGTATGGTTTTCAAAGGGTGAAGAAGATAACATGGCAATTATTAAGGAGTTTATGAGATTCAAAGTTCATATG
GAAGGTTCTGTTAACGGTCATGAATTTGAAATCGAAGGTGAAGGTGAAGGTAGACCATATGAAGGTACTCAAACAGCTA
AATTGAAGGTTACTAAAGGTGGTCCATTACCATTTGCATGGGATATTTGCTCCACAATTCATGTACGGTTCAAAAGC
ATATGTTAAGCATCCAGCAGATATTCCAGATTACTTGAATTTATCTTTTCTGAAGGTTTTAAATGGGAAAGAGTTATG
AATTCGAAGATGGTGGTGTGTTACTGTTACACAAGATTTCTCATTACAAGATGGCGAGTTTATATATAAGGTTAAAT
TGAGAGGTACAAATTTCCATCAGATGGTCCAGTTATGCAAAAGAAAATATGGGTTGGGAAGCATCTTCTGAAAGAAT
GTACCCAGAAGATGGTGCATTGAAGGGTGAATTAACAAAGATTGAAATTGAAGGATGGTGGTGCATTACGATGCTGAA
GTTAAGACTACATACAAGGCTAAGAAACCAGTTCAATTACCAGGTGCTTACAACGTTAAACATCAAATGGATATTACTT
CTCATAACGAAGATTACACAATTTGTTGAACAATATGAAAGAGCCGAAGGTAGACACTCAACAGGTGGTATGGATGAATT
GTATAAGTAACTCGAG

>NAPstar4.2

TCTAGAACCATGGGATCCAAAGTACCAGAAGCCGCTATTTCCAGATTGATAACATATTTGAGAATTTTAGAAGAATTAG
 AAGCACAAAGGTGTCCACAGAACCCTTCTGAACAATTGGGTGAATTAGCTCAAGTTACAGCATTCCAAGTTGATAAAGA
 TTTGTCATACTTTGGTTCTTACGGTACTGATGGTGTGGTTACACAGTCCAGTTTTGAAGAGAGAATTGAGACATATC
 TTGGGTTTAAACAGAAAGTGGGGTTTATGTATCGTTGGTATGGGTgacTTAGGTTCTGCTTTGGCAGATTGGCCAGGTT
 TTGGTGAATCATTTGAATTGAGAGGTTTCTTTTCAAGATCAGCTCAAAAAGTTGGTAGACCAGTTAGAGGTGGTGTAT
 TGAACATGTTGATTTGTTGCCACAAAGAGTTCCAGGTAGAATTGAAATTGCTTTGTTAACTGTTCCAAGAGAAGCTGCA
 CAAAAGCTGCAGATTTGTTAGTTGCTGCAGGTATTAAGGTATTTTAACTTCGCACCAGTTGTTTTGGAAGTTCCAA
 AAGAAGTTGCTGTTGAAAACGTTGATATTTGGCAGGTTTAACTAGATTGCTTTTGTATCTTGAATCCAACATGGTC
 AGCTGCAGGTGGTCATGGTTTTACTGCTCATAACGTTTACATCATGGCAGATAAGCAAAAGAATGGTATTAAGCTAAC
 TTCAAGATCAGACATAATATTGAAGATGGTGGTGTCAATTGGCAGATCATTACCAACAAAACACTCCAATTGGTGACG
 GTCCAGTTTTGTTACCAGATAACCATTACTTATCTATCCAATCAAAATTGTCTAAAGATCCAACGAAAAGAGAGATCA
 TATGGTTTTGTTAGAATTTGTTACTGCTGCAGGTATCACACATGGTATGGATGAATTATACAAAGGTGGTACAGGTGGT
 TCAATGGTTTTCTAAAGGTGAAGAATTGTTTACTGGTGTGTTCCAATTTTAGTTGAATTGGATGGTGACGTTAATGGTC
 ATAAATTTCTGTTTCAGGTGAAGGTGAAGGTGACGCTACTTACGGTAAATTGACATTGAAGTTTATTTGACTACTGG
 TAAATTACCAGTTCCTTGGCCAACATTGGTTACTACATTTTCTTACGGTGTATGGTTTTGCTAGATACCCAGATCAT
 ATGAAGCAACATGATTTCTTTAAGTCAGCAATGCCAGAAGGTTACGTTCAAGAAAGAACTATTTCTTTAAAGATGATG
 GTAACTACAAGACAAGAGCTGAGGTTAAGTTTCAAGGTGACACTTTAGTTAACAGAATCGAATTGAAAGGTATCGATTT
 CAAAGAAGATGGTAACATCTTAGGTACAAAATTGGAATATAATACAAAAGTTCCAGAAGCTGCTATTTCAAGATTGATC
 ACTTACTTAAGAATTTTGAAGAATTAGAAGCTCAAGGTGTTTATAGAACAGCATCAGAACAATTAGGTGAATTAGCTC
 AAGTCACTGCATTTCAAGTTGATGAAGATTTGTCATACTTCGGTCTTATGGTACTGACGGTGTCCGGTTATACAGTCC
 AGTCTTAAAAAGAGAATTGAGACACATTTTAGGTTTAAATAGAAAATGGGGTTTATGCATTGTCGGCATGGGTAGATTA
 GGTCTGCTTTGGCAGACTGGCCTGGTTTCGGCGAATCATTTGAATTGCGTGGTTTTCTTTCAAGATCAGCGGAAAAGG
 TCGGTAGACCAGTTAGAGGTGGTGTATTGAGCACACCGATTTGTTACCTCAGAGAGTTCCAGGCAGAATCGAAATCGC
 TTTGTTAACAGTTCCAAGAGAAGCCGCTCAAAAGGCCGAGATTTGTTAGTTGCCGCTGGTATTAAGGTATTTTAAAT
 TTCGCTCCTGTCGTTTTGGAAGTTCCAAAAGAAGTTGCGGTTGAAAACGTTGATTTCTTGGCTGGTTTAAACAAGATTGT
 CTTTTGCAATCTGAACCCAAAGTGGAGAGAAGAAATGATGGGTTCCAGGTACTGGTGGTAAATGCTTCAGATGGTGGTGG
 TTCTGGTGGTATGGTTTCAAAGGGTGAAGAAGATAACATGGCAATTATTAAGGAGTTTATGAGATTCAAAGTTCATATG
 GAAGGTTCTGTTAACGGTCAATGATTTGAAATCGAAGGTGAAGGTGAAGGTAGACCATATGAAGGTACTCAAACAGCTA
 AATTGAAGTTACTAAAGGTGGTCCATTACCATTGTCATGGGATATTTGCTCCACAATTCATGTACGGTTCAAAAGC
 ATATGTTAAGCATCCAGCAGATATTCAGATTACTTGAATTTATCTTTTCTGAAGGTTTTAAATGGGAAAGAGTTATG
 AACTTCAAGATGGTGGTGTGTTACTGTTACACAAGATTTCTTATTACAAGATGGCAGTTTATATATAAGGTTAAAT
 TGAGAGGTACAAAATTTCCATCAGATGGTCCAGTTATGCAAAAGAAAACATGGGTTGGGAAGCATCTTCTGAAAGAAT
 GTACCCAGAAGATGGTGCATTGAAGGGTGAATTAACAAAGATTGAAATGAAGGATGGTGGTCAATACGATGCTGAA
 GTTAAGACTACATAACAGCTAAGAAACCAGTTCAATTACCAGGTGCTTACAACGTTAACATCAAATTTGGATATTACTT
 CTCATAACGAAGATTACACAATTGTTGAACAATATGAAAAGAGCCGAAGGTAGACACTCAACAGGTGGTATGGATGAATT
 GTATAAGTAACTCGAG

>NAPstar4.3

TCTAGAACCATGGGATCCAAAGTACCAGAAGCCGCTATTTCCAGATTGATAACATATTTGAGAATTTTAGAAGAATTAG
 AAGCACAAAGGTGTCCACAGAACCCTTCTGAACAATTGGGTGAATTAGCTCAAGTTACAGCATTCCAAGTTGATAAAGA
 TTTGTCATACTTTGGTTCTTACGGTACTGATGGTGTGGTTACACAGTCCAGTTTTGAAGAGAGAATTGAGACATATC
 TTGGGTTTAAACAGAAAGTGGGGTTTATGTATCGTTGGTATGGGTgacTTAGGTTCTGCTTTGGCAGATTGGCCAGGTT
 TTGGTGAATCATTTGAATTGAGAGGTTTCTTTTCAAGATCAGCTCAAAAAGTTGGTAGACCAGTTAGAGGTGGTGTAT
 TGAACATGTTGATTTGTTGCCACAAAGAGTTCCAGGTAGAATTGAAATTGCTTTGTTAACTGTTCCAAGAGAAGCTGCA
 CAAAAGCTGCAGATTTGTTAGTTGCTGCAGGTATTAAGGTATTTTAACTTCGCACCAGTTGTTTTGGAAGTTCCAA
 AAGAAGTTGCTGTTGAAAACGTTGATATTTGGCAGGTTTAACTAGATTGCTTTTGTATCTTGAATCCAACATGGTC
 AGCTGCAGGTGGTCATGGTTTTACTGCTCATAACGTTTACATCATGGCAGATAAGCAAAAGAATGGTATTAAGCTAAC
 TTCAAGATCAGACATAATATTGAAGATGGTGGTGTCAATTGGCAGATCATTACCAACAAAACACTCCAATTGGTGACG
 GTCCAGTTTTGTTACCAGATAACCATTACTTATCTATCCAATCAAAATTGTCTAAAGATCCAACGAAAAGAGAGATCA
 TATGGTTTTGTTAGAATTTGTTACTGCTGCAGGTATCACACATGGTATGGATGAATTATACAAAGGTGGTACAGGTGGT
 TCAATGGTTTTCTAAAGGTGAAGAATTGTTTACTGGTGTGTTCCAATTTTAGTTGAATTGGATGGTGACGTTAATGGTC
 ATAAATTTCTGTTTCAGGTGAAGGTGAAGGTGACGCTACTTACGGTAAATTGACATTGAAGTTTATTTGACTACTGG
 TAAATTACCAGTTCCTTGGCCAACATTGGTTACTACATTTTCTTACGGTGTATGGTTTTGCTAGATACCCAGATCAT
 ATGAAGCAACATGATTTCTTTAAGTCAGCAATGCCAGAAGGTTACGTTCAAGAAAGAACTATTTCTTTAAAGATGATG
 GTAACTACAAGACAAGAGCTGAGGTTAAGTTTCAAGGTGACACTTTAGTTAACAGAATCGAATTGAAAGGTATCGATTT
 CAAAGAAGATGGTAACATCTTAGGTACAAAATTGGAATATAATACAAAAGTTCCAGAAGCTGCTATTTCAAGATTGATC
 ACTTACTTAAGAATTTTGAAGAATTAGAAGCTCAAGGTGTTTATAGAACAGCATCAGAACAATTAGGTGAATTAGCTC

AAGTCACTGCATTCCAAGTTGATGAAGATTTGTCATACTTCGGTCTTATGGTACTGACGGTGTGGTTATACAGTTCC
AGTCTTAAAAAGAGAATTGAGACACATTTTAGGTTTAAATAGAAAATGGGGTTTATGCATTGTCGGCATGGGTAGATTA
GGTTCGCTTTGGCAGACTGGCCTGGTTTCGGCGAATCATTTGAATTGCGTGGTTTCTTTCAAGAaagGCgaaAAGG
TCGGTAGACCAGTTAGAGGTGGTGTATTGAGCACTacGATTTGTTACCTCAGAGAGTTCAGGCAGAATCGAAATCGC
TTTGTTAACAGTTCCAAGAGAAGCCGCTCAAAAAGCCGCAGATTTGTTAGTTGCCGCTGGTATTAAGGTATTTAAAT
TTCGCTCCTGTCGTTTTGGAAGTTCCAAAAGAAGTTGCGGTTGAAAACGTTGATTTCTTGCTGGTTTAAACAAGATTGT
CTTTTGAATCTTGAACCCAAAGTGGAGAGAAGAAATGATGGGTTACGGTACTGGTGGTAATGCTTCAGATGGTGGTGG
TTCTGGTGGTATGGTTTTCAAAGGGTGAAGAAGATAACATGGCAATTATTAAGGAGTTTATGAGATTCAAAGTTCATATG
GAAGGTTCTGTTAACGGTCATGAATTTGAAATCGAAGGTGAAGGTGAAGGTAGACCATATGAAGGTACTCAAACAGCTA
AATTGAAGGTTACTAAAGGTGGTCCATTACCATTTGCATGGGATATTTGCTCCACAATTCATGTACGGTTCAAAAGC
ATATGTTAAGCATCCAGCAGATATTCCAGATTACTTGAAATTATCTTTTCTGAAGGTTTTAAATGGGAAAGAGTTATG
AACTTCGAAGATGGTGGTGTGTTACTGTTACACAAGATTCTTCATTACAAGATGGCGAGTTTATATATAAGGTTAAAT
TGAGAGGTACAAATTTCCATCAGATGGTCCAGTTATGCAAAAAGAAAATATGGGTTGGGAAGCATCTTCTGAAAGAAT
GTACCCAGAAGATGGTGCATTGAAGGGTGAATTTAAACAAAGATTGAAATTGAAGGATGGTGGTCAATTACGATGCTGAA
GTTAAGACTACATAACAAGCTAAGAAACCAGTTCAATTACCAGGTGCTTACAACGTTAACATCAAATTGGATATTACTT
CTCATAACGAAGATTACACAATTGTTGAACAATATGAAAGAGCCGAAGGTAGACACTCAACAGGTGGTATGGATGAATT
GTATAAGTAACTCGAG

>NAPstar5

TCTAGAACCATGGGATCCAAAGTACCAGAAGCCGCTATTTCCAGATTGATAACATATTTGAGAATTTAGAAAGAATTAG
AAGCACAAGGTGTCCACAGAACCGCTTCTGAACAATTGGGTGAATTAGCTCAAGTTACAGCATTCCAAGTTGATAAAGA
TTTGTCACTTTGGTCTTACGGTACTGATGGTGTGGTTACACAGTTCCAGTTTTGAAGAGAGAATTGAGACATATC
TTGGGTTTAAACAGAAAGTGGGTTTTATGTATCGTTGGTATGGGTTaTTAGGTTCTGCTTTGGCAGATTGGCCAGGTT
TTGGTGAATCATTTGAATTGAGAGGTTTCTTTCAAGATCAGCTCAAAAAGTTGGTAGACCAGTTAGAGGTGGTGTAT
TGAACATGTTGATTTGTTGCCACAAAGAGTTCAGGTAGAATTGAAATTGCTTTGTTAACTGTTCCAAGAGAAGCTGCA
CAAAAAGCTGCAGATTTGTTAGTTGCTGCAGGTATTAAGGTATTTTAAACTTCGCACCAGTTGTTTTGGAAGTTCCAA
AAGAAGTTGCTGTTGAAAACGTTGATATTTGGCAGGTTAACTAGATTGCTTTTGCTATCTTGAATCCAACATGGTC
AGCTGCAGGTGGTCATGGTTTTACTGCTCATAACGTTTACATCATGGCAGATAAGCAAAAAGAATGGTATTAAGCTAAC
TTCAAGATCAGACATAATATTGAAGATGGTGGTGTCAATTGGCAGATCATTACCAACAAAACACTCCAATTGGTGACG
GTCCAGTTTTGTTACCAGATAACCATTACTTATCTATCCAATCAAATTTGCTAAAGATCCAAACGAAAAGAGAGATCA
TATGGTTTTGTTAGAATTTGTTACTGCTGCAGGTATCACACATGGTATGGATGAATTATACAAAGGTGGTACAGGTGGT
TCAATGGTTTTCAAAGGTGAAGAATGTTTACTGGTGTGTTCCAATTTTAGTTGAATTGGATGGTGACGTTAATGGTC
ATAAATTTTCTGTTTCAGGTGAAGGTGAAGGTGACGCTACTTACGGTAAATTGACATTGAAGTTTATTTGTACTACTGG
TAAATTACCAGTTCCTTGGCCAACATTGGTTACTACATTTTCTTACGGTGTATGGTTTTTGCTAGATACCCAGATCAT
ATGAAGCAACATGATTTCTTTAAGTCAGCAATGCCAGAAGGTTACGTTCAAGAAAGAACTATTTTCTTTAAAGATGATG
GTAACACAAGACAAGAGCTGAGGTTAAGTTCGAAGGTGACACTTTAGTTAACAGAATCGAATTGAAAGGTATCGATTT
CAAAGAAGATGGTAACATCTTAGGTCACAAATTTGGAATATAATACAAAAGTTCCAGAAGCTGCTATTTCAAGATTGATC
ACTTACTTAAGAATTTGGAAGAATTAGAAGCTCAAGGTGTTATAGAACAGCATCAGAACAATTAGGTGAATTAGCTC
AAGTCACTGCATTCCAAGTTGATGAAGATTTGTCATACTTCGGTCTTATGGTACTGACGGTGTGGTTATACAGTTCC
AGTCTTAAAAAGAGAATTGAGACACATTTTAGGTTTAAATAGAAAATGGGGTTTATGCATTGTCGGCATGGGTTaTTA
GGTTCGCTTTGGCAGACTGGCCTGGTTTCGGCGAATCATTTGAATTGCGTGGTTTCTTTCAAGATCAGCGCAAAGG
TCGGTAGACCAGTTAGAGGTGGTGTATTGAGCACGTTGATTTGTTACCTCAGAGAGTTCAGGCAGAATCGAAATCGC
TTTGTTAACAGTTCCAAGAGAAGCCGCTCAAAAAGCCGCAGATTTGTTAGTTGCCGCTGGTATTAAGGTATTTAAAT
TTCGCTCCTGTCGTTTTGGAAGTTCCAAAAGAAGTTGCGGTTGAAAACGTTGATTTCTTGCTGGTTTAAACAAGATTGT
CTTTTGAATCTTGAACCCAAAGTGGAGAGAAGAAATGATGGGTTACGGTACTGGTGGTAAATGCTTCAGATGGTGGTGG
TTCTGGTGGTATGGTTTTCAAAGGGTGAAGAAGATAACATGGCAATTATTAAGGAGTTTATGAGATTCAAAGTTCATATG
GAAGGTTCTGTTAACGGTCATGAATTTGAAATCGAAGGTGAAGGTGAAGGTAGACCATATGAAGGTACTCAAACAGCTA
AATTGAAGGTTACTAAAGGTGGTCCATTACCATTTGCATGGGATATTTGCTCCACAATTCATGTACGGTTCAAAAGC
ATATGTTAAGCATCCAGCAGATATTCCAGATTACTTGAAATTATCTTTTCTGAAGGTTTTAAATGGGAAAGAGTTATG
AACTTCGAAGATGGTGGTGTGTTACTGTTACACAAGATTCTTCATTACAAGATGGCGAGTTTATATATAAGGTTAAAT
TGAGAGGTACAAATTTCCATCAGATGGTCCAGTTATGCAAAAAGAAAATATGGGTTGGGAAGCATCTTCTGAAAGAAT
GTACCCAGAAGATGGTGCATTGAAGGGTGAATTTAAACAAAGATTGAAATTGAAGGATGGTGGTCAATTACGATGCTGAA
GTTAAGACTACATAACAAGCTAAGAAACCAGTTCAATTACCAGGTGCTTACAACGTTAACATCAAATTGGATATTACTT
CTCATAACGAAGATTACACAATTGTTGAACAATATGAAAGAGCCGAAGGTAGACACTCAACAGGTGGTATGGATGAATT
GTATAAGTAACTCGAG

>NAPstar6

TCTAGAACCATGGGATCCAAAGTACCAGAAGCCGCTATTTCCAGATTGATAACATATTTGAGAATTTAGAAAGAATTAG
AAGCACAAGGTGTCCACAGAACCGCTTCTGAACAATTGGGTGAATTAGCTCAAGTTACAGCATTCCAAGTTGATAAAGA

TTTGTCACTTTGGTTCCTACGGTACTGATGGTGTGGTTACACAGTCCAGTTTTGAAGAGAGAATTGAGACATATC
 TTGGGTTTAAACAGAAAGTGGGGTTTATGTATCGTTGGTATGGGTAGATTAGGTTCTGCTTTGGCAGATTGGCCAGGTT
 TTGGTGAATCATTGAATTGAGAGGTTCTTTTCAAGAAagGCTgaaAAAGTTGGTAGACCAGTTAGAGGTGGTGTAT
 TGAACATgttGATTTGTTGCCACAAAGAGTCCAGGTAGAATTGAAATGCTTTGTTAACTGCTCCAAGAGAAGCTGCA
 CAAAAAGCTGCAGATTTGTTAGTTGCTGCAGGTATTAAGGTATTTTAACTTCGCACCAGTTGTTTTGGAAGTCCAA
 AAGAAGTTGCTGTTGAAAACGTTGATATTTGGCAGGTTAACTAGATTGCTTTTGTATCTTGAATCCAACATGGTC
 AGCTGCAGGTGGTCATGGTTTTACTGCTCATAACGTTACATCATGGCAGATAAGCAAAAGAATGGTATTAAGCTAAC
 TTCAAGATCAGACATAATATTGAAGATGGTGGTGTCAATTGGCAGATCATTACCAACAAAACACTCCAATTGGTGACG
 GTCCAGTTTTGTTACCAGATAACCATTACTTATCTATCCAATCAAAATGCTAAAGATCCAAACGAAAAGAGAGATCA
 TATGGTTTTGTTAGAATTTGTTACTGCTGCAGGTATCACACATGGTATGGATGAATTATACAAAGGTGGTACAGGTGGT
 TCAATGGTTTCTAAAGGTGAAGAATTGTTTACTGGTGTGTTCCAATTTAGTTGAATTGGATGGTGACGTTAATGGTC
 ATAAATTTCTGTTTCAGGTGAAGGTGAAGGTGACGCTACTTACGGTAAATTTGACATTGAAGTTATTTGACTACTGG
 TAAATTACCAGTTCCTTGGCCAACATTGGTTACTACATTTTCTTACGGTGTATGGTTTTGCTAGATACCCAGATCAT
 ATGAAGCAACATGATTTCTTTAAGTCAGCAATGCCAGAAGGTTACGTTCAAGAAAGAACTATTTCTTTAAAGATGATG
 GTAACTACAAGACAAGAGCTGAGGTTAAGTTCGAAGGTGACACTTTAGTTAACAGAATCGAATTGAAAGGTATCGATTT
 CAAAGAAGATGGTAACATCTTAGGTACAAAATTGGAATATAATACAAAAGTTCAGAAGCTGCTATTTCAAGATTGATC
 ACTTACTTAAGAATTTTGAAGAATTAGAAGCTCAAGGTGTTTATAGAACAGCATCAGAACAATTAGGTGAATTAGCTC
 AAGTCACTGCATTCCAAGTTGATGAAGATTTGTCATACTTCGGTCTTATGGTACTGACGGTGTCCGTTATACAGTTCC
 AGTCTTAAAAAGAGAATTGAGACACATTTTAGGTTTAAATAGAAAATGGGGTTTATGCATTGTCCGGCATGGGTAGATTA
 GGTCTGCTTTGGCAGACTGGCCTGGTTTCGGCGAATCATTTGAATTGCGTGGTTTTCTTTCAAGAAagGCGgaaAAGG
 TCGGTAGACCAGTTAGAGGTGGTGTATTGAGCACgttGATTTGTTACCTCAGAGAGTCCAGGCAGAATCGAAATCGC
 TTTGTTAACAGCTCCAAGAGAAGCCGCTCAAAGGCCGAGATTTGTTAGTTGCCGCTGGTATTAAGGTATTTTAAAT
 TTCGCTCCTGTCGTTTTGGAAGTTCAAAAGAAGTTCGGGTTGAAAACGTTGATTTCTTGGCTGGTTAACAAAGATTGT
 CTTTTGCAATCTTGAACCCAAAGTGGAGAGAAGAAATGATGGGTTGAGTACTGGTGGTAATGCTTCAGATGGTGGTGG
 TTCTGGTGGTATGGTTTCAAAGGTGAAGAAGATAACATGGCAATTATTAAGGAGTTTATGAGATTCAAAGTTCATATG
 GAAGTCTGTAAACGGTCAATTTGAAATCGAAGGTGAAGGTGAAGGTAGACCATATGAAGGTACTCAAACAGCTA
 AATTGAAGTTACTAAAGGTGGTCCATTACCATTGTCATGGGATATTTGCTCCACAATTCATGTACGGTTCAAAAGC
 ATATGTTAAGCATCCAGCAGATATCCAGATTACTTGAATTTATCTTTTCTGAAGTTTTAAATGGGAAAGAGTTATG
 AACTTCAAGATGGTGGTGTGTTACTGTTACACAAGATTTCTTATTACAAGATGGCGAGTTATATATAAGGTTAAAT
 TGAGAGGTACAAATTTCCATCAGATGGTCCAGTTATGCAAAAGAAAACATGGGTTGGGAAGCATCTTCTGAAAGAAAT
 GTACCCAGAAGATGGTGCATTGAAGGGTGAATTAACCAAAGATTGAAATGAAGGATGGTGGTCAATTACGATGCTGAA
 GTTAAGACTACATACAAGGCTAAGAAACCAGTTCAAATACCAGGTGCTTACAACGTTAACATCAAATGGATATTAAT
 CTCATAACGAAGATTACACAATGTTGAACAATATGAAAGAGCCGAAGGTAGACACTCAACAGGTGGTATGGATGAATT
 GTATAAGTAACTCGAG

>NAPstar7

TCTAGAACCATGGGATCCAAAGTACCAGAAGCCGCTATTTCCAGATTGATAACATATTTGAGAATTTTAGAAGAATTAG
 AAGCACAAAGGTGTCCACAGAACCCTTCTGAACAATTGGGTGAATTAGCTCAAGTTACAGCATTCCAAGTTGATAAAGA
 TTTGTCACTTTGGTTCCTACGGTACTGATGGTGTGGTTACACAGTCCAGTTTTGAAGAGAGAATTGAGACATATC
 TTGGGTTTAAACAGAAAGTGGGGTTTATGTATCGTTGGTATGGGTAGATTAGGTTCTGCTTTGGCAGATTGGCCAGGTT
 TTGGTGAATCATTGAATTGAGAGGTTCTTTTCAAGAAAGGCTGAAAAAGTTGGTAGACCAGTTAGAGGTGGTGTAT
 TGAACATGTTGATTTGTTGCCACAAAGAGTCCAGGTAGAATTGAAATGCTTTGTTAACTACTCCAAGAGAAGCTGCA
 CAAAAAGCTGCAGATTTGTTAGTTGCTGCAGGTATTAAGGTATTTTAACTTCGCACCAGTTGTTTTGGAAGTCCAA
 AAGAAGTTGCTGTTGAAAACGTTGATATTTGGCAGGTTAACTAGATTGCTTTTGTATCTTGAATCCAACATGGTC
 AGCTGCAGGTGGTCATGGTTTTACTGCTCATAACGTTACATCATGGCAGATAAGCAAAAGAATGGTATTAAGCTAAC
 TTCAAGATCAGACATAATATTGAAGATGGTGGTGTCAATTGGCAGATCATTACCAACAAAACACTCCAATTGGTGACG
 GTCCAGTTTTGTTACCAGATAACCATTACTTATCTATCCAATCAAAATGCTAAAGATCCAAACGAAAAGAGAGATCA
 TATGGTTTTGTTAGAATTTGTTACTGCTGCAGGTATCACACATGGTATGGATGAATTATACAAAGGTGGTACAGGTGGT
 TCAATGGTTTCTAAAGGTGAAGAATTGTTTACTGGTGTGTTCCAATTTAGTTGAATTGGATGGTGACGTTAATGGTC
 ATAAATTTCTGTTTCAGGTGAAGGTGAAGGTGACGCTACTTACGGTAAATTTGACATTGAAGTTATTTGACTACTGG
 TAAATTACCAGTTCCTTGGCCAACATTGGTTACTACATTTTCTTACGGTGTATGGTTTTGCTAGATACCCAGATCAT
 ATGAAGCAACATGATTTCTTTAAGTCAGCAATGCCAGAAGGTTACGTTCAAGAAAGAACTATTTCTTTAAAGATGATG
 GTAACTACAAGACAAGAGCTGAGGTTAAGTTCGAAGGTGACACTTTAGTTAACAGAATCGAATTGAAAGGTATCGATTT
 CAAAGAAGATGGTAACATCTTAGGTACAAAATTGGAATATAATACAAAAGTTCAGAAGCTGCTATTTCAAGATTGATC
 ACTTACTTAAGAATTTTGAAGAATTAGAAGCTCAAGGTGTTTATAGAACAGCATCAGAACAATTAGGTGAATTAGCTC
 AAGTCACTGCATTCCAAGTTGATGAAGATTTGTCATACTTCGGTCTTATGGTACTGACGGTGTCCGTTATACAGTTCC
 AGTCTTAAAAAGAGAATTGAGACACATTTTAGGTTTAAATAGAAAATGGGGTTTATGCATTGTCCGGCATGGGTAGATTA
 GGTCTGCTTTGGCAGACTGGCCTGGTTTCGGCGAATCATTTGAATTGCGTGGTTTTCTTTCAAGAAAGCGGAAAAAGG

TCGGTAGACCAGTTAGAGGTGGTGTATTGAGCACGTTGATTTGTTACCTCAGAGAGTTCCAGGCAGAATCGAAATCGC
TTTGTTAACTCCAAGAGAAGCCGCTCAAAGGCCGAGATTTGTTAGTTGCCGCTGGTATTAAGGTATTTAAAT
TTCGCTCCTGTCGTTTTGGAAGTTCCAAAAGAAGTTGCGGTTGAAAACGTTGATTTCTTGGCTGGTTAAACAAGATTGT
CTTTGCAATCTTGAACCCAAAGTGGAGAGAAGAAATGATGGGTTGAGTACTGGTGGTAATGCTTCAGATGGTGGTGG
TTCTGGTGGTATGGTTTTCAAAGGTGAAGAAGATAACATGGCAATTATTAAGGAGTTTATGAGATTCAAAGTTCATATG
GAAGGTTCTGTTAACGGTCATGAATTTGAAATCGAAGGTGAAGGTGAAGGTAGACCATATGAAGGTACTCAAACAGCTA
AATTGAAGGTTACTAAAGGTGGTCCATTACCATTTGCATGGGATATTTGTCTCCACAATTCATGTACGGTTCAAAGC
ATATGTTAAGCATCCAGCAGATATTCCAGATTACTTGAAATTATCTTTTCTGAAGGTTTTAAATGGGAAAGAGTTATG
AACTTCGAAGATGGTGGTGTGTTACTGTTACACAAGATTCTTCATTACAAGATGGCGAGTTTATATATAAGGTTAAAT
TGAGAGGTACAAATTTCCATCAGATGGTCCAGTTATGCAAAGAAAAGTATGGGTTGGGAAGCATCTTCTGAAAGAAT
GTACCAGAAGATGGTGCATTGAAGGGTGAATTAACAAAGATTGAAATTGAAGGATGGTGGTTCATTACGATGCTGAA
GTTAAGACTACATACAAGGCTAAGAAACCAGTTCAATTACCAGGTGCTTACAACGTTAACATCAAATTGGATATTACTT
CTCATAACGAAGATTACACAATTGTTGAACAATATGAAAGAGCCGAAGGTAGACACTCAACAGGTGGTATGGATGAATT
GTATAAGTAACTCGAG

Acknowledgement

An erster Stelle möchte ich Herrn Prof. Dr. Bruce Morgan danken, der mich in seine noch junge Arbeitsgruppe aufnahm und der es mir ermöglicht hat zu promovieren. Ich danke ihm für die stetige, wissenschaftliche Unterstützung sowie die Gestaltung einer sehr konstruktiven und angenehmen Arbeitsatmosphäre innerhalb der Gruppe.

Ein großer Dank gilt außerdem Herrn Prof. Dr. Robert Ernst für die Übernahme des Zweitgutachtens.

Des Weiteren danke ich Herrn Prof. Dr. Schwarzländer für die fruchtbare Kollaboration und die anregenden Diskussionen, ohne die es womöglich nicht zu der Entwicklung der NAPstar-Sensoren gekommen wäre. Ich danke Jan-Ole Niemeyer für die Durchführung der wichtigen und erkenntnisreichen in-vitro-Studien. Ebenso möchte ich Frau Jun.-Prof. Leticia Prates Roma, Herrn Prof. Dr. Jan Riemer sowie Markus Hoffmann und Lianne Jacobs danken, die das Projekt weiterhin mit Leben füllen.

Ein besonderer Dank geht an Dr. Jannik Zimmermann für den kontinuierlichen wissenschaftlichen Austausch und seine herausragende Unterstützung, auf die ich mich während meiner gesamten Promotion verlassen konnte. Neben Jannik sind Dr. Gurleen Khandpur und Dr. Julian Oestreicher einen Großteil des Weges mit mir gegangen. Euch dreien danke ich für eure Freundschaft und die schöne gemeinsame Zeit.

Dr. Frank Hannemann, Birgit Heider-Lips, Antje Eiden-Plach, sowie Gabi Schon legten die organisatorischen Grundlagen für eine weitestgehend ‚reibungslose‘ Promotion in Saarbrücken. Dafür, und für den netten zwischenmenschlichen Austausch, möchte ich euch von Herzen danken. Außerdem danke ich Frau Prof. Dr. habil. Rita Bernhardt für ihre fachlichen Ratschläge und die Unterstützung über meine Masterarbeit hinaus.

Weiterhin möchte ich allen Studenten, deren Abschlussarbeiten ich im Zuge des Promotionsprojektes betreuen durfte, für die wertvolle und konstruktive Zusammenarbeit danken: Kim, Linda, Pascal, Jochen, Michel und Julia.

Abschließend möchte ich von ganzem Herzen meinen Eltern, meinem Bruder Marko und Lukas, sowie seiner Familie, für ihre liebevolle und bedingungslose Unterstützung danken, ohne die mir sicherlich alles sehr viel schwerer gefallen wäre. Insbesondere mein Bruder, der leider viel zu früh von uns gegangen ist, war mir in vielerlei Hinsicht ein großes Vorbild. Vielen Dank für alles!